12-2014

Determining DNA Damage Prevention Mechanisms for Multifunctional Selenium and Sulfur Antioxidants and the DNA-Damaging Capabilities of Clotrimadozle and Pseudoephedrine-Derived Metal Complexes

Matthew Todd Zimmerman
Clemson University

DETERMINING DNA DAMAGE PREVENTION MECHANISMS FOR MULTIFUNCTIONAL SELENIUM AND SULFUR ANTIOXIDANTS AND THE DNA-DAMAGING CAPABILITIES OF CLOTRIMADOZLE AND PSEUDOEPHEDRINE-DERIVED METAL COMPLEXES

A Dissertation
Presented to
the Graduate School of
Clemson University

In Partial Fulfillment
of the Requirements for the Degree
Doctor of Philosophy
Chemistry

---

by
Matthew Todd Zimmerman
December 2014

Accepted by:
Dr. Julia L. Brumaghim, Committee Chair
Dr. Jeffrey N. Anker
Dr. Gautam Bhattacharyya
Dr. William T. Pennington

ABSTRACT

DNA damage by reactive oxygen species (ROS) is a cause of many chronic diseases. This work examines the ability of sulfur and selenium antioxidants to prevent oxidative DNA damage and the mechanisms for this activity. Although iron- and copper-generated hydroxyl radical are primary causes of damage under oxidative stress conditions, studies typically focus on ROS scavenging rather than antioxidant-metal binding as a mechanism for sulfur and selenium antioxidant behavior.

Mass spectrometry studies of sulfur and selenoamino acids (Chapter 2) show that most form Cu^{I} and Fe^{II} complexes, regardless of their metal-mediated DNA damage prevention abilities. Because their electrochemical properties do not correlate to antioxidant activity, metal binding rather than ROS scavenging is the major mechanism for these sulfur and selenium antioxidants.

DNA damage assays with *N,N'*-dimethylimazole thione (dmit) and selone (dmise) determined that both prevent Cu^{I}-mediated DNA damage (IC_{50} = 1550 and ~240 μM, respectively; Chapter 3). Surprisingly, dmit and dmise more effectively inhibit Fe^{II}-mediated DNA damage (IC_{50} = 89.1 and 3.2 μM, respectively), an ability not previously observed for this class of antioxidants. Dmise and dmit coordinate Cu^{I} and Fe^{II} and prevent DNA damage by peroxynitrite (IC_{50} = 171.4 and 155.2, respectively). Studies with similar thiones, selones, and their derivatives (Chapter 4) showed that these compounds are also multifunctional antioxidants, preventing DNA damage by Cu^{I} (IC_{50} = 22-1023 μM), Fe^{II} (IC_{50} = 2.3-1000 μM) and peroxynitrite (IC_{50} = 57.4-594 μM). Many

of these compounds readily undergo oxidation and reduction, and mass spectrometry studies show Cu^{I} or Fe^{II} coordination, regardless of antioxidant activity. These are the first sulfur and selenium compounds with multifunctional antioxidant activity, and the structure-activity relationships established in this work will allow development of more potent antioxidants for disease treatment and prevention.

Studies in Chapter 5 focus on how metal binding alters drug properties. Clotrimazole-metal complexes kill cancer cells, yet their cytotoxic mechanisms are not understood. Similarly, studies have not examined the effects of metal coordination on the biological properties of pseudoephedrine-derived compounds. DNA damage studies with copper complexes of both compounds found that they significantly damage DNA (EC_{50} = 10.5-21.7 μM), likely by copper-mediated ROS generation.

DEDICATION

I dedicate this dissertation to my parents, Carl and Deborah Zimmerman, my sister Amy, and my friends for their support and encouragement over the years.

ACKNOWLEDGEMENTS

Firstly, I would like to thank Dr. Julia Brumaghim for allowing me the opportunity to continue my academic growth in an exciting and ever expanding field of chemistry. Her mentorship and support throughout my time at Clemson has been invaluable, and catalyzed my desire to continue my career in academia.

I would like to thank Dr. Gautam Bhattacharyya, who provided very insightful and hilarious conversations over the years, and who always believed in me even though he did not receive a doughnut during my defense. I would like to acknowledge my collaborators, Dr. Daniel Rabinovich and Dr. Norah Barba-Behrens. A special thanks to Dr. Sean O'Connor and Dr. Andy Tennyson, for allowing me to teach some amazing chemistry courses.

To my colleagues in the Brumaghim group, I cannot thank you enough for your conversations and encouragement over the years. A special thanks to Dr. Sabina Wang and Dr. Martin Kimani for making late nights lost in lab enjoyable and memorable. I'm also grateful for the incredible friendships of Dr. Marcel Fallet, Charlie Lowe, and Sara Comer for their constant ability to find humor in any situation, and to always cheer me up during the darkest times of research.

Lastly, none of this would be possible without the support from my parents and sister, who never let me give up when times were rough, and always encouraged me to pursue my dreams.

TABLE OF CONTENTS

Page

Table of Contents (Continued) **Page**

Table of Contents (Continued) **Page**

LIST OF TABLES

Table **Page**

Table **Page**

Table **Page**

Table **Page**

Table **Page**

Table **Page**

LIST OF FIGURES

Figure **Page**

Figure **Page**

Figure **Page**

Figure **Page**

Figure **Page**

Figure **Page**

Figure **Page**

Figure **Page**

Figure **Page**

Figure **Page**

Figure **Page**

Figure **Page**

LIST OF SCHEMES

Scheme **Page**

CHAPTER ONE

SULFUR AND SELENIUM ANTIOXIDANTS: CHALLENGING RADICAL SCAVENGING MECHANISMS AND DEVELOPING STRUCTURE-ACTIVITY RELATIONSHIPS BASED ON METAL BINDING

1.1. Introduction

Reactive oxygen species (ROS) such as superoxide ($O_2^{\bullet-}$), hydrogen peroxide (H_2O_2), hydroxyl radical ($^{\bullet}OH$), peroxynitrite ($ONOO^-$), and singlet oxygen ($^1O_2$) are natural byproducts of cellular respiration that can cause cellular oxidative damage but also serve as cell signaling agents.[1-3] Hydroxyl radical is the most damaging ROS,[4-7] although peroxynitrite also directly damages lipids, proteins, and DNA. In contrast, H_2O_2 and superoxide are only indirect contributors to oxidative DNA damage.[3,8-11] This DNA damage is linked to development of cancer, inflammation, neurodegenerative diseases, and cardiovascular diseases.[12-16]

Cellular generation of $^{\bullet}OH$ typically occurs by iron- or copper-mediated hydrogen peroxide (H_2O_2) reduction (Reactions 1 and 2, respectively). In fact, metal-mediated $^{\bullet}OH$ generation is the major cause of DNA damage and cell death in *E. coli* and human cells.[17-19]

$$Fe^{II} + H_2O_2 \rightarrow Fe^{III} + {}^-OH + {}^{\bullet}OH \qquad (1)$$

$$Cu^{I} + H_2O_2 \rightarrow Cu^{II} + {}^-OH + {}^{\bullet}OH \qquad (2)$$

Hydroxyl radical generation is catalytic in the presence of cellular reductants such as ascorbic acid or nicotinamide adenine dinucleotide (NADH) that can reduce the oxidized metal ions back to their $^{\bullet}OH$-generating reduced states.[20,21] Cells typically control labile

(non-protein-bound) metal ions, but under conditions of oxidative stress, mis-regulation of iron and copper can lead to a significant increase in labile metal ion concentrations and $^{\bullet}$OH generation.[22-24] Labile (non-protein-bound) iron levels are typically 1-30 μM in human cells, with concentrations up to 210 μM in the mitochondria.[25-27] Similarly, reports show labile copper pools in mouse mitochondria and human brain tissue from 1 to ~1300 μM.[28,29] Sulfur and selenium antioxidants may promote cellular survival by scavenging radicals;[30-32] however, due to hydroxyl radical's short half-life (~1 ns),[33,34] scavenging of this radical is unlikely. In contrast to focusing exclusively on the damaging radical species (a process that can be compared to trying to catch bullets after they are fired from a gun), we have instead focused on exploring the ability of sulfur and selenium antioxidants to bind iron and copper and prevent radical formation or release (a process analogous to removing the gun). Our studies over the past decade have proven that metal coordination is the primary mechanism by which sulfur and selenium antioxidants prevent DNA damage.[18,35-37]

Numerous studies have demonstrated the beneficial health effects of sulfur and selenium compounds:[38,39] garlic extracts protect against the toxic effects of arsenic,[40] selenomethionine (Figure 1.1) has been used to treat sepsis,[41] and selenium supplementation can reduce oxidative damage in pulmonary tuberculosis patients.[42] In the past ten years, interest in selenium-containing antioxidants has significantly increased due to studies focused on the disease prevention and chemopreventative activity of selenium supplementation.[43-46] However, the Nutritional Prevention of Cancer (NPC) clinical trial and the Selenium and Vitamin E Cancer Prevention Trial (SELECT),

reported conflicting cancer-preventative abilities for selenium supplementation. In both double-blind trials, patients were given selenium supplements (200 μg/day). The 8-year NPC trial reported a 37 % decrease in cancer incidence, a total that included a 63 % reduction in prostate cancer.[47] In contrast, the SELECT trial determined that selenium supplementation did not consistently prevent prostate cancer, and this trial was canceled in 2008, the fifth year of the study.[18,48-50]

In 2009, El-Bayoumy discussed the difference in the selenium supplement between these trials as the possible source of discrepancy in these trial results.[51] Selenium-enriched yeast, the selenium supplement in the NPC trial, is comprised of 54-62 % selenomethionine, < 1 % selenite, and 36-46 % unidentified selenium species,[50] whereas the SELECT study used only selenomethionine. In a separate report, El-Bayoumy and Sinha reported that methyl-selenocysteine (Figure 1.1), another selenium species in selenium-enriched yeast is a more effective anticancer agent than selenomethionine,[52] and Menter *et al.* observed that selenomethionine inhibits growth of malignant prostate cells only at extremely high levels.[53] As these conflicting results demonstrate, a comprehensive understanding of sulfur and selenium antioxidant activity at the mechanistic level is critical for the success of future animal and clinical trials for disease prevention.

In addition to their ROS scavenging abilities, small-molecule selenium compounds are also extensively investigated as mimics of the selenoenzyme glutathione peroxidase.[54] However, many of these *in vitro* studies are not reliably reproducible, are typically conducted using non-physiological conditions, such as in organic solvents or

acidic solution, and most have not led to significant promising results in cellular and animal trials.[18,55-59] In a recent notable exception, selenium-containing glutathione peroxidase mimics improved glucose-stimulated insulin secretion in GPX1 knockout mice.[60]

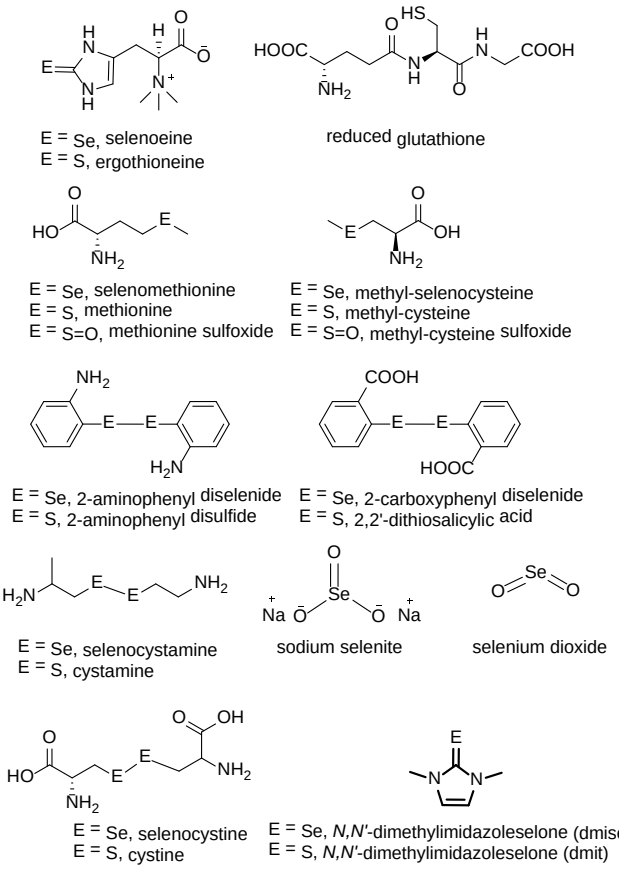

Figure 1.1. Selected sulfur and selenium compounds studied for their antioxidant activities.

Interest in thione (C=S) and selone (C=Se) antioxidants can be attributed to naturally occurring ergothioneine and selenoneine (Figure 1.1). Ergothioneine has been studied for its anti-inflammation effects, oxidative DNA damage prevention, and the scavenging of peroxynitrite and hydrogen peroxide.[61-66] Ergothioneine concentration in human tissue is typically 100-2000 μM.[67] A recent study reports ergothioneine levels in

human blood serum from 0.4-308 μM,[68] and intracellular ergothioneine levels are reported to be 2 to 9 times higher than plasma levels in the same patient.[69] Akanmu *et al.* reported that ergothioneine addition (1000 μM) resulted in 100 % inhibition of Cu^{I}-mediated deoxyribose degradation.[61] Similarly, Zhu *et. al* reported that ergothioneine inhibits Cu^{I}-mediated DNA damage between 100-1000 μM, with complete damage prevention by 1000 μM.[66]

Selenoneine was recently discovered in the blood of bluefin tuna (0.46 μM),[70] and effectively scavenges 1-diphenyl-2-picrylhydrazyl (DPPH) radical.[70,71] A recent study measured selenoneine blood concentrations up to 9 nM in a Japanese population with high bluefin tuna consumption.[72]

Traditionally, ROS scavenging is investigated as the primary mechanism for sulfur and selenium antioxidant activity; however, due to our work and others',[3,58,73,74] metal coordination has recently started to gain consideration as an independent antioxidant mechanism. This review discusses our investigations into the mechanisms by which various sulfur and selenium compounds prevent metal-mediated DNA damage and how copper and iron coordination contributes to this activity. Figure 1.2 compares the traditional ROS scavenging antioxidant mechanisms (top) with two potential metal-binding mechanisms for DNA damage prevention (bottom). Metal binding to sulfur and selenium antioxidants could either prevent copper and iron redox cycling and hydroxyl radical generation (redox control mechanism) or allow targeted scavenging of hydrogen peroxide or hydroxyl radical by the metal-bound antioxidant, preventing oxidative damage (targeted scavenging mechanism). Because no stability constants have been

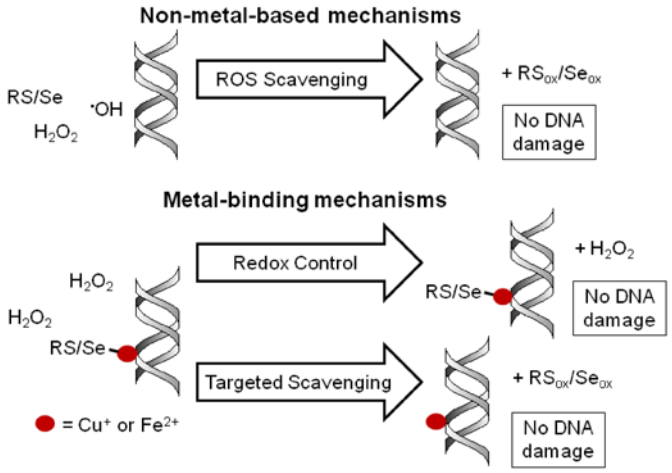

Figure 1.2. Proposed mechanisms for sulfur and selenium DNA damage prevention. A) Currently accepted reactive oxygen species (ROS) scavenging mechanisms involve no metal ions. B) Metal-binding mechanisms include sulfur or selenium binding to shift redox potentials of the metal ion outside of the biological window for hydroxyl radical formation (redox control), and/or metal-bound sulfur or selenium antioxidants preferentially reacting with hydrogen peroxide to prevent metal oxidation and hydroxyl radical formation (targeted scavenging).

measured for sulfur or selenium antioxidant binding to Cu^{I} or Fe^{II}, it is unknown whether the metal ion can remain on the DNA after binding and oxidation. Oxidation studies with *N,N'*-dimethylimidazole thione (dmit) and selone (dmise) indicate that these oxidized sulfur and selenium species do not remain bound to the metal (see section 1.6), but similar studies have not been conducted with other sulfur and selenium species to determine metal binding after oxidation. From this improved mechanistic understanding we have determined the chemical properties necessary for DNA damage prevention and developed predictive models for sulfur and selenium antioxidant activity based on metal binding.

The work presented in this chapter was conducted in collaboration with Professor Craig Bayse (Old Dominion University), who provided the DFT calculation results, and Professor Ria Ramoutar (Georgia Southern University), who conducted experiments with

the oxosulfur and oxoselenium compounds and obtained mass spectrometry data with the sulfur-containing amino acids.

1.2. Sulfur and Selenium Compounds Prevent Metal-Mediated DNA Damage

1.2.1 Quantifying DNA damage prevention by selenium antioxidants. The sulfur and selenium compounds selected for investigation were chosen due to their presence in biological systems (such as methionine, selenocystine, or glutathione), or because of their similarity to biologically relevant compounds (*N*,*N*'-dimethylimidazole thione (dmit) is an analog of ergothioneine). Guttormsen *et al.*[75] reported human plasma levels of cysteine and methionine around 256 μM and 23 μM, respectively, and cellular levels of these two amino acids are reported in the 100-200 μM range in skeletal muscle.[76] The intracellular concentration of glutathione is much higher, between 10,000-15,000 μM,[11,77] due to its critical role as a cellular antioxidant. Methimazole, a thione structurally similar to dmit but without one methyl group, is the primary drug used to treat hyperthyroidism in the United States. Blood concentrations of methimizole are reported to be in the range of 4-13 μM in hyperthyroid patients.[78,79]

Biological selenium concentrations are significantly lower than for analogous sulfur compounds. In the United States, human plasma Se concentrations average 1.5-1.6 μM, with more than 90% of this selenium present in selenoproteins or as non-specifically protein-incorporated selenomethionine, leaving less than 0.16 μM of non-protein-bound selenium.[80] Long-term human supplementation with selenomethionine or selenium-enriched yeast (up to 600 μg) raises plasma concentrations by 26% after 16 weeks, with

most of the selenium present as protein-incorporated selenomethionine.[80] Although selenium toxicity levels are currently debated, Reid *et al.* reported no toxic symptoms in prostate cancer patients supplemented with high doses of selenium-enriched yeast (1600 µg for 12 months), resulting in a selenium plasma concentration of ~10 µM.[81] Although many selenium supplementation studies use oral supplements of selenium-enriched yeast, selenomethionine, or inorganic selenite and selenate, treatment of acute oxidative stress using intravenously administered high-dose selenium also may reduce mortality in critically ill patients.[82] Human studies with selone compounds as the selenium source have not been conducted.

Most studies of sulfur and selenium antioxidant behavior focus on ROS scavenging, with little, if any, mention of metal coordination.[83] Many of these studies are not performed under expected biological conditions, including acidic or basic pH, the use of organic solvents such as dimethyl sulfoxide, or with oversimplified assumptions about the complex biological reactions that produce damaging ROS.[30,57,58,84] In contrast, our studies examine sulfur and selenium antioxidant behavior using copper- or iron-generated $^{\bullet}$OH radical to damage DNA, the primary mechanism for DNA oxidation and cell death under oxidative stress conditions.[85-89]

Studies with the selenium compounds in Figure 1.1 were performed to determine their ability to prevent Cu^{I}-mediated oxidative damage (single-strand nicking) to plasmid DNA (in MOPS buffer at pH 7 with 130 mM NaCl); all Fenton and Fenton-like reactions were quenched with ethylenediaminetetraacetic acid (EDTA) after 30 min. In the example DNA damage gel shown in Figure 1.3A, it is clear that H_2O_2 alone (50 µM, lane

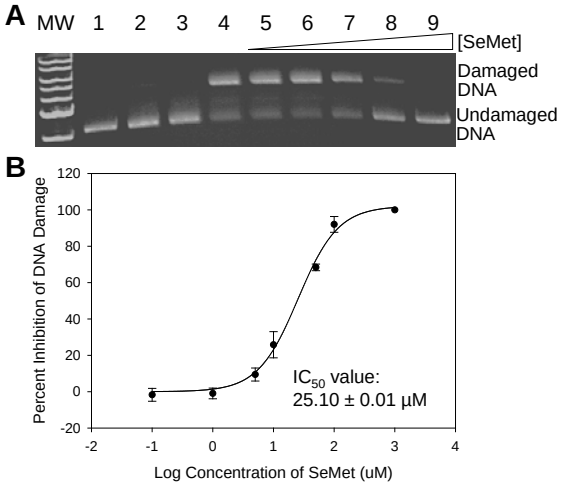

Figure 1.3. A) Gel electrophoresis image of Cu^{I}-mediated oxidative DNA damage prevention by selenomethionine (SeMet). Lane MW: 1 kb molecular weight marker; lane 1: plasmid DNA (p); lane 2: p + H_2O_2 (50 µM); lane 3: p + SeMet + H_2O_2; lane 4: p + ascorbate (7.5 µM) + $CuSO_4$ (6 µM) + H_2O_2 (50 µM); lanes 5-9: p + $CuSO_4$ + ascorbate + increasing concentrations of SeMet: 0.1, 1, 10, 100, and 1000 µM, respectively. B) The best-fit dose-response curve for prevention of Cu^{I}-mediated oxidative DNA damage by selenomethionine.

2) or with selenomethionine (lane 3) does not damage DNA. However, combining Cu^{I} (6 µM/7.5 µM ascorbic acid) and H_2O_2 generates $^{\bullet}OH$ and results in 98 % DNA damage (lane 4). Addition of selenomethionine in increasing concentrations decreases DNA damage (lanes 5-9), with 100 % DNA damage inhibition at 1000 µM. Quantification of band intensities, plotting the log of selenomethionine concentration versus percent DNA damage inhibition, and fitting the resultant sigmoidal dose-response curve allows calculation of an IC_{50} value, the antioxidant concentration necessary to inhibit 50 % of DNA damage (Figure 1.3B).[36] Since 6 µM Cu^{I} was used in these studies, coordination is expected to occur between 6-24 µM (1:1 to 1:4 metal-to-ligand molar ratio), and selenomethionine exhibits an IC_{50} value slightly higher than a 1:4 molar ratio (25.10 ± 0.01 µM). Of the nine selenium compounds examined, seven prevented copper-mediated damage (IC_{50} values in Table 1.1). Selenocystamine *promoted* DNA damage from 1-500

Table 1.1. DNA damage inhibition by sulfur and selenium antioxidants with H_2O_2 (50 μM) and Cu^I (6 μM) or Fe^{II} (2 μM) compared to mass spectrometry results showing coordination ratios of the compounds (1 equiv = 75 μM in 1:3 methanol:water solution).

Selenium Compound	**Cu^I IC_{50} (μM)[a]**	**Cu^I:Se/S Ligand**	**Fe^{II} IC_{50} (μM)[a]**	**Fe^{II}:Se/S Ligand**	**Ref.**
Selenocystine	3.34 ± 0.08	1:1, 1:2	No activity	1:1, 1:2, 1:3	18, 36
Selenomethionine	25.10 ± 0.01	1:1, 1:2, 1:3	No activity	1:2, 1:3	18, 36
Methyl-selenocysteine	8.64 ± 0.02	1:1, 1:2, 1:3	378.4 ± 0.1	1:1, 1:2, 1:3	18, 36
Selenocystamine	59 ± 3% (1000 μM)	None	121.4 ± 0.3	1:3	18, 36
2-Aminophenyl diselenide	No activity	None	No activity	1:1	18
2-Carboxyphenyl diselenide	No activity	1:1	No activity	1:1	18
Sodium selenite	1479 ± 2	None	84.5 ± 0.2	None	90
Selenium dioxide	3802 ± 5	None	859 ± 2	1:1, 1:2	90
N,*N*'-Dimethylimidazole selone (dmise)[b]	~240	1:1	3.2 ± 0.9	1:3, 1:5[d]	97
Sulfur Compound					
Cystine	3.34 ± 0.07	1:1	No activity	1:1	37
Methionine	11.02 ± 0.02	1:1	No activity	None	37
Methyl-cysteine	10.02 ± 0.02	1:1	No activity	1:1, 1:2	37
Cystamine	No activity	None	No activity	None	37
2-Aminophenyl disulfide	No activity	None	No activity	None	37
2,2'-Dithiosalicylic acid	No activity	None	No activity	1:1	37
Methionine sulfoxide	18 ± 1	1:1	No activity	1:1	35
Methylcysteine sulfoxide	8.1 ± 0.5	1:1, 1:2	DNA damage	1:1, 1:2	35
Reduced glutathione	12.98 ± 0.01	1:2	23 ± 8% (10,000 μM)	1:1	37
Oxidized glutathione	6.82 ± 0.03	1:1, 1:2	10,372 ± 2	1:1	37
N,*N*'-Dimethylimidazole thione (dmit)[b]	1550 ± 3	1:2[c]	89.1 ± 0.2	1:3, 1:4[c]	97

[a]IC_{50} value is the concentration required to inhibit 50% of DNA damage; [b]MALDI mass spectrometry samples prepared in water with 1 equiv = 300 μM. [c]Coordination observed in both MADLI and ESI. [d]Coordination with H_2O: $[Fe^{II}(dmise)_3(H_2O)]^{2+}$ and $[Fe^{II}(dmise)_5(H_2O)]^{2+}$.

μM, but even this compound was an antioxidant at 1000 μM, preventing 59 % DNA damage.[18,36]

Similar DNA damage studies were conducted with these selenium compounds to determine their ability to prevent iron-mediated oxidative DNA damage (in MES buffer at pH 6 to prevent iron precipitation). Of the nine tested, selenocystamine and methyl-selenocysteine were the only two amino acid compounds to inhibit Fe^{II}-mediated DNA damage (Table 1.1).[18] This striking difference between prevention of copper- and iron-mediated DNA damage emphasizes the importance of metal interactions for selenium

antioxidant activity.

Sodium selenite (SeO_3^-) and sodium selenate (SeO_4^{2-}) are inorganic selenium compounds used as selenium supplements in multivitamins, animal feed, and infant formula, and have been extensively examined for their antioxidant and anticancer properties.[74,90,91] In a small clinical study, Mantovani *et al*. observed that selenium dioxide treatment inhibits progression of stage IV cancer tumors in the head, neck, lung, prostate, and biliary tract.[92] Davis *et al*. reported that selenite or selenate supplementation significantly reduces formation of the 3,2'-dimethyl-4-aminobiphenyl-DNA adduct (a mimic for various mutagens in cooked fish and meat) in rats.[93] Additionally, Ip and Hayes[94] found that selenite is more active than selenomethionine in reducing dimethylbenz[a]anthracene-induced tumors in rats. In cellular studies, Spyrou *et al.*[95] determined that both selenate and selenite inhibit human lymphocyte growth, and that selenite-induced effects are reversible if selenate is removed.

In our studies, sodium selenite treatment prevented 50 % of the copper-mediated DNA damage inhibition at 1479 μM, and selenium dioxide had a much higher IC_{50} value of 3802 μM.[96] Sodium selenite was significantly better at inhibiting Fe^{II}-mediated DNA damage (IC_{50} = 84.5 μM), whereas selenium dioxide showed prooxidant activity at lower concentrations (0.5-50 μM), but had an overall IC_{50} value of 859 μM.[96] As was observed for the organoselenium compounds, selenium speciation, rather than just the presence of the element itself is critical to DNA damage prevention.

In contrast to other selenium antioxidants tested, the selone compound dmise does not show a simple sigmoidal dose-response curve. Instead, initial dmise DNA damage

prevention increases between 1-10 μM before leveling off around 45 % and then increasing to 100 % between 300 and 3000 μM.[97] Thus, dmise effectively prevents Cu^{I}-mediated oxidative DNA damage, with an IC_{50} value around 240 μM (Table 1.1) but an IC_{40} of approximately 7.5 μM. Since Cu^{I} coordination should occur within the range of 6-24 μM, this initial increase in activity is likely due to copper binding. The second increase in activity is well above the expected dmise-Cu^{I} coordination range, and is likely due to ROS scavenging.

Surprisingly, dmise also prevented significantly more Fe^{II}-mediated DNA damage (IC_{50} = 3.2 μM; Table 1.1) than Cu^{I}-mediated DNA damage,[97] the first selenium compound to show such activity.[18,35-37,96] Notably, this activity with Fe^{II} occurs within the possible metal coordination window of 1:1 to 1:6 molar ratio (2 to 12 μM), since 2 μM Fe^{II} was used in these studies, a value at the low end of labile iron in human cells.[25-27]

Although human selenium concentrations are in the low micromolar range even upon high-dose supplementation (0.1-10 μM), selenocystine, methyl-selenocystine, and dmise prevent significant copper-mediated DNA damage within these concentrations. Notably, selenomethioneine, a major component of selenium-enriched yeast and an often-used selenium supplement, shows very little activity within this range. Of all the tested selenium compounds, only dmise prevents significant iron-mediated DNA damage at biological selenium concentrations. These results not only demonstrate the multifunctional antioxidant potential of selone compounds, but also illustrate the dramatic effects different selenium-containing functional groups have on antioxidant activity.

1.2.3 Quantifying DNA damage prevention by sulfur antioxidants. To compare sulfur and selenium antioxidant prevention of DNA damage, we also conducted Cu^{I} DNA damage assays with sulfur analogs of the selenium antioxidants in Figure 1.1. Cystine, methionine, and methyl-cysteine exhibited activity similar to their selenium-containing counterparts, with IC_{50} values from 3.3 to 11 μM (Table 1.1). In contrast, cystamine exhibited no ability to inhibit Cu^{I}-mediated DNA damage. Both of the oxo-sulfur compounds, methionine sulfoxide and methyl-cysteine sulfoxide prevented Cu^{I}-mediated DNA damage with similar IC_{50} values compared to their non-oxidized amino acid analogs.[35,37] Additionally, the endogenous cellular antioxidant glutathione, in both oxidized and reduced forms, effectively inhibited Cu^{I}-mediated oxidative DNA damage well within its biological concentration range (1-15 mM).[11,37,98] The thione-containing dmit (Figure 1.1) also inhibited Cu^{I}-mediated oxidative DNA damage, although at substantially higher concentrations than its selone analog, dmise, and outside of the concentration window for potential metal coordination.[97]

As with the selenium compounds, Fe^{II}-mediated DNA damage prevention by sulfur antioxidants (Figure 1.1), revealed completely different results from the Cu^{I} studies. Seven of the eleven sulfur compounds tested inhibited no Fe^{II}-mediated DNA damage. In fact, methyl-cysteine sulfoxide *promoted* a small amount (17 ± 3 %) of Fe^{II}-mediated DNA damage at high concentrations (1000 μM).[35] Both oxidized and reduced glutathione prevented approximately 50 % and 23 % Fe^{II}-mediated DNA damage, respectively, at 10,000 μM,[37] the only sulfur-amino-acid compounds to inhibit both Cu^{I}- and Fe^{II}-mediated oxidative DNA damage. Dmit showed substantially stronger inhibition

of Fe^{II}-mediated DNA damage than Cu^{I}-mediated DNA damage, with an IC_{50} value of 89.1 μM.[97] Except for dmit, DNA damage prevention effects for these sulfur-containing antioxidants are well within the biological concentrations measured for these or similar compounds. The diverse abilities of these sulfur compounds to inhibit DNA damage by Cu^{I} and Fe^{II} illustrate that the metal ion generating $^{\bullet}OH$, as well as the chemical environment of the sulfur, can radically alter antioxidant behavior.

The antioxidant activity of sulfur and selenium amino acids and related compounds are primarily examined using ROS scavenging investigations.[99,100] Kim *et al.*[57] determined that *S*-allyl-L-cysteine sulfoxide and *S*-allyl-L-cysteine were the only two compounds capable of scavenging $^{\bullet}OH$ *in vitro* and preventing neuronal cells from ischemic damage. Similarly, Yildiz and Demiryurek[30] used chemiluminescence studies to determine that methionine scavenges $^{\bullet}OH$. Ergothioneine (Figure 1.1) scavenges harmful ROS such as $ONOO^{-}$ and $^{\bullet}OH$, and may act as a possible trigger for immune system responses.[63,65,66] Ergothioneine also inhibits Cu^{I}-mediated deoxyribose degradation at high concentrations (1 mM).[61]

Our studies established that, with the exception of selones and thiones, sulfur- and selenium-containing amino acid compounds showed strong inhibition of Cu^{I}-mediated DNA damage, yet were generally ineffective at preventing Fe^{II}-mediated DNA damage. Clearly, the presence of a sulfur or selenium atom alone is not sufficient for antioxidant activity. If ROS scavenging were the major antioxidant mechanism, then similar DNA damage inhibition would be expected for both Fe^{II} and Cu^{I} studies. Because this was decidedly not the case, and because the tested sulfur and selenium antioxidants exhibited

activity close to expected coordination ratios for copper and iron, our DNA damage prevention results strongly supported metal coordination as a significant antioxidant mechanism.

1.3. Establishing metal coordination as a primary mechanism for sulfur and selenium antioxidant activity

Current research into metal binding for the sulfur and selenium complexes in Figure 1.1 is limited, with the majority of publications focused on structural determination rather than potential biological activity. McAuliffe *et al.*[101] and Sze *et al.*[102] investigated metal-methionine complexes with Cr^{III}, Mn^{II}, Fe^{III}, Co^{II}, Ni^{II}, Cu^{II}, Zn^{II}, Ag^{I}, Cd^{II}, Hg^{II}, and Rh^{III}. Similarly, complexes of cysteinate and methyl-cysteinate have been synthesized and characterized for Cd^{II}, Pb^{II}, Hg^{II}, and Zn^{II},[102,103] and methyl-cysteine complexes with Mn^{II}, Co^{II}, Ni^{II}, Cu^{II}, Zn^{II}, Cd^{II}, Hg^{II}, Pd^{II}, and Pt^{II} have also been reported.[103,104]

Due to the incorporation of selenium into metalloenzymes, such as selenocysteine-molybdenum coordination in formate dehydrogenase H and selenocysteine-nickel coordination in [NiFeSe] hydrogenase,[105,106] seleno-amino acid-metal complexes also have been examined.[58] Zainal *et al.*[107] characterized $(SeMet)_2Cu$ and $(SeMet)_2Zn$ complexes using IR and Raman spectroscopic studies and determined that selenomethionine binds to Cu^{II} and Zn^{II} through the nitrogen and oxygen atoms of the amine and carboxylic acid groups, and that the selenium does not participate in metal coordination.

To prove our observed DNA damage prevention was a result of metal coordination, DNA damage assays (similar conditions as in Section 1.2) were performed using 50 μM $[Cu(bipy)_2]^+$ (bipy = 2,2'-bipyridine) or 400 μM $[Fe(EDTA)]^{2-}$ (EDTA = ethylenediaminetetraacetic acid) in place of unchelated Cu^I or Fe^{II}. Both $[Cu(bipy)_2]^+$ and $[Fe(EDTA)]^{2-}$ react with H_2O_2 to yield $^{\bullet}OH$, but fully chelate Cu^I and Fe^{II} to inhibit subsequent sulfur or selenium antioxidant binding. UV-vis spectroscopy and mass spectrometry studies were also conducted to determine whether metal complexes of the sulfur and selenium antioxidants could form in aqueous solutions at pH 6-7.

With $[Cu(bipy)_2]^+$ as the Cu^I source, no DNA damage prevention was observed for the sulfur and selenium-containing amino acids and related compounds in Figure 1.1,[18,37] proving that copper-antioxidant interactions are critical to DNA damage prevention. Methionine sulfoxide and methylcysteine sulfoxide prevented DNA damage only at concentrations 20 times higher than required for inhibition of Cu^I-mediated DNA damage: 43 ± 3 % and 88 ± 4 % inhibition at 1000 μM, respectively.[35] Similarly, dmise and dmit prevent DNA damage caused by $[Cu(bipy)_2]^+$ and H_2O_2 at much higher concentrations than Cu^I alone.[97]

Gel electrophoresis studies were also conducted with $[Fe(EDTA)]^{2-}$ in place of Fe^{II} to determine whether iron binding is required for the observed antioxidant behavior. Since the binding affinity of Fe^{II}-EDTA is 2×10^{14},[108] it is unlikely that the selenium and sulfur compounds investigated compete with EDTA for Fe^{II} binding. Methyl-selenocysteine at 1000 μM inhibited 27 % of DNA damage caused by $[Fe(EDTA)]^{2-}$ and H_2O_2; the same concentration of methyl-selenocysteine inhibited 60 % of Fe^{II}-mediated

DNA damage. Selenocystamine studies showed similar results, preventing 60 % of DNA damage with $[Fe(EDTA)]^{2-}$ at 1000 μM, significantly less than the 100 % inhibition observed with Fe^{II} at the same concentration.[18] Similarly, methylcysteine sulfoxide prevented no DNA damage in the presence of chelated Fe^{II}.[35] This limited activity observed only at very high antioxidant concentrations with chelated copper or iron as the hydroxyl radical generator is likely due to ROS scavenging, and suggests that this is only a secondary antioxidant mechanism for these compounds.

Oxidized and reduced glutathione (10,000 μM) prevent 68 % and 76 % DNA damage caused by $[Fe(EDTA)]^{2-}$, respectively, 18 % and 43 % more, respectively, than inhibition of non-chelated Fe^{II}-mediated DNA damage at the same concentrations.[37] This unique activity for glutathione indicates that it may prevent DNA damage by both ROS scavenging and iron coordination, a useful trait for the primary sulfur-containing cellular antioxidant.[109,110]

To establish copper and iron coordination and stoichiometry with sulfur and selenium antioxidants, UV-vis studies were conducted on all compounds, regardless of their ability to prevent metal-mediated DNA damage. UV-vis studies (in 10 mM MOPS buffer at pH 7) conducted with the selenium compounds that prevented Cu^{I}-mediated DNA damage revealed absorption bands around 226 nm,[18] the range expected for copper-selenium charge transfer bands,[111] whereas the selenium compounds that did not prevent DNA damage had no such bands. Although Fe^{II} coordination (in 10 mM MES buffer at pH 6) results in absorption bands of 316-340 nm for iron-thiolate clusters and 311-389 nm for iron-selenolate clusters,[112-115] UV-vis studies of all the sulfur and selenium

compounds with Fe^{II} revealed no absorption bands indicative of metal coordination, indicating that selenium- or sulfur-iron binding is weak, or that iron coordination may not occur through the selenium or sulfur atoms.[18,37]

Electrospray ionization mass spectrometry (ESI-MS) studies were also conducted with the antioxidants in Figure 1.1 with Fe^{II} or Cu^{I} to directly investigate their metal coordination. A majority of the compounds coordinated Cu^{I} in a 1:1 or 1:2 molar ratio of metal to ligand; only 2-aminophenyl diselenide, selenocystamine, sodium selenite, selenium dioxide, cystamine, 2-aminophenyl disulfide, and 2,2'-dithiosalicylic acid showed no copper coordination (Table 1.1).[18] Since many of the compounds investigated could coordinate Cu^{I} through the oxygen and/or nitrogen of the amino acid in addition to potential sulfur/selenium coordination, 1:1 or 1:2 metal-to-ligand molar ratios were expected.[96,116,117]

Similar mass spectrometry studies with Fe^{II} revealed that all of the tested organoselenium compounds formed Fe^{II} complexes with 1:1 and/or 1:2 metal-to-ligand ratios (Table 1.1), regardless of their ability to prevent iron-mediated DNA damage. Most of the organosulfur compounds also formed Fe^{II} complexes with the same ratios, with the exceptions of methionine, cystamine, and 2-aminophenyl disulfide. Fe^{II} has up to six possible binding sites, so expected metal-to-ligand ratios are 1:1 to 1:3 for potentially bidentate amino acids.[118,119] Although most of the compounds coordinated Cu^{I} or Fe^{II}, not all of them prevented metal-mediated DNA damage. Thus, metal coordination is necessary but not sufficient for DNA damage inhibition.[18] To result in DNA damage prevention, binding of the sulfur or selenium compound would have to significantly alter

the metal redox potential to prevent Cu^{I} or Fe^{II} oxidation by H_2O_2 (Figure 1.2, redox control mechanism). Alternatively, direct metal-sulfur or –selenium coordination may be required to efficiently scavenge H_2O_2 before DNA damage occurs (Figure 1.2, targeted oxidation mechanism).

1.4. Investigating the electrochemistry of sulfur and selenium antioxidants

Since generation of $^{\bullet}OH$ from H_2O_2 is a one-electron redox reaction, we focused on electrochemical studies to determine the oxidation ability of the tested sulfur and selenium compounds since this property should be directly related to $^{\bullet}OH$ scavenging ability. Researchers commonly study selenium compounds using a gold or mercury electrode, both of which readily coordinate sulfur and selenium.[12,120,121] Thus, redox potentials observed using metallic electrodes are most likely of a metal-selenium complex. To better mimic biological conditions, we used a glassy carbon electrode and samples in in 10 mM MOPS buffer at pH 7 for our cyclic and differential pulse voltammetry experiments to determine correlations between antioxidant ability and redox activity.[18] All of the selenium compounds in Table 1.1 were readily oxidized (Table 1.3), except the oxo-selenium compounds and methyl-selenocysteine, suggesting that most could be effective ROS scavengers. Only three compounds were found to undergo both oxidation and reduction: selenocystamine, 2-aminophenyl diselenide, and 2-carboxyphenyl diselenide.[18] Two of the most active selenium antioxidants for copper-mediated DNA damage prevention, selenomethionine and selenocystine, showed irreversible oxidation, but the electrochemically inactive methyl-selenocysteine prevented

Table 1.2. Electrochemical results vs. normal hydrogen electrode for selected Cu^{I} complexes (1 mM) in acetonitrile with tetra-*n*-butylammonium hexafluorophosphate (100 mM) as the supporting electrolyte.

	$Cu^{II/I}$				
Compound	Ep_a **(V)**	Ep_c **(V)**	ΔE **(V)**	$E_{1/2}$ **(V)**	**Ref.**
$[Tpm^{iPr}Cu(NCCH_3)][BF_4]$	1.254	-0.340	1.594	0.457	122
$[Tpm^{Me}Cu(NCCH_3)][BF_4]$	1.158	-0.620	1.778	0.269	122
$[TpmCu(NCCH_3)][BF_4]$	0.203	-0.641	0.844	-0.219	122
Dmise	0.039	-0.773	0.812	-0.367	122
$[Tpm^{iPr}Cu(dmise)][BF_4]$	-0.049	-0.729	0.680	-0.390	122
$[Tpm^{Me}Cu(dmise)][BF_4]$	-0.088	-0.644	0.556	-0.366	122
$[TpmCu(dmise)][BF_4]$	-0.030	-0.536	0.506	-0.283	122
$[Cu(dmise)_4][OTf]$	-0.191	-0.555	0.364	-0.373	123
Dmit	0.424	-0.761	1.158	-0.167	122
$[Tpm^{iPr}Cu(dmit)][BF_4]$	0.187	-0.507	0.694	-0.160	122
$[Tpm^{Me}Cu(dmit)][BF_4]$	0.307	-0.518	0.825	-0.105	122
$[TpmCu(dmit)][BF_4]$	0.392	-0.252	0.644	0.070	122
$[Cu(dmit)_3][OTf]$	0.000	-0.434	0.434	-0.217	124

both copper- and iron-mediated DNA damage. Similarly, for the sulfur antioxidants, only methionine and cysteine exhibited oxidation waves (Table 1.3). Because the oxidation potentials of these sulfur and selenium antioxidants do not correlate with their antioxidant abilities, and because these compounds prevented little or no DNA damage with chelated $[Cu(bipy)_2]^+$ or $[Fe(EDTA]^{2-}$,[18,37] we established that ROS scavenging (Figure 1.2, top) is not a major mechanism for their activity.

To directly compare the electrochemistry of a Cu^{I}-coordinated selones and thiones, we synthesized dmit and dmise copper complexes with tris(pyrazolyl)methane (Tpm^{R}) ligands (Table 1.2). These selone and thione ligands are similar in structure to the natural antioxidants ergothioneine,[62,63,122] selenoneine,[70] respectively (Figure 1.1), as well methimazole, a drug used to treat hyperthyroidism.[123] The Tpm^{R} ligands were selected to mimic the guanine N7 binding typical for Cu^{I}- and Fe^{II}-DNA interactions,[124,125] and coordination of these tridentate ligands to Cu^{I} permitted only one selone or thione ligand to bind, mimicking expected cellular ratios for copper and selenium antioxidants.

Electrochemical studies of uncoordinated dmise and dmit in acetonitrile determined that the selone undergoes reduction more readily than the thione ($E_{1/2}$ values of -167 and -367 mV, respectively).[126] When coordinated to Cu^{I} in the $[Tpm^{R}Cu(dmise)]^{+}$ complexes, binding of a single dmise ligand shifted the $E_{1/2}$ values for $Cu^{II/I}$ reduction by an average of -234 mV compared to analogous dmit complexes (Table 1.2), indicating increased Cu^{II} stabilization.[126,127] Increased stabilization of Cu^{II} upon dmise complexation is also observed for the homoleptic $[Cu(dmise)_4]^{+}$ and $Cu(dmit)_3]^{+}$ complexes (Table 1.2). If metal complex reduction potentials are more negative than the reduction potential of NADH (-324 mV), cellular Cu^{II} or Fe^{III} reduction to the hydroxyl-radical-generating Cu^{I} and Fe^{II} is inhibited.[128] Most of the Cu-dmise complexes in Table 1.2 have $Cu^{II/I}$ reduction potentials more negative than -324 mV, but none of the Cu-dmit complexes have such low $Cu^{II/I}$ potentials.[126,127] Thus, if similar copper-selenium antioxidant complexes form in cells, they may prevent copper redox cycling and copper-mediated DNA damage significantly more efficiently than analogous sulfur antioxidant complexes (Figure 1.2, redox control mechanism). These results are consistent with the trend of increased copper-mediated DNA damage prevention observed for selenium antioxidants compared to their sulfur analogs (Table 1.1) and highlight the importance of metal-binding antioxidant mechanisms.

Although our electrochemical studies demonstrated that dmit and dmise stabilize Cu^{II} over Cu^{I}, subsequent UV-vis studies indicated that dmise reduces Cu^{II} to Cu^{I} at a rate three times faster than dmit.[129] This apparent contradiction of the electrochemical (thermodynamic) and UV-vis (kinetic) results underscores the complex redox behavior of

these ligands and their copper complexes and suggests that the biological antioxidant abilities of these two antioxidants may vary greatly, since copper redox cycling is critical to oxidative DNA damage.[130,131]

1.5. Determining Cu^{I} coordination modes and predictive models for sulfur and selenium antioxidants

To obtain structural details of copper-seleno-amino acid coordination, we characterized the first such Cu^{I} complexes with selenomethionine and methyl-selenocysteine. Upon adding 1 equiv $[Cu(NCCH_3)_4]^+$ to an aqueous solution of methyl-selenocysteine at pH 7, the ^1H NMR resonances shifted significantly, suggesting that Cu^{I} bound through the selenium as well as a carboxylic acid oxygen or amine nitrogen.[132] Similar results were observed for selenomethionine-Cu^{I} interactions,[132] and are consistent with methyl-cysteine and methionine coordination to Ag^{I}.[133] Selenium-Cu^{II} interactions have also been reported for selenocysteine-containing copper proteins.[134,135] X-ray absorption studies of these Cu^{I}-seleno-amino acid complexes confirmed trigonal planar Cu^{I} bound to methyl-selenocysteine and selenomethionine through the selenium atom in addition to two oxygen or nitrogen atoms.[132]

Density functional theory (DFT) models of these trigonal planar $[Cu(L)(OH_2)]^+$ complexes (L = methyl-selenocysteine and selenomethionine), as well as their sulfur analogs (unpublished data), indicated that coordination through the chalcogen and the amine is slightly more favorable than through the carboxylate, and that trigonal planar coordination of the complex was completed with water.[132] These studies revealed both

the ability of sulfur and selenium compounds to readily form Cu^{I} complexes and strengthened the link between antioxidant-metal coordination and DNA damage prevention.

Transition metal complexes with heterocyclic thione and thione-derived scorpionate ligands, are well known.[136-139] Williams *et al.* have explored the metal complexes of *N*,*N'*-dimethylimidazole thione (dmit) and selone (dmise) with Cd^{II},[140] Zn^{II},[141,142] and Co^{II}.[143] Although many researchers have investigated copper coordination by various thione-containing ligands,[144-148] only a few have reported copper coordination by selone ligands.[139,149-151] To compare the reactivity of analogous Cu^{I} selone and thione complexes, the $[Tpm^{R}Cu(dmit/dmise)][BF_4]$ complexes were obtained by treating $[Cu(NCCH_3)_4][BF_4]$ with one equivalent of dmise/dmit, followed by addition of an equimolar amount of the tris(pyrazolyl) ligand (Scheme 1.1A).[126] We synthesized Cu^{I} complexes with the hydrotris(3,5-dimethylpyrazolyl)borate (Tp*) ligand, Tp*Cu(dmit/dmise) using similar methods.[126]

Scheme 1.1. Synthesis of selone and thione Cu^{I} complexes.

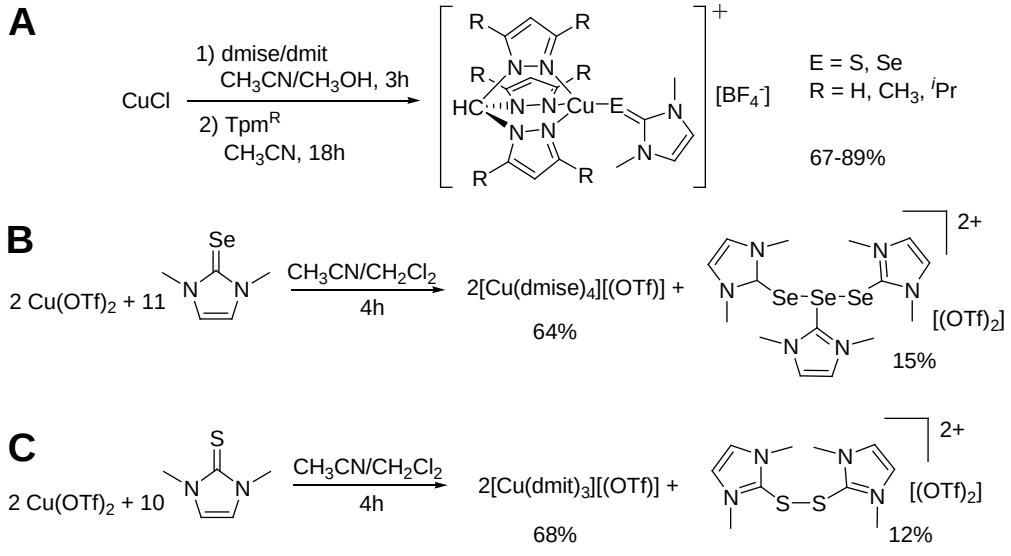

We also synthesized homoleptic Cu^{I} complexes of dmise and dmit (Scheme 1.1B and 1.1C) by treating $Cu(OTf)_2$ with an excess of dmit or dmise in a mixture of acetonitrile and dichloromethane.[127] Surprisingly, these reactions yielded sulfur and selenium complexes with different coordination numbers: a trigonal planar $[Cu(dmit)_3]^+$ complex and a distorted tetrahedral $[Cu(dmise)_4]^+$ complex, in addition to a disulfide dication and triselenide dication, respectively.[127] These synthetic results highlight the significant differences between sulfur and selenium coordination chemistry, and reinforce the fact that both sulfur and selenium complexes must be fully characterized and compared to develop a complete understanding of their antioxidant activity.

DFT calculations of $[Tpm^{Me}Cu(L)]^+$ (L = CH_3CN, dmit, dmise) showed that protection of the Cu^{I} center may be attributed to an important change in the HOMO of the complex upon dmit/dmise coordination.[152] Whereas the HOMO of the CH_3CN complex is localized on the metal d orbitals, a p-type lone pair of dmit/dmise is the major contributor to the HOMO of these complexes (Figure 1.4). Metal coordination destabilizes the lone pair of the thiolate/selenolate resonance structure of dmit/dmise

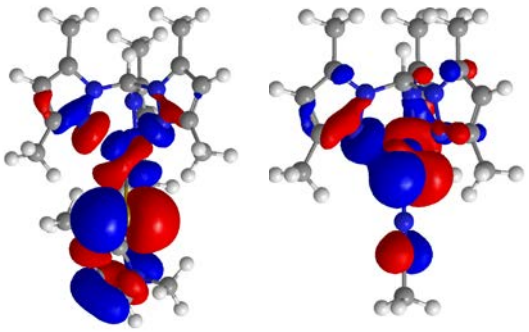

Figure 1.4. HOMOs for $[Tpm^{Me}Cu(dmit)]^+$ (left) and $[Tpm^{Me}Cu(NCCH_3)]^+$ (right). Reprinted with permission from Kimani, M. M.; Bayse, C. A.; Stadelman, B. S.; Brumaghim, J. L. *Inorg. Chem.* **2013**, *52*, 11685-11687 (Appendix A). Copyright 2013 American Chemical Society.

Scheme 1.2. Molecular orbital diagram showing the destabilization of the thiolate lone pair upon Cu^{I} coordination.

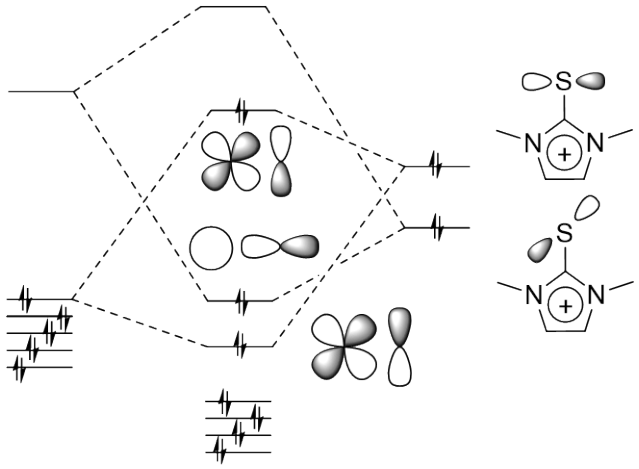

perpendicular to the Cu-S(Se) bond to make it more susceptible to oxidation (Scheme 1.2). This effect may be of general importance to the prevention of Fenton-type chemistry by S/Se compounds because for free, hydrated metal ions, the frontier MOs are metal-based, so that electrons will be drawn from these MOs in an oxidation process. Because most S/Se ligands act as p-donors, electrons will be removed from the destabilized lone pair to protect the metal.

Therefore, instead of a one-electron oxidation of Cu(I) producing $^{\bullet}OH$, the chalcogen is targeted for a two-electron oxidation, fully reducing H_2O_2. The HOMO energy of a series of $[Cu(L)(OH_2)]^{+}$ complexes with a S/Se compound L correlates well with the ability of the compound to protect DNA against oxidative damage based upon the IC_{50} data (Figure 1.5 and Table 1.4 at the end of the Experimental Methods section). Note that there is no correlation with the HOMO of the free S/Se compounds, again indicating that metal coordination is central to the protection mechanism.

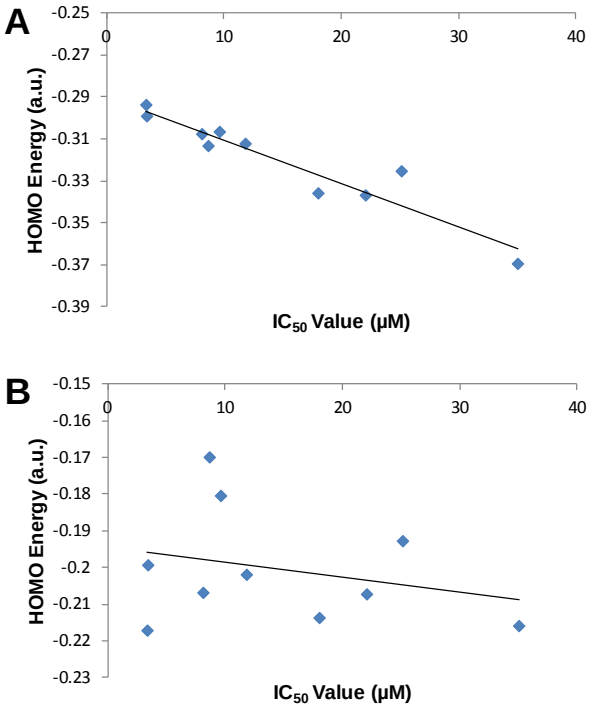

Figure 1.5. Correlations between the HOMO energies for a series of A) $[Cu(L)(OH_2)]^+$ complexes (R^2 = 0.90) and B) the free ligands (L; R^2 = 0.07). IC_{50} values are from references 18 and 35-37.

This destabilization of the lone pairs may explain why S/Se compounds are more effective against Cu^I-mediated oxidative damage. Because Fe^{II} is a borderline Lewis acid, it has less affinity for the soft S/Se ligands and prefers linkage isomers that bond through the N,O donors. Because no Fe-S/Se bond forms, the sulfur or selenium lone pairs are not activated for ROS scavenging and no protection from oxidative damage is observed except at very high concentrations. The main exception to this rule are dmit/dmise which are significantly more effective against Fe^{II}. These ligands can only form Fe-S/Se bonds with Fe^{II} and their greater effectiveness may be attributed to both the activation of the lone pairs and the delocalization of the spin density to the chalcogen. These results clearly demonstrate that only by understanding the metal-binding

mechanisms for antioxidant behavior can meaningful predictive models be developed for sulfur and selenium compounds.

1.6. Establishing targeted scavenging as an antioxidant mechanism linked to metal binding

Synthesis of the $[Tpm^{Me}Cu(dmit/dmise)]^+$ complexes also afforded us a system to examine whether these coordinated sulfur and selenium ligands protected Cu^I from oxidation. First, unbound dmise and dmit were treated with up to three equivalents of H_2O_2, and the results were observed by ^1H, ^{13}C, and ^{77}Se (for dmise) NMR spectroscopy in CD_3CN. Significant downfield shifts in the NMR resonances upon oxidation and indicated the formation of the *N,N'*-dimethylimidazolium cation and oxidized sulfur and selenium species, products that were confirmed by electrospray ionization mass spectrometry results (ESI-MS).[152] In the ^{77}Se NMR spectrum, this oxidation was unmistakable, since the selenium resonance shifted from δ -29.5 for dmise to an SeO_2 species at δ 1345.[152] Bhabak *et al.* determined that both dmise and dmit are similarly oxidized when treated with peroxynitrite.[99] As expected from the electrochemical results (Table 1.2), dmise is more sensitive to oxidation than dmit, requiring addition of only two equivalents of H_2O_2 for complete oxidation compared to the three equivalents required for complete oxidation of dmit.[152]

Similar oxidation studies with $[Tpm^{Me}Cu(dmise)]^+$ and $[Tpm^{Me}Cu(dmit)]^+$ were also performed to determine if dmise or dmit coordination could prevent Cu^I oxidation by H_2O_2. ^1H and ^{13}C NMR studies with the Cu^I-selone complex in acetonitrile treated with

0.5, 1, and 2 equivalents of H_2O_2 showed sharp peaks, indicative of Cu^I, with shifts in the bound dmise resonances the same as those seen for unbound oxidized dmise.[152] These results were again corroborated by ESI-MS, and the $[Tpm^{Me}Cu(NCCH_3)]^+$ complex was also isolated from the oxidized reaction mixture, confirming the presence of Cu^I. Treatment of $[Tpm^{Me}Cu(NCCH_3)]^+$ with H_2O_2 resulted in only Cu^{II} formation.[152] Similarly, treatment of $[Tpm^{Me}Cu(NCCH_3)]^+$ with O_2 resulted in immediate oxidation of Cu^I to Cu^{II} and formation of $[\{Tpm^{Me}(Cu(OH)\}_2]^{2+}$.[129] Thus, dmise binding protects Cu^I from H_2O_2 oxidation (Figure 1.6). Similar results were observed when the thione complex was treated with up to three equivalents of H_2O_2, confirming that dmise is a more effective H_2O_2 scavenger than dmit.[152]

Dmise and dmit are extremely versatile antioxidants, preventing oxidative DNA damage from oxidation by both copper or iron coordination and ROS scavenging. Their ability to protect bound Cu^I is the first example of metal-antioxidant binding leading to targeted ROS scavenging (Figure 1.2, bottom) and proves that metal coordination mechanisms are required to fully understand sulfur and selenium antioxidant activity.

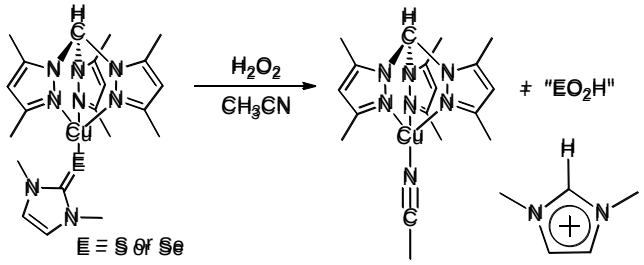

Figure 1.6. Reaction of $[Tpm^{Me}Cu(L)]^+$ (L = dmise or dmit) with H_2O_2. Reprinted with permission from Kimani, M. M.; Bayse, C. A.; Stadelman, B. S.; Brumaghim, J. L. *Inorg. Chem.* **2013**, *52*, 11685-11687 (Appendix A). Copyright 2013 American Chemical Society.

1.7. Conclusions and future directions

1.7.1 Conclusions. Sulfur and selenium antioxidants prevent metal-mediated oxidative DNA damage by coordinating Cu^{I} or Fe^{II} at biologically relevant concentrations. Whereas previous studies have almost exclusively focused on ROS scavenging as a primary antioxidant mechanism, our work has established the importance of metal interactions in antioxidant mechanisms. Three of the nine tested selenium compounds and seven of the eleven tested sulfur compounds more efficiently inhibited Cu^{I}-mediated DNA damage compared to Fe^{II}-mediated DNA damage. Our studies have also revealed that merely the presence of a sulfur or selenium atom is not sufficient for the prevention of DNA damage, and that functional groups with the ability to interact with metal ions substantially affect antioxidant behavior. Mass spectrometry confirmed copper and iron coordination for all sulfur and selenium compounds, regardless of antioxidant ability, indicating that metal binding is necessary but not sufficient for sulfur and selenium prevention of DNA damage. Because sulfur and selenium antioxidants can prevent DNA damage through multiple pathways, it is critical to fully understand the structural properties necessary for potent antioxidant activity for ROS scavenging and metal-binding mechanisms.

NMR and X-ray absorption spectroscopy studies of methyl-selenocysteine and selenomethionine with Cu^{I} confirmed that coordination occurs through the selenium or sulfur atoms in addition to the nitrogen and/or oxygen atoms. DFT calculations of Cu^{I} complexes with dmise and dmit revealed the destabilization of the selenium or sulfur lone pair upon coordination that makes dmise and dmit more susceptible to oxidation than Cu^{I}.

In addition, electrochemical studies showed that, upon dmise-Cu^{I} coordination, the $Cu^{II/I}$ redox potential is shifted outside the biological window for hydroxyl radical generation. Our results not only identify the chemical properties that contribute to antioxidant activity and prove that metal coordination is the key to fully understanding sulfur and selenium antioxidant mechanisms, but have established the first predictive models for sulfur and selenium prevention of metal-mediated DNA damage.

1.7.2. Future research directions. Future studies will focus on testing second-generation sulfur and selenium antioxidants with different functionalities to determine the effects of coordination mode and denticity on antioxidant behavior. Additional studies will focus on determining the formation constants of sulfur and selenium compounds with copper and iron, to determine the correlation between complex stability and antioxidant behavior. Our work over the past ten years has challenged the traditional mindset that sulfur and selenium antioxidant activity is controlled only by ROS scavenging and continues to illuminate the importance of metal-binding antioxidant mechanisms.

The research presented in this dissertation focuses on determining the DNA damage prevention mechanisms of sulfur and selenium compounds *in vitro*. The review in this introductory Chapter is submitted for publication in the *Journal of Inorganic Biochemistry* (Zimmerman, M. T.; Bayse, C. A.; Ramoutar, R. R.; Brumaghim, J. L. *J. Inorg. Biochem.,* submitted) Currently, the general consensus in the field is that sulfur and selenium compounds prevent oxidative DNA damage through ROS scavenging, while the role of redox active metal ions has been relatively unexplored. Thus, the sulfur

and selenium compounds discussed in Chapters 3 and 4 have been shown to exhibit metal-coordinating abilities and prevent oxidative DNA damage caused by metal- and nonmetal-mediated pathways.

The work presented in Chapter 2 examines the redox and metal coordinating properties of sulfur and selenium amino acids, and determines the correlation between these properties and DNA damage prevention capabilities. Furthermore, these studies show the significance of metal coordination in preventing DNA damage. Chapter 3 discusses the DNA damage prevention abilities of *N,N'*-dimethylimidazole selone (dmise) and thione (dmit), the first sulfur and selenium compounds to inhibit DNA damage from Fe^{II}/H_2O_2, Cu^{I}/H_2O_2, and peroxynitrite *in vitro*. These results also confirm the first selenium and sulfur compounds that prevent oxidative DNA damage through both metal coordination and ROS scavenging. The research in Chapter 4 examines how secondary functional groups, S/Se species, and methylation of the imidazole nitrogens affect the DNA damage prevention abilities of various selenium and sulfur compounds *in vitro*. This chapter also compares the ability of the hyperthyroid drug, methimazole, and the natural thione, ergothioneine, to prevent oxidative DNA damage from Fe^{II}/H_2O_2, Cu^{I}/H_2O_2, and peroxynitrite for the first time. Since interest in selenium and sulfur antioxidants has dramatically grown over the past decade, knowing how they prevent oxidative damage, and which chemical properties are necessary for activity, will permit better development of selenium and sulfur antioxidants for animal and clinical trials; leading to more effective treatment of diseases linked to oxidative damage.

Chapter 5 explores the redox properties of clotrimazole and pseudoephedrine metal complexes. This work describes the significance of transition metals on the antifungal mechanisms of clotrimazole, and suggests that one mechanism may be the metal-mediated generation of ROS. DNA damage studies with a copper clotrimazole complex suggest that Cu^{II}-clotrimazole complexes produce the harmful $^{\bullet}OH$ similar to Reaction 2.

Pseudoephedrine is commonly used as an antitussive drug or nasal decongestant, but little is known about the effect metal interactions have on its function. The electrochemical studies in Chapter 5 indicate that the presence of redox-active metal ions greatly reduces the oxidation potential of pseudoephedrine derivatives. In addition, DNA damage studies with trinuclear copper pseudoephedrine-derivative complexes suggest that DNA damage is dose-dependent and similar to Reaction 2. Understanding the significance of metal binding interactions for endogenous and exogenous antioxidants and drugs is critical for the development and targeting of future therapies to treat a wide array of diseases.

1.8. Abbreviations

bipy	2,2'-bipyridine
DFT	density functional theory
Dmise	*N*,*N*'-dimethylimidazole selone
Dmit	*N*,*N*'-dimethylimidazole thione
EDTA	ethylenediaminetetraacetic acid

ESI-MS	electrospray ionization mass spectrometry
MALDI	matrix-assisted laser-desorption ionization
MES	2-(*N*-morpholino)ethanesulfonic acid
MOPS	3-(*N*-morpholino)propanesulfonic acid
NADH	nicotinamide adenine dinucleotide
NPC	Nutritional Prevention of Cancer
OTf	trifluoromethane sulfonate
ROS	reactive oxygen species
SELECT	Selenium and Vitamin E Cancer Prevention Trial
SeMet	selenomethionine
Tpm	tris(pyrazolyl)methane
Tp^*	hydrotris(3,5-dimethylpyradzolyl)borate

1.9 Experimental Methods

Electrochemical measurements for sulfur compounds. Cyclic voltammetry samples were prepared by dissolving the sulfur compounds (300 μM) in MOPS buffer (10 mM, pH 7) with KNO_3 (10 mM) as a supporting electrolyte. Solutions were degassed for 5 min with N_2 before each experiment. All CV experiments were conducted at 100 mV/s. Differential pulse voltammetry experiments (pulse amplitude of 0.080 V, pulse width of 0.100, sample width of 0.045, and pulse period of 0.200) were also performed and showed similar results to the CV data. Samples of each compound were cycled between -1000 mV and 1000 mV using a glassy carbon working electrode, a Pt counter-electrode, and a Ag/AgCl (197 mV vs. NHE)[153] reference electrode.

Theoretical methods. The HOMO energies used for the graphs in Figure 1.5 were obtained from the minimum energy conformations of methionine, *S*-methylcysteine, cystine, methionine sulfoxide, *S*-methylcysteine sulfoxide, methyl methanethiosulfonate (MMTS), selenomethionine, *Se*-methylselenocysteine, selenocystine and glycine and their complexes with Cu(I) $[Cu(OH_2)L]^+$ (Table 1.3). Geometries were optimized using the BP86 xc functional,[154,155] as implemented in PQS version 3.3,[156] as previously reported in our study of Cu(I) with selenoamino acids.[132] Copper and selenium were represented by the Hurley et al relativistic effective core potentials.[157] The copper basis set was further modified by the 4p Couty-Hall contraction.[158] Sulfur was represented by the Wadt-Hay basis set augmented with diffuse and polarization functions.[159] Dunning split-valence triple-ζ basis sets,[160] modified with polarization and diffuse (heavy atoms only) functions were used for nitrogen, oxygen and hydrogen atoms attached to non-carbon heavy atoms. Hydrocarbon fragments used Dunning double-ζ basis sets with

Table 1.3. Electrochemical properties of sulfur and selenium compounds *versus* normal hydrogen electrode (NHE).

Selenium Compound[a]	Ep_a **(mV)**	Ep_c **(mV)**	ΔE**(mV)**	$E_{1/2}$ **(mV)**
Selenocystine	-115	—	—	—
Selenomethionine	693	—	—	—
Methyl-selenocysteine	—	—	—	—
Selenocystamine	-131	-526	394	-329
2-Aminophenyl diselenide	593, 120	24, -978	569, 1099	308, -429
2-Carboxyphenyl diselenide	501	569	67	535
Sulfur Compound				
Cystine	458	617	159	538
Methionine	-244	—	—	—
Methyl-cysteine	—	—	—	—
Cystamine	—	—	—	—
2,2'-Dithiosalicylic acid	—	—	—	—
Reduced glutathione	—	—	—	—

[a]Electrochemical values from reference 18.

polarization functions on carbon only.[161] Structures were shown to be minima of the potential energy surface by frequency calculations.

Amino acids were modeled as bidentate ligands. $[Cu(OH_2)L]^+$ complexes preferred to coordinate through S/Se and the amine over the S/Se and the carboxylate or the amine and carboxylate (N,O).[132] Glycine prefers to coordinate to the amino acid only (N,O-coordination). MMTS is a monodentate ligand through the sulfoxide oxygen.

Table 1.4. IC_{50} data and DFT(BP86) HOMO energies for selected sulfur and selenium compounds (L), free and in complex with Cu(I) $[Cu(OH_2)L]^+$.

Compound	**IC_{50} (μM)[a]**	**HOMO L (a. u.)**	**HOMO $[Cu(OH_2)L]^+$ (a. u.)**
Methionine	11.8	-0.20184	-0.31208
S-methylcysteine	9.6	-0.18036	-0.30642
cystine	3.4	-0.19924	-0.29899
methionine sulfoxide	18.0	-0.21360	-0.33569
S-methylcysteine sulfoxide	8.1	-0.20676	-0.30748
MMTS	35.0	-0.21579	-0.36929
selenomethionine	25.1	-0.19268	-0.32517
Se-methylselenocysteine	8.64	-0.16986	-0.31314
selenocystine	3.34	-0.21704	-0.29358
glycine	22.04	-0.20716	-0.33668

[a]IC_{50} values are from references 18 and 35-37.

1.10. References

(1) Lloyd, D. R.; Philips, D. H.; Carmichael, P. L. *Chem. Res. Toxicol.* **1997**, *10*, 393-400.

(2) Fridovich, I. *Annu. Rev. Pharmacol. Toxicol.* **1983**, *23*, 239-257.

(3) Imlay, J. A. *Annu. Rev. Biochem.* **2008**, *77*, 755-776.

(4) Henle, E. S.; Han, Z.; Tang, N.; Rai, P.; Luo, Y.; Linn, S. *J. Biol. Chem.* **1999**, *274*, 962-971.

(5) Henle, E. S.; Linn, S. *J. Biol. Chem.* **1997**, *272*, 19095-19098.

(6) Imlay, J. A. *Annu. Rev. Microbiol.* **2003**, *57*, 395-418.

(7) Seaver, L. C.; Imlay, J. A. *J. Biol. Chem.* **2004**, *279*, 48742-48750.

(8) Afonso, V.; Champy, R.; Mitrovic, D.; Collin, P.; Lomri, A. *Joint Bone Spine* **2007**, *74*, 324-329.

(9) Cadet, J.; Sage, E.; Douki, T. *Mutat. Res.* **2005**, *571*, 3-17.

(10) Valko, M.; Leibfritz, D.; Moncol, J.; Cronin, M. T. D.; Mazur, M.; Telser, J. *Inter. J. Biochem. Cell Biol.* **2007**, *39*, 44-84.

(11) Valko, M.; Rhodes, C. J.; Moncol, J.; Izakovic, M.; Mazur, M. *Chem. Biol. Interact.* **2006**, *160*, 1-40.

(12) Collins, C. A.; Fry, F. H.; Holme, A. L.; Yiakouvaki, A.; Al-Qenaei, A.; Pourzand, C.; Jacob, C. *Org. Biomol. Chem.* **2005**, *3*, 1541-1546.

(13) Fry, F. H.; Holme, A. L.; Giles, N. M.; Giles, G. I.; Collins, C.; Holt, K.; Pariagh, S.; Gelbrich, T.; Hursthouse, M. B.; Gutowski, N. J.; Jacob, C. *Org. Biomol. Chem.* **2005**, *3*, 2579-2587.

(14) Loft, S.; Deng, X. S.; Tuo, J.; Wellejus, A.; Sorensen, M.; Poulsen, H. E. *Free Radic. Res.* **1998**, *29*, 525-539.

(15) Brewer, G. J. *Exp. Biol. Med.* **2007**, *232*, 323-335.

(16) De Flora, S.; Izzotti, A. *Mutat. Res.* **2007**, *621*, 5-17.

(17) Bar-Or, D.; Thomas, G. W.; Rael, L. T.; Lau, E. P.; Winkler, J. V. *Biochem. Biophys. Res. Commun.* **2001**, *282*, 356-360.

(18) Battin, E. E.; Zimmerman, M. T.; Ramoutar, R. R.; Quarles, C. E.; Brumaghim, J. L. *Metallomics* **2011**, *3*, 503-512.

(19) Park, S.; Imlay, J. A. *J. Bacteriol.* **2003**, *185*, 1942-1950.

(20) Andrade, R. G., Jr.; Dalvi, L. T.; Silva, J. M., Jr.; Lopes, G. K.; Alonso, A.; Hermes-Lima, M. *Arch. Biochem. Biophys.* **2005**, *437*, 1-9.

(21) Miguel, F.; Augusto, A. C.; Gurgueira, S. A. *Free Radic. Res.* **2009**, *43*, 340-347.

(22) Angel, I.; Bar, A.; Horovitz, T.; Taler, G.; Krakovsky, M.; Resnitsky, D.; Rosenberg, G.; Striem, S.; Friedman, J. E.; Kozak, A. *Drug Dev. Res.* **2002**, *56*, 300-309.

(23) Keyer, K.; Imlay, J. A. *Proc. Natl. Acad. Sci. USA* **1996**, *93*, 13635-13640.

(24) Perry, G.; Cash, A. D.; Srinivas, R.; Smith, M. A. *Drug Dev. Res.* **2002**, *56*, 293-299.

(25) Jhurry, N. D.; Chakrabarti, M.; McCormick, S. P.; Holmes-Hampton, G. P.; A., L. P. *Biochemistry* **2012**, *51*, 5276-5284.

(26) Weiss, G.; Fuchs, D.; Hausen, A.; Reibnegger, G.; Werner, E. R.; Werner-Felmayer, G.; Wachter, H. *Exp. Hematol.* **1992**, *20*, 605-610.

(27) Ma, Y.; Liu, Z.; Hider, R. C.; Petrat, F. C. *Anal. Chem. Insights* **2007**, *2*, 61-67.

(28) Que, E. L.; Domaille, D. W.; Chang, C. J. *Chem. Rev.* **2008**, *108*, 1517-1549.

(29) Yang, L.; McRae, R.; Henary, M. M.; Patel, R.; Lai, B.; Vogt, S.; Fahrni, C. J. *Proc. Nat. Acad. Sci. USA* **2005**, *102*, 11179-11184.

(30) Yildiz, G.; Demiryurek, A. T. *J. Pharmacol. Toxicol. Methods* **1998**, *39*, 179-184.

(31) Karoui, H.; Hogg, N.; Frejaville, C.; Tordo, P.; Kalyanaraman, B. *J. Biol. Chem.* **1996**, *271*, 6000-6009.

(32) Kunwar, A.; Mishra, B.; Barik, A.; Kumbhare, L. B.; Pandey, R.; Jain, V. K.; Priyadarsini, K. I. *Chem. Res. Toxicol.* **2007**, *20*, 1482-1487.

(33) Emerit, J.; Beaumont, C.; Trivin, F. *Biomed. Pharmacother.* **2001**, *55*, 333-339.

(34) Pastor, N.; Weinstein, H.; Jamison, E.; Brenowitz, M. *J. Mol. Biol.* **2000**, *304*, 55-68.

(35) Ramoutar, R. R.; Brumaghim, J. L. *Main Group Chem.* **2007**, *6*, 143-153.

(36) Battin, E. E.; Perron, N. R.; Brumaghim, J. L. *Inorg. Chem.* **2006**, *45*, 499-501.

(37) Battin, E. E.; Brumaghim, J. L. *J. Inorg. Biochem.* **2008**, *102*, 2036-2042.

(38) Kieliszek, M.; Blazejak, S. *Nutrition* **2013**, *29*, 713-718.

(39) Zwolak, I.; Zaporowska, H. *Cell Biol. Toxicol.* **2012**, *28*, 31-46.

(40) Chowdhury, R.; Dutta, A.; Chaudhuri, S. R.; Sharma, N.; Giri, A. K.; Chaudhuri, K. *Food Chem. Toxicol.* **2008**, *46*, 740-751.

(41) Huang, Z.; Rose, A. H.; Hoffmann, P. R. *Antioxid. Redox. Signal* **2012**, *16*, 705-743.

(42) Seyedrezazadeh, E.; Ostadrahimi, A.; Mahboob, S.; Assadi, Y.; Ghaemmagami, J.; Pourmogaddam, M. *Respirology* **2008**, *13*, 294-298.

(43) Krehl, S.; Loewinger, M.; Florian, S.; Kipp, A. P.; Banning, A.; Wessjohann, L. A.; Brauer, M. N.; Iori, R.; Esworthy, R. S.; Chu, F. F.; Brigelius-Flohe, R. *Carcinogenesis* **2012**, *33*, 620-628.

(44) Letavayova, L.; Vlckova, V.; Brozmanova, J. *Toxicology* **2006**, *227*, 1-14.

(45) Raich, P. C.; Lu, J.; Thompson, H. J.; Combs, G. F., Jr. *Cancer Invest.* **2001**, *19*, 540-553.

(46) Zeng, H.; Combs, G. F., Jr. *J. Nutr. Biochem.* **2008**, *19*, 1-7.

(47) Clark, L. C.; Dalkin, B.; Krongrad, A.; Combs, G. F., Jr.; Turnbull, B. W.; Slate, E. H.; Witherington, R.; Herlong, J. H.; Janosko, E.; Carpenter, D.; Borosso, C.; Falk, S.; Rounder, J. *Br. J. Urol.* **1998**, *81*, 730-734.

(48) Combs, G. F.; Jr *Br. J. Cancer* **2004**, *91*, 195-199.

(49) Lippman, S. M.; Klein, E. A.; Goodman, P. J.; Lucia, M. S.; Thompson, I. M.; Ford, L. G.; Parnes, H. L.; Minasian, L. M.; Gaziano, J. M.; Hartline, J. A.; Parsons, J. K.; Bearden, J. D., III; Crawford, E. D.; Goodman, G. E.; Claudio, J.; Winquist, E.; Cook, E. D.; Karp, D. D.; Walther, P.; Lieber, M. M.; Kristal, A. R.; Darke, A. K.; Arnold, K. B.; Ganz, P. A.; Santella, R. M.; Albanes, D.; Taylor, P. R.; Probstfield, J. L.; Jagpal, T. J.; Crowley, J. J.; Meyskens, F. L., Jr.; Baker, L. H.; Coltman, C. A., Jr. *J. Am. Med. Assoc.* **2009**, *301*, 39-51.

(50) Reid, M. E.; Duffield-Lillico, A. J.; Slate, E.; Natarajan, N.; Turnbull, B.; Jacobs, E.; Combs, G. F.; Alberts, D. S.; Clark, L. C.; Marshall, J. R. *Nutr. Cancer* **2008**, *60*, 155-163.

(51) El-Bayoumy, K. *Nutr. Cancer* **2009**, *61*, 285-286.

(52) El-Bayoumy, K.; Sinha, R. *Mutat. Res.* **2005**, *591*, 224-236.

(53) Menter, D. G.; Sabichi, A. L.; Lippman, S. M. *Cancer Epidemiol. Biomarkers Prev.* **2000**, *9*, 1171-1182.

(54) Molina-Holgado, F.; Hider, R. C.; Gaeta, A.; Williams, R.; Francis, P. *Biometals* **2007**, *20*, 639-654.

(55) Ates, B.; Abraham, L.; Ercal, N. *Free Radic. Res.* **2008**, *42*, 372-377.

(56) Zhao, G.-R.; Xiang, Z.-J.; Ye, T.-X.; Yuan, Y.-J.; Guo, Z.-X. *Food Chemistry* **2006**, *99*, 767-774.

(57) Kim, J. M.; Chang, H. J.; Kim, W. K.; Chang, N.; Chun, H. S. *J. Agric. Food Chem.* **2006**, *54*, 6547-6553.

(58) Battin, E. E.; Brumaghim, J. L. *Cell. Biochem. Biophys.* **2009**, *55*, 1-23.

(59) Sarma, B. K.; Mugesh, G. *J. Am. Chem. Soc.* **2005**, *127*, 11477-11485.

(60) Wang, X.; Yun, J. W.; Lei, X. G. *Antioxid. Redox Signal.* **2014**, *20*, 191-203.

(61) Akanmu, D.; Cecchini, R.; Aruoma, O. I.; Halliwell, B. *Arch. Biochem. Biophys.* **1991**, *288*, 10-16.

(62) Aruoma, O. I.; Whiteman, M.; England, T. G.; Halliwell, B. *Biochem. Biophys. Res. Commun.* **1997**, *231*, 389-391.

(63) Ey, J.; Schomig, E.; Taubert, D. *J. Agric. Food Chem.* **2007**, *55*, 6466-6474.

(64) Markova, N. G.; Karaman-Jurukovska, N.; Dong, K. K.; Damaghi, N.; Smiles, K. A.; Yarosh, D. B. *Free Radic. Biol. Med.* **2009**, *46*, 1168-1176.

(65) Rahman, I.; Gilmour, P. S.; Jimenez, L. A.; Biswas, S. K.; Antonicelli, F.; Aruoma, O. I. *Biochem. Biophys. Res. Commun.* **2003**, *302*, 860-864.

(66) Zhu, B. Z.; Mao, L.; Fan, R. M.; Zhu, J. G.; Zhang, Y. N.; Wang, J.; Kalyanaraman, B.; Frei, B. *Chem. Res. Toxicol.* **2011**, *24*, 30-34.

(67) Hartman, P. E. *Methods Enzymol.* **1990**, *186*, 310-318.

(68) Sotgia, S.; Zinellu, A.; Mangoni, A. A.; Pintus, G.; Attia, J.; Carru, C.; McEvoy, M. *PLoS One* **2014**, *9*, e84918.

(69) Mitsuyama, H.; May, J. M. *Clin. Sci.* **1999**, *97*, 407-411.

(70) Yamashita, Y.; Yamashita, M. *J. Biol. Chem.* **2010**, *285*, 18134-18138.

(71) Klein, M.; Ouerdane, L.; Bueno, M.; Pannier, F. *Metallomics* **2011**, *3*, 513-520.

(72) Yamashita, M.; Yamashita, Y.; Ando, T.; Wakamiya, J.; Akiba, S. *Biol. Trace Elem. Res.* **2013**, *156*, 36-44.

(73) Fontecave, M. *Nat. Chem. Biol.* **2006**, *4*, 171-174.

(74) Ramoutar, R. R.; Brumaghim, J. L. *Cell Biochem. Biophys.* **2010**, *58*, 1-23.

(75) Guttormsen, A. B.; Schneede, J.; Fiskerstrand, T.; Ueland, P. M.; Refsum, H. M. *J. Nutr.* **1993**, *124*, 1934-1941.

(76) Bergstroem, J.; Fuerst, P.; Noree, L. O.; Vinnars, E. *J. Appl. Physiol.* **1974**, *36*, 693-697.

(77) Smith, C. V.; Jones, D. P.; Guenthner, T. M.; Lash, L. H.; Lauterburg, B. H. *Toxicol. Appl. Pharmacol.* **1996**, *140*, 1-12.

(78) Skellern, G. G.; Stenlake, J. B.; Williams, W. D. *Br. J. Clin. Pharmac.* **1974**, *1*, 265-269.

(79) Okuno, A.; Yano, K.; Inyaku, F.; Suzuki, Y.; Sanae, N.; Kumai, M.; Naitoh, Y. *Acta Endocrinol.* **1987**, *115*, 112-118.

(80) Burk, R. F.; Norsworthy, B. K.; Hill, K. E.; Motley, A. K.; Byrne, D. W. *Cancer Epidemiol. Biomarkers* **2006**, *15*, 804-810.

(81) Reid, M. E.; Stratton, M. S.; Lillico, A. J.; Fakih, M.; Natarajan, R.; Clark, L. C.; Marshall, J. R. *J. Trace Elem. Med. Biol.* **2004**, *18*, 69-74.

(82) Landucci, F.; Mancinelli, P.; De Gaudio, A. R.; Virgili, G. *J. Crit. Care* **2014**, *29*, 150-156.

(83) Seifried, H. E.; Anderson, D. E.; Fisher, E. I.; Milner, J. A. *J. Nutr. Biochem.* **2007**, *18*, 567-579.

(84) Roussyn, I.; Briviba, K.; Masumoto, H.; Sies, H. *Arch. Biochem. Biophys.* **1996**, *330*, 216-218.

(85) Giles, N. M.; Watts, A. B.; Giles, G. I.; Fry, F. H.; Littlechild, J. A.; Jacob, C. *Chem. Biol.* **2003**, *10*, 677-693.

(86) Quig, D. *Altern. Med. Rev.* **1998**, *3*, 262-270.

(87) Waalkes, M. P.; Liu, J.; Goyer, R. A.; Diwan, B. A. *Cancer Res.* **2004**, *64*, 7766-7772.

(88) Wetli, H. A.; Buckett, P. D.; Wessling-Resnick, M. *Chem. Biol.* **2006**, *13*, 965-972.

(89) Oikawa, T.; Esaki, N.; Tanaka, H.; Soda, K. *Proc. Natl. Acad. Sci. USA* **1991**, *88*, 3057-3059.

(90) Finley, J. W.; Ip, C.; Lisk, D. J.; Davis, C. D.; Hintze, K. J.; Whanger, P. D. *J. Agric. Food Chem.* **2001**, *49*, 2679-2683.

(91) Schrauzer, G. N. *J. Am. Coll. Nutr.* **2001**, *20*, 1-4.

(92) Mantovani, G.; Maccio, A.; Madeddu, C.; Serpe, R.; Massa, E.; Gramignano, G.; Lusso, M. R.; Curreli, N.; Rinaldi, A. *J. Exp. Ther. Oncol.* **2004**, *4*, 69-78.

(93) Davis, C. D.; Feng, Y.; Hein, D. W.; Finley, J. W. *J. Nutr.* **1999**, *129*, 63-69.

(94) Ip, C.; Hayes, C. *Carcinogenesis* **1989**, *10*, 921-925.

(95) Spyrou, G.; Bjornstedt, M.; Skog, S.; Holmgren, A. *Cancer Res.* **1996**, *56*, 4407-4412.

(96) Ramoutar, R. R.; Brumaghim, J. L. *J. Inorg. Biochem.* **2007**, *101*, 1028-1035.

(97) Zimmerman, M. T.; Brumaghim, J. L. *in preparation*.

(98) Burk, R. F. *Nutr. Clin. Care* **2002**, *5*, 75-79.

(99) Bhabak, K. P.; Mugesh, G. *Chem. Eur. J.* **2010**, *16*, 1175-1185.

(100) Bhabak, K. P.; Satheeshkumar, K.; Jayavelu, S.; Mugesh, G. *Org. Biomol. Chem.* **2011**, *9*, 7343-50.

(101) McAuliffe, C. A.; Quagliano, J. V.; Vallarino, L. M. *Inorg. Chem.* **1966**, *5*, 1996-2003.

(102) Sze, Y. K.; Davis, A. R.; Neville, G. A. *Inorg. Chem.* **1970**, *14*, 1969-1974.

(103) Shindo, H.; Brown, T. L. *J. Am. Chem. Soc.* **1965**, *87*, 1904-1909.

(104) Livingstone, S. E.; Nolan, J. D. *Inorg. Chem.* **1968**, *7*, 1447-1451.

(105) Boyington, J. C.; Gladyshev, V. N.; Khangulov, S. V.; Stadtman, T. C.; Sun, P. D. *Science* **1997**, *275*, 1305-1308.

(106) Garcin, E.; Vernede, X.; Hatchikian, E. C.; Volbeda, A.; Frey, M.; Fontecilla-Camps, J. C. *Structure* **1999**, *7*, 557-566.

(107) Zainal, H. A.; Wolf, W. R. *Trans. Metal Chem.* **1995**, *20*, 225-227.

(108) Christian, G. D. *Analytical Chemistry*, 4th ed.; John Wiley & Sons: New York, 1980, p. 616.

(109) Cheung, P. Y.; Danial, H.; Jong, J.; Schulz, R. *Arch. Biochem. Biophys.* **1998**, *350*, 104-108.

(110) Nakagawa, H.; Sumiki, E.; Takusagawa, M.; Ikota, N.; Matsushima, Y.; Ozawa, T. *Chem. Pharm. Bull.* **2000**, *48*, 261-265.

(111) Lu, Z.; Huang, W.; Vittal, J. J. *New J. Chem.* **2002**, *26*, 1122-1129.

(112) Breton, J. L.; Farrar, J. A.; Kennedy, M. C.; Beinert, H.; Thomson, A. J. *Biochem. J.* **1995**, *311*, 197-202.

(113) Ding, H.; Clark, R. J. *Biochem. J.* **2004**, *379*, 433-440.

(114) Lombardi, A.; Marasco, D.; Maglio, O.; Di Costanzo, L.; Nastri, F.; Pavone, V. *Proc. Natl. Acad. Sci. USA* **2000**, *97*, 11922-11927.

(115) Yu, S.-B.; Papaefthymiou, G. C.; Holm, R. H. *Inorg. Chem.* **1991**, *30*, 3476-3485.

(116) Poleć-Pawlak, K.; Ruzik, R.; Lipiec, E. *Talanta* **2007**, *72*, 1564-1572.

(117) Lavanant, H.; Hoppilliard, Y. *J. Mass Spectrom.* **1997**, *32*, 1037-1049.

(118) Chernyshova, O. S.; Boichenko, A. P.; Abdulrahman, H.; Loginova, L. P. *J. Mol. Liq.* **2013**, *182*, 1-6.

(119) Rimola, A.; Sodupe, M.; Tortajada, J.; Rodríguez-Santiago, L. *Int. J. Mass Spectrom.* **2006**, *257*, 60-69.

(120) Molter, A.; Mohr, F. *Coord. Chem. Rev.* **2010**, *254*, 19-45.

(121) Suzuki, K. T.; Sasakura, C.; Yoneda, S. *Biochim. Biophys. Acta* **1998**, *1429*, 102-112.

(122) Fahey, R. C. *Annu. Rev. Microbiol.* **2001**, *55*, 333-356.

(123) Cooper, D. S. *N. Engl. J. Med.* **2005**, *352*, 905-917.

(124) Rai, P.; Cole, T. D.; Wemmer, D. E.; Linn, S. *J. Mol. Biol.* **2001**, *312*, 1089-1101.

(125) Rai, P.; Wemmer, D. E.; Linn, S. *Nucl. Acids Res.* **2005**, *33*, 497-510.

(126) Kimani, M. M.; Brumaghim, J. L.; VanDerveer, D. *Inorg. Chem.* **2010**, *49*, 9200-9211.

(127) Kimani, M. M.; Bayse, C. A.; Brumaghim, J. L. *Dalton Trans.* **2011**, *40*, 3711-3723.

(128) Pierre, J. L.; Fontecave, M. *BioMetals* **1999**, *12*, 195-199.

(129) Kimani, M. M.; Wang, H. C.; Brumaghim, J. L. *Dalton Trans.* **2011**, *41*, 5248-5259.

(130) Opazo, C.; Barria, M. I.; Ruiz, F. H.; Inestrosa, N. C. *BioMetals* **2003**, *16*, 91-98.

(131) Achard-Joris, M.; Moreau, J. L.; Lucas, M.; Baudrimont, M.; Mesmer-Dudons, N.; Gonzalez, P.; Boudou, A.; Bourdineaud, J. P. *Biochimie* **2007**, *89*, 1474-1488.

(132) Wang, H. C.; Riahi, M.; Pothen, J.; Bayse, C. A.; Riggs-Gelasco, P.; Brumaghim, J. L. *Inorg. Chem.* **2011**, *50*, 10893-10900.

(133) Pettit, L. D.; Siddiqui, K. F. *Inorg. Chim. Acta* **1981**, *55*, 87-91.

(134) Ralle, M.; Berry, S. M.; Nilges, M. J.; Gieselman, M. D.; van der Donk, W. A.; Lu, Y.; Blackburn, N. J. *J. Am. Chem. Soc.* **2004**, *126*, 7244-7256.

(135) Siluvai, G. S.; Nakano, M.; Mayfield, M.; Blackburn, N. J. *J. Biol. Inorg. Chem.* **2011**, *16*, 285-297.

(136) Akrivos, P. D. *Coord. Chem. Rev.* **2001**, *213*, 181-210.

(137) Raper, E. S. *Coord. Chem. Rev.* **1985**, *61*, 115-184.

(138) Spicer, M. D.; Reglinski, J. *Eur. J. Inorg. Chem.* **2009**, *12*, 1553-1574.

(139) Stadelman, B. S.; Brumaghim, J. L. In *Biochalcogen Chemistry: The Biological Chemistry of Sulfur, Selenium, and Tellurium*; American Chemical Society: 2013; Vol. 1152, p 33-70.

(140) Williams, D. J.; McKinney, B. J.; Baker, B.; Gwaltney, K. P.; VanDerveer, D. J. *J. Chem. Crystallogr.* **2007**, *37*, 691-694.

(141) Williams, D. J.; Concepcion, J. J.; Koether, M. C.; Arrowood, A. K.; Carmack, A. L.; Hamilton, T. G.; Luck, S. M.; Ndomo, M.; Teel, R. C.; VanDerveer, D. J. *J. Chem. Crystallogr.* **2006**, *36*, 453-457.

(142) Williams, D. J.; White, K. M.; VanDerveer, D. J.; Wilkinson, A. P. *Inorg. Chem. Commun.* **2002**, *5*, 124-126.

(143) Williams, D. J.; Timothy, A. J.; Rice, E. D.; Davis, K. J.; Ritchie, J. A.; Pennington, W. T.; Schimek, G. L. *Acta Crystallogr.* **1997**, *C53*, 837-838.

(144) Lobana, T. S.; Sharma, R.; Butcher, R. J. Z. *Anorg. Allg. Chem.* **2008**, *634*, 1785-1790.

(145) Lobana, T. S.; Sultana, R.; Hundal, G. *Polyhedron* **2008**, *27*, 1008-1016.

(146) Kim, H. R.; Jung, I. G.; Yoo, K.; Jang, K.; Lee, E. S.; Yun, J.; Son, S. U. *Chem. Commun.* **2010**, *46*, 758-760.

(147) Lobana, T. S.; Castineiras, A. *Polyhedron* **2002**, *21*, 1603-1611.

(148) Aslanidis, P.; Hadjikakou, S. K.; Karagiannidis, P.; Cox, P. J. *Inorg. Chim. Acta* **1998**, *271*, 243-247.

(149) Blake, A. J.; Lippolis, V.; Pivetta, T.; Verani, G. *Acta Crystallogr.* **2007**, *63*, 364-367.

(150) Devillanova, F. A.; Diaz, A.; Isaia, F.; Verani, G. *Trans. Metal Chem.* **1989**, *14*, 153-154.

(151) Minoura, M.; Landry, V. K.; Melnick, J. G.; Pang, K.; Marchio, L.; Parkin, G. *Chem. Commun.* **2006**, 3990-3992.

(152) Kimani, M. M.; Bayse, C. A.; Stadelman, B. S.; Brumaghim, J. L. *Inorg. Chem.* **2013**, *52*, 11685-11687.

(153) Bard, A. J.; Faulkner, L. R. In *Electrochemical methods: Fundamentals and applications*; 2nd ed.; Wiley: New York, 2004, p 1-43.

(154) Becke, A. D. *Phys. Rev. A* **1988**, *38*, 3098-3100.

(155) Perdew, J. P. *Phys. Rev. B Condens Matter* **1986**, *33*, 8822-8824.

(156) In *Parallel Quantum Solutions* Fayetteville, AR, n.d.

(157) Hurley, M. M.; Pacios, L. F.; Christiansen, P. A.; Ross, R. B.; Ermler, W. C. *J. Chem. Phys.* **1986**, *84*, 6840-6853.

(158) Couty, M.; Hall, M. B. *J. Comput. Chem.* **1996**, *17*, 1359-1370.

(159) Wadt, W. R.; Hay, P. J. *J. Chem. Phys.* **1985**, *82*, 284-298.

(160) Dunning, T. H. *J. Chem. Phys.* **1971**, *55*, 716-723.

(161) Dunning, T. H. *J. Chem. Phys.* **1970**, *53*, 2823-2833.

CHAPTER TWO

THE RELATIONSHIP BETWEEN ELECTROCHEMICAL PROPERTIES AND METAL COORDINATION FOR SULFUR AND SELENIUM ANTIOXIDANTS

2.1 Introduction

Oxidative damage caused by reactive oxygen species (ROS) has been linked to cancer, neurodegenerative diseases, inflammation, and cardiovascular diseases.[1-5] One of the most prevalent and damaging ROS is $^{\bullet}OH$,[6-9] commonly generated from reduction of H_2O_2 by redox-active transition metals Fe^{II} and Cu^{I} (Reactions 1 and 2).[10-12]

$$Fe^{II} + H_2O_2 \rightarrow Fe^{III} + {}^{-}OH + {}^{\bullet}OH \qquad (1)$$

$$Cu^{I} + H_2O_2 \rightarrow Cu^{II} + {}^{-}OH + {}^{\bullet}OH \qquad (2)$$

Although cells maintain metal homeostasis through various mechanisms, mis-regulation of this homeostasis can occur, resulting in rapid increases in the concentrations of non-protein bound Fe^{II} and Cu^{I}. Infact, one study has reported that neuronal cells can store between 100-1000 μM non-protein bound Fe^{II} and Cu^{I} in cellular compartments.[13] These elevated metal concentrations can lead to a drastic increase in $^{\bullet}OH$ generation,[14-16] and cellular reductants make this reaction to be catalytic by reduction of Fe^{III} and Cu^{II} back to Fe^{II} and Cu^{I}.[17,18] To combat oxidative stress, cells incorporate antioxidant sulfur compounds such as cysteine, methionine, and glutathione to defend against oxidative damage.[19,20] Dietary organosulfur compounds, such as those in garlic, have shown promise for preventing stomach, colorectal, and prostate cancers in clinical trials.[20-23] Methionine is an essential amino acid with ROS scavenging capabilities, and glutathione, one of the most abundant cellular antioxidants, is present in concentrations between 1 and

15,000 μM and is a critical component in the glutathione peroxidase (GPx) antioxidant cycle.[24-26] Cell viability has been linked to the ROS scavenging capability of glutathione in GPx activity.[26]

Measuring the ability of selenium compounds to scavenge H_2O_2 in a manner similar to GPx is a standard method to assess their antioxidant efficacy.[27-29] Ebselen, the most promising and thoroughly studied GPx mimic, clinical trials have shown that it can protect against ischemic brain damage, and it is studied for the treatment of Parkinson's disease.[30-33] However, measuring selenium antioxidant activity based on GPx-like behavior is not without flaws. The greatest difficulty is that GPx activity measurements typically use non-physiological conditions such as acidic solutions[34-36] and that decreased activity can be observed due to unexpected thiol exchanges.[28,37,38] Additionally, H_2O_2 is a longer-lived and less reactive ROS compared to $^{\bullet}OH$ and is relatively harmless in metal-free environments.[11,12,39] Due to the extreme reactivity of hydroxyl radical, greater oxidative DNA damage prevention may occur from preventing metal-mediated $^{\bullet}OH$ formation or by reducing DNA damage from metal-generated $^{\bullet}OH$ rather than scavenging H_2O_2.[40] This prevention of hydroxyl radical generation or release could be accomplished by direct metal coordination of the selenium or sulfur antioxidant.

Interest in selenium antioxidant properties has also increased over the years due to the link between selenium deficiency and Keshan disease,[41] Kashin-Beck disease,[42,43] cancer,[44-48] and pulmonary tuberculosis.[49] The anticancer properties of selenium were the primary interest in two clinical trials with conflicting results. The Nutritional Prevention of Cancer (NPC) reported a 63 % decrease in prostate cancer incidence upon selenium-

enriched yeast supplementation (200 µg/day).[50] In contrast, the Selenium and Vitamin E Cancer Prevention Trial (SELECT) reported no decrease in prostate cancer incidence upon administering the same amount of selenium supplement.[51,52] The NPC trial used selenium-enriched yeast comprised of multiple selenium species, whereas the SELECT trial used only selenomethionine, the major selenium species in selenium-enriched yeast.[53,54] The difference in the outcomes of these trials indicates that it is not sufficient to simply supplement with selenium; understanding selenium antioxidant mechanisms is critical to identify effective selenium supplements for successful clinical trials.

Studies have suggested that copper-glutathione binding may reduce the cellular toxicity of copper.[55,56] In addition, gel electrophoresis studies by the Brumaghim group have shown the ability of several sulfur antioxidants (Figure 2.1) to effectively prevent Cu^{I}-mediated DNA damage from $^{\bullet}OH$ under physiological conditions.[20] None of these sulfur compounds, however, inhibit DNA damage when $[Cu(bipy)_2]^{I}$ (bipy =

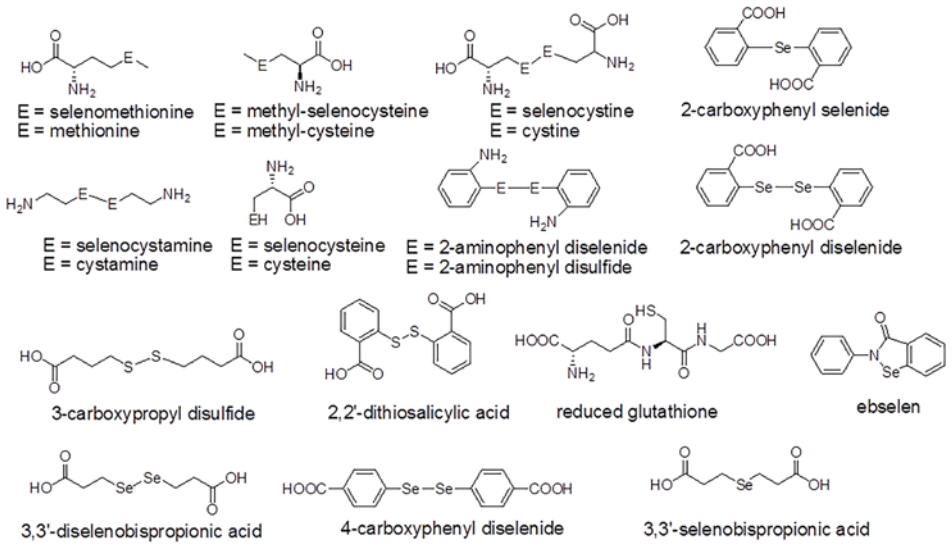

Figure 2.1. Structures of sulfur and selenium compounds discussed in Chapter 2.

2,2'-bipyridine) is substituted for unchelated Cu^{I}. The presence of the bipy ligands effectively prevents sulfur antioxidant binding to Cu^{I} and subsequent DNA damage inhibition, suggesting that metal coordination is necessary for the antioxidant abilities of these sulfur compounds.[20] These sulfur compounds much more effectively prevent copper-mediated DNA damage than that caused by iron; only oxidized glutathione, reduced glutathione, and 3-carboxypropyl disulfide prevent Fe^{II}-mediated DNA damage.[20]

Similar gel electrophoresis studies with the selenium compounds in Figure 2.1 revealed that selenocystine, methyl-selenocysteine, selenomethionine, and selenocystamine prevent Cu^{I}-mediated DNA damage and that this activity is significantly different from their measured abilities for scavenging H_2O_2 in a GPx-like mechanism.[11] In contrast to their sulfur analogs, 3,3'-diselenobispropionic acid, selenocystamine, methyl-selenocysteine, and 3,3'-selenobispropionic acid also prevent Fe^{II}-mediated DNA damage, but 3,3-diselenobispropionic acid and 3,3'-selenobispropionic acid exhibit no GPx-like activity.[11] Thus, H_2O_2 scavenging is not an accurate method for measuring selenium this antioxidant activity and is not a primary mechanism for metal-mediated DNA damage prevention.

Metal coordination is a separate mechanism from the traditional ROS scavenging mechanisms, and it has recently been the focus of many studies on the antioxidant abilities of sulfur and selenium compounds. Figure 2.2 compares the two accepted scavenging mechanisms, GPx-like activity (A) and direct ROS scavenging (B). Alternatively, metal binding to sulfur and selenium antioxidants could prevent oxidative

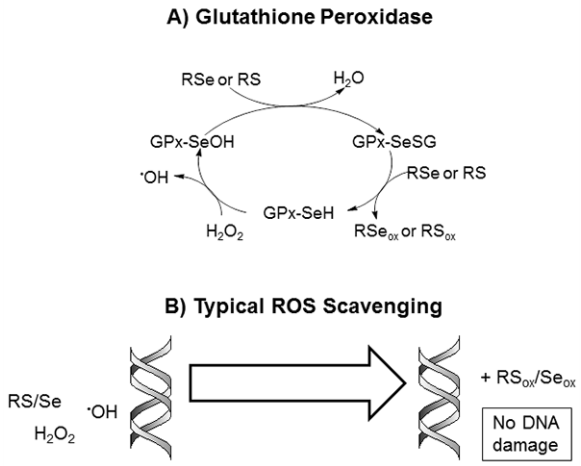

Figure 2.2. Proposed ROS scavenging mechanisms of sulfur and selenium compounds without metal ions. A) Glutathione peroxidase (GPx)-like cycle for H_2O_2 scavenging by selenium compounds. B) The typical ROS scavenging mechanism assumed for sulfur and selenium compounds.

damage by the targeted scavenging of H_2O_2 or $^{\bullet}OH$ at the site of generation (Figure 2.3). Since $^{\bullet}OH$ is a strong oxidizing agent, investigating the electrochemical properties of the compounds in Figure 2.1 will shed light on the ability of sulfur and selenium compounds to undergo oxidation, indicating possible ROS scavenging ability. Mass spectrometry studies with Cu^{I} and Fe^{II} will indicate metal coordination ability, and the capability to prevent oxidative damage through a targeted scavenging mechanism. The results of the studies with the selenium antioxidants (Figure 2.1) presented in this Chapter are published in Battin, E. E.; Zimmerman, M. T.; Ramoutar, R. R.; Quarles, C. E.; Brumaghim, J. L. *Metallomics* **2011**, 3, 503-512 (reproduced by permission of The Royal

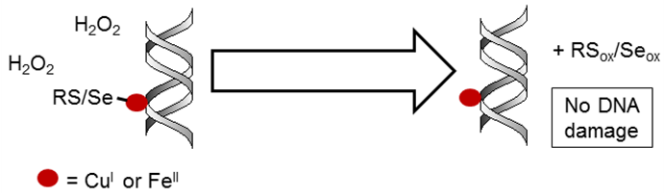

Figure 2.3. Metal coordination mechanism for sulfur and selenium compounds targeting H_2O_2, preventing metal oxidation and the generation of $^{\bullet}OH$.

Society of Chemistry http://pubs.rsc.org/en/content/articlepdf/2011/mt/c0mt00063a; Appendix A) and results of the sulfur compound studies were obtained in collaboration with Dr. Carolyn E. Quarles and Prof. Ria R. Ramoutar.

2.2 Results and Discussion

2.2.1. Electrochemistry of selenium compounds. To determine whether a correlation exists between selenium antioxidant activity and electrochemistry of the selenium compounds (Figure 2.1), cyclic voltammetry (CV; Figures 2.4 and 2.5) experiments were conducted in aqueous buffer at pH 7. Differential pulse voltammetry (DPV) experiments were also conducted to confirm the presence of any weak redox waves in the CV studies (Figures 2.8-2.11 in the Experimental Methods section).

Because hydroxyl radical is a strong oxidant, one might expect to observe high oxidation potentials for the most effective selenium antioxidants if hydroxyl radical scavenging is a major antioxidant mechanism. Only three of the ten selenium compounds have measureable $E_{1/2}$ values using a glassy carbon working electrode: selenocystamine (-329 mV), 2-carboxyphenyl diselenide (535 mV), and 2-aminophenyl diselenide (with two redox potentials at 308 and -429 mV; Table 2.1). In contrast, selenomethionine, 2-carboxyphenyl selenide, 3,3'-diselenobispropionic acid, and selenocystine show only a single oxidation wave, whereas 3,3'-selenobispropionic acid, 4-carboxyphenyl diselenide, and methyl-selenocysteine exhibit no electrochemical activity between -1000 mV and 1000 mV.

In contrast, Bai *et al.*[57] observed two anodic waves for selenocystine at 810 mV and ~1200 mV vs. Ag/AgCl as well as two anodic waves for selenomethionine at ~640 mV and 1100 mV. This discrepancy is likely due to the difference in both the pH and choice of working electrode; Bai and coworkers reported these potentials at pH 3.9 using a gold working electrode. Many electrochemical studies of selenium antioxidants have been performed with either mercury or gold electrodes;[57,58] however, both mercury[59] and gold[60] can form selenium complexes. As a result, the observed electrochemical behavior may be of the metal complex between the selenium compound and the electrode rather than the selenium compound alone.

Selenocystine, an antioxidant containing both amine and carboxylate functionalities, has a single irreversible anodic wave at -115 mV, whereas the amine-functionalized selenocystamine

Table 2.1. Electrochemical properties of selenium compounds versus normal hydrogen electrode (NHE).

Compound	E_{p_a} **(mV)**	E_{p_c} **(mV)**	ΔE**(mV)**	$E_{1/2}$ **(mV)**
Selenomethionine	693	—	—	—
Selenocystine	-115	—	—	—
Methyl-selenocysteine	—	—	—	—
Selenocystamine	-131	-526	394	-329
2-Aminophenyl diselenide	593, 120	24, -978	569, 1099	308, -429
2-Carboxyphenyl diselenide	501	569	67	535
2-Carboxyphenyl selenide	832	—	—	—
4-Carboxyphenyl diselenide	—	—	—	—
3,3'-Diselenobispropionic acid	907	—	—	—
3,3'-Selenobispropionic acid	—	—	—	—

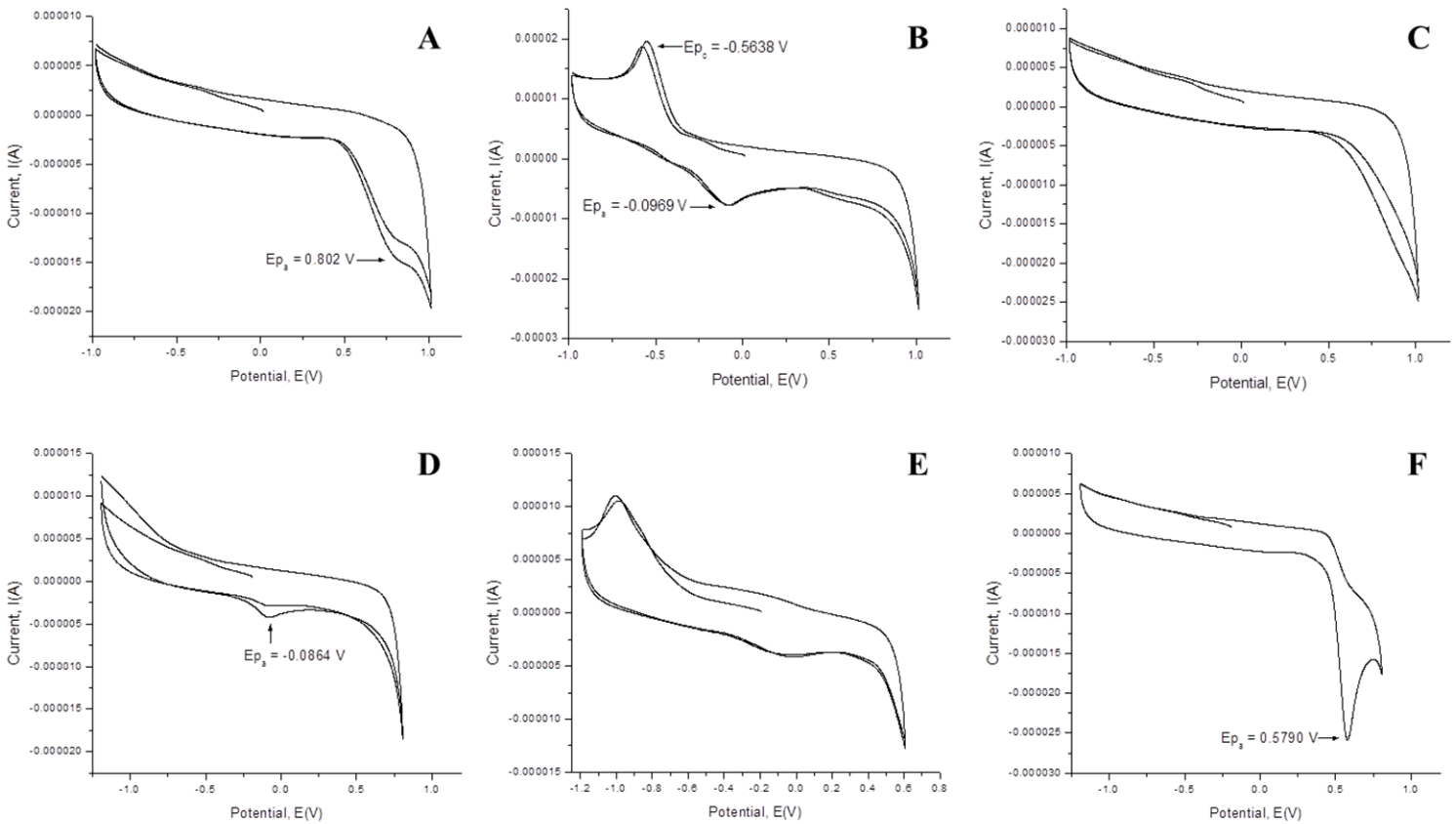

Figure 2.4. Cyclic voltammograms for A) selenomethionine, B) selenocystamine, C) methyl-selenocysteine, D) selenocystine, E) 2-aminophenyl diselenide, and F) 2-carboxyphenyl diselenide in MOPS buffer (10 mM, pH = 7.0) containing KNO_3 (10 mM) as a supporting electrolyte. Selenium compounds (300 µM) were cycled between -1000 mV and 1000 mV ($2APSe_2$ was cycled between -1200 mV and 800 mV) vs. NHE at a scan rate of 100 mV/s.

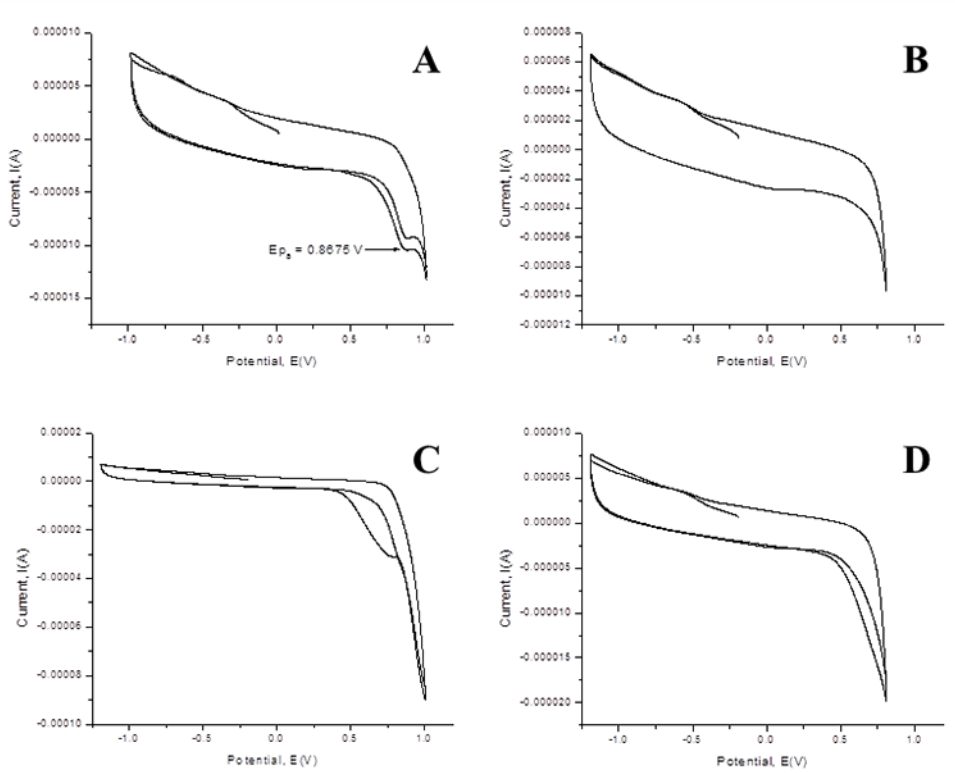

Figure 2.5. Cyclic voltammograms for A) 2-carboxyphenyl selenide, B) 4-carboxyphenyl diselenide, C) 3,3'-diselenobispropionic acid, and D) 3,3'-selenobispropionic acid in MOPS buffer (10 mM, pH =7.0) containing KNO_3 (10 mM) as a supporting electrolyte. Selenium compounds (300 µM) were cycled between -1000 mV and 1000 mV vs. NHE at a scan rate of 100 mV/s.

exhibits quasi-reversible behavior with a similar redox potential of -329 mV. In contrast, the similar amino acids selenomethionine and methyl-selenocysteine show very different electrochemical behavior; selenocystine has a single anodic wave at 693 mV, and methyl-selenocysteine exhibits no electrochemical behavior. These electrochemical differences are surprising, since selenomethionine and methyl-selenocysteine differ only by one methylene group.

The results of our DNA damage assays (Tables 2.2 and 2.3) do not correlate with the observed electrochemistry of the selenium compounds (Table 2.1). Selenocystine, the most effective selenium compound for preventing Cu^{I}-mediated DNA damage, exhibits the ability to undergo oxidation but lacked any activity towards Fe^{II}-, $[Fe(EDTA)]^{2-}$, and $[Cu(bipy)_2]^{+}$-

Table 2.2. IC_{50} values and mass spectrometry data for the tested selenium compounds with Cu^I, as well as GPx-like activity measurements.

Compound	Cu^I IC_{50} (μM)[a]	*m/z* (Da)	Cu^I : Se compound	Relative GPx Activity[b]
Selenocystine	3.34 ± 0.08[c]	397.8, 731.6	1:1, 1:2	4.5
Methyl-selenocysteine	8.64 ± 0.02	247.8, 427.8, 598.1	1:1, 1:2, 1:3	0.7
Selenomethionine	25.10 ± 0.01[c]	261.9, 456.9, 650.9	1:1, 1:2, 1:3	0.6
Selenocystamine	59 ± 3 % (1000 μM)[c]	—	—	8.8
2-Aminophenyl diselenide	—	—	—	6.4
2-Carboxyphenyl diselenide	—	466.9	1:1	~ 0
2-Carboxyphenyl selenide	—	383.9	1:1[d]	~ 0
4-Carboxyphenyl diselenide	—	466.9	1:1	~ 0
3,3'-Diselenobis(propionic acid)	—	370.6, 673.4	1:1, 1:2	~ 0
3,3'-Selenobis(propionic acid)	—	290.7, 515.6	1:1, 1:2	~ 0

[a]IC_{50} is defined as the concentration at which the compound inhibits 50% of DNA damage. [b]GPx relative activity values are reported relative to ebselen in methanol. [c]Values from reference 61. [d]ESI mass spectrometry voltage of 5500 V.

Table 2.3. IC_{50} values, and mass spectrometry data for the tested selenium compounds with Fe^{II}.

Compound	Fe^{II} IC_{50} (μM)[a]	*m/z* (Da)	Fe^{II} : Se compound
3,3'-Diselenobispropionic acid	~ 75[b]	360.6, 664.4	1:1, 1:2
Selenocystamine	121.4 ± 0.3	415.1	1:3
Methyl-selenocysteine	378.4 ± 0.1	239.1, 420.8, 601.8	1:1, 1:2, 1:3
3,3'-Selenobispropionic acid	42 ± 8% inhibition (1000 μM)	288.7, 506.6	1:1, 1:2
Selenocystine	—	390.8, 724.7, 1058.2	1:1, 1:2, 1:3
2-Aminophenyl diselenide	—	404.8	1:1[c]
2-Carboxyphenyl diselenide	—	465.7	1:1[c]
2-Carboxyphenyl selenide	—	376.9, 696.7	1:1, 1:2[c]
4-Carboxyphenyl diselenide	—	455.1	1:1
Selenomethionine	—	448.9, 643.9	1:2, 1:3

[a]IC_{50} is defined as the concentration at which the compound inhibited 50% of DNA damage. [b]Estimated value. [c]ESI mass spectrometry voltage of 5500 V.

mediated DNA damage.[61] Similarly, selenomethionine inhibits Cu^I-mediated DNA damage[61] and shows only an oxidation potential. Methyl-selenocysteine inhibits both Cu^I- and Fe^{II}-mediated DNA damage, but exhibits no electrochemical activity. 3,3'-Diselenobispropionic acid undergoes only oxidation and inhibits Fe^{II}-mediated DNA damage, whereas the analogous selenide 3,3'-selenobispropionic acid also inhibits Fe^{II}-mediated DNA damage, but has no observable electrochemical behavior. Both 2-carboxyphenyl selenide and 2-carboxyphenyl diselenide also differ by a single selenium atom, but 2-carboxyphenyl diselenide undergoes both oxidation and reduction, whereas 2-carboxyphenyl selenide exhibits only an oxidation potential. Despite their high oxidation potentials, neither 2-carboxyphenyl diselenide or 2-carboxyphenyl selenide inhibit Cu^I- or Fe^{II}-mediated DNA damage. Since no correlation is observed between

oxidation potential and DNA damage prevention, direct ROS scavenging is likely not a major mechanism for the observed antioxidant activity.

2.2.2. Electrochemistry of sulfur compounds. Similar electrochemical studies, both CV and DPV, were conducted on all the sulfur compounds in Figure 2.1 (except oxidized glutathione and 2-aminophenyl disulfide) in aqueous buffer at pH 7. Of the eight compounds investigated, only methionine and cystine show redox activity; methionine exhibits only a single irreversible anodic wave at -244 mV, and cystine exhibits a quasi-reversible redox couple with an $E_{1/2}$ value of 580 mV (Table 2.4). All cyclic voltammograms are provided in Figures 2.6, and DPV scans for methionine and cysteine are provided in Figure 2.7.

The electrochemical results for these sulfur compounds do not correlate with previous DNA damage prevention gel electrophoresis studies (Table 2.5). Cystine exhibited the lowest IC_{50} value for prevention of Cu^{I}-mediated DNA damage (3.4 μM), and undergoes both oxidation and reduction. In contrast, methyl-cysteine, reduced glutathione, and oxidized glutathione prevent Cu^{I}-mediated DNA damage (IC_{50} values of 9.6, 12.4, and 6.6 μM, respectively), but exhibit no redox activity under these conditions. In addition, cystamine, 2,2'-dithiosalicylic acid, and 3-carboxypropyl disulfide have no redox activity and did not prevent Cu^{I}-mediated DNA damage. Similarly, both reduced

Table 2.4. Electrochemical properties of sulfur compounds versus normal hydrogen electrode (NHE).

Compound	Ep_a (mV)	Ep_c (mV)	ΔE(mV)	$E_{1/2}$ (mV)
Methionine	-244[a]	—	—	—
Cystine	428[a]	617[a]	75[a]	580[a]
Cysteine	—	—	—	—
Methyl-cysteine	—	—	—	—
Reduced glutathione	—	—	—	—
Cystamine	—	—	—	—
3-Carboxypropyl disulfide	—	—	—	—
2,2'-Dithiosalicylic acid	—	—	—	—

[a] Potentials from DPV scans.

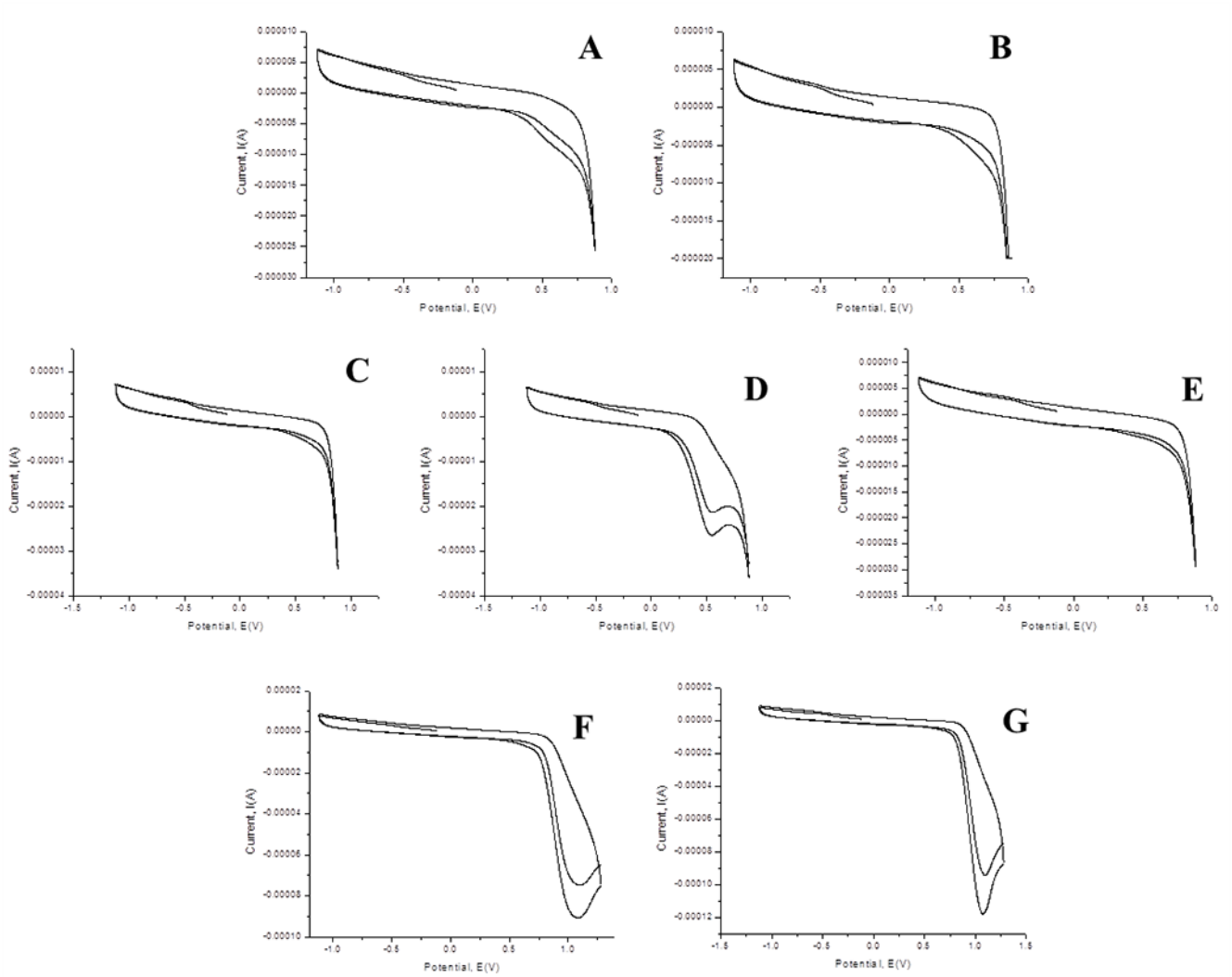

Figure 2.6. Cyclic voltammograms for A) reduced glutathione, B) methionine, C) methyl-cysteine, D) cystine, E) cystamine, F) 22'-dithiosalicylic acid, and G) 3-carboxypropyl disulfide in MOPS buffer (10 mM, pH = 7.0) containing KNO_3 (10 mM) as a supporting electrolyte. Sulfur compounds (300 µM) were cycled between -1000 mV and 1000 mV vs. NHE, and a scan rate of 100 mV/s.

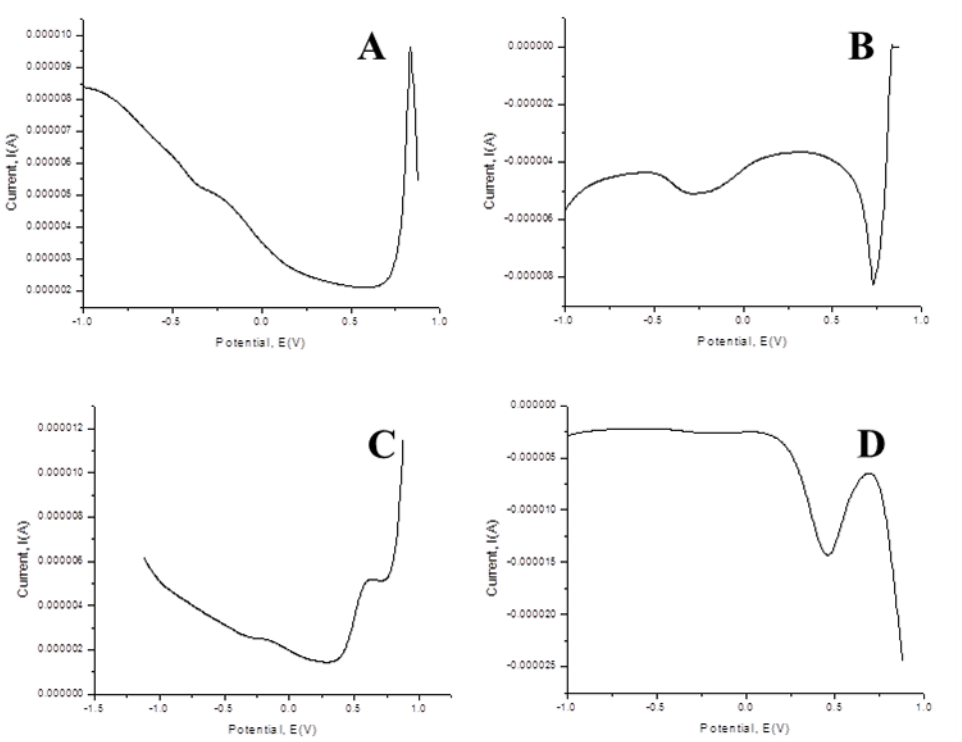

Figure 2.7. Differential pulse voltammograms of A) negative scan of methionine, B) positive scan of methionine, C) negative scan of cystine, and D) positive scan of cysteine. in MOPS buffer (10 mM, pH = 7.0) containing KNO_3 (10 mM) as a supporting electrolyte. Sulfur compounds (300 µM) were scanned between -1000 mV and 1000 mV vs. NHE.

and oxidized glutathione prevented Fe^{II}-mediated DNA damage, but exhibited no redox activity. Since no correlation exists between metal-mediated DNA damage prevention and the redox activities of these sulfur compounds, direct ROS scavenging is likely not a major antioxidant mechanism.

2.2.3. Mass spectrometry evidence for metal coordination to selenium antioxidants. Electrospray ionization mass spectroscopy (ESI-MS) was used to examine Cu^{I} and Fe^{II} coordination of the selenium compounds in Figure 2.1. Most selenium compounds form 1:1 and 1:2 (Cu:ligand) complexes with Cu^{I}, except for 2-aminophenyl diselenide, which forms only a 1:1 complex, and selenocystamine, which shows no coordination (Table 2.2). Both selenomethionine and

Table 2.5. IC_{50} values and mass spectrometry data for the tested sulfur compounds with Cu^{I} and Fe^{II}.

Compound	**Cu^{I} IC_{50} (µM)[a]**	***m/z* (Da)[b]**	**Cu^{I} : S compound**	**Fe^{II} IC_{50} (µM)[a]**	***m/z* (Da)[b]**	**Fe^{II} : S compound**
Oxidized glutathione	6.82 ± 0.03[c]	674.0	1:1	10,372 ± 2[c]	667.0	1:1
Reduced glutathione	12.98 ± 0.01[c]	369.0, 674.0	1:1, 1:2	23 ± 8 % (10,000 µM)[c]	362.0	1:1
Cystine	3.34 ± 0.07[c]	302.9	1:1	—	294.9	1:1
Cysteine	7.6 ± 1.2[c]	302.9	1:2	—	175.9, 296.9, 415.2	1:1, 1:2, 1:3
Methyl-cysteine	10.02 ± 0.02[c]	198.0	1:1	—	190.0, 325.0	1:1, 1:2
Methionine	11.02 ± 0.02[c]	212.0	1:1	—	—	—
Cystamine	—	—	—	—	—	—
3-Carboxypropyl disulfide	—	—	—	22 ± 6 % (1000 µM)[c]	—	—
2-Aminophenyl disulfide	—	—	—	—	—	—
2,2'-Dithiosalicylic acid	—	—	—	—	360.9	1:1

[a]IC_{50} is defined as the concentration at which the compound inhibited 50% of DNA damage. [b]ESI mass spectrometry voltage of 5500 V. [c]Values from reference 20.

methyl-selenocysteine also form complexes with Cu^{I} in a 1:3 ratio.

Because Cu^{I} typically adopts tetrahedral coordination geometry, it is probable that many of these selenium compounds bind Cu^{I} through the selenium atom, as well as through the amine nitrogen and/or carboxylate oxygen atom(s), similar to the geometry found for Cu^{I} methyl-selenocystine and selenomethionine complexes.[62] Since the majority of selenium compounds show metal coordination regardless of antioxidant activity, these results indicate that metal coordination is necessary but not sufficient for prevention of copper-mediated DNA damage.

Similar mass spectrometry studies with Fe^{II} reveal iron binding to all of tested selenium compounds (Table 2.3). Both 1:1 and 1:2 stoichiometries (Fe:ligand) are observed for all compounds except 4-carboxyphenyl diselenide, which binds in only a 1:1 ratio, and selenocystamine, which binds in only a 1:3 ratio. A 1:3 coordination ratio was also observed for selenomethionine, selenocystine, and methyl-selenocysteine. Again, all the selenium compounds coordinate Fe^{II}, regardless of antioxidant activity, indicating that iron coordination is necessary but not sufficient for the observed DNA damage prevention. Metal-antioxidant binding may prevent DNA damage by either altering the redox potential of the metal ion and preventing H_2O_2 reduction to $^{\bullet}OH$ or preventing Cu^{II} and Fe^{III} reduction by cellular reductants.[63] Alternatively, the metal-bound selenium antioxidant may be poised to efficiently scavenge $^{\bullet}OH$ immediately upon formation at the metal center before it is released (targeted scavenging mechanism in Figure 2.3).

2.2.4. Mass spectrometry evidence for metal coordination to sulfur antioxidants. Similar mass spectrometry studies were conducted on the sulfur compounds to determine their ability to coordinate Cu^{I} and Fe^{II}. Of the ten compounds investigated, five formed either 1:1 or 1:2 (Cu^{I} : ligand) complexes, and five exhibited no metal coordination under the conditions investigated

(Table 2.5). Due to the similar chemical properties of sulfur and selenium, these sulfur amino acid compounds will likely bind through the sulfur atom, in addition to the amine nitrogen or carboxylate oxygen to adopt the stable tetrahedral geometry typical for Cu^{I}. Similar coordination to Ag^{I} has previously been observed with methyl-cysteine and methionine.[64] Since all of the compounds inhibit Cu^{I}-mediated DNA damage also coordinate Cu^{I}, metal coordination is required for this antioxidant activity. The necessity for Cu^{I} coordination is further supported by the lack of DNA damage prevention by the sulfur compounds when $[Cu(bipy)_2]^{+}$ is used in place of unchelated Cu^{I} to damage DNA.

Similar studies with Fe^{II} revealed the ability of most sulfur amino acid compounds to coordinate Fe^{II} regardless of antioxidant activity. Molar ratios of 1:1 (Fe:ligand) are observed for cysteine, cystine, methyl-cysteine, 2,2'-dithiosalicylic acid, reduced glutathione, and oxidize glutathione (Table 2.5); and the thiols cystine and reduced glutathione also form 1:2 complexes. Methionine, cystamine, 2-aminophenyl disulfide, and 3-carboxypropyl disulfide show no Fe^{II} coordination under our experimental conditions. Of the sulfur compounds investigated, only oxidized glutathione prevented Fe^{II}-mediated DNA damage and exhibited Fe^{II} coordination. Since the majority of the sulfur compounds coordinate Fe^{II} but do not prevent iron-mediated DNA damage, these studies suggest that metal coordination alone is not sufficient for antioxidant activity of both sulfur and selenium compounds.

2.3. Conclusions

Sulfur and selenium compounds exhibit the ability to prevent metal-mediated oxidative DNA damage with IC_{50} values between 3.34-1000 μM with Cu^{I}, and 75-10,300 μM with Fe^{II}. This ability to prevent DNA damage does not correlate with electrochemical properties of these

compounds, suggesting that typical ROS scavenging (Figure 2.2) is not the primary mechanism for prevention of metal-mediated DNA damage. Similarly, mass spectrometry studies revealed that the majority of sulfur and selenium compounds coordinate to Cu^{I} and Fe^{II}, regardless of antioxidant activity. Thus, metal binding alone is not sufficient to prevent metal-mediated oxidative DNA damage. These results illustrate the complex nature of sulfur and selenium antioxidant mechanisms and that further investigations must be completed to understand the chemical properties required for effective antioxidant activity. This knowledge will be invaluable for the future development of effective sulfur and selenium compounds and their testing in animal and human trials to treat the wide array of diseases linked to oxidative stress.

2.4. Experimental and Methods

Materials. Water was deionized (diH_2O) using a Nano Pure DIamond Ultrapure H_2O system (Barnstead International). $CuSO_4$ was purchased from Fisher. Selenocystamine, and selenocystine were purchased from Sigma-Aldrich; 3-(*N*-morpholino)propanesulfonic acid (MOPS), selenomethionine, 2-aminophenyl diselenide, and methyl-selenocysteine were obtained from Acros. $FeSO_4$ was purchased from Alfa Aesar. 2-Carboxyphenyl selenide, 2-carboxyphenyl diselenide, and 4-carboxyphenyl diselenide were purchased from Focus. Ascorbic acid was obtained from J. T. Baker.

Mass spectroscopy measurements. Electrospray ionization (ESI) mass spectra were obtained using the QSTAR XL Hybrid MS/MS System (Applied Biosystems), with direct injection of the sample (flow rate = 0.05 mL/min) into the Turbo Ionspray ionization source. Samples were run under positive mode, with an ionspray voltage of 3000 V (except as otherwise indicated) in time-of-flight scan mode (error ± 2 *m/z*). Mass spectrometry samples for a 1:3

metal to ligand ratio were prepared by combining $CuSO_4$ (75 μM) and ascorbic acid (94 μM) in methanol/water, and allowed to stand for 3 min at room temperature. The selenium or sulfur compounds (225 μM) were added to the solution to obtain a final volume of 1 mL, and allowed to stand for 5 min at room temperature. A similar procedure was followed for studies with Fe^{II}, combining $FeSO_4$ (75 μM) and the selenium/sulfur compounds (225 μM), for a 1:3 metal to ligand ratio. All concentrations indicated are the final concentrations in a 1 μL volume. All reported *m/z* peak envelopes matched theoretical peak envelopes for the assigned complexes.

Electrochemical measurements. Electrochemical experiments were conducted on CH Electrochemical Analyzer (CH Instruments, Inc.). Cyclic voltammetry samples were prepared by dissolving the selenium or sulfur compounds (300 μM) in MOPS buffer (10 mM, pH 7) with KNO_3 (10 mM) as a supporting electrolyte. Solutions were degassed for 5 min with N_2 before each experiment. All CV experiments were conducted at 100 mV/s. For differential pulse voltammetry experiments (Figures 2.8-2.11), a pulse amplitude of 0.080 V, a pulse width of 0.100, a sample width of 0.045, and a pulse period of 0.200 were used. Samples of each compound were cycled between -1000 mV and 1000 mV ($2APSe_2$ was cycled between -1200 mV and 800 mV) using a glassy carbon working electrode, a Pt counter electrode, and a Ag/AgCl (197 mV vs. NHE[65]) reference electrode.

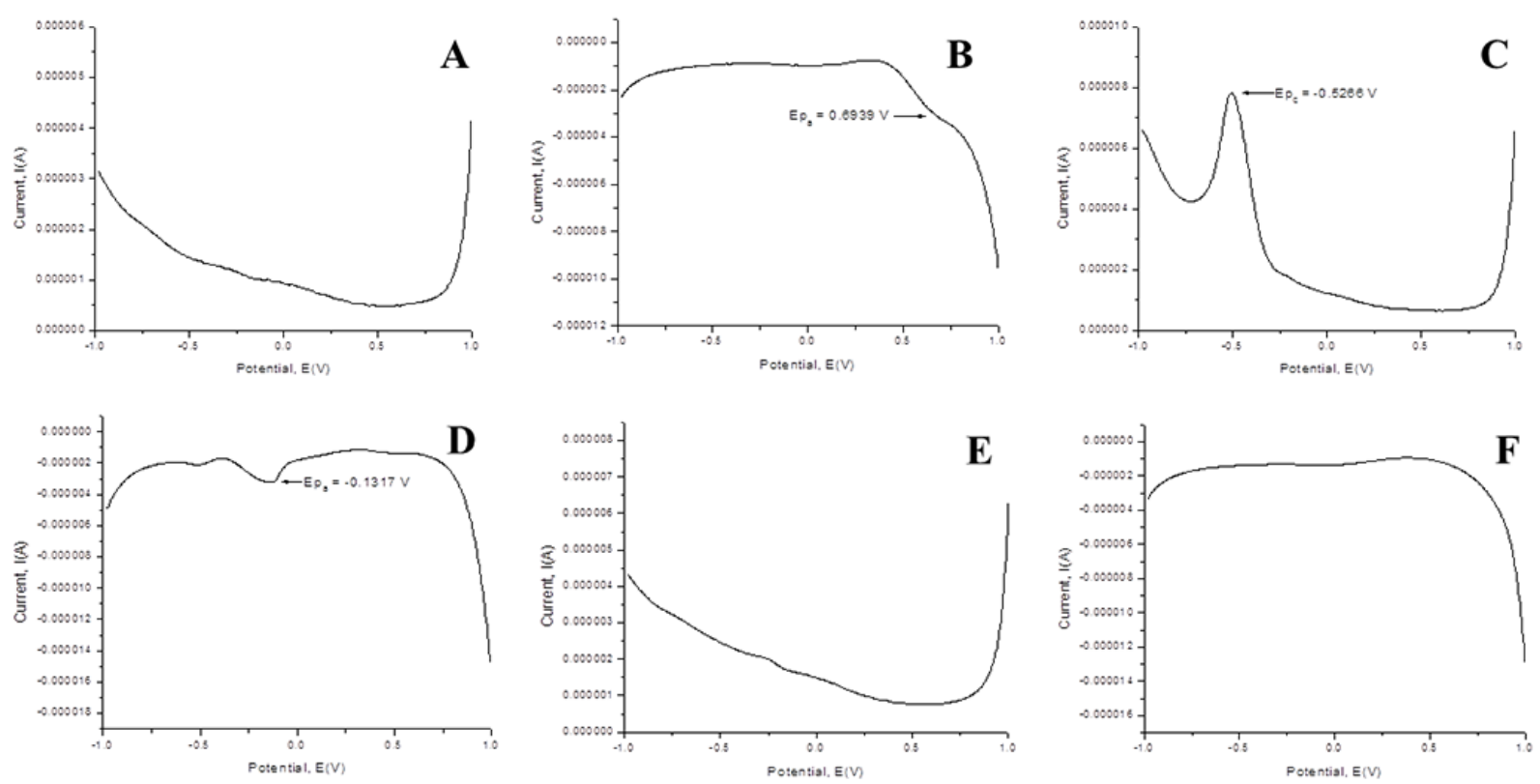

Figure 2.8. Differential pulse voltammetry scans for A) positive scan of selenomethionine, B) negative scan of selenomethionine, C) positive scan of selenocystamine, D) negative scan of selenocystamine, E) negative scan of methyl-selenocysteine, and D) positive scan of methyl-selenocysteine in MOPS buffer (10 mM, pH 7.0) containing KNO_3 (10 mM) as a supporting electrolyte. Selenium compounds (300 µM) were cycled between -1000 mV and 1000 mV vs NHE, using a pulse width of 0.100, a sample width of 0.045, and a pulse period of 0.200.

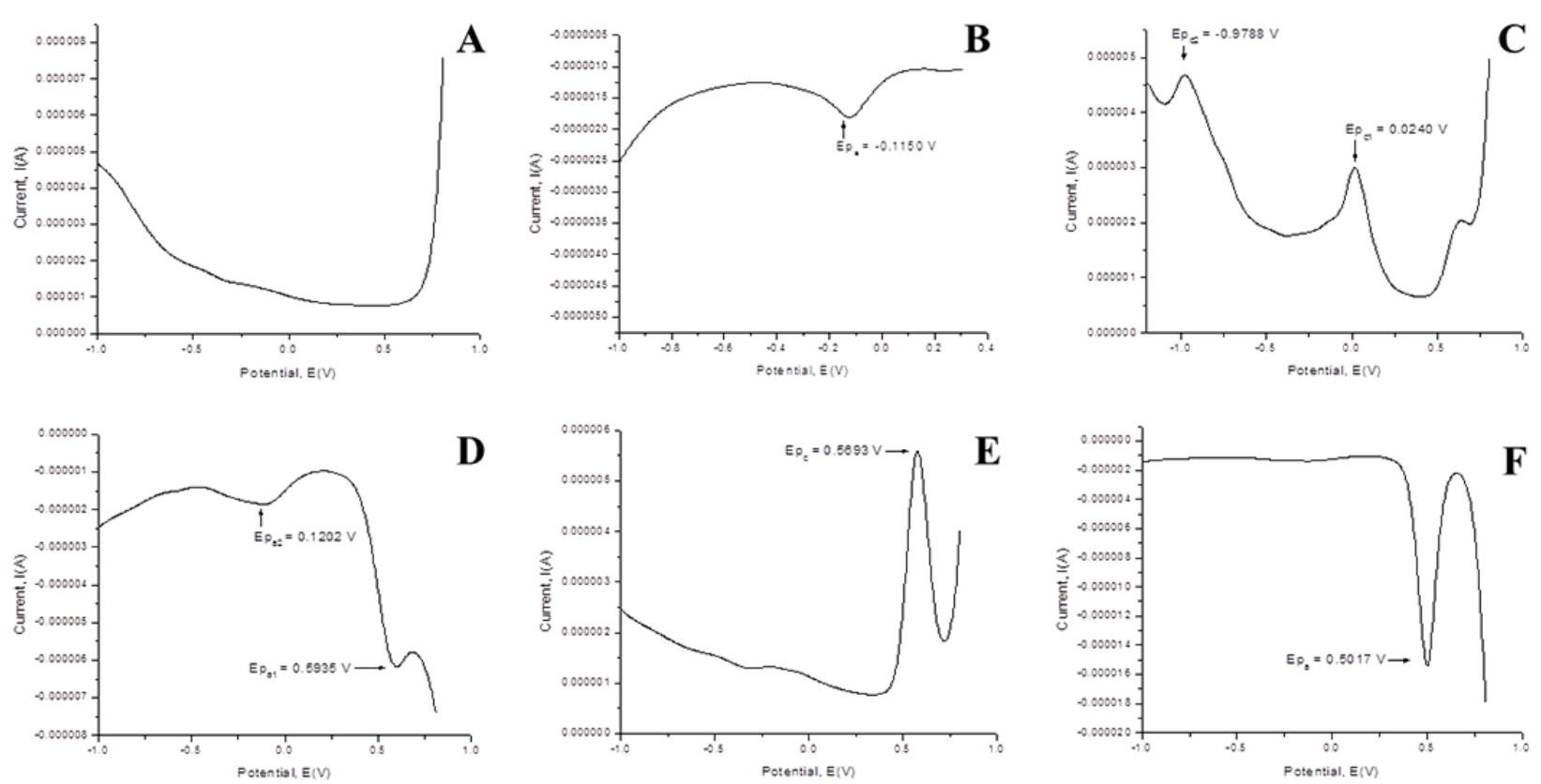

Figure 2.9. Differential pulse voltammetry scans for A) positive scan of selenocystine, B) negative scan of selenocystine, C) positive scan of 2-aminophenyl diselenide, D) negative scan of 2-aminophenyl diselenide, E) negative scan of 2-carboxyphenyl diselenide, and D) positive scan of 2-carboxyphenyl diselenide in MOPS buffer (10 mM, pH 7.0) containing KNO_3 (10 mM) as a supporting electrolyte. Selenium compounds (300 µM) were cycled between -1000 mV and 1000 mV vs. NHE, using a pulse width of 0.100, a sample width of 0.045, and a pulse period of 0.200.

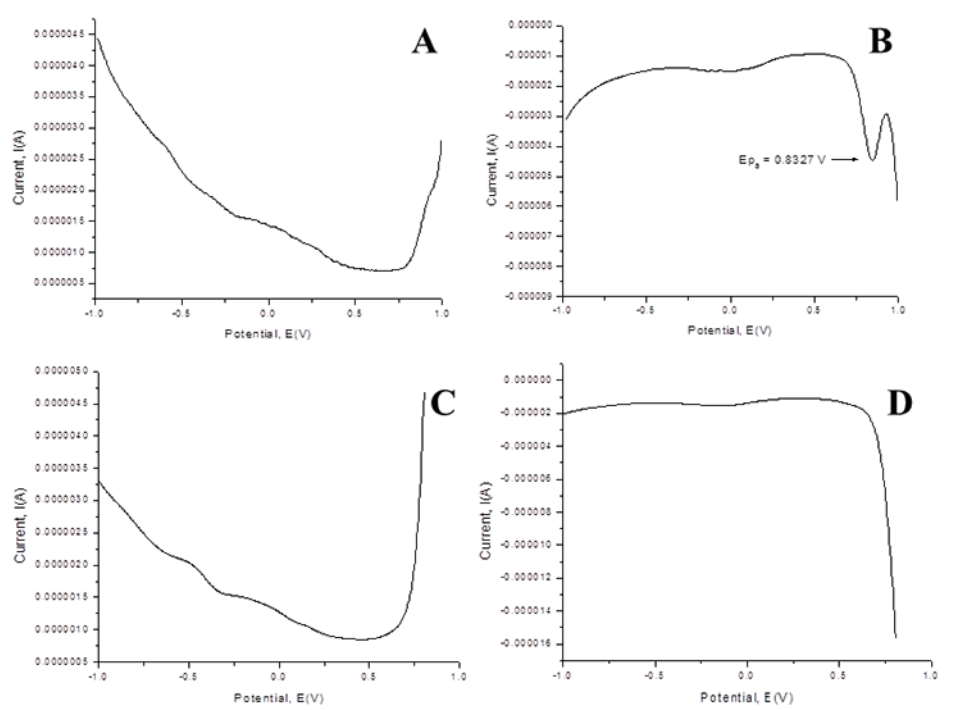

Figure 2.10. Differential pulse voltammetry scans for A) positive scan of 2-carboxylphenyl selenide, B) negative scan of 2-carboxyphenyl selenide, C) positive scan of 4-carboxyphenyl diselenide, and D) negative scan of 4-carboxyphenyl diselenide in MOPS buffer (10 mM, pH 7.0) containing KNO_3 (10 mM) as a supporting electrolyte. Selenium compounds (300 µM) were cycled between -1000 mV and 1000 mV vs. NHE, using a pulse width of 0.100, a sample width of 0.045, and a pulse period of 0.200.

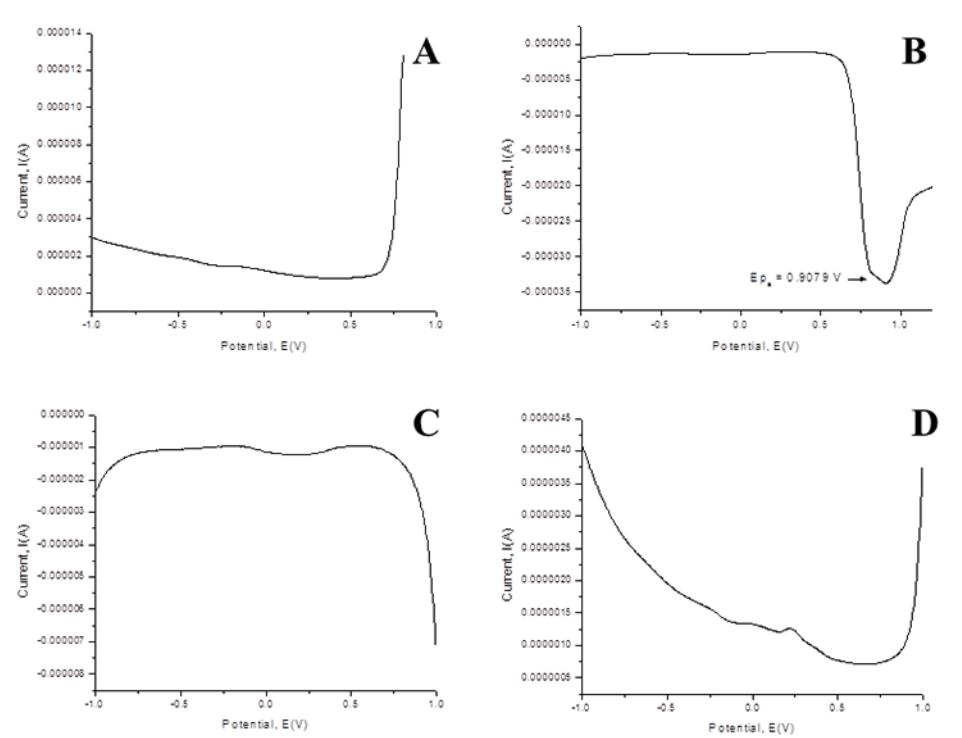

Figure 2.11. Differential pulse voltammetry scans for A) positive scan of 3,3'-diselenobispropionic acid, B) negative scan of 3,3'-diselenobispropionic acid, C) positive scan of 3,3'-selenobispropionic acid, and D) negative scan of 3'3'-selenobispropionic acid in MOPS buffer (10 mM, pH 7.0) containing KNO_3 (10 mM) as a supporting electrolyte. Selenium compounds (300 µM) were cycled between -1000 mV and 1000 mV vs. NHE, a pulse width of 0.100 , a sample width of 0.045, and a pulse period of 0.200 were used.

2.5. References

(1) Brewer, G. J. *Exp. Biol. Med.* **2007**, *232*, 323-335.

(2) Collins, C. A.; Fry, F. H.; Holme, A. L.; Yiakouvaki, A.; Al-Qenaei, A.; Pourzand, C.; Jacob, C. *Org. Biomol. Chem.* **2005**, *3*, 1541-1546.

(3) De Flora, S.; Izzotti, A. *Mutat. Res.* **2007**, *621*, 5-17.

(4) Fry, F. H.; Holme, A. L.; Giles, N. M.; Giles, G. I.; Collins, C.; Holt, K.; Pariagh, S.; Gelbrich, T.; Hursthouse, M. B.; Gutowski, N. J.; Jacob, C. *Org. Biomol. Chem.* **2005**, *3*, 2579-2587.

(5) Loft, S.; Deng, X. S.; Tuo, J.; Wellejus, A.; Sorensen, M.; Poulsen, H. E. *Free Radic. Res.* **1998**, *29*, 525-539.

(6) Henle, E. S.; Han, Z.; Tang, N.; Rai, P.; Luo, Y.; Linn, S. *J. Biol. Chem.* **1999**, *274*, 962-971.

(7) Henle, E. S.; Linn, S. *J. Biol. Chem.* **1997**, *272*, 19095-19098.

(8) Imlay, J. A. *Annu. Rev. Microbiol.* **2003**, *57*, 395-418.

(9) Seaver, L. C.; Imlay, J. A. *J. Biol. Chem.* **2004**, *279*, 48742-48750.

(10) Bar-Or, D.; Thomas, G. W.; Rael, L. T.; Lau, E. P.; Winkler, J. V. *Biochem. Biophys. Res. Commun.* **2001**, *282*, 356-360.

(11) Battin, E. E.; Zimmerman, M. T.; Ramoutar, R. R.; Quarles, C. E.; Brumaghim, J. L. *Metallomics* **2011**, *3*, 503-512.

(12) Park, S.; Imlay, J. A. *J. Bacteriol.* **2003**, *185*, 1942-1950.

(13) Crichton, R. R.; Dexter, D. T.; Ward, R. J. *Coord. Chem. Rev.* **2008**, *252*, 1189-1199.

(14) Angel, I.; Bar, A.; Horovitz, T.; Taler, G.; Krakovsky, M.; Resnitsky, D.; Rosenberg, G.; Striem, S.; Friedman, J. E.; Kozak, A. *Drug Dev. Res.* **2002**, *56*, 300-309.

(15) Keyer, K.; Imlay, J. A. *Proc. Natl. Acad. Sci. USA* **1996**, *93*, 13635-13640.

(16) Perry, G.; Cash, A. D.; Srinivas, R.; Smith, M. A. *Drug Dev. Res.* **2002**, *56*, 293-299.

(17) Andrade, R. G., Jr.; Dalvi, L. T.; Silva, J. M., Jr.; Lopes, G. K.; Alonso, A.; Hermes-Lima, M. *Arch. Biochem. Biophys.* **2005**, *437*, 1-9.

(18) Miguel, F.; Augusto, A. C.; Gurgueira, S. A. *Free Radic. Res.* **2009**, *43*, 340-347.

(19) Beeh, K. M.; Beier, J.; Haas, I. C.; Kornmann, O.; Micke, P.; Buhl, R. *Eur. Respir. J.* **2002**, *19*, 1119-1123.

(20) Battin, E. E.; Brumaghim, J. L. *J. Inorg. Biochem.* **2008**, *102*, 2036-2042.

(21) Fleischauer, A. T.; Arab, L. *J. Nutr.* **2001**, *131*, 1032S-1040S.

(22) Pinto, J. T.; Rivlin, R. S. *J. Nutr.* **2001**, *131*, 1058S-1060S.

(23) Tanaka, S.; Haruma, K.; Yoshihara, M.; Kajiyama, G.; Kira, K.; Amagase, H.; Chayama, K. *J. Nutr.* **2006**, *136*, 821S-826S.

(24) Mugush, G.; Singh, H. B. *Chem. Soc. Rev.* **2000**, *29*, 347-357.

(25) Smith, C. V.; Jones, D. P.; Guenthner, T. M.; Lash, L. H.; Lauterburg, B. H. *Toxicol. Appl. Pharmacol.* **1996**, *140*, 1-12.

(26) Valko, M.; Rhodes, C. J.; Moncol, J.; Izakovic, M.; Mazur, M. *Chem. Biol. Interact.* **2006**, *160*, 1-40.

(27) Mishra, B.; Priyadarsini, K. I.; Mohan, H.; Mugesh, G. *Bioorg. Med. Chem. Lett.* **2006**, *16*, 5334-5338.

(28) Mishra, B.; Barik, A.; Kunwar, A.; Kumbhare, L. B.; Priyadarsini, K. I.; Jain, V. K. *Phosphorus, Sulfur, Silicon Relat. Elem.* **2008**, *183*, 1018-1025.

(29) Mugesh, G.; Panda, A.; Singh, H. B.; Punekar, N. S.; Butcher, R. J. *J. Am. Chem. Soc.* **2001**, *123*, 839-850.

(30) Yamaguchi, T.; Sano, K.; Takakura, K.; Saito, I.; Shinohara, Y.; Asano, T.; Yasuhara, H. *Stroke* **1998**, *29*, 12-17.

(31) Blum, D.; Torch, S.; Lambeng, N.; Nissou, M.; Benabid, A. L.; Sadoul, R.; Verna, J. M. *Prog. Neurobiol.* **2001**, *65*, 135-172.

(32) Moussaoui, S.; Obinu, M. C.; Daniel, N.; Reibaud, M.; Blanchard, V.; Imperato, A. *Exp. Neurol.* **2000**, *166*, 235-245.

(33) Parnham, M.; Sies, H. *Expert Opin. Investig. Drugs* **2000**, *9*, 607-619.

(34) Ates, B.; Abraham, L.; Ercal, N. *Free Radic. Res.* **2008**, *42*, 372-377.

(35) Kim, J. M.; Chang, H. J.; Kim, W. K.; Chang, N.; Chun, H. S. *J. Agric. Food Chem.* **2006**, *54*, 6547-6553.

(36) Zhao, G.-R.; Xiang, Z.-J.; Ye, T.-X.; Yuan, Y.-J.; Guo, Z.-X. *Food Chem.* **2006**, *99*, 767-774.

(37) Mouithys-Mickalad Mareque, A.; Faez, J. M.; Chistiaens, L.; Kohnen, S.; Deby, C.; Hoebeke, M.; Lamy, M.; Deby-Dupont, G. *Redox Rep.* **2004**, *9*, 81-87.

(38) Sarma, B. K.; Mugesh, G. *J. Am. Chem. Soc.* **2005**, *127*, 11477-11485.

(39) Halliwell, B.; Gutteridge, J. M. *Arch. Biochem. Biophys.* **1986**, *246*, 501-514.

(40) Yu, B. P. *Physiol. Rev.* **1994**, *74*, 139-162.

(41) Burk, R. F. *Nutr. Clin. Care* **2002**, *5*, 75-79.

(42) Moreno-Reyes, R.; Mathieu, F.; Boelaert, M.; Begaux, F.; Suetens, C.; Rivera, M. T.; Neve, J.; Perlmutter, N.; Vanderpas, J. *Am. J. Clin. Nutr.* **2003**, *78*, 137-44.

(43) Zou, K.; Liu, G.; Wu, T.; Du, L. *Osteoarthr. Cartilage* **2009**, *17*, 144-151.

(44) Gromadzinska, J.; Reszka, E.; Bruzelius, K.; Wasowicz, W.; Akesson, B. *Eur. J. Nutr.* **2008**, *47*, 29-50.

(45) Koriyama, C.; Campos, F. I.; Yamamoto, M.; Serra, M.; Carrasquilla, G.; Carrascal, E.; Akiba, S. *J. Toxicol. Sci.* **2008**, *33*, 227-235.

(46) Pourmand, G.; Salem, S.; Moradi, K.; Nikoobakht, M. R.; Tajik, P.; Mehrsai, A. *Nutr. Cancer* **2008**, *60*, 171-176.

(47) Letavayova, L.; Vlckova, V.; Brozmanova, J. *Toxicology* **2006**, *227*, 1-14.

(48) Raich, P. C.; Lu, J.; Thompson, H. J.; Combs, G. F., Jr. *Cancer Invest.* **2001**, *19*, 540-553.

(49) Seyedrezazadeh, E.; Ostadrahimi, A.; Mahboob, S.; Assadi, Y.; Ghaemmagami, J.; Pourmogaddam, M. *Respirology* **2008**, *13*, 294-298.

(50) Clark, L. C.; Dalkin, B.; Krongrad, A.; Combs, G. F., Jr.; Turnbull, B. W.; Slate, E. H.; Witherington, R.; Herlong, J. H.; Janosko, E.; Carpenter, D.; Borosso, C.; Falk, S.; Rounder, J. *Br. J. Urol.* **1998**, *81*, 730-734.

(51) Combs Jr., G. F. *Br. J. Cancer* **2004**, *91*, 195-199.

(52) Lippman, S. M.; Klein, E. A.; Goodman, P. J.; Lucia, M. S.; Thompson, I. M.; Ford, L. G.; Parnes, H. L.; Minasian, L. M.; Gaziano, J. M.; Hartline, J. A.; Parsons, J. K.; Bearden, J. D., III; Crawford, E. D.; Goodman, G. E.; Claudio, J.; Winquist, E.; Cook, E. D.; Karp, D. D.; Walther, P.; Lieber, M. M.; Kristal, A. R.; Darke, A. K.; Arnold, K. B.; Ganz, P. A.; Santella, R. M.; Albanes, D.; Taylor, P. R.; Probstfield, J. L.; Jagpal, T. J.; Crowley, J. J.; Meyskens, F. L., Jr.; Baker, L. H.; Coltman, C. A., Jr. *J. Am. Med. Assoc.* **2009**, *301*, 39-51.

(53) El-Bayoumy, K. *Nutr. Cancer* **2009**, *61*, 285-286.

(54) Reid, M. E.; Duffield-Lillico, A. J.; Slate, E.; Natarajan, N.; Turnbull, B.; Jacobs, E.; Combs, G. F.; Alberts, D. S.; Clark, L. C.; Marshall, J. R. *Nutr. Cancer* **2008**, *60*, 155-163.

(55) Freedman, J. H.; Ciriolo, M. R.; Peisach, J. *J. Biol. Chem.* **1989**, *264*, 5598-5605.

(56) Jiang, J.; St Croix, C. M.; Sussman, N.; Zhao, Q.; Pitt, B. R.; Kagan, V. E. *Chem. Res. Toxicol.* **2002**, *15*, 1080-1087.

(57) Bai, Y.; Wang, T.; Liu, Y.; Zheng, W. *Colloids Surf.* **2009**, *B74*, 150-153.

(58) Collins, C. A.; Fry, F. H.; Holme, A. L.; Yiakouvaki, A.; Al-Qenaei, A.; Pourzand, C.; Jacob, C. *Org. Biomol. Chem.* **2005**, *3*, 1541-6.

(59) Suzuki, K. T.; Sasakura, C.; Yoneda, S. *Biochim. Biophys. Acta, Protein Struct. Mol. Enzymol.* **1998**, *1429*, 102-112.

(60) Molter, A.; Mohr, F. *Coord. Chem. Rev.* **2010**, *254*, 19-45.

(61) Battin, E. E.; Perron, N. R.; Brumaghim, J. L. *Inorg. Chem.* **2006**, *45*, 499-501.

(62) Wang, H. C.; Riahi, M.; Pothen, J.; Bayse, C. A.; Riggs-Gelasco, P.; Brumaghim, J. L. *Inorg. Chem.* **2011**, *50*, 10893-10900.

(63) Pierre, J. L.; Fontecave, M.; Crichton, R. R. *BioMetals* **2002**, *15*, 341-346.

(64) Pettit, L. D.; Siddiqui, K. F. *Inorg. Chim. Acta* **1981**, *55*, 87-91.

(65) Bard, A. J.; Faulkner, L. R. *Electrochemical Methods, Fundamentals and Applications*; Second ed.; Wiley: New York, 2004, p 3.

CHAPTER THREE

MULTIFUNCTIONAL SELONE AND THIONE ANTIOXIDANTS PREVENT DNA DAMAGE BY METAL COORDINATION AND SCAVENGING REACTIVE OXYGEN SPECIES

3.1. Introduction

Multifunctional antioxidants are compounds that prevent oxidative damage by multiple mechanisms, including (but not limited to) scavenging of reactive oxygen species (ROS), redox signaling interference,[1-3] and metal coordination (either by inhibiting ROS production, or by targeted ROS scavenging). Due to the increase in diseases caused by cellular oxidative stress such as Alzheimer's, age-related macular degeneration, and amyotrophic lateral sclerosis, as well as the pharmaceutical prospect of developing compounds that target multiple pathways in which a disease is induced, recent interest in multifunctional antioxidants has risen over the past decade.[4-6]

A major source of cellular ROS, including superoxide ($O_2^{\bullet-}$), hydrogen peroxide (H_2O_2), and hydroxyl radical ($^{\bullet}OH$) is the cytochrome P450 enzyme in mitochondria.[7,8] To maintain low concentrations of these damaging ROS, mitochondria also have high concentrations of antioxidant enzymes such as superoxide dismutase (SOD) and glutathione peroxidase (GPx) to actively scavenge $O_2^{\bullet-}$ and H_2O_2, respectively. However, the primary source of damage is from $^{\bullet}OH$ generation in the Fenton (Fe) or Fenton-like (Cu) reactions with H_2O_2 (Reaction 1).[9]

$$Fe^{II}/Cu^{I} + H_2O_2 \rightarrow Fe^{III}/Cu^{II} + {}^{-}OH + {}^{\bullet}OH \qquad (1)$$

Under physiological conditions, this process is controlled by the relatively low

concentrations of non-protein-bound Fe^{II}, Cu^{I}, and H_2O_2, but during oxidative stress, H_2O_2 concentrations rise sufficiently to damage iron-sulfur clusters. H_2O_2 oxidizes the proteins containing these clusters, releasing Fe^{II} and leading to an increased concentration of non-protein-bound Fe^{II}, which can then react with excessive H_2O_2 to generate $^{\bullet}OH$.[10] Additionally, non-protein bound Cu^{I} can interact with excess H_2O_2 to generate $^{\bullet}OH$.[11,12] This process can be particularly acute in patients suffering from hemochromatosis (iron overload) and Wilson's disease (copper overload).[13-15] Thus, excessive concentrations of iron and copper leads to increased oxidative damage, resulting in cell death and disease.

In the past decade, the most widely examined class of multifunctional antioxidants has been polyphenols. Various studies have shown the ability of polyphenol antioxidants to directly scavenge ROS such as $^{\bullet}OH$ and $ONOO^{-}$ [16-19] in addition to coordinating redox-active metals such as Fe, Cu, Cr, Co, and V.[20-23] Chelation of redox-active metals promotes cellular survival by preventing metal-mediated oxidative stress.[24,25] Furthermore, polyphenols have been shown to bind to various proteins and enzymes linked to inflammation. Joven *et al.*[26] reported that polyphenols in the extract of *Hibiscus sabdariffa* were effective peroxyl radical scavengers, inhibited the radical generating enzyme xanthine oxidase, and reduced the production of cytokines during the misregulation of tumor necrosis factor α (TNF-α) in endothelial cells. Studies by Patel *et al.*[27] revealed that polymeric black tea polyphenols decreased cell proliferation induced by 12-*O*-tetradecanoylphorbol-13-acetate (used to chemically promote skin cancer) in mice by reducing the activation of signaling kinases and the inflammatory protein cyclooxygenase 2.

The vast majority of antioxidant research with sulfur and selenium compounds over the years has focused on their ability to scavenge ROS, leaving the role of metal coordination relatively unexplored. However, our group discovered that some sulfur- and selenium-containing antioxidants effectively prevent oxidative copper-mediated DNA damage by binding copper, but were substantially less effective at preventing Fe^{II}-mediated DNA damage.[28-30]

N,N'-dimethylimidazole selone (dmise) and thione (dmit; Figure 5.1) were selected for the investigation of their DNA damage inhibition properties due to their structural similarities to ergothioneine and selenoneine. Ergothioneine (ESH; Figure 5.1), is a natural thione found in animals and plants, and has been found to prevent oxidative DNA damage, scavenge ROS, and promote anti-inflammatory effects in cells.[31-35] The concentration of ergothioneine varies in the human body, ranging from 100-2000 μM in tissue,[36] to 0.4-308 μM in blood serum.[37] Its selenium analog, selenoneine, was only recently discovered in bluefin tuna (0.46 μM in blood)[38] and in humans (up to 9 nM in blood),[39] and it can scavenge 1-diphenyl-2-picrylhydrazyl (DPPH) radical.[38,40] Both dmise and dmit are similar to methimazole, the primary drug used in the United States to treat hyperthyroidism.[41,42]

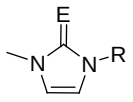

E = Se, R = CH_3: *N,N'*-Dimethylimidazoleselone (Dmise)
E = S, R = CH_3: *N,N'*-Dimethylimidazoleselone (Dmit)
E = S, R = H: Methimazole

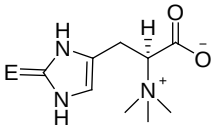

E = Se, Selenoeine
E = S, Ergothioneine (ESH)

Figure 3.1. Selones and thiones discussed in Chapter 3.

Previous antioxidant studies with dmit and related compounds have shown their ability to prevent the peroxynitrite nitration of tyrosine by ROS scavenging.[43,44] In contrast, studies of sulfur- and selenium-containing amino acids have established the importance of metal coordination for their antioxidant activity.[28,29] Coordination chemistry studies with dmise and dmit have shown their ability to readily bind copper(I),[45] suggesting that these compounds may potentially prevent DNA damage through metal coordination similar to the sulfur- and selenoamino acids. Thus, these two compounds showed promise as multifunctional antioxidants. In this work, dmise and dmit were tested for their ability to inhibit copper-, iron-, and peroxynitrite- mediated DNA damage using gel electrophoresis methods,[28-30,46] and their ability to coordinate Fe^{II} and Cu^{I} in aqueous solution was determined using mass spectrometry.

3.2. Results and Discussion

3.2.1. Prevention of copper(I)-mediated DNA damage. Plasmid DNA damage assays were used to determine the ability of dmise and dmit to prevent DNA single-strand backbone nicking caused by Cu^{I}/H_2O_2 (Reaction 1). These studies observe a biological endpoint (DNA damage) rather than relying on traditional methods for determining radical scavenging that use non-aqueous solutions, aromatic radical species that do not have the very short lifetime of hydroxyl radical, or highly acidic or basic pH.[47-50] For our experiments, 6 μM Cu^{I} is combined with H_2O_2 (50 μM) to generate $^{\bullet}OH$. This copper concentration is within the reported concentration in human neuronal tissue of 1-1300 μM.[51,52] Figure 3.2 shows the results of a gel electrophoresis experiment to measure

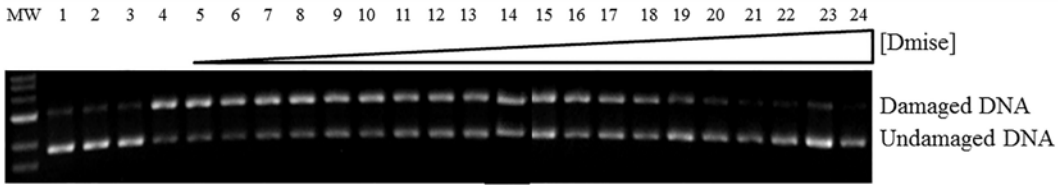

Figure 3.2. Gel electrophoresis image of Cu^{I}-mediated DNA damage inhibition by *N,N'*-dimethylimidazole selone (dmise) in MOPS buffer (10 mM, pH 7). Lane: MW = 1 kb molecular weight marker; lane 1: plasmid DNA (p); lane 2: p + H_2O_2; lane 3: p + dmise (2000 μM) + H_2O_2; lane 4: p + ascorbate (7.5 μM) + $CuSO_4$ (6 μM) + H_2O_2 (50 μM); lanes 5-24: p + $CuSO_4$ + ascorbate + increasing concentrations of dmise: 0.2, 0.5, 0.75, 0.9, 1, 2.5, 5, 7.5, 10, 50, 100, 200, 300, 400, 600, 800, 1000, 1200, 1500, and 2000 μM dmise, respectively.

dmise inhibition of Cu^{I}-mediated DNA damage. Lane 2 shows that combining plasmid DNA with H_2O_2 does not result in DNA damage (single-strand DNA nicking), nor does combining the highest concentration of dmise (2000 μM, lane 3) with H_2O_2, although combining H_2O_2, $CuSO_4$ (6 μM), and ascorbic acid (7.5 μM) results in 85% DNA damage (lane 4). As the concentration of dmise increases (lanes 5-26), the percentage of DNA damage decreases.

A plot of the percent DNA damage inhibition versus the log concentration of dmise is shown in Figure 3.3. From this plot, the concentration of dmise required to inhibit 50% oxidative DNA damage (IC_{50} value), of approximately 240 μM was determined. Surprisingly, the DNA damage prevention activity of dmise did not fit a typical dose-response curve; an initial increase in activity is observed between 1-10 μM, and a second increase occurs between 300-3000 μM. The appearance of a second increase in activity has not been observed in previous studies of sulfur and selenium antioxidants using similar methods, and suggests that dmise inhibits DNA damage through more than one mechanism. Since Cu^{I} typically coordinates four monodentate ligands in a tetrahedral geometry, the approximate concentration range for DNA damage

prevention for these studies with 6 μM Cu^{I} is expected to occur around dmise concentrations of 6-24 μM. Since dmise inhibits 40% of DNA damage at 7.5 μM, at low concentrations, dmise may inhibit oxidative DNA damage through copper coordination.

To confirm that metal coordination is essential for this antioxidant activity of dmise, further gel electrophoresis experiments were conducted using $[Cu(bipy)_2]^+$ (bipy = 2,2'-bipyridine) in place of Cu^{I}. In these experiments, the Cu^{I} ions are fully coordinated prior to the addition of dmise, preventing copper-dmise binding (all gel figures are provided at the end of the Experimental Methods section in Figures 3.5-3.9). Although

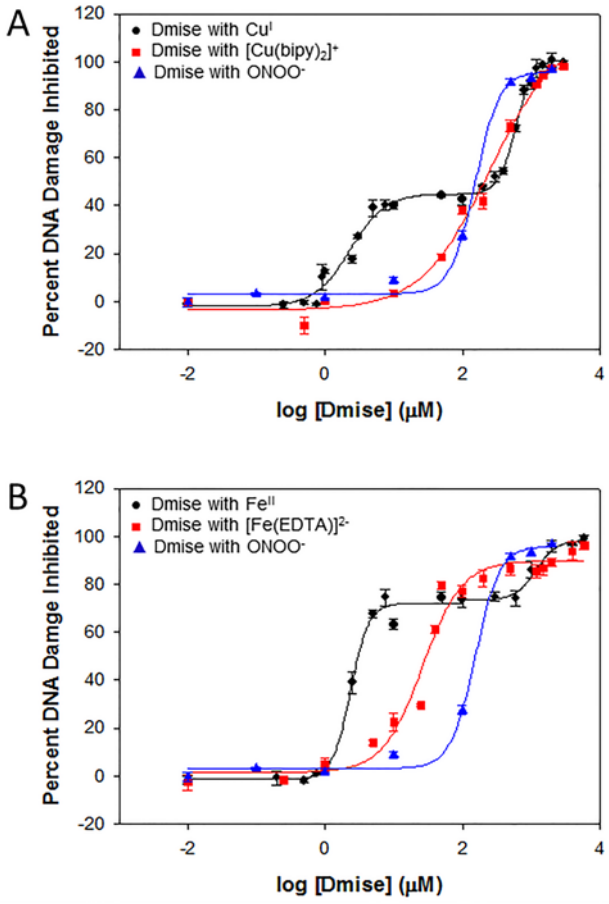

Figure 3.3. Dose-response curves for dmise prevention of DNA damage by A) Cu^{I}/H_2O_2, $[Cu(bipy)_2]^+/H_2O_2$, and peroxynitrite; and B) Fe^{II}/H_2O_2, $[Fe(EDTA)]^{2-}/H_2O_2$, and peroxynitrite ($ONOO^-$).

the IC_{50} value calculated from the best-fit dose-response curve for dmise inhibition of $[Cu(bipy)_2]^+$-mediated DNA damage (205.5 ± 0.4 μM; Table 3.1) is about the same concentration as the IC_{50} value for prevention of copper-mediated DNA damage, dmise activity in the $[Cu(bipy)_2]^+$ studies exhibits a typical dose-response curve, without the increased DNA damage inhibition observed at low concentrations in the Cu^I studies (Figure 3.3A). Because copper binding is prevented by using $[Cu(bipy)_2]^+$, this marked difference supports the conclusion that primary mode of DNA damage inhibition is due to metal coordination at low concentrations and that ROS scavenging may be a secondary mechanism at significantly higher concentrations.

Dmit also prevents copper-mediated DNA damage, but with a high IC_{50} value of 1550 ± 1 μM (Table 3.1; IC_{50} plots are provided at the end of the Experimental Methods section in Figure 3.10) with no activity observed within the expected range for tetrahedral copper coordination (6-24 μM). When $[Cu(bipy)_2]^+$ is used to damage DNA instead of Cu^I, the IC_{50} value increases by more than two-fold to 3470 ± 5 μM, suggesting that dmit inhibits DNA damage by different mechanisms for labile and chelated Cu^I-mediated DNA damage. From their IC_{50} values, dmise is at least six time more effective than dmit at inhibiting Cu^I-mediated DNA damage.

Table 3.1. IC_{50} values for dmise and dmit prevention of DNA damage and MALDI mass spectrometry results with metal coordination.

IC_{50} Value	**Dmise (μM)**	**M:L Ratio (*m/z*, Da)**	**Dmit (μM)**	**M:L Ratio (*m/z*, Da)**
Cu^I	~240[a]	1:1 (242)	1550 ± 3	1:2 (320)[c]
Fe^{II}	3.2 ± 0.9	1:3 (301; $[Fe^{II}(dmise)_3(H_2O)]^{2+}$)	89.1 ± 0.2	1:3 (220)[c]
		1:5 (480; $[Fe^{II}(dmise)_5(H_2O)]^{2+}$)		1:4 (284)[b]
$[Fe(EDTA)]^{2-}$	34.0 ± 0.1		353.2 ± 0.4	
$[Cu(bipy)_2]^+$	205.5 ± 0.4		3470 ± 5	
$ONOO^-$	155.2 ± 0.1		171.4 ± 0.2	

[a]Estimated value. [b]Coordination observed only by ESI mass spectrometry. [c]Coordination observed inboth ESI and MALDI studies.

3.2.2. Prevention of iron(II)-mediated DNA damage. Gel electrophoresis studies were also conducted on dmise and dmit to determine their ability to prevent iron-mediated DNA damage. All iron studies were conducted at pH 6.0 in to maintain Fe^{II} solubility.[53] These Fe^{II}-mediated DNA damage prevention studies were conducted with 2 μM $FeSO_4$, a concentration at the low end of the intracellular labile iron concentration (1-30 μM).[54-56] Figure 3.4 shows the results of a gel electrophoresis experiment with dmise under these conditions. Lane 2 shows that addition of H_2O_2 alone (50 μM) to plasmid DNA results in no DNA damage (nicking), nor does the highest concentration of dmise (6000 μM, lane 3) combined with H_2O_2, but combining H_2O_2 and $FeSO_4$ (2 μM) results in 85 % DNA damage (lane 4). As the concentration of dmise increases (lanes 5-26), the percentage of DNA damage decreases. Fitting the dose-response curve for these data gives an IC_{50} value of 3.2 ± 0.9 μM for dmise inhibition of Fe^{II}-mediated DNA damage (Figure 3.3B). This is especially significant, since dmise is the first selenium compound to show greater efficacy at preventing iron-mediated DNA damage than copper-mediated damage.

Once again, the iron-mediated DNA damage prevention ability of dmise did not fit a typical dose-response curve; an initial increase in activity is observed between 1-50

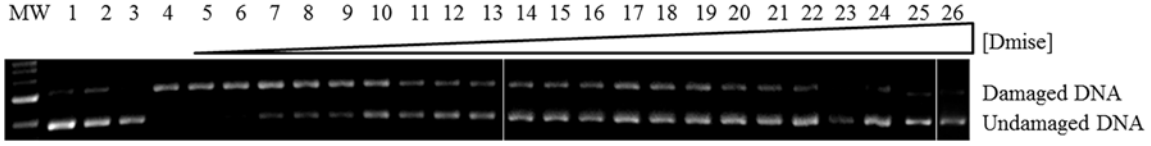

Figure 3.4. Gel electrophoresis image of Fe^{II}-mediated DNA damage inhibition by *N,N'*-dimethylimidazole selone (Dmise) in MES buffer (10 mM, pH 6). Lane: MW = 1 kb molecular weight marker; lane 1: plasmid DNA (p); lane 2: p + H_2O_2; lane 3: p + dmise (6000 μM) + H_2O_2; lane 4: p + $FeSO_4$ (2 μM) + H_2O_2 (50 μM); lanes 5-24: p + $FeSO_4$ + increasing concentrations of dmise: 0.01, 0.2, 0.5, 0.75, 1, 2.5, 5, 7.5, 10, 50, 100, 200, 300, 400, 600, 800, 1000, 1200, 1500, 2000, 4000, and 6000 μM, respectively.

μM, with a second increase between 600-6000 μM. This second increase in activity again suggests that dmise inhibits DNA damage through two distinct mechanisms. The first increase is observed in the range expected for possible octahedral dmise-iron binding (up to 12 μM for 2 μM Fe^{II} with 63 % DNA damage inhibition at 10 μM dmise), indicating that dmise may inhibit oxidative DNA damage by iron coordination at low concentrations. In contrast, sulfur and selenoamino acids exhibit little or no ability to prevent Fe^{II}-mediated DNA damage. Only methyl-selenocysteine, selenocystamine, and reduced and oxidized glutathione inhibited Fe^{II}-mediated DNA damage with IC_{50} values ranging from 120-10,000 μM.[28-30] Thus, dmise compounds is almost 40 times more effective at preventing Fe^{II}-mediated DNA damage than the most effective selenoamino acid, methylselenocysteine.

To confirm that iron coordination is essential for the observed antioxidant activity of dmise, further gel electrophoresis experiments were conducted using $[Fe(EDTA)]^{2-}$ (EDTA = ethylenediaminetetraacetic acid) in place of Fe^{II}. In these experiments, Fe^{II} is fully chelated prior to dmise addition, thus preventing dmise-iron coordination. Dmise prevents 50 % DNA damage by $[Fe(EDTA)]^{2-}/H_2O_2$ at 34.0 ± 0.1 μM, approximately 10 times higher than dmise with unchelated Fe^{II} (Figure 3.3B). This difference suggests that the antioxidant activity at low concentrations of dmise is due to Fe^{II} coordination and ROS scavenging is a likely secondary mechanism at significantly higher concentrations.

Using the same DNA damage assays, dmit prevents iron-mediated DNA damage with an IC_{50} value of 89.1 μM and $[Fe(EDTA)]^{2-}$-mediated DNA damage at four times this concentration (IC_{50} = 353 μM). In the unchelated Fe^{II} studies, 40 % of DNA damage

is prevented at 10 μM dmit, well within the 12 μM limit for octahedral Fe^{II} binding. Thus, these results suggest that dmit, while a less effective antioxidant than dmise, also prevents metal-mediated DNA damage through multiple antioxidant mechanisms. At more biologically relevant, lower concentrations, metal coordination is critical to activity, and at high concentrations ROS scavenging is more prevalent.

Akanmu *et al.* reported that ESH inhibits 100% of Cu^{I}-mediated deoxyribose degradation at a concentration of 1 mM,[57] well within biological concentrations (1-3 mM).[58,59] Surprisingly, both dmise and dmit inhibit Fe^{II}-mediated DNA damage at substantially lower concentrations than Cu^{I}-mediated DNA damage, in contrast to other sulfur- and selenium-containing antioxidants.[28-30] The effectiveness of these two compounds at preventing Fe^{II}-mediated DNA damage is unexpected, since Cu^{I} is a soft Lewis acid and should favor binding the soft sulfur and selenium atoms more than borderline Fe^{II}.

3.2.3. Significance of metal coordination. Mass spectrometry studies in water were conducted to determine the Fe^{II} and Cu^{I} coordination ability of dmise and dmit (Table 3.1). Dmise coordinates Fe^{II} in both 1:3 and 1:5 Fe:dmise molar ratios, whereas dmit shows coordination only in a 1:3 Fe:dmit ratio. Similar studies with Cu^{I} revealed signals for a 1:1 complex with Cu^{I} and dmise and a 1:2 complex with dmit. Thus, both these antioxidants are capable of binding iron and copper in aqueous solution, with higher coordination numbers for the potentially octahedral Fe^{II} compared to the potentially tetrahedral Cu^{I}. In addition, Stadelman *et al.*[60] have reported that dmise and dmit form isolable complexes with iron(II) in 1:2 and 1:4 molar ratios.

3.2.4. Prevention of peroxynitrite-mediated DNA damage. To determine the extent to which dmise and dmit prevent DNA damage by ROS scavenging, gel electrophoresis studies with peroxynitrite were performed. Peroxynitrite ($ONOO^-$) anion is produced *in vivo* by the reaction of nitric oxide with superoxide[61,62] and can directly damage DNA.[63,64] Around pH 7, peroxynitrite is protonated to form peroxynitrous acid that decomposes into nitrogen dioxide ($NO_2^{\bullet}$) and $^{\bullet}OH$ with a half-life of about 1 s.[65] Thus, peroxynitrite causes hydroxyl radical damage to DNA without the presence of metal ions. Peroxynitrite DNA damage studies were performed similarly to the metal-based studies, but with the addition of peroxynitrite (1450 μM) at pH 6.8 (10 mM MOPS buffer) for stability.

Dmise and dmit effectively prevent peroxynitrite-mediated DNA damage with IC_{50} values of 155.2 and 171.4 μM, respectively. Since these studies with $ONOO^-$ are conducted in the absence of metals, the ability of dmise and dmit to prevent this oxidative DNA damage only at higher micromolar concentrations suggests that ROS scavenging is not the primary antioxidant mechanism at lower concentrations. Studies by Bhabak and Mugesh have reported that dmise has a low IC_{50} value (12.2 μM) for the prevention of tyrosine nitration by peroxynitrite, supporting the fact that these compounds possess the ability to act as ROS scavengers,[43] but these IC_{50} values cannot be realistically compared due to the very different reactions that were examined.

3.3. Conclusions

These results demonstrate the first example of multifunctional sulfur and selenium compounds that prevent oxidative DNA damage through copper coordination, iron coordination, and ROS scavenging. Dmit DNA damage prevention activity falls within the concentration ranges found for the biological thiones ergothioneine (0.4-308 μM in human blood serum, and between 100-2000 μM in human tissue)[36,66] and methimazole (4-13 μM in blood of hyperthyroid patients).[67,68] Human plasma concentrations of selenium are typically about 1.5μM, and selenium supplementation studies have reported non-toxic concentrations up to ~10 μM,[69,70] within the activity window for dmise prevention of iron-mediated DNA damage.

These multifunctional antioxidants prevent DNA damage by two separate mechanisms. At low concentrations, copper or iron coordination is the primary mechanism at very low micromolar concentrations, whereas ROS scavenging occurs at concentrations above 100 μM, as confirmed by peroxynitrite-mediated DNA damage studies. Surprisingly, both compounds exhibited more potent prevention of Fe^{II}-mediated than Cu^{I}-mediated DNA damage, an ability not previously reported for sulfur or selenium antioxidants. Thus, these results have opened the doors for the development of future selone- and thione-derived compounds that can be tuned for antioxidant activity by targeted coordination to specific redox-active metals and prevention of disease-causing oxidative damage caused by metal-mediated DNA damage.

3.4. Experimental Methods

Materials. A NANOpure Diamond water deionization system (Barnstead International) was used to prepare deionized H_2O. NaCl (99.999%) and $FeSO_4 \cdot 7H_2O$ were purchased from Alfa Aesar; $CuSO_4 \cdot 5H_2O$, yeast extract, tryptone (peptone), and 30% H_2O_2 were purchased from Fisher. MOPS and MES were obtained from Alfa Aesar. Ethanol (200 proof) and ascorbic acid were from Acros Organics. Dmise and dmit were prepared according to a previous report.[71] Glucose and ampicillin were from EMD. Ethidium bromide and agar were from Lancaster. TRIS hydrochloride and microcentrifuge tubes were from VWR. Metal-free microcentrifuge tubes were prepared by washing the tubes in 1 M HCl for ~1 h, and then triple rinsing three times with deionized H_2O.

Plasmid transfection, amplification, and purification. Plasmid DNA (pBSSK) was purified from DH1 *E.* coli competent cells using a 5 Prime PerfectPrep^{TM} Spin Kit (Fisher). Tris-EDTA buffer (pH 8.01) was used to elute the plasmid from the spin columns. Plasmid DNA was dialyzed against 130 mM NaCl for 24 h at 4 °C to ensure all Tris-EDTA buffer and metal contaminates were removed, and its concentration was determined through the use of UV-vis spectroscopy at a wavelength of 260 nm. Absorbance ratios of $A_{250}/A_{260} \leq 0.95$ and $A_{260}/A_{280} \geq 1.8$ were determined via UV-vis for DNA used in all experiments. Plasmid purity was determined through digestion of plasmid (0.1 pmol) with *Sac 1* and *KpN1* in a mixture of NEB buffer and bovine serum albumin was conducted at 37 °C for 90 minutes. Comparison to an undigested plasmid sample and a 1 kb molecular weight marker was conducted by gel electrophoresis.

DNA damage gel electrophoresis experiments. Deionized H_2O, MOPS buffer (10 mM, pH 7.0), NaCl (130 mM), ethanol (10 mM), $CuSO_4 \cdot 5H_2O$ (6 μM), ascorbate (7.5 μM), and the indicated concentrations of sulfur or selenium compounds were combined in a microcentrifuge tube and allowed to stand for 5 min at room temperature. Plasmid (pBSSK, 0.1 pmol in 130 mmol NaCl solution) was then added to the reaction mixture and allowed to stand for 5 min at room temperature. Hydrogen peroxide (50 μM) was then added and allowed to react at room temperature for 30 min. EDTA (50 μM) was added after 30 min to quench the reaction. For Fe^{2+} DNA damage experiments, $FeSO_4 \cdot 7H_2O$ (2 μM) and MES (10 mM, pH 6.0) were used in place of $CuSO_4$, ascorbic acid, MOPS buffer. All concentrations are final concentrations in a 10 μL volume. All samples were loaded into a 1% agarose gel in TAE running buffer; damaged and undamaged plasmid was separated by electrophoresis (140 V for 30 min). Gels were then stained using ethidium bromide and imaged under UV light. The amounts of nicked (damaged) and circular (undamaged) DNA were quantified using UViProMW (Jencons Scientific Inc., 2007). The intensity of the circular plasmid band was multiplied by 1.24, due to the lesser binding ability of ethidium bromide to supercoiled plasmid.[72,73] Experiments using $[Cu(bipy)_2]^{2+}$ (50 μM) or $[Fe(EDTA)]^{2-}$ (400 μM) in the place of Cu^{2+} and Fe^{2+} were conducted using a similar procedure. For gels with $[Cu(bipy)_2]^{2+}$, 62.5 μM ascorbic acid was also added. Tabular data for all metal-containing gel experiments can be found at the end of this section in Tables 5.2-5.9.

Calculating percent inhibition of DNA damage. The formula 1-[%N-%B]*100 was used to calculate percent DNA damage inhibition; %N = percent of nicked DNA in

lanes 6 and higher, and %B = the percent of nicked DNA in the Cu^{+}/H_2O_2 or Fe^{2+}/H_2O_2 control lane. All percentages were corrected for residual nicked DNA (lane 2) prior to calculation. Results were obtained from an average of three trials, with indicated standard deviations.

Synthesis of peroxynitrite anion ($ONOO^-$). Synthesis of peroxynitrite followed the method of Keith and Powell,[74] resulting in the bright yellow-colored $ONOO^-$. The concentration of $ONOO^-$ was calculated from its absorbance at 302 nm, using an extinction coefficient of 1670 cm^{-1} mol^{-1} dm^3.[75] Samples of $ONOO^-$ were stored at -80 °C for up to two weeks before use.

Gel electrophoresis experiments with $ONOO^-$. Selenium or sulfur compounds were combined with ethanol (10 mM 100%), NaCl (130 mM), MOPS buffer (10 mM, pH 6.8), and plasmid DNA (pBSSK, 0.1 mmol in 130 mM NaCl) in an acid-washed microcentrifuge tube and allowed to stand for 5 min. Peroxynitrite (1450 µM) was added at 4°C, and the reaction was allowed to stand for an additional 5 min at room temperature. All concentrations indicated are the final concentrations in a 10 µL volume. After the 5 min incubation with $ONOO^-$, loading dye was added to obtain a final volume of 12 µL. All samples were loaded into a 1% agarose gel in TAE running buffer, and gel electrophoresis was performed as previously stated. Data for all peroxynitrite gels are presented at the end of this section in Tables 5.10 and 5.11.

Mass spectrometry studies. MALDI mass spectrometry experiments were performed using a Bruker Microflex MALDI-TOF mass spectrometer with *trans*-2-[3-(4-tert-butylphenyl)-2-methyl-2-propenyldiene (250.34 *m/z*) as the matrix. Stock solutions

of $FeSO_4$ (900 µM), $CuSO_4$ (900 µM), ascorbic acid (900 µM), dmise (900, 3600, and 5400 µM), and dmit (900, 3600, and 5400 µM) were prepared in deionized H_2O. Mass spectrometry samples for 1:4 metal-to-ligand ratios were prepared by combining $CuSO_4$ (300 µL, 900 µM) and ascorbic acid (300 µL, 900 µM) solutions and allowing the samples to stand for 5 min at room temperature. Dmise or dmit (300 µL or 3600 µM) was then added to the solution, and allowed to stand for an additional 5 min. A similar procedure was followed for studies with Fe^{II}, by combining $FeSO_4$ (300 µL, 900 µM in deionized H_2O) and either dmise or dmit (300 µL, 5400 µM in deionized H_2O) for 1:1 and 1:6 metal-to-ligand ratios. ESI-MS studies were conducted on a Waters Alliance 2695 LC / Waters Micromass ZQ Mass Spectrometer by Emily Kurfman and Prof. Sandra K. Wheeler (Furman University). Experiments were conducted in diH_2O and at the same concentration as MALDI studies. All concentrations indicated are final concentrations in 900 µL volumes. All reported *m/z* peak envelopes matched theoretical peak envelopes for the assigned complexes.

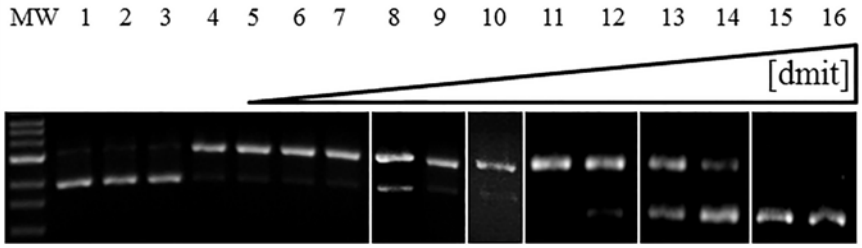

Figure 3.5. Gel electrophoresis image of Cu^{I}-mediated DNA damage inhibition by *N,N'*-dimethylimidazole thione (dmit) in MOPS buffer (10 mM, pH 7). Lane: MW = 1 kb molecular weight marker; lane 1: plasmid DNA (p); lane 2: p + H_2O_2; lane 3: p + dmit (6000 µM) + H_2O_2; lane 4: p + ascorbate (AA, 7.5 µM) + $CuSO_4$ (6 µM) + H_2O_2 (50 µM); lanes 5-16: p + $CuSO_4$ + AA + increasing concentration of dmit: 0.1, 1, 10, 50, 100, 250, 500, 1000, 1500, 2000, 4000, and 6000 µM, respectively.

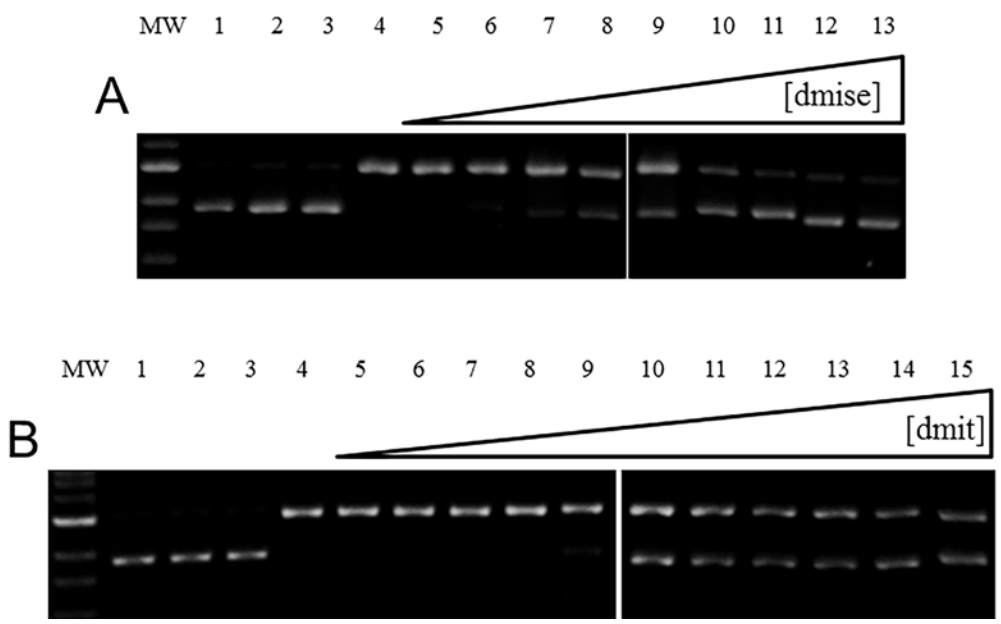

Figure 3.6. Gel electrophoresis images of $[Cu(bipy)_2]^+$-mediated DNA damage inhibition by A) *N*,*N*'-dimethylimidazole selone (dmise) and B) *N*,*N*'-dimethylimidazole thione (dmit) in MOPS buffer (10 mM, pH 7). Lane: MW = 1 kb molecular weight marker; lane 1: plasmid DNA (p); lane 2: p + H_2O_2; lane 3: p + S/Se compound (dmise = 1200; dmit = 6000 μM) + H_2O_2; lane 4: p + ascorbate (63 μM) + $[Cu(bipy)_2]^+$ (50 μM) + H_2O_2 (50 μM); lanes 5+: p + $FeSO_4$ + increasing concentrations of compound: A) 1, 10, 50, 100, 200, 500, 1200, 1500, and 2000 μM dmise, respectively, and B) 0.1, 1, 10, 100, 1000, 1500, 2000, 2500, 3000, 4000, and 6000 μM dmit, respectively.

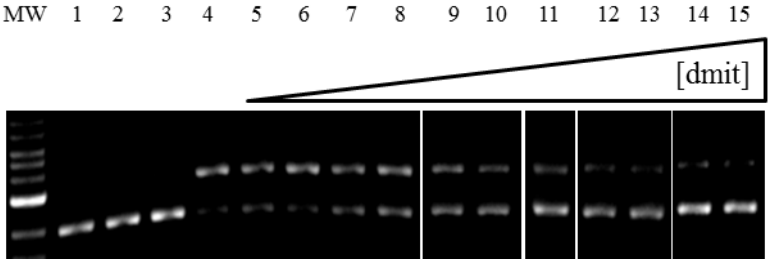

Figure 3.7. Gel electrophoresis images of Fe^{II}-mediated DNA damage inhibition by *N*,*N*'-dimethylimidazole thione (dmit) in MES buffer (10 mM, pH 6). Lane: MW = 1 kb molecular weight marker; lane 1: plasmid DNA (p); lane 2: p + H_2O_2; lane 3: p + dmit (6000 μM) + H_2O_2; lane 4: p + $FeSO_4$ (2 μM) + H_2O_2 (50 μM); lanes 5-15: p + $FeSO_4$ + increasing concentrations of dmit: 0.1, 1, 10, 100, 250, 500, 1000, 1500, 2000, 4000, and 6000 μM, respectively.

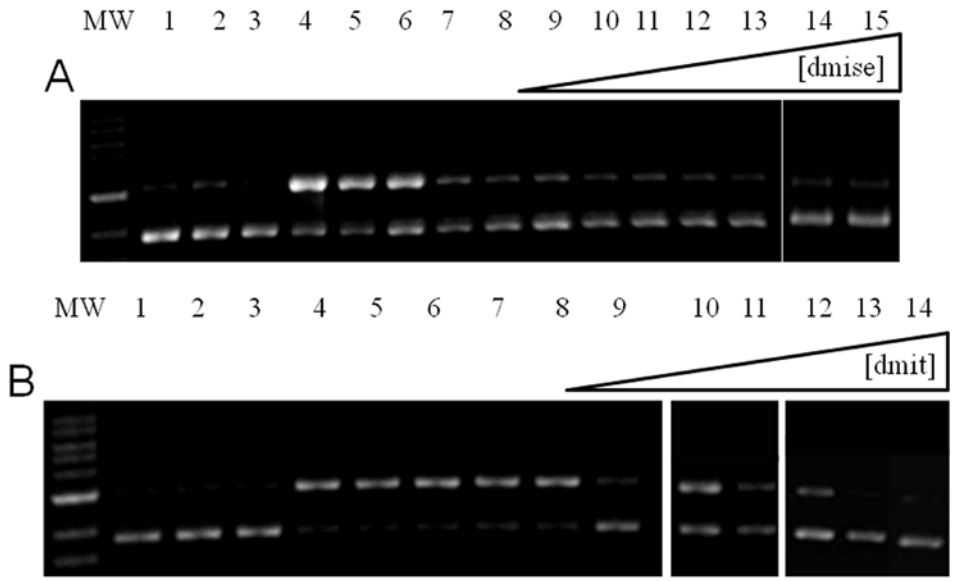

Figure 3.8. Gel electrophoresis images of $[Fe(EDTA)]^{2-}$-mediated DNA damage inhibition by A) *N*,*N*'-dimethylimidazole selone (dmise) and B) *N*,*N*'-dimethylimidazole thione (dmit) in MES buffer (10 mM, pH 6). Lane: MW = 1 kb molecular weight marker; lane 1: plasmid DNA (p); lane 2: p + H_2O_2; lane 3: p + S/Se compound (dmise = 6000 or dmit = 2000 μM) + H_2O_2; lane 4: p + $[Fe(EDTA)]^{2-}$ (400 μM) + H_2O_2 (50 μM); lanes 5+: p + $[Fe(EDTA)]^{2-}$ + increasing concentrations of compound: A) 1, 10, 50, 100, 200, 500, 1200, 1500, 2000, 4000, and 6000 μM dmise, respectively, and B) 0.1, 1, 10, 100, 250, 500, 750, 1000, 1500, and 2000 μM dmit, respectively.

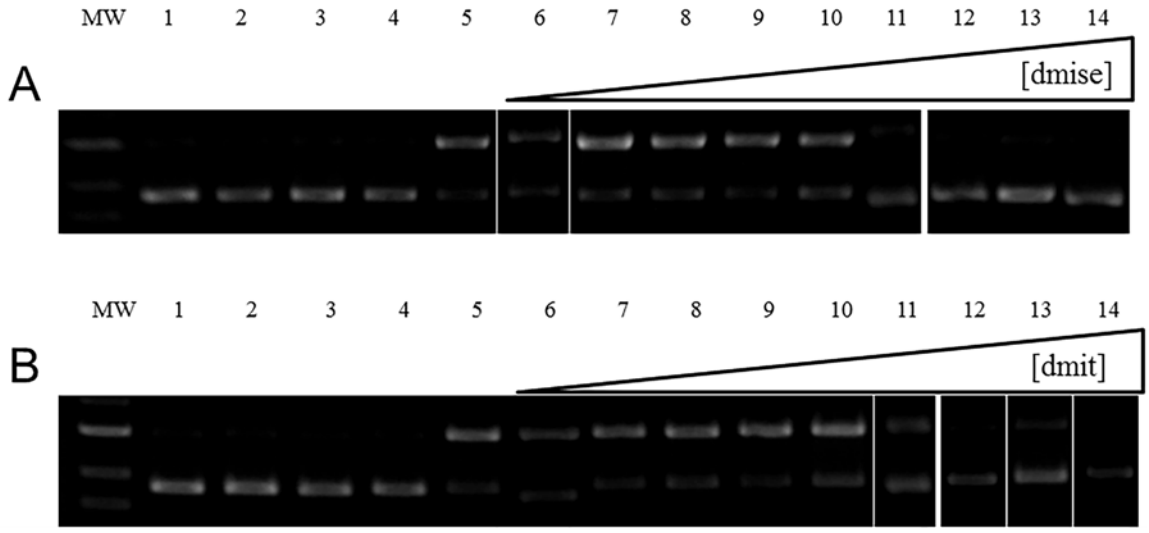

Figure 3.9. Gel electrophoresis images of peroxynitrite ($ONOO^-$)-mediated DNA damage inhibition by A) *N*,*N*'-dimethylimidazole selone (dmise) and B) *N*,*N*'-dimethylimidazole thione (dmit) in MOPS buffer (10 mM, pH 6.8). Lane: MW = 1 kb molecular weight marker; lane 1: plasmid DNA (p); lane 2: p + $NaNO_2$; lane 3: p + KNO_3; lane 4: p + S/Se compound (1000 μM); lane 5: p + $ONOO^-$ (1450 μM); lanes 6-14: p + $ONOO^-$ + increasing concentrations of compounds: 0.01, 0.1, 1, 10, 100, 250, 500, 1000 and 2000 μM, respectively.

Table 3.2. Gel electrophoresis results for *N*,*N*'-dimethylimidazole selone (dmise) DNA damage assays with 6 μM Cu^{I} and 50 μM H_2O_2.[a]

Gel Lane	[Dmise] (μM)	% Supercoiled	% Nicked	% Damage Inhibition	*P* Value
1: plasmid DNA (p)	0	97.30 ± 0.79	2.70 ± 0.79	–	–
2: p + H_2O_2	0	97.10 ± 1.40	2.9 ± 1.40	–	–
3: p + H_2O_2 + dmise	2000	98.90 ± 0.96	1.10 ± 0.96	–	–
4: p + Cu^{I} + H_2O_2	0	17.69 ± 6.64	82.31 ± 6.64	0	–
5: p + Cu^{I} + H_2O_2 + dmise	0.25	16.07 ± 1.19	83.92 ± 1.19	-1.44 ± 1.48	0.233
6	0.5	1.29 ± 0.70	98.71 ± 0.70	-0.59 ± 0.74	0.301
7	0.75	0.47 ± 0.44	99.53 ± 0.44	-1.15 ± 0.46	0.049
8	0.9	21.59 ± 4.64	78.41 ± 4.64	9.90 ± 5.44	0.088
9	1	13.73 ± 0.90	86.27 ± 0.90	12.55 ± 0.93	0.002
10	2.5	18.59 ± 1.72	81.41 ± 1.72	17.57 ± 1.77	0.003
11	5	39.18 ± 3.52	60.82 ± 3.52	38.94 ± 3.54	0.003
12	7.5	40.46 ± 2.01	59.54 ± 2.01	40.17 ± 2.08	< 0.001
13	10	49.38 ± 5.40	50.62 ± 5.40	39.95 ± 1.48	< 0.001
14	50	51.43 ± 1.02	48.56 ± 1.02	44.32 ± 0.83	< 0.001
15	100	46.25 ± 2.01	53.74 ± 2.01	42.65 ± 2.28	< 0.001
16	200	50.77 ± 0.96	49.22 ± 0.96	47.78 ± 1.09	< 0.001
17	300	59.80 ± 2.44	40.20 ± 2.44	51.97 ± 2.16	< 0.001
18	400	56.55 ± 1.06	43.44 ± 1.06	54.31 ± 1.20	< 0.001
19	600	72.35 ± 0.98	27.64 ± 0.98	72.20 ± 1.11	< 0.001
20	800	88.10 ± 1.29	11.90 ± 1.29	88.20 ± 1.82	< 0.001
21	1000	88.64 ± 1.71	11.35 ± 1.71	90.64 ± 1.93	< 0.001
22	1200	95.22 ± 1.30	4.78 ± 1.30	97.23 ± 3.58	< 0.001
23	1500	96.21 ± 1.01	3.79 ± 1.0	98.51 ± 0.93	< 0.001
24	2000	98.01 ± 0.86	1.99 ± 0.86	100.77 ± 3.08	< 0.001

[a]Data are reported as the average of three trials with calculated standard deviations.

Table 3.3. Gel electrophoresis results for *N*,*N*'-dimethylimidazole thione (dmit) DNA damage assays with 6 μM Cu^I and 50 μM H_2O_2.[a]

Gel Lane	[Dmit] (μM)	% Supercoiled	% Nicked	% Damage Inhibition	*p* Value
1: plasmid DNA (p)	0	95.50 ± 0.10	4.50 ± 0.10	–	–
2: p + H_2O_2	0	95.00 ± 0.20	5.00 ± 0.20	–	–
3: p + H_2O_2 + dmit	6000	98.90 ± 0.96	1.10 ± 0.96	–	–
4: p + Cu^I + H_2O_2	0	3.42 ± 2.85	96.58 ± 2.85	0	–
5: p + Cu^I + H_2O_2 + dmit	0.1	6.47 ± 0.76	93.53 ± 0.76	3.10 ± 3.61	0.275
6	1	4.19 ± 1.29	95.81 ± 1.29	0.73 ± 3.08	0.721
7	10	4.52 ± 2.90	95.48 ± 2.90	1.10 ± 3.90	0.673
8	50	14.37 ± 3.91	85.63 ± 3.91	5.34 ± 4.53	0.178
9	100	9.66 ± 6.38	90.34 ± 6.38	6.57 ± 4.85	0.143
10	250	20.15 ± 1.22	79.85 ± 1.22	12.03 ± 1.41	0.005
11	500	10.51 ± 1.85	89.48 ± 1.85	10.51 ± 1.85	0.010
12	1000	14.81 ± 2.31	85.18 ± 2.31	14.81 ± 2.31	0.008
13	1500	46.78 ± 0.83	53.21 ± 0.83	46.78 ± 0.83	< 0.001
14	2000	81.74 ± 1.60	18.25 ± 1.60	81.74 ± 1.60	< 0.001
15	4000	99.91 ± 0.03	0.08 ± 0.03	99.91 ± 0.03	< 0.001
16	6000	99.88 ± 0.07	0.11 ± 0.07	99.88 ± 0.07	< 0.001

[a]Data are reported as the average of three trials with calculated standard deviations.

Table 3.4. Gel electrophoresis results for *N*,*N*'-dimethylimidazole selone (dmise) DNA damage assays with 50 μM $[Cu(bipy)_2]^+$ and 50 μM H_2O_2.[a]

Gel Lane	[Dmise] (μM)	% Supercoiled	% Nicked	% Damage Inhibition	*p* value
1: plasmid DNA (p)	0	97.75 ± 0.84	2.25 ± 0.84	–	–
2: p + H_2O_2	0	97.20 ± 1.53	2.80 ± 1.53	–	–
3: p + H_2O_2 + dmise	2000	96.71 ± 0.70	3.29 ±0.70	–	–
4: p + $[Cu(bipy)_2]^+$ + H_2O_2	0	0.10 ± 0.21	99.86 ± 0.21	0	–
5: p + $[Cu(bipy)_2]^+$ + H_2O_2 + dmise	1	0.26 ± 0.14	99.74 ± 0.14	0.00 ± 0.06	1.000
6	10	3.26 ± 1.13	96.74 ± 1.13	3.32 ± 1.16	0.038
7	50	17.77 ± 1.27	82.22 ± 1.27	18.54 ± 1.33	0.002
8	100	37.02 ± 1.61	62.98 ± 1.61	38.11 ± 1.65	< 0.001
9	200	40.11 ± 3.00	59.88 ± 3.00	41.90 ± 3.14	< 0.001
10	500	71.03 ± 2.28	28.97 ± 2.28	73.15 ± 2.35	< 0.001
11	1200	88.14 ± 1.61	11.86 ± 1.61	90.77 ± 1.66	< 0.001
12	1500	90.37 ± 1.26	9.62 ± 1.26	94.45 ± 1.32	< 0.001
13	2000	93.24 ± 0.94	6.75 ± 0.94	97.45 ± 0.99	< 0.001

[a]Data are reported as the average of three trials with calculated standard deviations.

Table 3.5. Gel electrophoresis results for *N*,*N*'-dimethylimidazole thione (dmit) DNA damage assays with 50 μM $[Cu(bipy)_2]^+$ and 50 μM H_2O_2.[a]

Gel Lane	[Dmit] (μM)	% Supercoiled	% Nicked	% Damage Inhibition	*p* Value
1: plasmid DNA (p)	0	98.94 ± 0.62	1.06 ± 0.62	–	–
2: p + H_2O_2	0	98.66 ± 0.47	1.34 ± 0.47	–	–
3: p + dmit + H_2O_2	6000	96.71 ± 0.70	3.29 ± 0.70	–	–
4: p + $[Cu(bipy)_2]^+$ + H_2O_2	0	0.28 ± 0.03	99.72 ± 0.03	0	–
5: p + $[Cu(bipy)_2]^+$ + H_2O_2 + dmit	0.1	0.36 ± 0.33	99.64 ± 0.33	0.07 ± 0.34	0.755
6	1	0.31 ± 0.03	99.69 ± 0.03	0.03 ± 0.01	0.035
7	10	0.27 ± 0.12	99.73 ± 0.12	-0.01 ± 0.09	0.865
8	100	0.21 ± 0.15	99.79 ± 0.15	-0.07 ± 0.13	0.449
9	1000	8.55 ± 0.45	91.45 ± 0.45	8.35 ± 0.45	< 0.001
10	1500	31.52 ± 2.41	68.48 ± 2.41	33.35 ± 5.01	0.007
11	2000	36.21 ± 2.93	67.79 ± 2.93	38.83 ± 2.17	0.001
12	2500	36.37 ± 8.52	63.63 ± 8.52	42.07 ± 1.06	< 0.001
13	3000	42.95 ± 1.07	57.05 ± 1.07	44.28 ± 0.88	< 0.001
14	4000	53.65 ± 0.63	46.35 ± 0.63	55.99 ± 0.66	< 0.001
15	6000	61.13 ± 2.96	38.87 ± 2.96	60.04 ± 1.11	< 0.001

[a]Data are reported as the average of three trials with calculated standard deviations.

Table 3.6. Gel electrophoresis results for *N*,*N*'-dimethylimidazole selone (dmise) DNA damage assays with 2 μM Fe^{II} and 50 μM H_2O_2.[a]

Gel Lane	[Dmise] (μM)	% Supercoiled	% Nicked	% Damage Inhibition	*p* Value
1: plasmid DNA (p)	0	98.03 ± 1.10	1.97 ± 1.10	–	–
2: p + H_2O_2	0	95.48 ± 0.49	4.52 ± 0.49	–	–
3: p + dmise + H_2O_2	6000	98.21 ± 1.81	1.79 ± 1.81	–	–
4: p + Fe^{II} + H_2O_2	0	4.40 ± 1.35	95.60 ± 1.35	0	–
5: p + Fe^{II} + H_2O_2 + dmise	0.01	4.91 ± 3.24	95.09 ± 3.24	-1.78 ± 1.48	0.172
6	0.2	5.85 ± 4.31	94.15 ± 4.31	-0.73 ± 3.01	0.715
7	0.5	3.84 ± 0.88	96.15 ± 0.88	-2.00 ± 0.96	0.069
8	0.75	6.55 ± 0.54	93.44 ± 0.54	0.94 ± 0.59	0.110
9	1	9.05 ± 1.82	90.94 ± 1.82	3.64 ± 1.99	0.087
10	2.5	41.56 ± 4.15	58.43 ± 4.15	39.03 ± 4.52	0.004
11	5	67.86 ± 1.56	32.13 ± 1.56	67.64 ± 1.70	< 0.001
12	7.5	74.03 ± 3.14	25.96 ± 3.14	74.46 ± 3.37	< 0.001
13	10	62.86 ± 3.72	37.14 ± 3.72	63.08 ±2.12	< 0.001
14	50	76.99 ± 1.83	23.01 ± 1.83	74.38 ± 2.44	< 0.001
15	100	76.47 ± 0.66	23.53 ± 0.66	73.69 ± 3.47	< 0.001
16	200	71.41 ± 1.86	28.58 ± 1.86	72.12 ± 1.96	< 0.001
17	300	73.89 ± 1.74	26.10 ± 1.74	74.70 ± 1.84	< 0.001
18	400	76.49 ± 2.17	23.50 ± 2.17	77.48 ± 2.29	< 0.001
19	600	76.83 ± 0.82	23.17 ± 0.82	74.14 ± 3.33	< 0.001
20	800	83.13 ± 4.27	16.86 ± 4.27	84.48 ± 4.50	< 0.001
21	1000	84.21 ± 2.88	15.78 ± 2.88	86.04 ± 3.48	< 0.001
22	1200	88.08 ± 1.10	11.92 ± 1.10	87.59 ± 4.33	< 0.001
23	1500	87.35 ± 2.04	12.65 ± 2.04	86.91 ± 0.94	< 0.001
24	2000	92.51 ± 1.96	7.48 ± 1.96	96.09 ± 2.38	< 0.001
25	4000	94.66 ± 0.20	5.33 ± 0.20	96.56 ± 0.21	< 0.001
26	6000	98.54 ± 1.28	1.45 ± 1.28	99.04 ± 1.58	< 0.001

[a]Data are reported as the average of three trials with calculated standard deviations.

Table 3.7. Gel electrophoresis results for *N,N*'-dimethylimidazole thione (dmit) DNA damage assays with 2 μM Fe^{II} and 50 μM H_2O_2.[a]

Gel Lane	[Dmit] (μM)	% Supercoiled	% Nicked	% Damage Inhibition	*p* Value
1: plasmid DNA (p)	0	98.72 ± 1.07	1.28 ± 1.07	–	–
2: p + H_2O_2	0	98.91 ± 1.10	1.09 ± 1.10	–	–
3: p + dmit + H_2O_2	6000	98.09 ± 1.76	1.91 ± 1.76	–	–
4: p + Fe^{II} + H_2O_2	0	20.01 ± 0.90	79.98 ± 0.90	0	–
5: p + Fe^{II} + H_2O_2 + dmit	0.1	33.73 ± 5.48	66.26 ± 5.48	5.21 ± 0.89	0.010
6	1	38.98 ± 1.47	61.01 ± 1.47	24.67 ± 1.83	0.002
7	10	51.29 ± 3.92	48.70 ± 3.92	40.03 ± 4.89	0.005
8	100	60.99 ± 2.71	39.00 ± 2.71	52.12 ± 3.39	0.001
9	250	60.45 ± 1.48	39.54 ± 1.48	51.30 ± 1.87	< 0.001
10	500	72.59 ± 0.86	27.40 ± 0.86	66.64 ± 1.08	< 0.001
11	1000	84.86 ± 1.67	15.13 ± 1.67	81.90 ± 2.09	< 0.001
12	1500	81.85 ± 1.53	18.14 ± 1.53	78.34 ± 1.94	< 0.001
13	2000	87.39 ± 3.33	12.60 ± 3.33	85.34 ± 4.21	< 0.001
14	4000	89.19 ± 0.71	10.80 ± 0.71	87.74 ± 0.92	< 0.001
15	6000	94.04 ± 1.08	5.95 ± 1.08	93.97 ± 1.39	< 0.001

[a]Data are reported as the average of three trials with calculated standard deviations.

Table 3.8. Gel electrophoresis results for *N,N*'-dimethylimidazole selone (dmise) DNA damage assays with 400 μM $[Fe(EDTA)]^{2-}$ and 50 μM H_2O_2.[a]

Gel Lane	[Dmise] (μM)	% Supercoiled	% Nicked	% Damage Inhibition	*p* Value
1: plasmid DNA (p)	0			–	–
2: p + H_2O_2	0			–	–
3: p + dmise + H_2O_2	6000	97.42 ± 2.00	2.58 ± 2.00	–	–
4: p + $Fe(EDTA)^{2-}$ + H_2O_2	0	16.08 ± 1.98	83.92 ± 1.98	0	–
5: p + $Fe(EDTA)^{2-}$ + H_2O_2 + dmise	1	20.13 ± 0.52	79.87 ± 0.52	4.93 ± 2.57	0.080
6	10	34.29 ± 4.43	65.71 ± 4.43	22.38 ± 3.90	0.010
7	50	78.56 ± 1.47	21.44 ± 1.47	79.38 ± 1.73	< 0.001
8	100	78.80 ± 2.09	21.20 ± 2.09	77.07 ± 2.60	< 0.001
9	200	83.21 ± 3.52	16.79 ± 3.52	82.45 ±3.38	< 0.001
10	500	86.41 ± 3.43	13.59 ± 3.43	86.40 ± 2.51	< 0.001
11	1200	85.54 ± 1.95	14.46 ± 1.95	85.37 ± 2.47	< 0.001
12	1500	86.66 ± 3.80	13.34 ± 3.80	86.69 ± 2.77	< 0.001
13	2000	88.52 ± 1.72	11.48 ± 1.72	89.09 ± 1.59	< 0.001
14	4000	94.41 ± 3.10	5.58 ± 3.10	93.87 ± 3.63	< 0.001
15	6000	96.28 ± 1.45	3.71 ± 1.45	96.06 ± 1.69	< 0.001

[a]Data are reported as the average of three trials with calculated standard deviations.

Table 3.9. Gel electrophoresis results for *N*,*N*'-dimethylimidazole thione (dmit) DNA damage assays with 400 μM $[Fe(EDTA)]^{2-}$ and 50 μM H_2O_2.[a]

Gel Lane	[Dmit] (μM)	% Supercoiled	% Nicked	% Damage Inhibition	*p* Value
1: plasmid DNA (p)	0	99.28 ± 0.63	0.71 ± 0.63	–	–
2: p + H_2O_2	0	98.66 ± 0.74	1.33 ± 0.74	–	–
3: p + dmit + H_2O_2	2000	99.40 ± 0.99	0.60 ± 0.99	–	–
4: p + $[Fe(EDTA)]^{2-}$ + H_2O_2	0	10.80 ± 3.86	89.20 ± 3.86	0	–
5: p + $[Fe(EDTA)]^{2-}$ + H_2O_2 + dmit	0.1	11.33 ± 3.54	88.67 ± 3.54	0.58 ± 0.35	0.103
6	1	10.02 ± 3.32	89.98 ± 3.32	-0.92 ± 1.73	0.454
7	10	12.01 ± 3.61	87.99 ± 3.61	1.35 ± 0.36	0.023
8	100	17.49 ± 2.10	82.51 ± 2.10	7.51 ± 2.05	0.024
9	250	46.10 ± 0.26	53.90 ± 0.26	41.04 ± 0.31	< 0.001
10	500	66.62 ± 1.34	33.38 ± 1.34	64.93 ± 1.56	< 0.001
11	750	78.94 ± 0.60	21.06 ± 0.60	79.27 ± 0.70	< 0.001
12	1000	88.54 ± 1.16	11.46 ± 1.16	87.73 ± 0.59	< 0.001
13	1500	95.94 ± 2.61	4.06 ± 2.61	99.06 ± 3.04	< 0.001
14	2000	96.98 ± 0.61	3.02 ± 0.61	100.27 ± 0.71	< 0.001

[a]Data are reported as the average of three trials with calculated standard deviations.

Table 3.10. Gel electrophoresis results for *N*,*N*'-dimethylimidazole selone (dmise) DNA damage assays with 1450 μM $ONOO^-$.[a]

Gel Lane	[Dmise] (μM)	% Supercoiled	% Nicked	% Damage Inhibition	*p* Value
1: plasmid DNA (p)	0	96.02 ± 2.45	3.98 ± 2.45	–	–
2: p + Na_2NO_2	0	95.17 ± 1.42	4.83 ± 1.42	–	–
3: p + KNO_3	0	95.41 ± 1.15	4.59 ± 1.15	–	–
4: p + dmise	1000	94.04 ± 2.09	5.96 ± 2.09	–	–
5: p + $ONOO^-$	0	15.59 ± 1.48	84.41 ± 1.48	0	–
6: p + $ONOO^-$ + dmise	0.01	18.07 ± 1.04	81.93 ± 1.04	3.10 ± 0.51	0.009
7	0.1	18.07 ± 1.04	81.93 ± 1.04	3.10 ± 0.51	0.009
8	1	16.72 ± 1.63	83.28 ± 1.63	1.43 ± 0.29	0.013
9	10	22.53 ± 0.35	77.47 ± 0.35	8.70 ± 1.51	0.010
10	100	37.49 ± 0.91	62.51 ± 0.91	27.48 ± 1.77	< 0.001
11	250	75.62 ± 1.55	24.37 ± 1.55	73.60 ± 2.02	< 0.001
12	500	91.78 ± 1.23	8.22 ± 1.23	91.66 ± 1.53	< 0.001
13	1000	90.05 ± 1.78	9.95 ± 1.78	93.58 ± 1.59	< 0.001
14	2000	95.81 ± 0.42	4.19 ± 0.42	96.69 ± 0.53	< 0.001

[a]Data are reported as the average of three trials with calculated standard deviations.

Table 3.11. Gel electrophoresis results for *N*,*N*'-dimethylimidazole thione (dmit) DNA damage assays with 1450 μM $ONOO^-$.[a]

Gel Lane	[Dmit] (μM)	% Supercoiled	% Nicked	% Damage Inhibition	*p* Value
1: plasmid DNA (p)	0	96.57 ± 0.34	3.43 ± 0.34	–	–
2: p + Na_2NO_2	0	96.75 ± 0.66	3.25 ±0.66	–	–
3: p + KNO_3	0	97.37 ± 0.30	2.63 ± 0.30	–	–
4: p + dmit	1000	96.60 ± 0.78	3.40 ± 0.78	–	–
5: p + $ONOO^-$	0	17.70 ± 2.12	82.30 ± 2.12	0	–
6: p + $ONOO^-$ + dmit	0.01	19.61 ± 0.62	80.38 ± 0.62	1.22 ± 0.79	0.116
7	0.1	17.59 ± 1.75	82.41 ± 1.75	-0.15 ± 0.49	0.649
8	1	19.13 ± 0.60	80.87 ± 0.60	1.73 ± 3.30	0.460
9	10	32.15 ± 1.23	67.85 ± 1.23	18.26 ± 1.34	0.002
10	100	39.89 ± 3.23	60.11 ± 3.23	28.13 ± 2.33	0.002
11	250	56.91 ± 0.54	43.09 ± 0.54	49.23 ± 0.71	< 0.001
12	500	84.58 ± 0.90	15.42 ± 0.90	84.98 ± 1.17	< 0.001
13	1000	88.17 ± 1.06	11.83 ± 1.06	89.20 ± 1.68	< 0.001
14	2000	89.91 ± 0.72	10.09 ± 0.72	91.85 ± 0.93	< 0.001

[a]Data are reported as the average of three trials with calculated standard deviations.

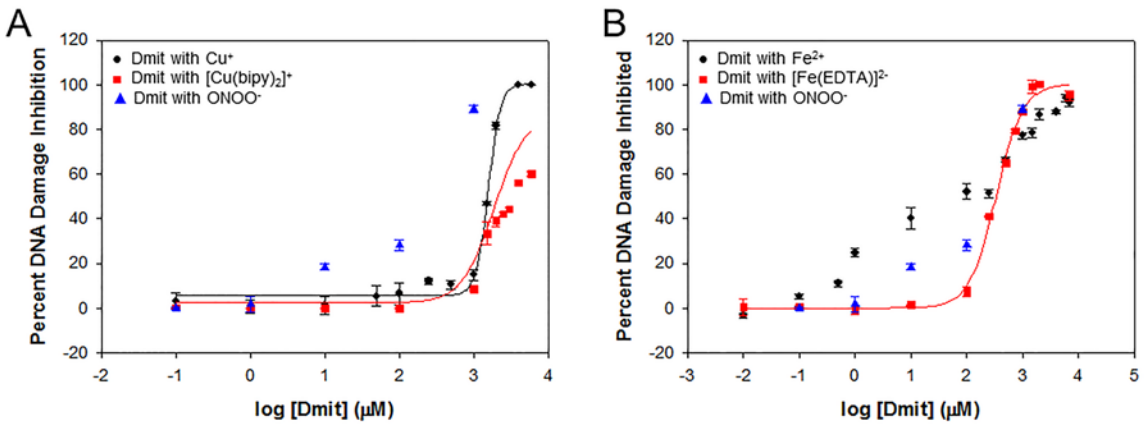

Figure 3.10. Dose-response curves for the inhibition of oxidative DNA damage by *N*,*N*'-dimethylimidazole thione (dmit). A) Studies with CuI and [Cu(bipy)]+ were conducted in MOPS buffer (10 mM, pH 7) and B) Studies with Fe^{II} and $[Fe(EDTA)]^{2-}$ were conducted in MES buffer (10 mM, pH 6). Studies with $ONOO^-$ were conducted in MOPS buffer (10 mM, pH 6.9). All error bars are standard deviations of three trials.

3.5. References

(1) Jamier, V.; Ba, L. A.; Jacob, C. *Chemistry* **2010**, *16*, 10920-10928.

(2) Mecklenburg, S.; Collins, C. A.; Döring, M.; Burkholz, T.; Abbas, M.; Fry, F. H.; Pourzand, C.; Jacob, C. *Phosphorus, Sulfur Silicon Relat. Elem.* **2008**, *183*, 863-888.

(3) Mecklenburg, S.; Shaaban, S.; Ba, L. A.; Burkholz, T.; Schneider, T.; Diesel, B.; Kiemer, A. K.; Roseler, A.; Becker, K.; Reichrath, J.; Stark, A.; Tilgen, W.; Abbas, M.; Wessjohann, L. A.; Sasse, F.; Jacob, C. *Org. Biomol. Chem.* **2009**, *7*, 4753-62.

(4) Jin, H.; Randazzo, J.; Zhang, P.; Kador, P. F. *J. Med. Chem.* **2006**, *53*, 1117-1127.

(5) Zhang, H.-Y.; Yang, D.-P.; Tang, G.-Y. *Drug Discovery Today* **2006**, *11*, 749-754.

(6) Linares, E.; Seixas, L. V.; dos Prazeres, J. N.; Ladd, F. V. L.; Ladd, A. A. B. L.; Coppi, A. A.; Augusto, O. *PLoS One* **2013**, *8*, 1-11.

(7) Imlay, J. A. *Annu. Rev. Biochem.* **2008**, *77*, 755-776.

(8) Yasui, H.; Hayashi, S.; Sakurai, H. *Drug Metab. Pharmacokinet.* **2005**, *20*, 1-13.

(9) Imlay, J. A.; Linn, S. *Science* **1988**, *240*, 1302-1309.

(10) Chantrel-Groussard, K.; Geromel, V.; Puccio, H.; Koenig, M.; Munnich, A.; Rotig, A.; Rustin, P. *Hum. Mol. Genet.* **2001**, *10*, 2061-2067.

(11) Bremmer, I. *Am. J. Clin. Nutr.* **1998**, *67*, 1069S-1073S.

(12) Turnlund, J. R.; Jacob, R. A.; Keen, C. L.; Strain, J. J.; Kelley, D. S.; Domek, J. M.; Keyes, W. R.; Ensunsa, J. L.; Lykkesfeldt, J.; Coulter, J. *Am. J. Clin. Nutr.* **2004**, *79*, 1037-1044.

(13) Lee, D. H.; Zacharski, L. R.; Jacobs, D. R., Jr. *Am. Heart J.* **2006**, *151*, 1247 e1-7.

(14) Mendes, J. F.; Arruda, S. F.; Siqueira, E. M.; Ito, M. K.; Silva, E. F. *Nutrition* **2009**, *25*, 379-384.

(15) Preedy, V. R.; Reilly, M. E.; Mantle, D.; Peters, T. J. *J. Inter. Fed. Clin. Chem.* **1998**, *10*, 16-20.

(16) Borkowski, T.; Szymusiak, H.; Gliszczynska-Rwiglo, A.; Rietjens, I. M.; Tyrakowska, B. *J. Agric. Food Chem.* **2005**, *53*, 5526-34.

(17) Muzolf, M.; Szymusiak, H.; Gliszczynska-Swiglo, A.; Rietjens, I. M.; Tyrakowska, B. *J. Agric. Food Chem.* **2008**, *56*, 816-823.

(18) Visioli, F.; Bellomo, G.; Galli, C. *Biochem. Biophys. Res. Commun.* **1998**, *247*, 60-64.

(19) Kapiszewska, M.; Cierniak, A.; Elas, M.; Lankoff, A. *Toxicol. In Vitro* **2007**, *21*, 1020-1030.

(20) Perron, N. R.; Hodges, J. N.; Jenkins, M.; Brumaghim, J. L. *Inorg. Chem.* **2008**, *47*, 6153-6161.

(21) Sang, S.; Hou, Z.; Lambert, J. D.; Yang, C. S. *Antioxid. Redox Signal.* **2005**, *7*, 1704-1714.

(22) Ullah, M. F.; Shamim, U.; Hanif, S.; Azmi, A. S.; Hadi, S. M. *Mol. Nutr. Food Res.* **2009**, *53*, 1376-1385.

(23) Kim, B. Y.; Kim, K. A.; Kwon, O.; Kim, S. O.; Kim, M. S.; Kim, B. S.; Oh, W. K.; Kim, G. D.; Jung, M.; Ahn, J. S. *Carcinogenesis* **2005**, *26*, 1395-1403.

(24) Perron, N. R.; Brumaghim, J. L. *Cell Biochem. Biophys.* **2009**, *53*, 75-100.

(25) Wang, H. C.; Brumaghim, J. L. In *Oxidative Stress: Diagnostics, Prevention, and Therapy*; American Chemical Society: 2011; Vol. 1083, pp 99-175.

(26) Joven, J.; March, I.; Espinel, E.; Fernandez-Arroyo, S.; Rodriguez-Gallego, E.; Aragones, G.; Beltran-Debon, R.; Alonso-Villaverde, C.; Rios, L.; Martin-Paredero, V.; Menendez, J. A.; Micol, V.; Segura-Carretero, A.; Camps, J. *Mol. Nutr. Food Res.*, *58*, 1374-1378.

(27) Patel, R.; Krishnan, R.; Ramchandani, A.; Maru, G. *Cell Prolif.* **2008**, *41*, 532-553.

(28) Battin, E. E.; Brumaghim, J. L. *J. Inorg. Biochem.* **2008**, *102*, 2036-2042.

(29) Battin, E. E.; Perron, N. R.; Brumaghim, J. L. *Inorg. Chem.* **2006**, *45*, 499-501.

(30) Battin, E. E.; Zimmerman, M. T.; Ramoutar, R. R.; Quarles, C. E.; Brumaghim, J. L. *Metallomics* **2011**, *3*, 503-512.

(31) Aruoma, O. I.; Whiteman, M.; England, T. G.; Halliwell, B. *Biochem. Biophys. Res. Commun.* **1997**, *231*, 389-391.

(32) Ey, J.; Schomig, E.; Taubert, D. *J. Agric. Food Chem.* **2007**, *55*, 6466-6474.

(33) Markova, N. G.; Karaman-Jurukovska, N.; Dong, K. K.; Damaghi, N.; Smiles, K. A.; Yarosh, D. B. *Free Radic. Bio. Med.* **2009**, *46*, 1168-1176.

(34) Rahman, I.; Gilmour, P. S.; Jimenez, L. A.; Biswas, S. K.; Antonicelli, F.; Aruoma, O. I. *Biochem. Biophys. Res. Commun.* **2003**, *302*, 860-864.

(35) Zhu, B. Z.; Mao, L.; Fan, R. M.; Zhu, J. G.; Zhang, Y. N.; Wang, J.; Kalyanaraman, B.; Frei, B. *Chem. Res. Toxicol.* **2011**, *24*, 30-34.

(36) Hartman, P. E. *Methods Enzymol.* **1990**, *186*, 310-318.

(37) Sotgia, S.; Zinellu, A.; Mangoni, A. A.; Pintus, G.; Attia, J.; Carru, C.; McEvoy, M. *PLoS One*, *9*, e84918.

(38) Yamashita, Y.; Yamashita, M. *J. Biol. Chem.* **2010**, *285*, 18134-18138.

(39) Yamashita, M.; Yamashita, Y.; Ando, T.; Wakamiya, J.; Akiba, S. *Biol. Trace Elem. Res.* **2013**, *156*, 36-44.

(40) Klein, M.; Ouerdane, L.; Bueno, M.; Pannier, F. *Metallomics* **2011**, *3*, 513-520.

(41) Okuno, A.; Yano, K.; Inyaku, F.; Suzuki, Y.; Sanae, N.; Kumai, M.; Naitoh, Y. *Acta Endocrinol.* **1987**, *115*, 112-118.

(42) Skellern, G. G.; Stenlake, J. B.; Williams, W. D.; McLarty, D. G. *Br. J. Clin. Pharmacol.* **1974**, *1*, 265-269.

(43) Bhabak, K. P.; Mugesh, G. *Chem. Eur. J.* **2010**, *16*, 1175-1185.

(44) Bhabak, K. P.; Satheeshkumar, K.; Jayavelu, S.; Mugesh, G. *Org. Biomol. Chem.* **2011**, *9*, 7343-7350.

(45) Kimani, M. M.; Brumaghim, J. L.; Vanderveer, D. *Inorg. Chem.* **2010**, *49*, 9200-9211.

(46) Ramoutar, R. R.; Brumaghim, J. L. *J. Inorg. Biochem.* **2007**, *101*, 1028-1035.

(47) Kim, J. M.; Chang, H. J.; Kim, W. K.; Chang, N.; Chun, H. S. *J. Agric. Food Chem.* **2006**, *54*, 6547-6553.

(48) Roussyn, I.; Briviba, K.; Masumoto, H.; Sies, H. *Arch. Biochem. Biophys.* **1996**, *330*, 216-218.

(49) Yildiz, G.; Demiryurek, A. T. *J. Pharmacol. Toxicol. Methods* **1998**, *39*, 179-184.

(50) Battin, E. E.; Brumaghim, J. L. *Cell. Biochem. Biophys.* **2009**, *55*, 1-23.

(51) Que, E. L.; Domaille, D. W.; Chang, C. J. *Chem. Rev.* **2008**, *108*, 1517-1549.

(52) Yang, L.; McRae, R.; Henary, M. M.; Patel, R.; Lai, B.; Vogt, S.; Fahrni, C. J. *Proc. Nat. Acad. Sci. USA* **2005**, *102*, 11179-11184.

(53) Henle, E. S.; Luo, Y.; Linn, S. *Biochemistry* **1996**, *35*, 12212-12219.

(54) Jhurry, N. D.; Chakrabarti, M.; McCormick, S. P.; Holmes-Hampton, G. P.; Lindahl, P. A. *Biochemistry* **2012**, *51*, 5276-5284.

(55) Ma, Y.; Liu, Z.; Hider, R. C.; Petrat, F. *Anal. Chem. Insights* **2007**, *2*, 61-67.

(56) Weiss, G.; Fuchs, D.; Hausen, A.; Reibnegger, G.; Werner, E. R.; Werner-Felmayer, G.; Wachter, H. *Exp. Hematol.* **1992**, *20*, 605-610.

(57) Akanmu, D.; Cecchini, R.; Aruoma, O. I.; Halliwell, B. *Arch. Biochem. Biophys.* **1991**, *288*, 10-16.

(58) Briggs, I. *J. Neurochem.* **1972**, *19*, 27-35.

(59) Epand, R. M.; Epand, R. F.; Wong, S. C. *J. Clin. Chem. Clin. Biochem.* **1988**, *26*, 623-626.

(60) Stadelman, B. S.; Kimani, M. M.; McMillen, C.; Brumaghim, J. L. *Inorg. Chem., submitted*.

(61) Koppenol, W. H.; Moreno, J. J.; Pryor, W. A.; Ischiropoulos, H.; Beckman, J. S. *Chem. Res. Toxicol.* **1992**, *5*, 834-842.

(62) Radi, R.; Peluffo, G.; Alvarez, M. N.; Naviliat, M.; Cayota, A. *Free Radic. Biol. Med.* **2001**, *30*, 463-488.

(63) De Silva, V.; Woznichak, M. M.; Burns, K. L.; Grant, K. B.; May, S. W. *J. Am. Chem. Soc.* **2004**, *126*, 2409-2413.

(64) Epe, B.; Ballmaier, D.; Roussyn, I.; Briviba, K.; Sies, H. *Nucleic Acids Res.* **1996**, *24*, 4105-4110.

(65) Beckman, J. S.; Beckman, T. W.; Chen, J.; Marshall, P. A.; Freeman, B. A. *Proc. Natl. Acad. Sci. USA* **1990**, *87*, 1620-1624.

(66) Sotgia, S.; Zinellu, A.; Mangoni, A. A.; Pintus, G.; Attia, J.; Carru, C.; McEvoy, M. *PLoS One* **2014**, *9*, e84918.

(67) Okuno, A.; Yano, K.; Inyaku, F.; Suzuki, Y.; Sanae, N.; Kumai, M.; Naitoh, Y. *Acta Endocrinol.* **1987**, *115*, 112-118.

(68) Skellern, G. G.; Stenlake, J. B.; Williams, W. D. *Br. J. Clin. Pharmac.* **1974**, *1*, 265-269.

(69) Burk, R. F.; Norsworthy, B. K.; Hill, K. E.; Motley, A. K.; Byrne, D. W. *Cancer Epidemiol. Biomarkers* **2006**, *15*, 804-810.

(70) Reid, M. E.; Stratton, M. S.; Lillico, A. J.; Fakih, M.; Natarajan, R.; Clark, L. C.; Marshall, J. R. *J. Trace Elem. Med. Biol.* **2004**, *18*, 69-74.

(71) Roy, G.; Das, D.; Mugesh, G. *Inorg. Chim. Acta* **2007**, *360*, 303-316.

(72) Hertzberg, R. P.; Dervan, P. B. *J. Am. Chem. Soc.* **1982**, *104*, 313-315.

(73) Lloyd, R. S.; Haidle, C. W.; Robberson, D. L. *Biochemistry* **1978**, *17*, 1890-1896.

(74) Keith, W. G.; Powell, R. E. *J. Chem. Soc. A* **1969**, 90.

(75) Hughes, M. N.; Nicklin, H. G. *J. Chem. Soc. A* **1971**, 164-168.

CHAPTER FOUR

IDENTIFYING CHEMICAL PROPERTIES THAT INFLUENCE THE DNA DAMAGE PREVENTION ABILITIES OF THIONES, SELONES, AND THEIR ANALOGS

4.1. Introduction

Antioxidant prevention of oxidative damage caused by reactive oxygen species (ROS) has resulted in increasing interest in determining how antioxidants can be used for the prevention or treatment of diseases caused by oxidative stress.[1-5] For this reason sulfur and selenium compounds have been extensively studied for their antioxidant activity.[6-13]

Initial interest in antioxidant selones, thiones, and their derivatives arose from the discovery of the naturally occurring thione amino acid, ergothioneine (ESH, Figure 4.1), found in concentrations 1-3 mM from in human plasma. ESH is a known ROS scavenger and effectively prevents Cu^{I}-mediated deoxyribose damage at a concentration of 1 mM.[14-19]; whereas, selenoneine (Figure 4.1), has been reported in concentrations up to 9 nM in human blood.[20] Although, very little is known about the antioxidant properties of selenoneine,[21] studies have shown that it can protect myoglobin and hemoglobin from oxidation by iron ions under hypoxic conditions[22,23] and act as a radical scavenger of 1,1-diphenyl-2-picrylhydrazyl (DPPH).[23]

Analogs of ergothioneine and selenoneine,*N*,*N'*-dimethylimidazole thione (dmit) and selone (dmise; Figure 4.1), prevent Fe^{II}, Cu^{I}-, and peroxynitrite-mediated oxidative DNA damage at low micromolar concentrations. Dmit and dmise were unique among sulfur and selenium antioxidants in that they not only prevent oxidative DNA damage

through multiple mechanisms, but that they more effectively prevent iron-mediated DNA damage than copper-mediated damage. Their ability to prevent DNA damage when metal coordination was blocked by chelation, using $[Fe(EDTA)]^{2-}$ (EDTA = ethylenediaminetetraacetic acid) and $[Cu(bipy)_2]^{+}$ (bipy – 2,2'-bipyridyl) as the damaging metal species, suggested that metal coordination is necessary for activity at low micromolar concentrations, and DNA damage studies with peroxynitrite ($ONOO^-$) confirmed that ROS scavenging is a major antioxidant mechanism at higher concentrations. In addition, oxidation studies conducted by Kimani *et al.*[24] found that H_2O_2 reacted preferentially with Cu^I-bound dmise or dmit instead of Cu^I, thus preventing Cu^I oxidation and concomitant $^{\bullet}OH$ generation (targeted scavenging).

Concentrations of non-protein bound copper in human brain tissue have been measured between 1-1300 µM,[25,26] and non-protein-bound iron concentrations have been reported between 1-30 µM in human cells.[27-29] Under oxidative stress, the cellular pathways used to maintain metal homeostasis can be overwhelmed, leading to increased non-protein-bound Fe^{II} and Cu^{I}[7,30-32] and overproduction of the damaging hydroxyl radical ($^{\bullet}OH$) *via* the Fenton (iron) and Fenton-like (copper) reactions (Reaction 1).[33-35] This catalytic metal-generated $^{\bullet}OH$ formation results in oxidative DNA damage.[8,30,32]

$$Cu^I/Fe^{II} + H_2O_2 \rightarrow Cu^{II}/Fe^{III} + {}^{-}OH + {}^{\bullet}OH \quad (1)$$

Clinical trials with sulfur and selenium antioxidants have been of great interest, due to their potential to prevent cancer.[7,36-38] However, clinical trials of selenium supplementation for prostate cancer prevention have concluded with mixed results. The Nutritional Prevention of Cancer trial (NPC) and Selenium and Vitamin E Cancer

Prevention Trial (SELECT) treated participants with selenium-enriched yeast and selenomethionine (200 μg/day), respectively. Results from the NPC trial revealed a 37% decrease in total cancer incidence, including a substantial reduction in prostate cancer,[39] yet the SELECT reported no significant effect of selenium supplementation on the prevention of prostate cancer.[40-42] These conflicting trial results highlight the need to understand the antioxidant mechanisms for specific sulfur and selenium compounds at the chemical level before continuing with animal and clinical studies.

The selected sulfur and selenium compounds in Figure 4.1 were investigated to determine if the multifunctional antioxidant activity observed for dmise and dmit was a universal trait for selones, thiones, and their derivatives, and to identify which mechanisms are primary in their DNA damage prevention ability. The compounds in Figure 4.1 were also chosen to identify specific relationships between chemical features and measured antioxidant activity.

For this work, gel electrophoresis studies were used to assess the ability of the compounds in Figure 4.1 to prevent Cu^{I}- and Fe^{II}-mediated DNA damage and to identify the chemical properties (speciation, aromaticity, substituent functional groups, and denticity) that enhance inhibition of metal-mediated DNA damage. Mass spectrometry studies were also conducted to determine whether these sulfur and selenium compounds form complexes with Cu^{I} and Fe^{II} in aqueous solution. Similar DNA damage assays were conducted with peroxynitrite ($ONOO^{-}$) as the damaging ROS source. Since no metal is required for peroxynitrite-mediated DNA damage, these studies determine the ROS scavenging abilities of the tested compounds. Additionally, electrochemical studies were

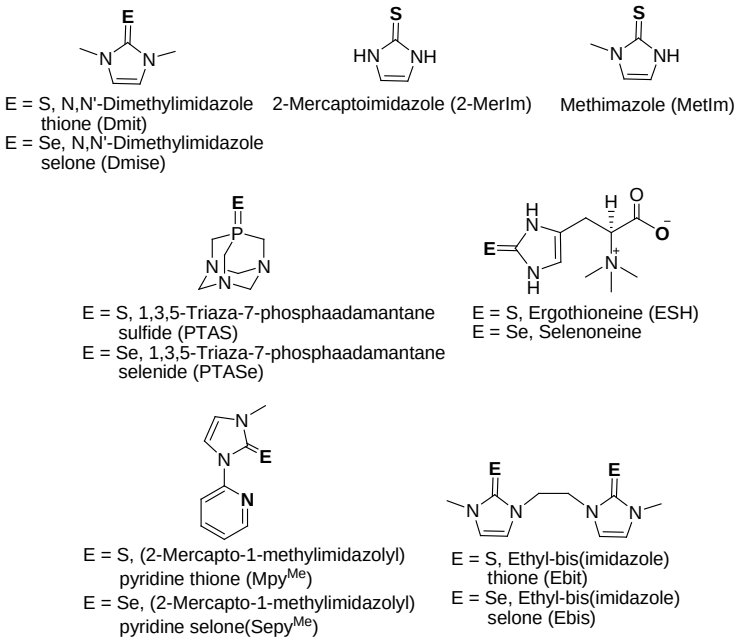

Figure 4.1. Sulfur and selenium compounds discussed in Chapter 4. Potential metal-binding sites are highlighted in bold.

performed to determine the ability of these compounds to readily undergo oxidation, an indication of ROS scavenging ability. This work is the first to explore the relationship between structure and DNA damage prevention ability of thiones, selones, and their analogs; and results from these studies will allow development of more effective selone and thione antioxidants for use as multifunctional drugs and supplements. The research presented in this Chapter was conducted in collaboration with of Prof. Daniel Rabinovich (University of North Carolina at Charlotte), who provided several selone and thione compounds for analysis, Prof. Sandra K. Wheeler and undergraduate researcher Emily Kurfman (Furman University) who conducted ESI-MS studies on many sulfur and selenium compounds, and with Clemson undergraduate researcher Alyssa D. Rabon, who conducted some of the DNA damage assays with PTAS and PTASe.

4.2. Results and Discussion

4.2.1. Copper(I)-mediated oxidative DNA damage prevention. Gel electrophoresis studies were used to investigate the thione- and selone-derived compounds in Figure 4.1 for their ability to prevent Cu^{I}-mediated oxidative DNA damage. All experiments were conducted with 6 μM Cu^{I} at pH 7 to mimic physiological conditions. Figure 4.2 shows a representative gel showing copper-mediated DNA damage prevention by ESH. Hydrogen peroxide alone (50 μM; lane 2) does not cause oxidative DNA damage, nor does ESH combined with H_2O_2 (lane 3). Upon addition of H_2O_2 to Cu^{I}, more than 90% DNA damage is observed (lane 4). Subsequent addition of ESH shows a decrease in DNA damage with increasing ESH concentration (lanes 5-14); by 2000 μM, more than 95 % of the DNA damage is prevented. Figure 4.3 shows the best-fit sigmodial dose-response curve obtained from the DNA damage assays with ESH, and the concentration needed to inhibit 50 % of copper-mediated DNA damage (IC_{50} value) was calculated as 22.0 μM (Table 4.1). Using similar methods, IC_{50} values (Table 4.1) were also determined for the dithione, ebit (31.9 μM), MetIm (102.3 μM), mpy^{Me} (383.7 μM), and PTAS (1023 μM;

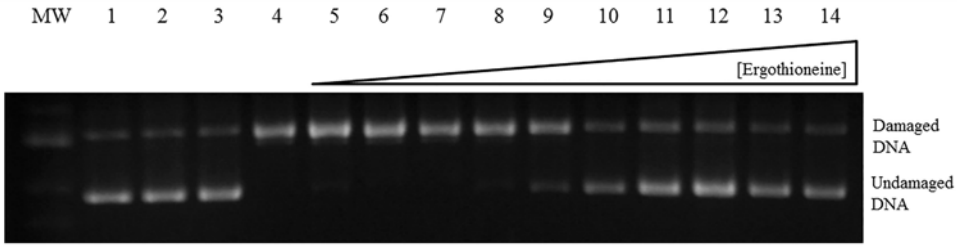

Figure 4.2. Gel electrophoresis image of Cu^{I}-mediated DNA damage inhibition by ergothioneine (ESH) in MOPS buffer (10 mM, pH 7). Lane MW: 1 kb molecular weight marker; lane 1: plasmid DNA (p); lane 2: p + H_2O_2 (50 μM); lane 3: p + ESH (2000 μM) + H_2O_2; lane 4: p + ascorbate (7.5 μM) + $CuSO_4$ (6 μM) + H_2O_2; lanes 5-14: p + $CuSO_4$ + ascorbate + H_2O_2 + increasing concentrations of ESH: 0.1, 1, 2, 5, 10, 50, 100, 500, 1000, and 2000 μM respectively.

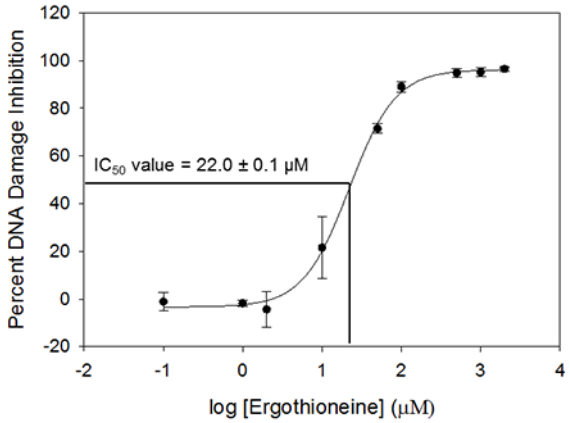

Figure 4.3. Dose-response curve for Cu^{I}-mediated DNA damage inhibition versus ergothioneine concentration (µM).

Figure 4.1; all gel images and IC_{50} plots are provided at the end of the Experimental Methods section in Figures 4.5 through 4.19).

All of the sulfur-containing compounds investigated inhibit Cu^{I}-mediated DNA damage, in stark contrast to the lack of activity observed for many of the amino acid-derived sulfur compounds previously studied.[7,9,10] Arranging the thione compounds from highest to lowest IC_{50} values, dmit < PTAS < mpy^{Me} < MetIm < ebit < 2-MerIm < ESH, shows that these compounds cover a wide range of activities (IC_{50} values from 22-1550 µM), indicating that structural or other properties play a significant role in enhancing antioxidant activity. As methyl groups are removed from the imidazole ring, the antioxidant activity is enhanced by 70-fold from dimethylated dmit (IC_{50} = 1550 µM) to the mono-methylated MetIm (102 µM) to the non-methylated ESH and 2-MerIm (IC_{50} = 22 µM). The presence of the pyridine ring in mpy^{Me} is not as effective as addition of a second thione in ebit or the amino acid group in ESH.

Thione compounds with the lowest IC_{50} values have multiple potential metal-binding sites (shown in bold in Figure 4.1), suggesting that metal coordination ability

Table 4.1. IC_{50} values[a] for the prevention of DNA damage by sulfur and selenium compounds.

Compound	Cu^{I} IC_{50} (μM)	Fe^{II} IC_{50} (μM)	$ONOO^-$ IC_{50} (μM)
Sulfur			
ESH	22.0 ± 0.1	5.78 ± 0.01	594 ± 5
2-MerIm	22.06 ± 0.03	2.31 ± 0.01	417 ± 1
Ebit	31.9 ± 0.1	88.3 ± 0.1	48 ± 6 % (100 μM)
MetIm	102.3 ± 0.2	5.78 ± 0.07	378 ± 2
Mpy^{Me}	383.7 ± 0.5	55 ± 2 % (1000 μM)	~289[b]
PTAS	1023 ± 4	44 ± 4 % (1000 μM)	49 ± 2 % (1000 μM)
Dmit	1550 ± 3[c]	89.1 ± 0.2	171.4 ± 0.2
Selenium			
$Sepy^{Me}$	11.85 ± 0.01	44.66 ± 0.07	67.61 ± 0.08
Ebis	13.09 ± 0.03	3.68 ± 0.01	71 ± 3 % (100 μM)
PTASe	57.3 ± 0.2	52.4 ± 0.1	57.5 ± 0.2
Dmise	~240[b,c]	3.2 ± 0.9	155.2 ± 0.1

[a]IC_{50} is the concentration at which the compound inhibits 50% DNA damage. [b]Estimated values. [c]Values from reference 43.

may contribute to DNA damage prevention for these compounds. The amino acid group in ESH increases activity more than the second thione in ebit and 70-fold over the monodentate dmit, but potential pyridine nitrogen coordination in mpy^{Me} increases DNA damage prevention only 4-fold compared to dmit.[43] Thus, the DNA damage prevention activities of the sulfur compounds investigated is heavily influenced by the secondary functional groups are present.

All the selone-derived compounds in Figure 4.1 inhibit Cu^{I}-mediated DNA damage. In contrast to the modest activity of the thione mpy^{Me}, its selenium analog, $sepy^{Me}$, is the most effective selone, inhibiting 50 % of Cu^{I}-mediated DNA damage at 11.85 μM. Similarly, the IC_{50} values of ebis and PTASe are 13.09 μM and 57.3 μM, respectively. Again, potential metal binding sites influence antioxidant activity; the potentially bidentate diselone ebis, and the potentially bidentate pyridine-containing $sepy^{Me}$ both have similar IC_{50} values that are lower than the monodentate PTASe and dmise.[43] Examining the effect of methyl substituents on the imidazole nitrogen atoms

was not possible, since removal of even one methyl group makes these selone compounds unstable to air oxidation.[44]

A comparison of the sulfur and selenium compounds reveals that the selenium compounds are substantially more effective at preventing Cu^{I}-mediated DNA damage than their sulfur analogs. $Sepy^{Me}$ is ~30 times more effective than mpy^{Me}, and PTASe is 17 times more effective than its sulfur analog, PTAS. A similar trend was previously observed for selenoamino acid compounds when compared to their sulfur analogs.[7,9,10]

4.2.2. Fe^{II}-mediated oxidative DNA damage prevention. A similar gel electrophoresis protocol was used to determine the ability of the compounds in Figure 4.1 to prevent metal-mediated DNA damage caused by Fe^{II}/H_2O_2. All Fe^{II} experiments were conducted at pH 6, due to Fe^{II} insolubility at pH > 6.[45-47] As with Cu^{I} DNA damage assays, all of the compounds investigated show the ability to prevent Fe^{II}-mediated DNA damage (gel images and IC_{50} plots are provided after the Experimental Methods section in Figures 4.5 and 4.19). This widespread ability to prevent Fe^{II}-mediated DNA damage was not observed with sulfur and selenium amino acid derivatives.[7,9,10] This increased activity for preventing iron-mediated DNA damage over copper is unprecedented for sulfur and selenium antioxidants. In actuality, the majority of the sulfur amino acids investigated showed no ability to prevent Fe^{II}-mediated DNA damage. The ability of the sulfur and selenium compounds investigated in this Chapter to effectively inhibit Fe^{II}-mediated DNA damage in addition to Cu^{I}-mediated DNA damage suggests that the antioxidant activity of these compounds can be tuned for various redox metals.

Under these conditions, 2-MerIm is the most effective antioxidant, inhibiting 50 % of Fe^{II}-mediated DNA damage at 2.31 μM. Both ESH and MetIm also have very low IC_{50} values of 5.78 μM (Table 4.1). Ebit inhibits 50 % of Fe^{II}-mediated DNA damage at 88.3 ± 0.1 μM, almost three times the concentration of its IC_{50} value for prevention of copper-mediated damage. Both mpy^{Me} and PTAS only weakly inhibit iron-mediated DNA damage, preventing 55 ± 3 % and 44 ± 4 % DNA damage at 1000 μM, respectively.

Selones and their analog compounds (Figure 4.1) also show significant ability to prevent iron-mediated DNA damage, with IC_{50} values ranging from 3-45 μM. The diselone ebis inhibits 50 % of Fe^{II}-mediated DNA damage at 3.68 μM. Ebis is 12 times more effective at preventing Fe^{II}-mediated DNA damage than $sepy^{Me}$ (IC_{50} = 52.4 ± 0.1 μM), indicating that the presence of two selone groups results in more effective antioxidant activity than one selone and one pyridine group. The non-selone PTASe (IC_{50} = 44.66 μM) is the least effective selenium compound at preventing Fe^{II}-mediated DNA damage.

In comparison to the sulfur compounds, the selenium compounds are substantially more effective than their sulfur analogs at preventing Fe^{II}-mediated DNA damage. Ebis is 24 times more effective than ebit, and dmise is almost 28 times more effective than dmit at preventing irom-mediated damage. Once again, methylation is a significant factor in the prevention of iron-mediated DNA damage, since the non-methylated 2-MerIm has the lowest IC_{50} value, followed by the non-methylated ESH the mono-methylated MetIm, with the dimethylated dmit a distant fourth. Overall, these results suggest that the

presence of the imidazole-based thione or selone is stronger than the effects of the substituent functional groups, such as an amino acid tail, or denticity of the compounds. Interestingly, all mono-thione compounds have similar IC_{50} values compared to their dithione analogs, a trend also observed for the selone analogs. This similarity is not observed for prevention of Cu^{I}-mediated DNA damage, and indicates that the metal ion greatly affects the behavior of these antioxidants.

4.2.3. Quantifying ROS scavenging using peroxynitrite ($ONOO^-$)-mediated oxidative DNA damage. Gel electrophoresis experiments with peroxynitrite ($ONOO^-$) as the DNA-damaging agent were conducted to investigate the ROS scavenging abilities of the sulfur and selenium compounds (Figure 4.1). Generation of $ONOO^-$ is metal-independent and occurs biologically through the reaction of superoxide and nitric acid.[48,49] Peroxynitrite directly damages biomolecules,[50-55] including plasmid and eukaryotic DNA.[56,57] At pH 6.8, $ONOO^-$ is protonated to peroxynitrous acid, which has half-life of 1 s, and rapidly decomposes into $^{\bullet}OH$ and nitrogen dioxide ($NO_2^{\bullet}$), leading to oxidative single-strand breaks in DNA similar to the Fenton and Fenton-like reactions (Reaction 1).[58] For these experiments, a protocol similar to the Fe^{II}-mediated oxidative DNA damage studies was used, in which $ONOO^-$ (1450 μM) in MES buffer (10 mM, pH 6.8) was substituted for Fe^{II} and H_2O_2.

All the investigated sulfur compounds prevent $ONOO^-$-mediated DNA damage (Table 4.2), all gel images and IC_{50} plots are provided at the end of the Experimental Methods section in Figures 4.5 and 4.19), but at significantly higher concentrations than those required to prevent Cu^{I}- and Fe^{II}-mediated DNA damage. ESH, 2-MerIm, and

MetIm prevent 50 % of $ONOO^-$-mediated DNA damage at 594 μM, 417 μM, and 378 μM, respectively. To inhibit 50 % $ONOO^-$-mediated DNA damage, ESH requires a concentration 27 times higher than that needed for similar prevention of Cu^I-mediated DNA damage. Similarly, 2-MerIm and MetIm require 19 and 4 times the concentrations needed to prevent 50 % of Cu^I-mediated damage, respectively, and 208 and 63 times the concentrations needed to prevent Fe^{II}-mediated DNA damage, respectively. At 1000 μM, PTAS inhibits 49 % of $ONOO^-$-mediated DNA damage, similar to its activity observed with Cu^I and Fe^{II}. At the maximum concentration (100 μM), ebit inhibits only 48 % of $ONOO^-$-mediated DNA damage, whereas lower concentrations are need for 50 % DNA damage prevention with Cu^I and Fe^{II}.

All of the selenium compounds exhibit significantly more activity towards $ONOO^-$-mediated DNA damage than their sulfur analogs (Table 4.2), similar to the trends for Cu^I and Fe^{II} DNA damage studies. The non-methylated and mono-methylated compounds, ESH, 2-MerIm, and MetIm all have close IC_{50} values, a trend previously

Table 4.2. IC_{50} values[a] for the prevention of $[Cu(bipy)_2]^+$-, $[Fe(EDTA)]^{2-}$-, and $ONOO^-$-mediated DNA damage by the sulfur and selenium compounds.

Compound	$[Cu(bipy)_2]^+$ IC_{50} (μM)	$[Fe(EDTA)]^{2-}$ IC_{50} (μM)
Sulfur		
Dmit	3470 ± 5[b]	353.2 ± 0.4[b]
Ebit	19 ± 1 % (100 μM)	35 ± 2 % (100 μM)
Mpy^{Me}	63 ± 2 % (100 μM)	167.9 ± 0.2
PTAS	19 ± 3 % (2000 μM)	13 ± 3 % (1000 μM)
MetIm	—	51.6 ± 0.1
ESH	—	238.2 ± 0.4
2-MerIm	—	139.9 ± 0.4
Selenium		
Dmise	205.5 ± 0.4[b]	34.04 ± 0.07[b]
Ebis	55 ± 2 % (100 μM)	38 ± 1 % (100 μM)
$Sepy^{Me}$	14.13 ± 0.01	4.72 ± 0.01
PTASe	2 ± 2 % (2000 μM)	57 ± 1 % (1000 μM)

[a] IC_{50} is the concentration at which the compound inhibits 50% DNA damage. [b]Values from reference 43.

observed with prevention of Fe^{II}-mediated DNA damage. Both mpy^{Me} and PTAS exhibit the least ability to prevent $ONOO^-$-mediated DNA damage, similar to their activities towards labile Cu^I and Fe^{II}; however, unlike the metal-based studies, ebit is the most effective sulfur compound at preventing $ONOO^-$-mediated DNA damage.

Metal-mediated DNA damage prevention by the sulfur and selenium compounds in Figure 4.1 is typically observed at much lower concentrations than required to inhibit non-metal-mediated peroxynitrite damage, indicating that ROS scavenging is not the active antioxidant mechanism at lower, more biologically relevant concentrations of these compounds. Thus, the peroxynitrite DNA damage studies in addition to the metal-mediated DNA damage results, confirm the ability of sulfur and selenium compounds to inhibit oxidative DNA damage through multiple pathways, not just ROS scavenging.

4.2.4. The effect of metal coordination on the prevention of DNA damage. Previous studies have shown the importance of metal coordination for sulfur and selenium prevention of Cu^I-mediated DNA damage.[7-13] To determine the significance metal coordination is to the DNA damage prevention abilities of the sulfur and selenium compounds investigated, experiments were conducted with $[Cu(bipy)_2]^+$ and H_2O_2, a combination that causes oxidative DNA damage, but where the Cu^I is chelated prior to antioxidant addition to prevent metal-antioxidant interactions. Under these conditions, no DNA damage inhibition should be observed if copper coordination is necessary for antioxidant activity.

Many of the sulfur and selenium compounds investigated show some ability to prevent oxidative DNA damage (Table 4.2) caused by $[Cu(bipy)_2]^+$ and H_2O_2, but most

only at high concentrations (1000 and 2000 μM). Only ESH, MetIm, 2-MerIm, and PTASe exhibit little to no activity under these conditions. Similar results were previously reported for dmit and dmise, with IC_{50} values of 3470 μM and 205 μM, respectively.[43] It is not clear why ESH prevents no $[Cu(bipy)_2]^+$-mediated oxidative DNA damage, although this may be due to its amino acid functionality; the sulfur-containing amino acids previously studied also showed no ability to inhibit $[Cu(bipy)_2]^+$- mediated DNA damage.[7,9,10]

Gel electrophoresis experiments were also conducted with $[Fe(EDTA)]^{2-}$ to investigate the extent that prior Fe^{II} chelation affects the antioxidant activity of the investigated sulfur and selenium compounds. Like $[Cu(bipy)_2]^+$, $[Fe(EDTA)]^{2-}$ reacts with H_2O_2 and generate DNA-damaging $^{\bullet}OH$,[7,9,10] but EDTA fully coordinates the octahedral Fe^{II} ion and prevents sulfur and selenium antioxidant coordination to Fe^{II}.

All of the investigated compounds show some ability to prevent $[Fe(EDTA)]^{2-}$-mediated DNA damage (Table 4.2), with IC_{50} values between 4 and 353 μM. PTAS and PTASe at 1000 μM have maximum inhibition percentages of 13 % and 57 %, respectively, and ebit and ebis show 35 % and 38 % inhibition at 100 μM, respectively. Surprisingly, both mpy^{Me} and $sepy^{Me}$ have lower IC_{50} values lower with $[Fe(EDTA)]^{2-}$ (Table 4.2) as compared to the studies with unchelated Fe^{II}, suggesting that ROS scavenging may be a more significant mechanism for mpy^{Me} and $sepy^{Me}$ DNA damage inhibition. In contrast, MetIm, 2-MerIm, and ESH prevent $[Fe(EDTA)]^{2-}$-mediated DNA damage at substantially higher concentrations compared to their IC_{50} values for the prevention of Fe^{II}-mediated damage.

The dimethylated dmit is less effective at inhibiting $[Fe(EDTA)]^{2-}$-mediated DNA damage than the mono-methylated MetIm and the non-methylated 2-MerIm, further indicating that removing methylation is critical to maximizing the antioxidant activity of thione compounds. Additionally, these results also indicate that metal coordination is the active mechanism at low concentrations of the compounds in Figure 4.2, and that a second mechanism, likely ROS scavenging, is active when $[Fe(EDTA)]^{2-}$ is used or at high concentrations of the investigated compounds.

Comparison between the $[Cu(bipy)_2]^{+}$ and $[Fe(EDTA)]^{2-}$ results reveals that most of the compounds investigated are more effective at preventing DNA damage caused by $[Fe(EDTA)]^{2-}$ than $[Cu(bipy)_2]^{+}$, with the exception of ebis and PTAS. Thus, antioxidant activity is affected by the metal species that causes the damage, not simply the ROS that is generated. It is likely that ROS scavenging is a primary mechanism for inhibition of this damage, since it is unlikely any of the compounds investigated can compete with bipy or EDTA for coordination sites of copper or iron; for example, the binding affinity of EDTA for Fe^{II} is 2×10^{14}.[59] Thus, these studies suggest that at biologically relevant, low concentrations of the investigated thione- and selone-containing compounds, metal coordination is the primary antioxidant mechanism, and at higher concentrations when the system is saturated with these compounds, ROS scavenging is a primary mechanism. Comparison of all the DNA damage inhibition results suggest that the metal complexes that cause oxidative DNA damage are just as important to the observed antioxidant activity as is the sulfur or selenium source.

4.2.5. Cu^{I} and Fe^{II} coordination studies by mass spectrometry. MALDI-TOF mass spectrometry studies were conducted on the investigated sulfur and selenium antioxidants to determine their ability to coordinate Cu^{I} and Fe^{II}. Ebit, ebis, and mpy^{Me} form only 1:1 (Cu^{I}:ligand) complexes, $sepy^{Me}$ forms both 1:1 and 1:2 complexes with Cu^{I}, ESH forms only a 1:2 complex, and MetIm forms complexes with 1:2 and 1:3 ratios (Table 4.3). PTAS and PTASe exhibit no metal coordination under these conditions, although coordination complexes of these ligands with Ag^{I} and Co^{II} are reported.[60,61]

Since Cu^{I} typically prefers tetrahedral coordination geometry, it is likely that the compounds such as ESH, mpy^{Me}, $sepy^{Me}$, ebit, and ebis will bind Cu^{I} through multiple sites (Figure 4.1). ESH can bind through the thione sulfur as well as the carboxylate oxygen. Both mpy^{Me} and $sepy^{Me}$ have been reported to coordinate Cu^{I} through the thione and selone, respectively, in addition to the pyridine nitrogen.[62] Similarly, studies have reported the ability of dmit and dmise to coordinate Cu^{I} through the sulfur or selenium atoms, respectively.[63,64] Although these studies confirm the ability of these sulfur and selenium compounds to bind Cu^{I}, they do not provide information on how copper binding

Table 4.3. MALDI mass spectrometry data for the tested sulfur and selenium compounds.

Compound	***m/z* (Da)**	**Cu^{I} : ligand**	***m/z* (Da)**	**Fe^{II} : ligand**
Sulfur				
ESH	521[a]	1:2[a]	304[b], 257	1:1 $[Fe^{II}(ESH)(OH)]^{+}$, 1:2
2-MerIm	263[a], 365[b]	1:2[a], 1:3[a]	332[a]	1:6[a]
Ebit	317.6[b]	1:1[b]	348, 282[a]	1:1 $[Fe^{II}(Ebit)(OH)(H_2O)]^{+}$, 1:2[a]
MetIm	292[b], 427.2	1:2[b], 1:3	332	1:6
Mpy^{Me}	254	1:1	318	1:3
PTAS	—	—	—	—
Selenium				
$Sepy^{Me}$	303, 541, 562	1:1, 1:2[a], 1:2 $[Cu(sepy^{Me})(H_2O)]^{+}$	267[a], 386[a]	1:2[a], 1:3[a]
Ebis	413[b]	1:1[b]	426	1:1 $[Fe^{II}(ebis)(OH)]^{+}$
PTASe	—	—	—	—

[a]Coordination observed in ESI studies. [b]Coordination observed in both MALDI and ESI.

results in the observed antioxidant activity.

Similar mass spectrometry studies conducted with Fe^{II} revealed the ability of these sulfur and selenium compounds to form Fe^{II} complexes in various ratios. Only PTAS and PTASe formed no complexes under these conditions. Ebis formed only a 1:1 (Fe^{II}:ligand), ESH forms both 1:1 and 1:2 (Fe^{II}:ligand) complexes, and mpy^{Me} only forms a 1:3 Fe^{II} complex, consistent with possible chelation. Ebit forms a 1:2 Fe^{II} complex, whereas $sepy^{Me}$ forms both 1:2 and 1:3 Fe^{II} complexes. Higher-order complexes were also observed for the monodentate compounds, in keeping with potentially octahedral Fe^{II} coordination, including both 1:4 and 1:6 complexes with MetIm and a 1:6 complex with 2-MerIm.

Since 6 μM Cu^{I} was used for the DNA damage studies, copper coordination is expected to occur between 6-24 μM for monodentate compounds, and between 3-12 μM for bidentate compounds. ESH, 2-MerIm, ebit, ebis, and $sepy^{Me}$ are among the most effective compounds at inhibiting copper-mediated DNA damage, with IC_{50} values within (or near) this range for copper coordination (Table 4.1). The similar activity between ESH and 2-MerIm, indicates that the non-methylated nitrogen atoms in 2-MerIm may provide some multidentate properties similar to ESH. Likewise, the similarity in activity of ebis and $sepy^{Me}$ may be due to bidentate copper binding.

Since 2 μM Fe^{II} was used in these DNA damage experiments, coordination of Fe^{II} is expected to occur between 2-12 μM for the monodentate compounds, and 1-6 μM for bidentate compounds. ESH, MetIm, and 2-MerIm exhibit activity within this 1-6 μM coordination ratio window. Most notably, even compounds that show no metal binding

by mass spectrometry methods were found to significantly prevent copper-and iron-mediated DNA damage, and even compounds with high IC_{50} values for prevention of metal-mediated DNA damage exhibit some ability to form metal complexes by mass spectrometry. Thus, these studies taken together show that metal coordination is necessary but not sufficient for antioxidant activity.

4.2.6. Relationship between electrochemical properties and DNA damage prevention. Generation of $^{\bullet}OH$ from H_2O_2 is a one-electron redox reaction, so if an antioxidant compound can undergo oxidation, ROS scavenging could occur. Cyclic voltammetry (CV) experiments were performed on the sulfur and selenium compounds to determine their electrochemical properties and their relationship to their antioxidant activities. Differential pulse voltammetry (DPV) experiments were simultaneously conducted to confirm weak waves observed in the CV experiments. All experiments were conducted in aqueous solution (10 mM MOPS buffer, pH 7.0) to mimic physiological conditions with potassium nitrate (0.1 M) as the supporting electrolyte. All potentials are reported relative to normal hydrogen electrode (NHE) and are provided in Table 4.4.

Table 4.4. Electrochemical potentials (versus NHE) of the tested sulfur and selenium compounds in MOPS buffer (10 mM, pH 7) with KNO_3 (0.1 M) as the supporting electrolyte.

Compound	E_{pa} **(V)**	E_{pc} **(V)**	ΔE **(V)**	$E_{1/2}$ **(V)**
Sulfur				
ESH	0.382[a]	0.655[a]	0.273[b]	0.518[b]
2-MerIm	0.528	-0.275	0.803	0.126
Ebit	0.590	0.507	0.083	0.548
MetIm	0.625	-0.539	1.164	0.043
Mpy^{Me}	0.534	0.650[a]	0.213[b]	0.726[b]
PTAS	—	-0.612	—	—
Selenium				
$Sepy^{Me}$	0.272, 0.592	0.017, 0.647[a]	0.249, 0.131[b]	0.142, 0.581[b]
Ebis	0.323	0.194	0.129	0.258
PTASe	—	-0.164	—	—

[a]Potential from DPV scan. [b]Calculation performed with values obtained from DPV scan

The CV of mpy^{Me} exhibits a single anodic wave at 0.534 V (Table 4.4 and Figure 4A). In contrast, the DPV scans of mpy^{Me} (data are provided in Figure 4.20 through Figure 4.22 at the end of the Experimental Methods section) reveal two redox couples; the first redox couple consists of an anodic wave at 0.650 V and a cathodic wave at 0.802 V ($E_{1/2}$ value of 0.726 V), and a second redox couple consisting of an anodic wave of 0.954 V and a cathodic wave of 1.041 V ($E_{1/2}$ value of 0.883 V). The more positive Ep_a values observed in the DPV compared to CV are a result of the different parameters used in these experiments.[65,66] Similar studies with ESH, 2-MerIm, MetIm, and ebit revealed their ability to undergo both oxidation and reduction with $E_{1/2}$ values of 0.518, 0.126, 0.043, and 0.548 V respectively. The more positive $E_{1/2}$ values for ESH, mpy^{Me}, and ebit are likely attributed to their secondary functional groups (amino acid tail, pyridine ring, or second thione) compared to the lone thione of 2-MerIm and MetIm.

In contrast to the trend observed for the Cu^{I}-mediated DNA damage studies, methylation of the imidazole nitrogens has less of an effect on the redox activity than denticity. Comparing $E_{1/2}$ values of the investigated compounds reveals that the observed

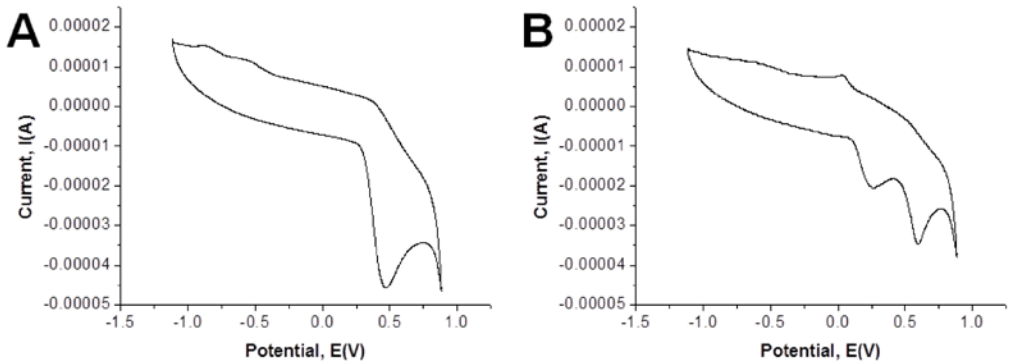

Figure 4.4. Cyclic voltammograms vs. NHE for A) mpy^{Me}, and B) sepy^{Me}. Samples are 1 mM in MOPS buffer (10 mM, pH 7) with 0.1 M KNO_3 as the supporting electrolyte.

trend is mpy^{Me} (potentially bidentate) > ESH (no methylated nitrogens, and potentially bidentate) > ebit (potentially bidentate) > 2-MerIm (no methylated nitrogens) > MetIm one methylated nitrogen). PTAS only undergoes a single reduction and is not likely to be a highly effective ROS scavenger.

The selenium compound sepy^{Me} exhibits two strong anodic waves in the cyclic voltammogram (Figure 4.4B; Ep$_a$ values of 0.272 and 0.592 V) and a single cathodic wave at 0.017 V. In contrast, the DPV scans of sepy^{Me} (provided in Figure 4.22 at the end of the Experimental Methods section) show two anodic waves (Ep$_a$ values of 0.114 and 0.647 V) and two cathodic waves (Ep$_c$ values of 0.157 and 0.516 V), similar to results observed for mpy^{Me}. The redox couple for sepy^{Me} exhibits quasi-reversible behavior with and $E_{1/2}$ value of 0.142 V and is highly susceptible to oxidation in aqueous solution. In contrast, the bidentate compound ebis only exhibits a single quasi-reversible couple with an $E_{1/2}$ of 0.258 V. The more positive $E_{1/2}$ value for sepy^{Me} compared to ebis indicates that the selone-pyridine compounds is more prone to oxidation than a di-selone compound and that sepy^{Me} may be a better ROS scavenger.

Comparison of these electrochemical findings to results for ONOO$^-$-mediated DNA damage reveals that compounds with more positive $E_{1/2}$ values generally are more effective at preventing ONOO$^-$-mediated DNA damage. In contrast, PTASe exhibits a single reductive wave ($E_{pc=}$ -0.164 V), similar to PTAS, indicating that ROS scavenging is not a likely mechanism for these two compounds. However, their ability to prevent ONOO$^-$-mediated DNA damage suggests that the antioxidant mechanisms of PTASe and PTAS are likely different from those of the selone and thione compounds.

The monodentate thione and selone ligands dmit and dmise oxidize in aqueous solution when treated with H_2O_2 and $ONOO^-$,[44,64,67] and they have $E_{1/2}$ values of 0.187 and 0.125 V, respectively. The more positive shift in the $E_{1/2}$ values for the sulfur and selenium compounds investigated in this Chapter compared to the values observed for dmise and dmit indicate that the potentially multidentate compounds are more readily oxidized than the monodentate sulfur and selenium compounds (including 2-MerIm and MetIm) and that this oxidation is readily accessible in aqueous solution. However, $ONOO^-$-mediated DNA damage studies revealed that dmit was one of the most effective ROS scavengers of the sulfur compounds, and indicates that directly comparing electrochemical results with prevention of DNA damage by ROS scavenging is not always accurate.

Additional electrochemical studies were conducted with Cu^I and Fe^{II}, focusing on the biological redox window of Fenton and Fenton-like reactions (-0.324 V < $E_{1/2}$ < 0.460 V). Pierre and Fontecave reported that when the potential for the $Fe^{III/II}$ (or $Cu^{II/I}$) couple is more positive than 0.460 V, H_2O_2 cannot oxidize Fe^{II} to Fe^{III} (or Cu^I to Cu^{II}). Similarly, when the potential falls below -0.324 V, natural cellular reductants such as NADH are unable to reduce Fe^{III} to Fe^{II} (or Cu^{II} to Cu^I).[68] Thus, if these sulfur and selenium compounds shift the redox potential of $Fe^{III/II}$ (or $Cu^{II/I}$) outside this window, metal-mediated $^{\bullet}OH$ formation may be effectively inhibited. For these studies, copper(II) sulfate or iron(II) sulfate was added to solutions of the sulfur and selenium prior to investigations. Copper studies were conducted in MOPS (10 mM, pH 7.0) to mimic biological conditions and for comparison to gel electrophoresis studies, whereas iron

studies were performed in MES buffer (10 mM, pH 6.0). All samples contained potassium nitrate (0.1 M) as the supporting electrolyte. Potentials are reported relative to normal hydrogen electrode (NHE) and are provided in Tables 4.5 and 4.6.

Iron sulfate alone revealed an anodic wave at -0.037 V and a cathodic wave at -0.145 V, with an $E_{1/2}$ of -0.091 V, attributed to the $Fe^{III/II}$ couple. A solution of Fe^{II}:ESH (1:6 molar ratio) exhibited an anodic wave at 0.017 V and a cathodic wave at -0.317 V with an $E_{1/2}$ = -0.150 V for the same redox reaction. The significant negative shift of the cathodic wave indicative of Fe^{III} reduction to Fe^{II}, indicates that ESH stabilizes the softer Fe^{II} oxidation state compared to the harder Fe^{III} oxidation state. Similar results are observed with Fe^{II}:MetIm (1:6), which exhibits a cathodic wave for $Fe^{III/II}$ at -0.205 V.

Table 4.5. Electrochemical potentials (versus NHE) of the tested sulfur and selenium compounds and $FeSO_4$ in MES buffer (10 mM, pH 6) with KNO_3 (0.1 M) as the supporting electrolyte.

	$Fe^{III/II}$			
Compound	E_{pa} **(V)**	E_{pc} **(V)**	ΔE **(V)**	$E_{1/2}$ **(V)**
$FeSO_4$	-0.037	-0.145	0.108	-0.091
1:1 Fe:2-MerIm	0.222	-0.147	0.369	-0.037
1:6 Fe:2-MerIm	0.120[a]	-0.073[a]	0.193[b]	0.023[b]
1:1 Fe:Ebit	0.220	-0.147	0.367	0.036
1:1 Fe:Ebis	0.065[a]	-0.128	0.193[b]	-0.032[b]
1:6 Fe:ESH	0.017	-0.317	0.334	-0.15
1:1 Fe:MetIm	-0.083	-0.195	0.112	-0.056
1:6 Fe:MetIm	-0.005	-0.205	0.200	-0.105

[a]Potential from DPV scan. [b]Calculation performed with values obtained from DPV scan.

Table 4.6. Electrochemical potentials (versus NHE) of the tested sulfur and selenium compounds and $CuSO_4$ in MOPS buffer (10 mM, pH 7) with KNO_3 (0.1 M) as the supporting electrolyte.

	$Cu^{I/0}$			
Compound	E_{pa} **(V)**	E_{pc} **(V)**	ΔE **(V)**	$E_{1/2}$ **(V)**
$CuSO_4$	—	—	—	—
1:1 Cu:2-MerIm	0.544	0.157	0.387	0.350
1:4 Cu:2-MerIm	0.470	-0.395	0.865	0.037
1:1 Cu:MetIm	0.590	0.194	0.396	0.392
1:4 Cu:MetIm	0.516	-0.220	0.736	0.148
1:1 Cu:Ebit	0.212, 0.599[a], 0.811[a]	0.111, 0.525[a]	0.101	0.162
1:1 Cu:Ebis	0.240, 0.525[a]	0.047	0.193	0.144
1:4 Cu:ESH	0.321[a,b]	-0.691, 0.169[a,b]	—	—

[a]Potential from ligand. [b]Potential from DPV scan.

A 1:1 solution of MetIm:Fe^{II} exhibits a significant shift for the anodic wave of the $Fe^{III/II}$ couple (E_{pa} = -0.083 V) compared to $FeSO_4$, in addition to a negative shift of 0.050 V for the cathodic wave. High concentrations of ESH and 2-MerIm stabilize Fe^{II} more than Fe^{III}, as indicated by the substantial negative $E_{1/2}$ values for the $Fe^{II/III}$ couple.

In contrast, 2-MerIm has the opposite effect on the redox activity of iron. In the presence of 2-MerIm, the cathodic wave of the $Fe^{III/II}$ couple is not affected at low concentrations of 2-MerIm (-0.147 V, 1:1 molar ratio), but shifts positive when additional 2-MerIm is added (-0.073 V, 1:6 molar ratio). The 1:1 molar ratio of 2-MerIm:Fe has an $E_{1/2}$ of -0.037 V, whereas a 1:6 solution has a more positive $E_{1/2}$ of 0.023 V, indicating that the Fe^{II} oxidation state is stabilized more with high concentrations of 2-MerIm. This is in agreement with DNA damage studies with Fe^{II}, which showed the ability to prevent > 75 % oxidative DNA damage by 10 μM. Studies with ebit (1:1 molar ratio) revealed a similar $E_{1/2}$ of 0.036 V, indicating that ebit stabilizes Fe^{II} over Fe^{III}. Ebis with iron (1:1) exhibited a slightly less positive shift for the $Fe^{III/II}$ couple ($E_{1/2}$ = -0.032 V), indicating that ebis is not as effective at stabilizing Fe^{II} compared to ebit.

All of the compounds studied with copper only revealed signals for the $Cu^{I/0}$ redox couple; the $Cu^{II/I}$ redox couple is completely absent from all cyclic and differential pulse voltammograms. However, a negative shift is observed for the $Cu^{I/0}$ couple when high concentrations of 2-MerIm and Metlm are used, suggesting that Cu^{I} is favored over Cu^{0}.

The DNA damage prevention studies conducted in this Chapter reveal that more effectively preventing Fe^{II}-mediated DNA damage than Cu^{I}-mediated DNA damage is a

general behavior of selones and thiones, similar to results obtained for dmise and dmit (Chapter 3). These sulfur and selenium compounds also show significant ability to prevent DNA damage by $[Fe(EDTA)]^{2-}$, $[Cu(bipy)_2]^{+}$, and $ONOO^{-}$, indicating that compounds with C=S/Se and P=S/Se functional groups are the first characterized multifunctional sulfur and selenium compounds. The relatively high concentrations required for activity with $[Fe(EDTA)]^{2-}$, $[Cu(bipy)_2]^{+}$, and $ONOO^{-}$ compared to unchelated Fe^{II} and Cu^{I} indicates that metal coordination is the primary mechanism for antioxidant activity at low micromolar concentrations. In addition, activity is greatly affected by chemical structure, with the most effective properties: selenium versus sulfur > nitrogen methylation > denticity > potential aromaticity > S/Se speciation (C=S/Se versus P=S/Se). Electrochemical studies revealed the majority of these compounds readily undergo oxidation, in general agreement with the ROS scavenging ability observed with $ONOO^{-}$-mediated DNA damage gels. Electrochemical studies with iron showed the ability of these sulfur and selenium compounds to stabilize Fe^{II} relative to Fe^{III}, although their potentials remain within the electrochemical window for metal-generated hydroxyl radical, indicating that these compounds likely prevent metal-mediated DNA damage by targeted scavenging rather than redox control. Thus, these studies have shown the first relationship between chemical structure and antioxidant activity, and a series of sulfur and selenium compounds that prevent oxidative DNA damage through multiple mechanisms.

4.3. Conclusions

The gel electrophoresis studies presented in this Chapter confirm the that thiones and selones inhibit oxidative DNA damage *via* at least two separate mechanisms. In the Cu^{I} studies at low concentrations, metal coordination is the primary mechanism when the metal-to-ligand ratios are between 1:1 and 1:4 for the monodentate compounds or between 1:1 and 1:2 for potentially bidentate compounds (in gel electrophoresis studies). Similarly, metal coordination occurs with Fe^{II}, between the metal-to-ligand ratios of 1:1 and 1:6 for the monodentate compounds, and 1:1 and 1:3 for potentially bidentate compounds (in gel electrophoresis studies). In contrast, ROS scavenging is likely the active mechanism once the solution is saturated by the thione and selone antioxidants. This conclusion is confirmed by the DNA damage prevention abilities observed for most of the compounds when bipy or EDTA is used to fully coordinate Cu^{I} or Fe^{II}, respectively, prior to antioxidant addition and from the lesser activities observed for peroxynitrite-mediated DNA damage inhibition.

Methylation of the imidazole nitrogens has the most significant effect on the antioxidant properties of the sulfur compounds investigated, since the non-methylated compounds, ESH and 2-MerIm, most effectively prevent Cu^{I}- and Fe^{II}-mediated DNA damage. Although the mono-methylated MetIm is not the most effective antioxidant at inhibiting Cu^{I}-mediated damage, its ability to prevent Fe^{II}-mediated DNA damage is similar to ESH. Adding chelating capability generally increases the antioxidant activity of these compounds in preventing Cu^{I}-mediated oxidative DNA damage. In contrast, many of the bidentate compounds exhibited similar abilities to prevent Fe^{II}-mediated oxidative

DNA damage as their monodentate analogs. These results suggest that while denticity is important to activity, it is not consistent between metals, suggesting that these compounds can be tuned for specific metal ions.

In the case of ESH, addition of the amino acid substituent to the thione results in behavior similar to that observed for selenomethione prevention of DNA damage by Cu^{I} and $[Cu(bipy)_2]^{+}$. Similarly, the presence of the pyridine functional group in mpy^{Me} and $sepy^{Me}$ results in more effective inhibition of DNA damage by $[Fe(EDTA)]^{2-}$ and $[Cu(bipy)_2]^{+}$; however, having two thiones or selones in one compound (ebit and ebis) resulted in stronger activity in preventing DNA damage by both Fe^{II} and Cu^{I}. Thus, the identity of the secondary functional groups on the thione or selone compound has a drastic effect on the antioxidant activity. The presence of aromatic imidazole ring also increases the observed antioxidant ability, whereas PTAS and PTASe coordinate only through the P=S/Se bond required higher concentrations compared to the other compounds. Perhaps the largest contributor to antioxidant activity was the presence of selenium versus sulfur, since all of the selenium compounds are significantly more effective than their sulfur analogs at preventing oxidative DNA damage under all conditions.

Not only are these compounds multifunctional antioxidants, similar to the previously reported dmise and dmit, but these results provide a glimpse as to how thiones, selones and their analogs might be tuned to maximize their antioxidant activity at biological concentrations. The significance of these studies also arises from the observed relationship between chemical structure and antioxidant activity, which has been difficult

to observe with the limited activity or number of tested compounds in previous studies. The information gained from this work has provided the groundwork for effective selection and synthesis of potent sulfur and selenium compounds for multifunctional antioxidant studies at biological concentrations.

4.4. Experimental Methods

Materials. Potassium nitrate was from Fisher. MOPS and MES were obtained from Alfa Aesar. PTAS, PTASe, mpy^{Me}, and $sepy^{Me}$ were provided by Prof. Daniel Rabinovich (University of North Carolina at Charlotte). Ebit and ebis were synthesized according to previously published methods.[69] NaCl (99.999%), glycerol, $FeSO_4 \cdot 7H_2O$, 2-MerIm, and bromophenol blue were all from Alfa Aesar. MetIm was purchased from Spectrum Chemical. Yeast extract, 30% H_2O_2, sodium EDTA, tryptone (peptone), $CuSO_4 \cdot 5H_2O$, and agarose were all from Fisher. Glucose and ampicillin were from EMD. Ethidium bromide and agar were from Lancaster. Ethanol (200 proof) and ascorbic acid were from Acros Organics. Xylene cyanol FF was from J. T. Baker. Tris hydrochloride and microcentrifuge tubes were from VWR. A NANOpure Diamond water deionization system (Barnstead International) was used to prepare diH_2O. Metal-free microcentrifuge tubes were prepared by washing the tubes in 1M HCl for ~1 hour, and then triple rinsing three times with diH_2O.

Plasmid transfection, amplification, and purification. Plasmid DNA (pBSSK) was purified from DH1 *E.* coli competent cells using a 5 Prime PerfectPrep^{TM} Spin Kit (250 count, Fisher). Tris-EDTA buffer (pH 8.0) was used to elute the plasmid from the

spin columns. Plasmid was dialyzed against 130 mM NaCl for 24 hours at 4°C to ensure all Tris-EDTA buffer and metal contaminates were removed, and plasmid concentration was determined by UV-vis spectroscopy at a wavelength of 260 nm. Absorbance ratios of $A_{250}/A_{260} \leq 0.95$ and $A_{260}/A_{280} \geq 1.8$ were determined for DNA used in all experiments. Plasmid purity was determined through digestion of plasmid (0.1 pmol) with *Sac 1* and *KpN1* in a mixture of NEB buffer and bovine serum albumin was conducted at 37°C for 90 minutes. Comparison to an undigested plasmid sample and a 1 kb molecular weight marker was conducted by gel electrophoresis.

DNA damage gel electrophoresis experiments: DiH_2O, MOPS buffer (10 mM, pH 7.0), NaCl (130 mM), ethanol (100% metal free, 10 mM), $CuSO_4 \cdot 5H_2O$ (6000 nM), ascorbate (7500 nM), and the indicated concentrations of sulfur (or selenium) compounds were combined in an acid-washed microcentrifuge tube and allowed to stand for 5 min at room temperature. Plasmid (pBSSK, 0.1 pmol in 130 mmol NaCl) was then added to the reaction mixture and allowed to stand for 5 min at room temperature. H_2O_2 (50 μM) was then added and allowed to react at room temperature for 30 min. EDTA (50 μM) was added after 30 min to quench the reaction. For Fe^{II} DNA damage experiments, $FeSO_4 \cdot 7H_2O$ (2 μM) and MES (10 mM, pH 6.0) were used in place of $CuSO_4$, ascorbic acid, MOPS buffer. All concentrations mentioned are final concentrations in a 10 μL volume. All samples were loaded into a 1% agarose gel in a TAE running buffer (50X); damaged and undamaged plasmid was separated by electrophoresis (140 V for 30 min). Gels were stained using ethidium bromide and imaged under UV light. The amounts of nicked (damaged) and circular (undamaged) were analyzed using UViProMW (Jencons

Scientific Inc., 2007). Intensity of circular plasmid was multiplied by 1.24, due to the poor binding ability of ethidium bromide to undamaged plasmid.[7,9] Experiments using $[Cu(bipy)_2]^{2+}$ (50 µM) or $[Fe(EDTA)]^{2-}$ (400 µM) in the place of Cu^{II} and Fe^{II} were conducted using a similar procedure. For gels with $[Cu(bipy)_2]^{2+}$, 62.5 µM ascorbic acid was also added.

Synthesis of peroxynitrite anion ($ONOO^-$). Synthesis of peroxynitrite followed the method of Keith and Powell,[70] resulting in the bright yellow-colored $ONOO^-$. The concentration of $ONOO^-$ was calculated from its absorbance at 302 nm using an extinction coefficient of 1670 cm^{-1} mol^{-1} dm^3.[71] Samples of $ONOO^-$ were stored at -80°C for up to two weeks.

Gel electrophoresis experiments with $ONOO^-$. Selenium or sulfur compounds were combined with ethanol (10 mM, 100%), NaCl (130 mM), MOPS buffer (10 mM, pH 6.8), and plasmid DNA (pBSSK, 0.1 mmol in 130 mM NaCl) in an acid-washed microcentrifuge tube and allowed to stand for 5 min. Peroxynitrite (1450 µM) was added at 4°C, and the reaction was allowed to stand for an additional 5 min at room temperature. All concentrations indicated are the final concentrations in a 10 µL volume. After the 5 min incubation with $ONOO^-$, loading dye (bromophenol blue) was added to obtain a final volume of 12 µL. All samples were loaded into a 1% agarose gel in TAE running buffer, and gel electrophoresis was conducted as previously stated.

Calculating percent inhibition of DNA damage. The formula 1-[%N-%B]*100 was used to calculate percent DNA damage inhibition; %N = percent of nicked DNA in the thione- or selone-containing lanes, and %B = the percent of nicked DNA in the

Cu^{+}/H_2O_2 or Fe^{2+}/H_2O_2 control lane. All percentages were corrected for residual nicked DNA prior to calculation. Results were obtained from an average of three trials, with indicated standard deviations.

Mass spectrometry studies. MALDI mass spectrometry experiments were performed using a Bruker Microflex MALDI-TOF mass spectrometer with *trans*-2-[3-(4-tert-butylphenyl)-2-methyl-2-propenyldiene (250.34 *m/z*) as the matrix. A 1:1 Cu^{I}:ligand sample was prepared by adding 300 µL of $CuSO_4$ (900 µM) to 300 µL of ascorbic acid (900 µM) and allowed to incubate at room temperature for 5 min, followed by the addition of 300 µL of the sulfur or selenium compounds (900 µM). Similar samples with Fe^{II} were made by combining 300 µL of $FeSO_4$ (900 µM) with 300 µL of the sulfur or selenium compounds, and 300 µL of deionized H_2O. For higher ratio samples, the metal concentration remained the same (900 µM), with increased concentrations of the sulfur and selenium compounds (3600 µM for 1:4 ratios, and 5400 µM for 1:6 µM). ESI-MS studies were conducted on a Waters Alliance 2695 LC / Waters Micromass ZQ Mass Spectrometer by Emily Kurfman and Prof. Sandra K. Wheeler (Furman University). Experiments were conducted in diH_2O and at the same concentration as MALDI studies.

Electrochemical studies. Cyclic voltammetry (CV) and differential pulse voltammetry (DPV) experiments were conducted with a CH Electrochemical Analyzer (CH Instruments, Inc.). Studies were conducted in dry, degassed MOPS buffer (10 mM, pH 7.0) or MES buffer (10 mM, pH 6.0) with KNO_3 (0.1 M) as a supporting electrolyte, respectively. Final concentrations of all sulfur and selenium compounds absent of $CuSO_4$ or $FeSO_4$ were 1 mM with a final volume of 9 mL. All samples were degassed for 10

minutes with N_2 before each experiment. For metal studies, a solution of 1:1 metal-to-ligand ratio was made by adding 3 mL of $FeSO_4$ or $CuSO_4$ (900 µM) to 3 mL of a sulfur or selenium compound (900 µM), then diluted with the respectively buffer (3 mL, 30 mM). Final concentration of a 1:1 sample in 9 mL was 300 µM. A similar method was used to prepare 1:4 and 1:6 metal-to-ligand samples. All samples were degassed for 10 minutes with N_2 before each experiment. All CV experiments were conducted at 100 mV/s. A pulse amplitude of 0.080 V and a pulse width of 0.050 were used for all DPV experiments, in conjunction with a sample width of 0.045 and a pulse period of 0.200. Samples of each complex were cycled between -1.0 V and 1.0 V, using a glassy carbon working electrode, a Pt counter electrode, and a Ag/AgCl (+0.197 V vs. NHE[72]) reference electrode. All experiments were externally referenced to potassium ferricyanide (0.361 V vs. NHE[73]).

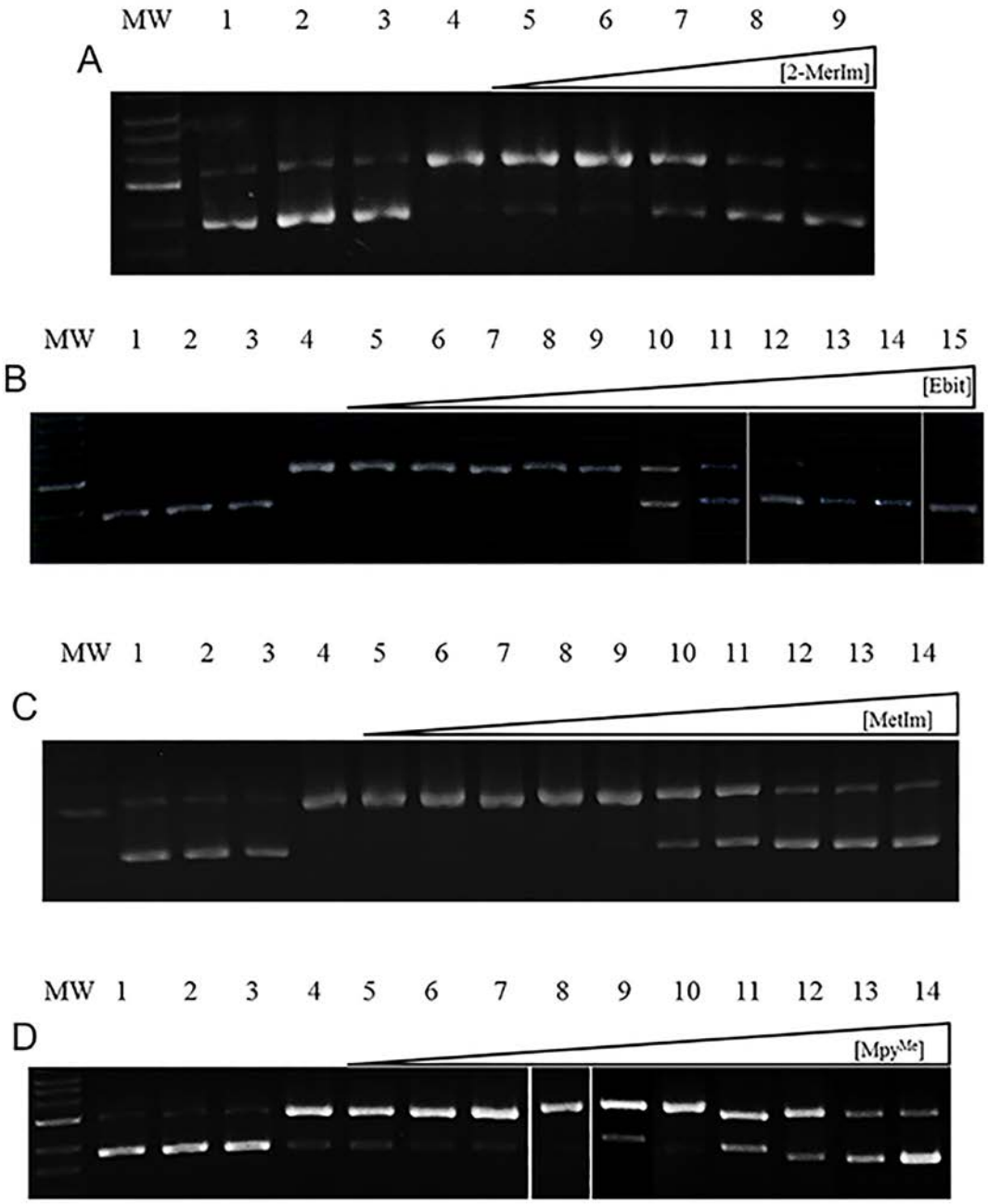

Figure 4.5. Gel electrophoresis images of Cu^{I}-mediated DNA damage inhibition by A) 2-mercaptoimidazole (2-MerIm), B) ethyl-bis(imidazole) thione (ebit), C) methimazole (MetIm), and D) (2-mercapto-1-methyimidazolyl)pyridine thione (mpy^{Me}) in MOPS buffer (10 mM, pH 7). Lane: MW = 1 kb molecular weight marker; lane 1: plasmid DNA (p); lane 2: p + H_2O_2; lane 3: p + S/Se compound (2-MerIm = 1000, ebit = 100 μM, MetIm = 2000 μM, mpy^{Me} = 1000 μM) + H_2O_2; lane 4: p + ascorbate (7.5 μM) + $CuSO_4$ (6 μM) + H_2O_2 (50 μM); lanes 5+: p + $CuSO_4$ + ascorbate + H_2O_2 + increasing concentrations of compound: A) 0.1, 1, 10, 100, and 1000 μM 2-MerIm, respectively, B) 0.1, 1, 5, 10, 25, 35, 40, 50, 75, 90, and 100 μM ebit, respectively, C) 0.1, 1, 2, 5, 10, 50, 100, 500, 1000, and 2000 μM MetIm, respectively, and D) 0.1, 1, 10, 25, 50, 75, 100, 250, 500, and 1000 μM mpy^{Me}, respectively.

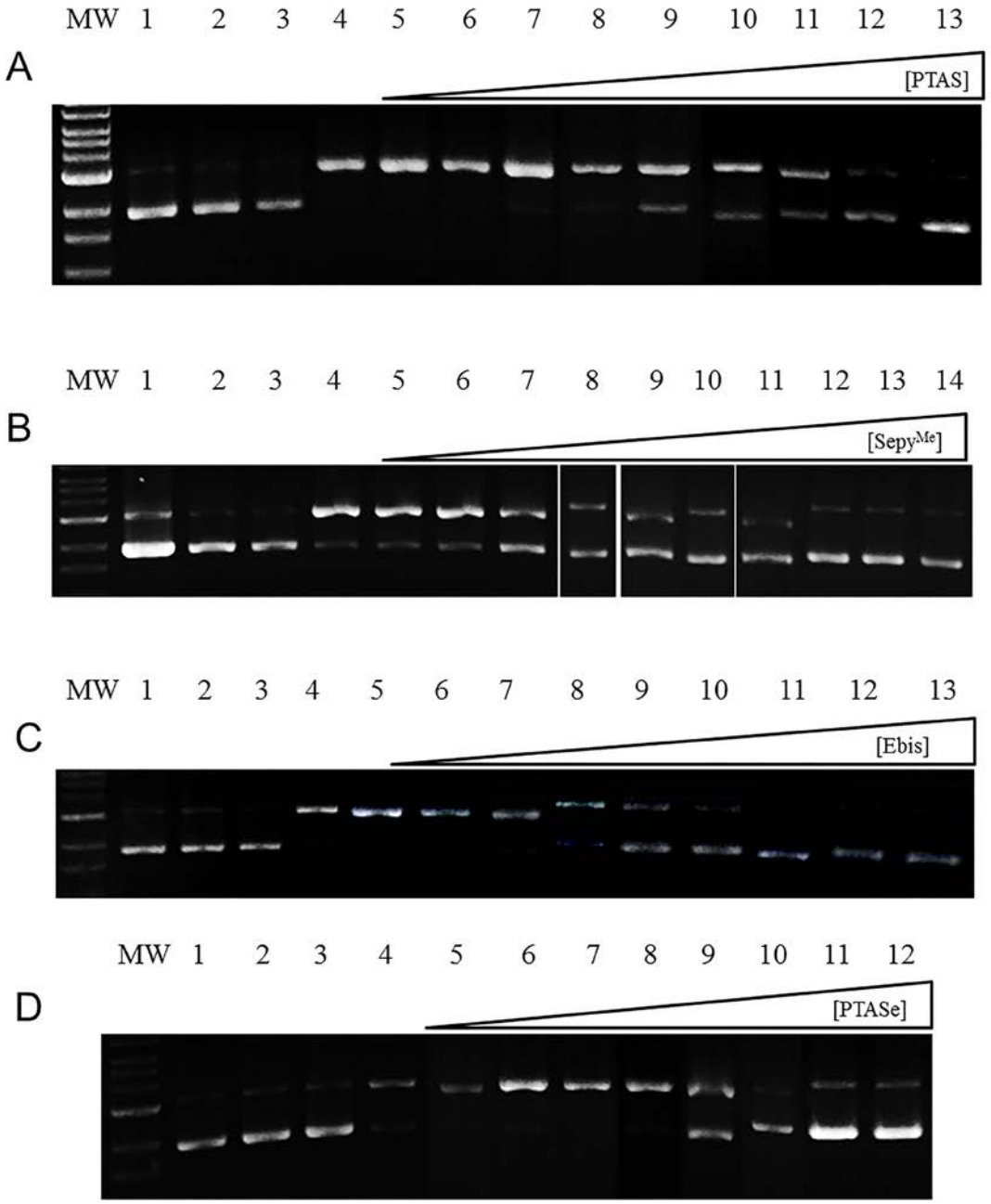

Figure 4.6. Gel electrophoresis images of Cu^{I}-mediated DNA damage inhibition by A) 1,3,5-triaza-7-phospaadamantane sulfide (PTAS), B) (2-mercapto-1-methyimidazolyl)pyridine selone ($sepy^{Me}$), C) ethyl-bis(imidazole) selone (ebis), and D) 1,3,5-triaza-7-phospaadamantane selenide (PTASe) in MOPS buffer (10 mM, pH 7). Lane: MW = 1 kb molecular weight marker; lane 1: plasmid DNA (p); lane 2: p + H_2O_2; lane 3: p + S/Se compound (PTAS = 1500, $sepy^{Me}$ = 1000 µM, ebis = 100 µM, PTASe = 1000 µM) + H_2O_2; lane 4: p + ascorbate (7.5 µM) + $CuSO_4$ (6 µM) + H_2O_2 (50 µM); lanes 5+: p + $CuSO_4$ + ascorbate + H_2O_2 + increasing concentrations of compound: A) 0.1, 1, 10, 100, 250, 500, 1000, 1100 and 1500 µM PTAS, respectively, B) 0.1, 1, 10, 25, 50, 75, 100, 250, 500 and 1000 µM $sepy^{Me}$, respectively, C) 0.1, 1, 5, 10, 25, 40, 50, 75, 90, and 100 µM ebis, respectively, and D) 1, 5, 10, 50, 75, 100, 500, and 1000 µM PTASe, respectively.

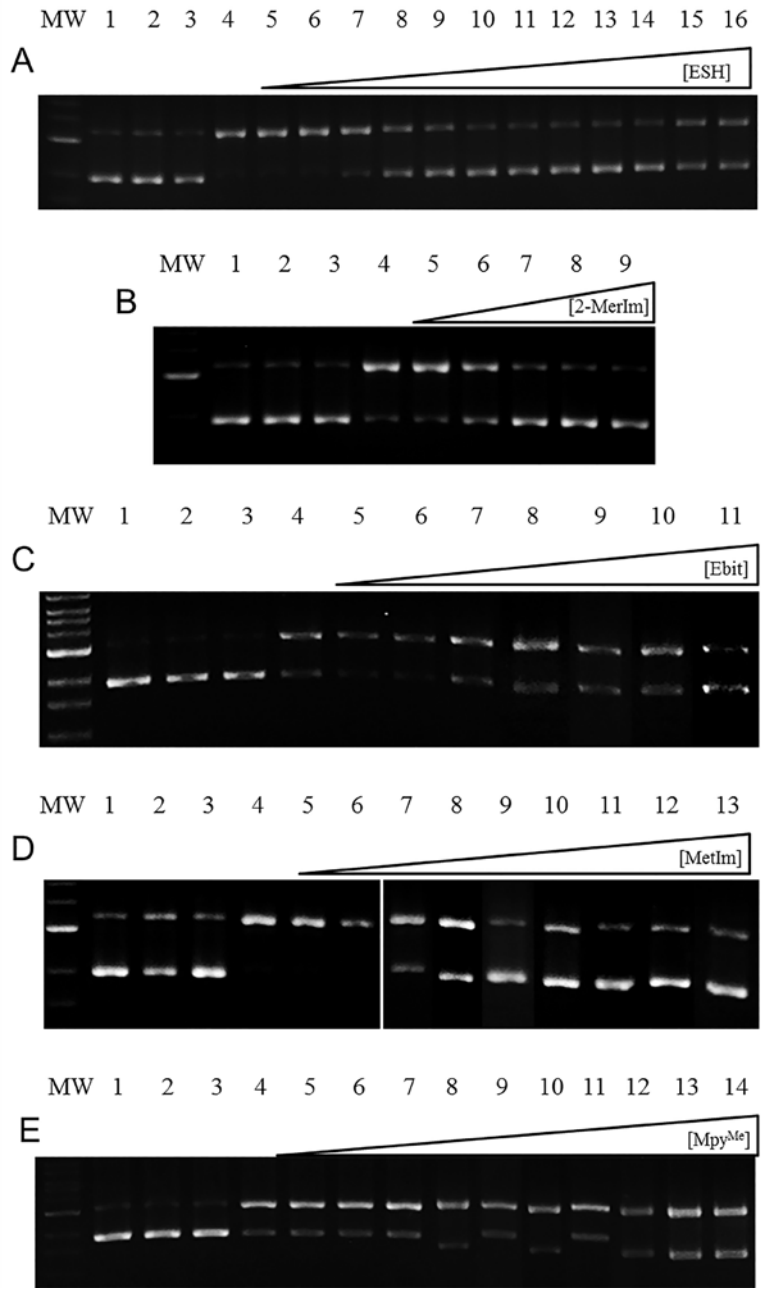

Figure 4.7. Gel electrophoresis images of Fe^{II}-mediated DNA damage inhibition by A) ergothioneine (ESH), B) 2-mercaptoimidazole (2-MerIm), C) ethyl-bis(imidazole) thione (ebit),D) methimazole (MetIm), and E) (2-mercapto-1-methyimidazolyl)pyridine thione (mpy^{Me}) in MES buffer (10 mM, pH 6). Lane: MW = 1 kb molecular weight marker; lane 1: plasmid DNA (p); lane 2: p + H_2O_2; lane 3: p + S/Se compound (ESH = 2000 µM, 2-MerIm = 1000, ebit = 100 µM, MetIm = 2000 µM, mpy^{Me} = 1000 µM) + H_2O_2; lane 4: p + $FeSO_4$ (2 µM) + H_2O_2 (50 µM); lanes 5+: p + $FeSO_4$ + H_2O_2 + increasing concentrations of compound: A) 0.01, 0.1, 1, 10, 50, 100, 1000, 1500, and 2000 µM ESH, respectively, B) 0.1, 1, 10, 100, and 1000 µM 2-MerIm, respectively, C) 0.1, 1, 10, 25, 50, 75, and 100 µM ebit, respectively, D) 0.1, 1, 5, 10, 50, 100, 500, 1000, and 2000 µM MetIm, respectively, and E) 0.1, 1, 10, 25, 50, 75, 100, 250, 500, and 1000 µM mpy^{Me}, respectively.

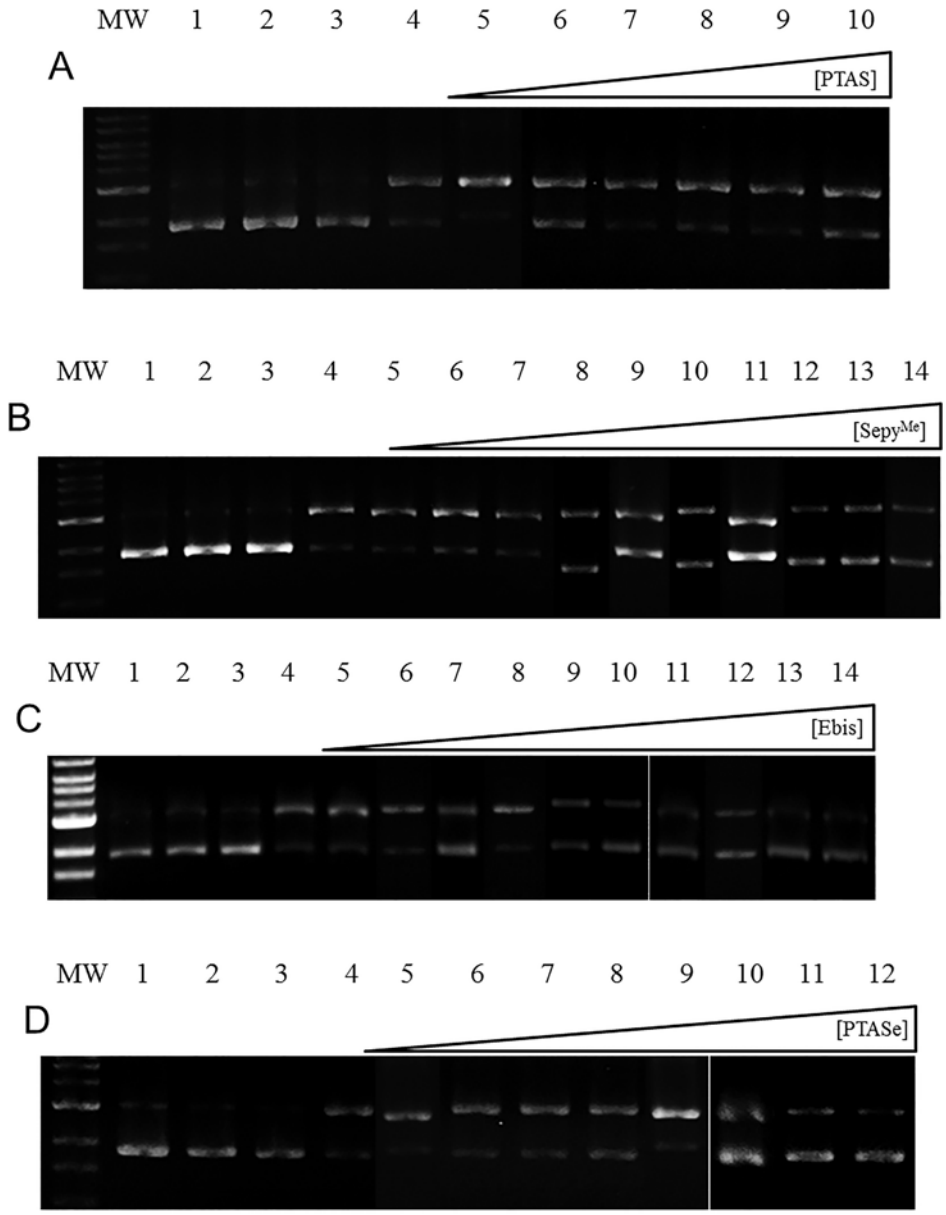

Figure 4.8. Gel electrophoresis images of Fe^{II}-mediated DNA damage inhibition by A) 1,3,5-triaza-7-phospaadamantane sulfide (PTAS), B) (2-mercapto-1-methyimidazolyl)pyridine selone ($sepy^{Me}$), C) ethyl-bis(imidazole) selone (ebis), and D) 1,3,5-triaza-7-phospaadamantane selenide (PTASe) in MOPS buffer (10 mM, pH 7). Lane: MW = 1 kb molecular weight marker; lane 1: plasmid DNA (p); lane 2: p + H_2O_2; lane 3: p + S/Se compound (PTAS = 1500, $sepy^{Me}$ = 1000 µM, ebis = 100 µM, PTASe = 1000 µM) + H_2O_2; lane 4: p + $FeSO_4$ (2 µM) + H_2O_2 (50 µM); lanes 5+: p + $FeSO_4$ + H_2O_2 + increasing concentrations of compound: A) 0.1, 1, 10, 100, 250, 500, 1000, 1100 and 1500 µM PTAS, respectively, B) 0.1, 1, 10, 25, 50, 75, 100, 250, 500 and 1000 µM $sepy^{Me}$, respectively, C) 0.1, 0.2, 1, 2, 3, 8, 10, 25, 50, and 100 µM ebis, respectively, and D) 1, 5, 10, 50, 75, 100, 500, and 1000 µM PTASe, respectively.

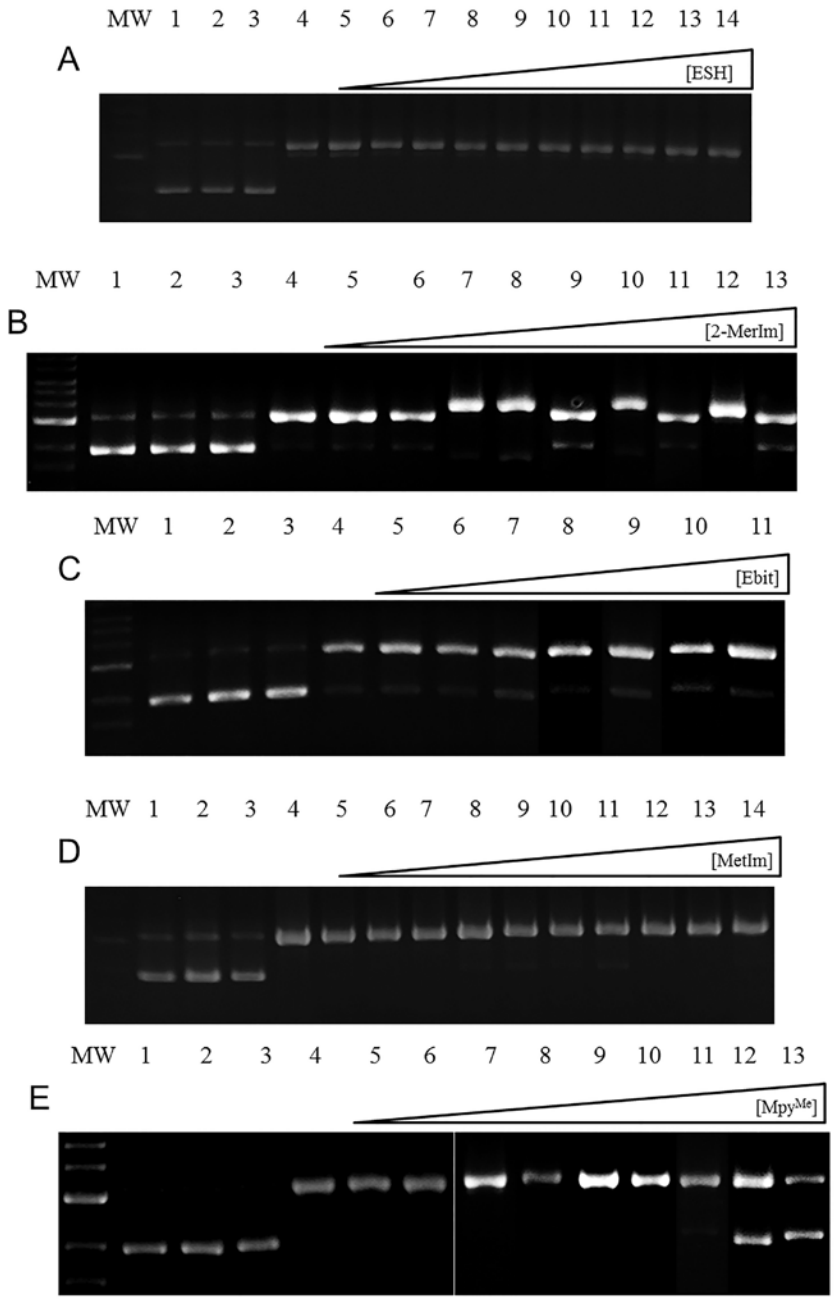

Figure 4.9. Gel electrophoresis images of $[Cu(bipy)_2]^+$-mediated DNA damage inhibition by A) ergothioneine (ESH), B) 2-mercaptoimidazole (2-MerIm), C) ethyl-bis(imidazole) thione (ebit),D) methimazole (MetIm), and E) (2-mercapto-1-methyimidazolyl)pyridine thione (mpy^{Me}) in MOPS buffer (10 mM, pH 7). Lane: MW = 1 kb molecular weight marker; lane 1: plasmid DNA (p); lane 2: p + H_2O_2; lane 3: p + S/Se compound (ESH = 2000 µM, 2-MerIm = 1000, ebit = 100 µM, MetIm = 2000 µM, mpy^{Me} = 1000 µM) + H_2O_2; lane 4: p + $[Cu(bipy)_2]^{2+}$ (50 µM) + ascorbate (63 µM) + H_2O_2 (50 µM); lanes 5+: p + $[Cu(bipy)_2]^{2+}$ + ascorbate + H_2O_2 + increasing concentrations of compound: A) 0.01, 0.1, 1, 10, 50, 100, 1000, 1500, and 2000 µM ESH, respectively, B) 0.1, 1, 10, 100, and 1000 µM 2-MerIm, respectively, C) 0.1, 1, 10, 25, 50, 75, and 100 µM ebit, respectively, D) 0.1, 1, 5, 10, 50, 100, 500, 1000, and 2000 µM MetIm, respectively, and E) 0.1, 1, 10, 25, 50, 75, 100, 250, 500, and 1000 µM mpy^{Me}, respectively.

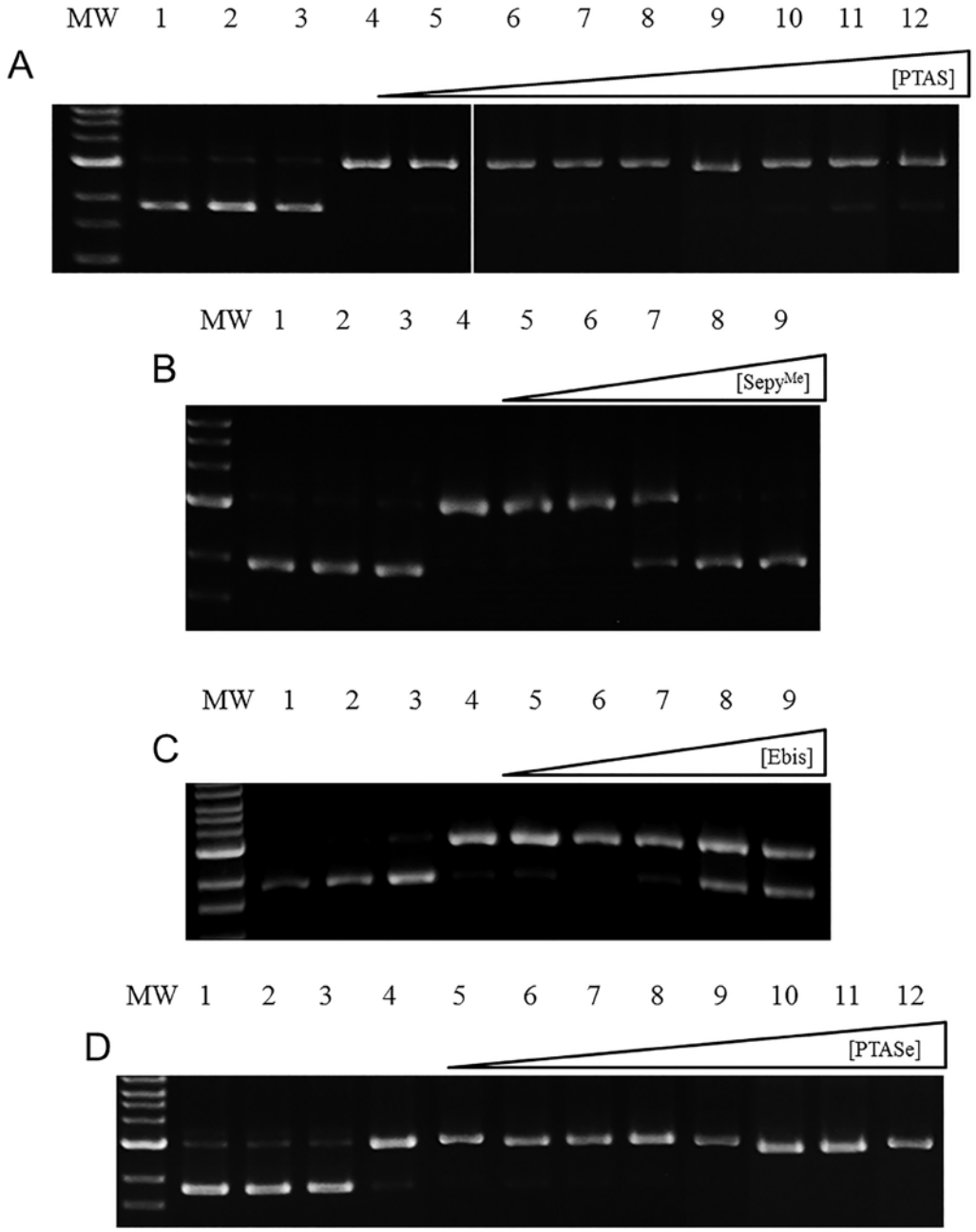

Figure 4.10. Gel electrophoresis images of $[Cu(bipy)_2]^+$-mediated DNA damage inhibition by A) 1,3,5-triaza-7-phospaadamantane sulfide (PTAS), B) (2-mercapto-1-methyimidazolyl)pyridine selone ($sepy^{Me}$), C) ethyl-bis(imidazole) selone (ebis), and D) 1,3,5-triaza-7-phospaadamantane selenide (PTASe) in MOPS buffer (10 mM, pH 7). Lane: MW = 1 kb molecular weight marker; lane 1: plasmid DNA (p); lane 2: p + H_2O_2; lane 3: p + S/Se compound (PTAS = 1500, $Sepy^{Me}$ = 1000 µM, ebis = 100 µM, PTASe = 1000 µM) + H_2O_2; lane 4: p + $[Cu(bipy)_2]^{2+}$ (50 µM) + ascorbate (63 µM) + H_2O_2 (50 µM); lanes 5+: p + $[Cu(bipy)_2]^{2+}$ + ascorbate + H_2O_2 + increasing concentrations of compound: A) 0.1, 1, 10, 100, 250, 500, 1000, 1100 and 1500 µM PTAS, respectively, B) 0.1, 1, 10, 25, 50, 75, 100, 250, 500 and 1000 µM $sepy^{Me}$, respectively, C) 0.1, 1, 5, 10, 25, 40, 50, 75, 90, and 100 µM ebis, respectively, and D) 1, 5, 10, 50, 75, 100, 500, and 1000 µM PTASe, respectively.

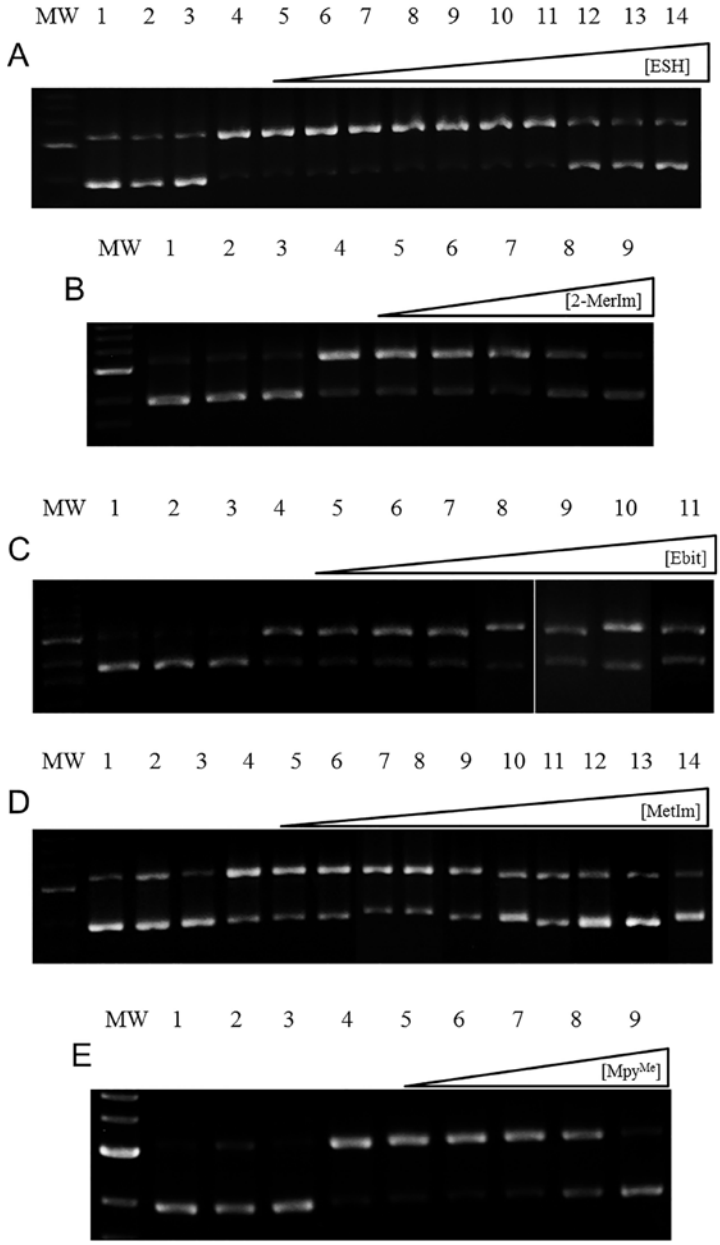

Figure 4.11. Gel electrophoresis images of $[Fe(EDTA)]^{2-}$-mediated DNA damage inhibition by A) ergothioneine (ESH), B) 2-mercaptoimidazole (2-MerIm), C) ethyl-bis(imidazole) thione (ebit), D) methimazole (MetIm), and E) (2-mercapto-1-methyimidazolyl)pyridine thione (mpy^{Me}) in MOPS buffer (10 mM, pH 7). Lane: MW = 1 kb molecular weight marker; lane 1: plasmid DNA (p); lane 2: p + H_2O_2; lane 3: p + S/Se compound (ESH = 2000 µM, 2-MerIm = 1000, ebit = 100 µM, MetIm = 2000 µM, mpy^{Me} = 1000 µM) + H_2O_2; lane 4: p + $[Fe(EDTA)]^{2-}$ (400 µM) + H_2O_2 (50 µM); lanes 5+: p + $[Fe(EDTA)]^{2-}$ + H_2O_2 + increasing concentrations of compound: A) 0.01, 0.1, 1, 10, 50, 100, 1000, 1500, and 2000 µM ESH, respectively, B) 0.1, 1, 10, 100, and 1000 µM 2-MerIm, respectively, C) 0.1, 1, 10, 25, 50, 75, and 100 µM ebit, respectively, D) 0.1, 1, 5, 10, 50, 100, 500, 1000, and 2000 µM MetIm, respectively, and E) 0.1, 1, 10, 25, 50, 75, 100, 250, 500, and 1000 µM mpy^{Me}, respectively.

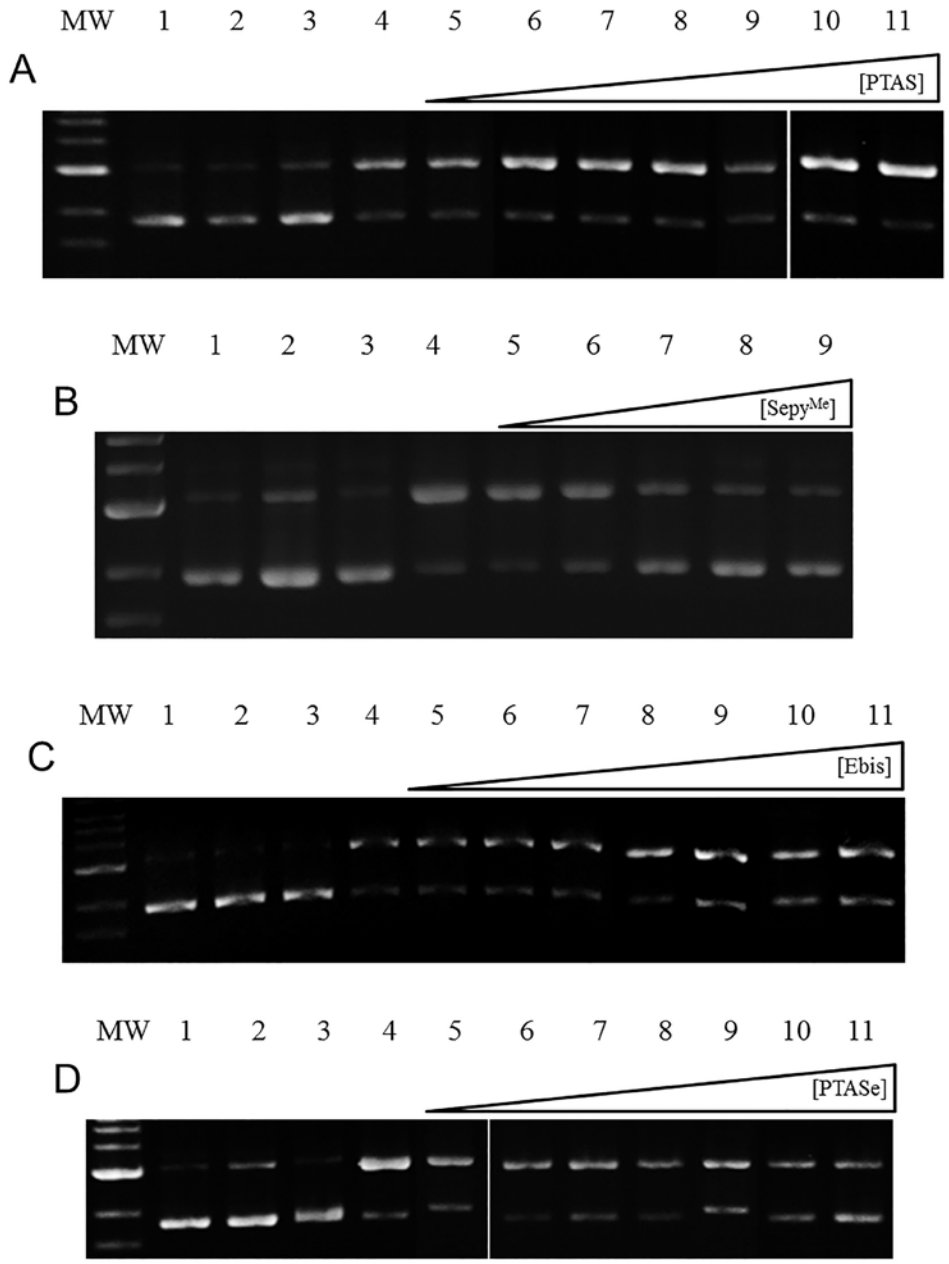

Figure 4.12. Gel electrophoresis images of $[Fe(EDTA)]^{2-}$-mediated DNA damage inhibition by A) 1,3,5-triaza-7-phospaadamantane sulfide (PTAS), B) (2-mercapto-1-methyimidazolyl)pyridine selone ($sepy^{Me}$), C) ethyl-bis(imidazole) selone (ebis), and D) 1,3,5-triaza-7-phospaadamantane selenide (PTASe) in MOPS buffer (10 mM, pH 7). Lane: MW = 1 kb molecular weight marker; lane 1: plasmid DNA (p); lane 2: p + H_2O_2; lane 3: p + S/Se compound (PTAS = 1500, $sepy^{Me}$ = 1000 µM, ebis = 100 µM, PTASe = 1000 µM) + H_2O_2; lane 4: p + $[Fe(EDTA)]^{2-}$ (400 µM) + H_2O_2 (50 µM); lanes 5+: p + $[Fe(EDTA)]^{2-}$ + H_2O_2 + increasing concentrations of compound: A) 0.1, 1, 10, 100, 250, 500, 1000, 1100 and 1500 µM PTAS, respectively, B) 0.1, 1, 10, 25, 50, 75, 100, 250, 500 and 1000 µM $sepy^{Me}$, respectively, C) 0.1, 1, 5, 10, 25, 40, 50, 75, 90, and 100 µM ebis, respectively, and D) 1, 5, 10, 50, 75, 100, 500, and 1000 µM PTASe, respectively.

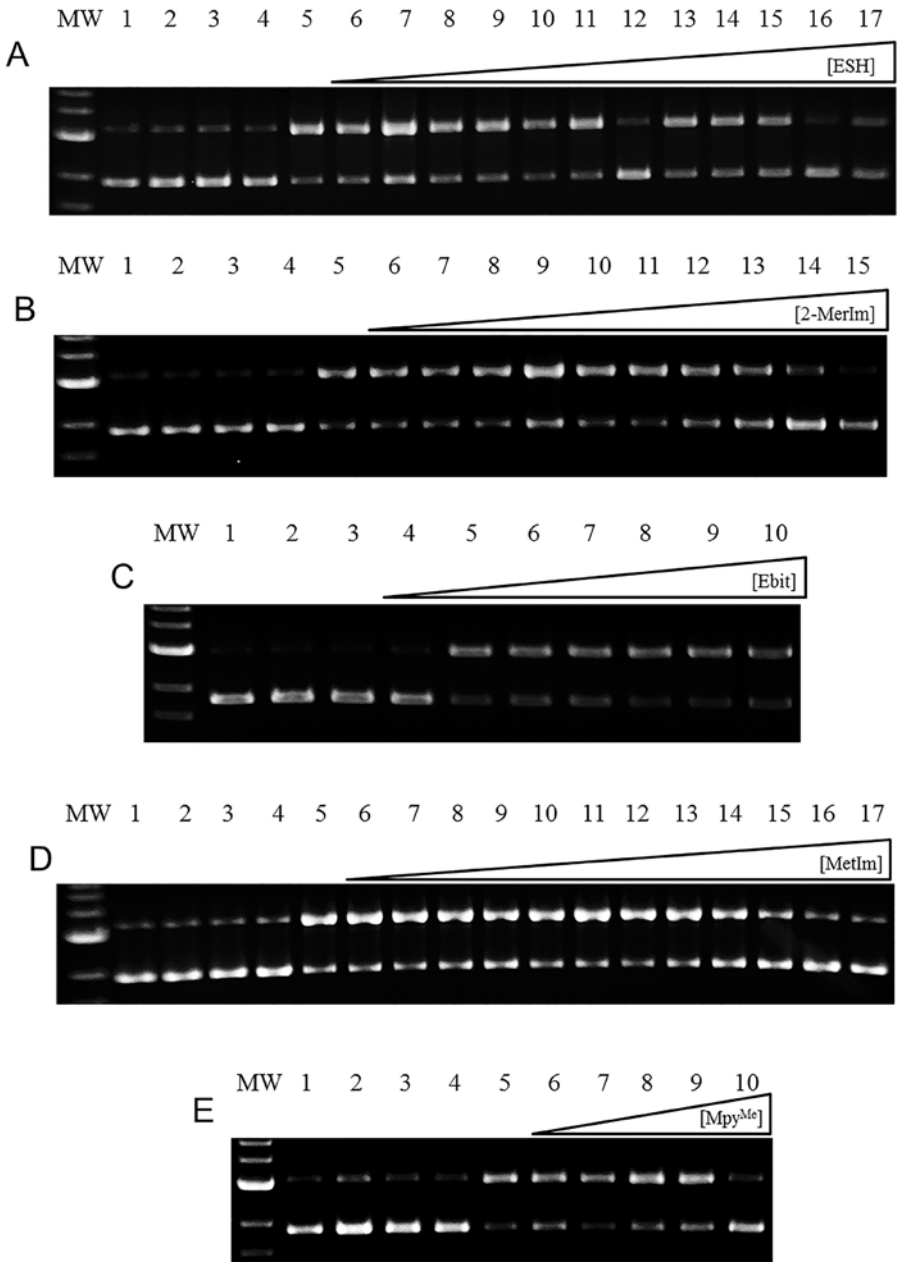

Figure 4.13. Gel electrophoresis images of peroxynitrite ($ONOO^-$)-mediated DNA damage inhibition by A) ergothioneine (ESH), B) 2-mercaptoimidazole (2-MerIm), C) ethyl-bis(imidazole) thione (ebit),D) methimazole (MetIm), and E) (2-mercapto-1-methyimidazolyl)pyridine thione (mpy^{Me}) in MOPS buffer (10 mM, pH 6.8). Lane: MW = 1 kb molecular weight marker; lane 1: plasmid DNA (p); lane 2: p + $NaNO_2$; lane 3: p + KNO_3; lane 4: p + S/Se compound (ESH = 2000 µM, 2-MerIm = 1000, ebit = 100 µM, MetIm = 2000 µM, mpy^{Me} = 1000 µM); lane 5: p + $ONOO^-$ (1450 µM); lanes 6-14: p + $ONOO^-$ + increasing concentrations of compounds: A) 0.01, 0.1, 1, 10, 50, 100, 1000, 1500, and 2000 µM ESH, respectively, B) 0.1, 1, 10, 100, and 1000 µM 2-MerIm, respectively, C) 0.1, 1, 10, 25, 50, 75, and 100 µM ebit, respectively, D) 0.1, 1, 5, 10, 50, 100, 500, 1000, and 2000 µM MetIm, respectively, and E) 0.1, 1, 10, 25, 50, 75, 100, 250, 500, and 1000 µM mpy^{Me}, respectively.

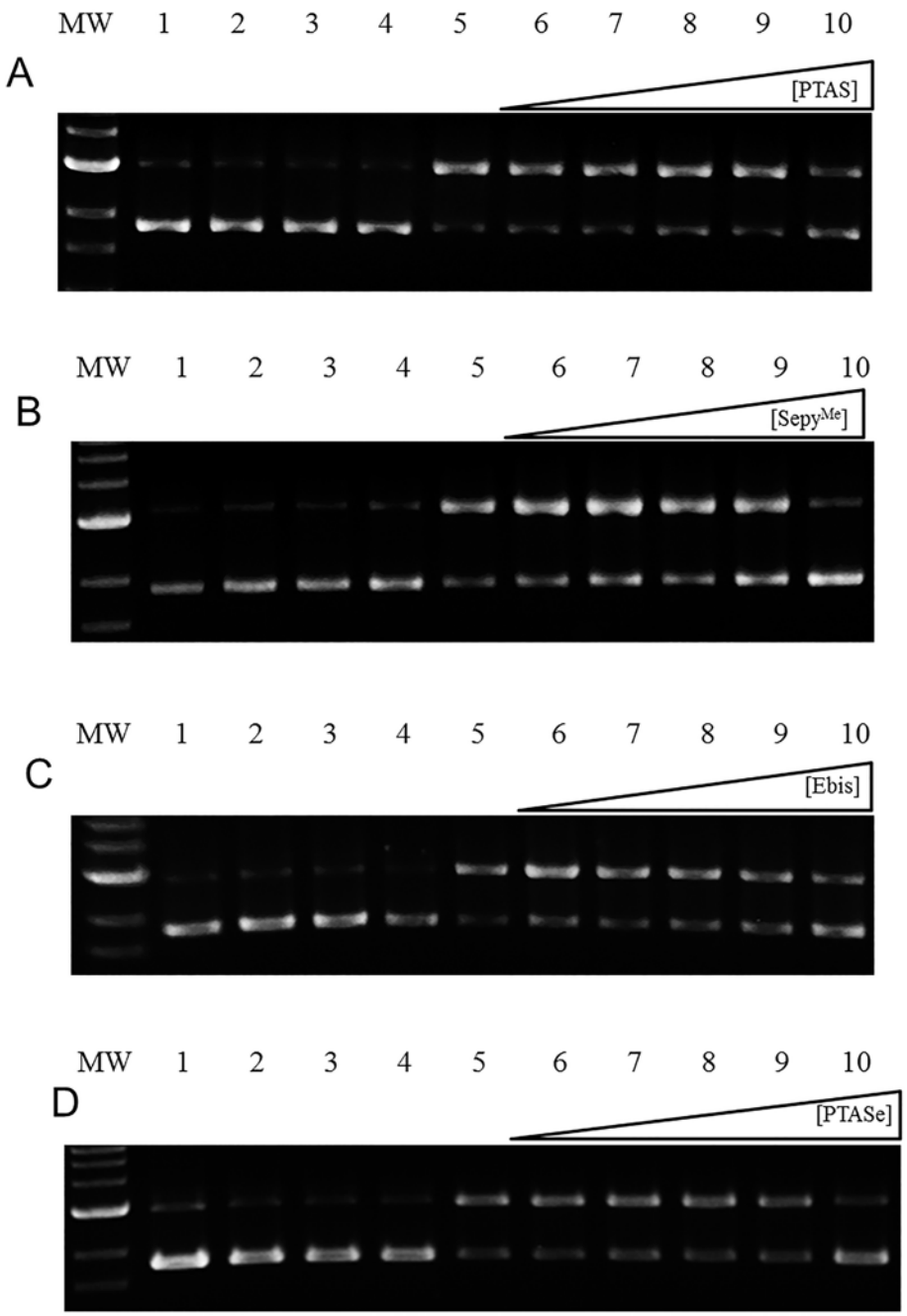

Figure 4.14. Gel electrophoresis images of peroxynitrite ($ONOO^-$)-mediated DNA damage inhibition by A) 1,3,5-triaza-7-phospaadamantane sulfide (PTAS), B) (2-mercapto-1-methyimidazolyl)pyridine selone ($sepy^{Me}$), C) ethyl-bis(imidazole) selone (ebis), and D) 1,3,5-triaza-7-phospaadamantane selenide (PTASe) in MOPS buffer (10 mM, pH 6.8). Lane: MW = 1 kb molecular weight marker; lane 1: plasmid DNA (p); lane 2: p + $NaNO_2$; lane 3: p + KNO_3; lane 4: p + S/Se compound (PTAS = 1500, $sepy^{Me}$ = 1000 µM, ebis = 100 µM, PTASe = 1000 µM); lane 5: p + $ONOO^-$ (1450 µM); lanes 6-14: p + $ONOO^-$ + increasing concentrations of compounds: A) 0.1, 1, 10, 100, 250, 500, 1000, 1100 and 1500 µM PTAS, respectively, B) 0.1, 1, 10, 25, 50, 75, 100, 250, 500 and 1000 µM $sepy^{Me}$, respectively, C) 0.1, 1, 5, 10, 25, 40, 50, 75, 90, and 100 µM ebis, respectively, and D) 1, 5, 10, 50, 75, 100, 500, and 1000 µM PTASe, respectively.

Table 4.7. Gel electrophoresis results for ergothioneine (ESH) DNA damage assays with 6 µM Cu^{I} and 50 µM H_2O_2.[a]

Gel lane	[ESH], µM	% Supercoiled	% Nicked	% Damage Inhibition	*p* Value
1: plasmid DNA (p)	0	93.25 ± 2.59	6.75 ± 2.59	–	–
2: p + H_2O_2	0	91.84 ± 2.80	8.16 ± 2.80	–	–
3: p + ESH + H_2O_2	2000	91.88 ± 3.56	8.12 ± 3.56	–	–
4: p + Cu^+ + H_2O_2	0	7.82 ± 6.30	92.18 ± 6.30	0	–
5: p + Cu^+ + H_2O_2 + ESH	0.1	6.95 ± 4.07	93.05 ± 4.07	-1.15 ± 3.96	0.665
6	1	6.34 ± 5.36	93.66 ± 5.36	-1.81 ± 1.31	0.139
7	2	4.41 ± 6.12	95.59 ± 6.12	-4.39 ± 7.62	0.423
8	5	18.00 ± 0.76	82.00 ± 0.76	6.12 ± 0.94	0.007
9	10	40.31 ± 1.33	59.69 ± 1.33	33.66 ± 1.64	< 0.001
10	50	67.90 ± 0.92	32.10 ± 0.92	71.49 ± 2.07	< 0.001
11	100	82.56 ± 1.74	17.44 ± 1.74	89.05 ± 2.15	< 0.001
12	500	87.38 ± 2.67	12.62 ± 2.67	94.79 ± 1.69	< 0.001
13	1000	87.76 ± 1.55	12.24 ± 1.55	95.14 ± 1.78	< 0.001
14	2000	88.87 ± 2.01	11.13 ± 2.01	96.49 ± 0.86	< 0.001

[a]Data are reported as the average of three trials with calculated standard deviations shown.

Table 4.8. Gel electrophoresis results for 2-mercaptoimidazole (2-MerIm) DNA damage assays with 6 µM Cu^{I} and 50 µM H_2O_2.[a]

Gel lane	[2-MerIm], µM	% Supercoiled	% Nicked	% Damage Inhibition	*p* Value
1: plasmid DNA (p)	0	94.8 ± 1.2	5.2 ± 1.2	–	–
2: p + H_2O_2	0	94.2 ± 1.5	5.8 ± 1.5	–	–
3: p + 2-MerIm + H_2O_2	1000	94.7 ± 0.5	5.3 ± 0.5	–	–
4: p + Cu^+ + H_2O_2	0	8.2 ± 1.9	91.8 ± 1.9	0	–
5: p + Cu^+ + H_2O_2 + 2-MerIm	0.1	8.4 ± 1.8	91.6 ± 1.8	0.15 ± 0.28	0.451
6	1	8.7 ± 2.7	91.3 ± 2.7	0.56 ± 1.71	0.628
7	10	35.5 ± 1.3	64.5 ± 1.3	31.69 ± 1.25	< 0.001
8	100	73.8 ± 3.8	26.2 ± 3.8	76.32 ± 4.02	< 0.001
9	1000	92.1 ± 3.6	7.9 ± 3.6	97.52 ± 2.58	< 0.001

[a]Data are reported as the average of three trials with calculated standard deviations shown.

Table 4.9. Gel electrophoresis results for ethyl-bis(imidazole) thione (ebit) DNA damage assays with 6 μM Cu^{I} and 50 μM H_2O_2.[a]

Gel lane	[ebit], μM	% Supercoiled	% Nicked	% Damage Inhibition	*p* Value
1: plasmid DNA (p)	0	96.85 ± 0.14	3.15 ± 0.14	–	–
2: p + H_2O_2	0	96.11 ± 0.30	3.89 ± 0.30	–	–
3: p + ebit + H_2O_2	100	97.11 ± 0.72	2.89 ± 0.72	–	–
4: p + Cu^{+} + H_2O_2	0	1.59 ± 2.06	98.41 ± 2.06	0	–
5: p + Cu^{+} + H_2O_2 + ebit	0.1	2.10 ± 3.64	97.90 ± 3.64	0.57 ± 1.80	0.638
6	1	1.58 ± 2.70	98.42 ± 2.70	-0.09 ± 4.55	0.976
7	5	7.85 ± 3.28	92.15 ± 3.28	3.19 ± 3.67	0.271
8	10	13.43 ± 2.22	86.57 ± 2.22	3.48 ± 2.57	0.144
9	25	13.82 ± 1.17	86.18 ± 1.17	9.86 ± 1.31	0.006
10	35	67.50 ± 0.82	32.50 ± 0.82	66.08 ± 0.95	< 0.001
11	40	65.02 ± 2.30	34.98 ± 2.30	67.03 ± 2.57	< 0.001
12	50	77.36 ± 2.88	22.64 ± 2.88	79.27 ± 2.96	< 0.001
13	75	78.05 ± 1.21	21.95 ± 1.21	81.59 ± 1.35	< 0.001
14	90	87.91 ± 1.09	12.09 ± 1.09	89.72 ± 1.26	< 0.001
15	100	89.94 ± 2.78	10.06 ± 2.78	92.45 ± 2.46	< 0.001

[a]Data are reported as the average of three trials with calculated standard deviations shown.

Table 4.10. Gel electrophoresis results for methimazole (MetIm) DNA damage assays with 6 μM Cu^{I} and 50 μM H_2O_2.[a]

Gel lane	[MetIm], μM	% Supercoiled	% Nicked	% Damage Inhibition	*p* Value
1: plasmid DNA (p)	0	95.0 ± 0.3	5.0 ± 0.3	–	–
2: p + H_2O_2	0	95.2 ± 0.1	4.8 ± 0.1	–	–
3: p + MetIm + H_2O_2	2000	94.6 ± 0.8	5.4 ± 0.8	–	–
4: p + Cu^{+} + H_2O_2	0	4.9 ± 1.5	95.1 ± 1.5	0	–
5: p + Cu^{+} + H_2O_2 + MetIm	0.1	1.4 ± 1.2	98.6 ± 1.2	-3.99 ± 2.80	0.132
6	1	1.8 ± 0.6	98.2 ± 0.6	-3.54 ± 1.39	0.048
7	2	1.8 ± 1.2	98.2 ± 1.2	-3.51 ± 2.58	0.143
8	5	1.0 ± 1.0	99.0 ± 1.0	-4.45 ± 2.68	0.103
9	10	4.0 ± 1.3	96.0 ± 1.3	-1.05 ± 2.49	0.541
10	50	28.5 ± 2.0	71.5 ± 2.0	26.16 ± 1.02	< 0.001
11	100	47.7 ± 1.2	50.3 ± 1.2	49.62 ± 0.75	< 0.001
12	500	80.8 ± 2.6	19.2 ± 2.6	84.08 ± 2.57	< 0.001
13	1000	84.9 ± 2.3	15.1 ± 2.3	88.63 ± 2.27	< 0.001
14	2000	89.6 ± 1.8	10.4 ± 1.8	93.81 ± 1.78	< 0.001

[a]Data are reported as the average of three trials with calculated standard deviations shown.

Table 4.11. Gel electrophoresis results for (2-mercapto-1-methylimidazolyl)pyridine thione (mpy^{Me}) DNA damage assays with 6 μM Cu^{I} and 50 μM H_2O_2.[a]

Gel lane	[mpy^{Me}], μM	% Supercoiled	% Nicked	% Damage Inhibition	*p* Value
1: plasmid DNA (p)	0	96.48 ± 0.38	3.52 ± 0.38	–	–
2: p + H_2O_2	0	95.92 ± 1.46	4.08 ± 1.46	–	–
3: p + mpy^{Me} + H_2O_2	100	95.80 ± 0.45	4.20 ± 0.45	–	–
4: p + Cu^{+} + H_2O_2	0	15.29 ± 1.18	84.71 ± 1.18	0	–
5: p + Cu^{+} + H_2O_2 + mpy^{Me}	0.1	14.37 ± 0.45	85.63 ± 0.45	-1.17 ± 1.26	0.249
6	1	16.65 ± 1.43	83.35 ± 1.43	1.69 ± 0.55	0.033
7	10	16.34 ± 1.27	83.66 ± 1.27	1.30 ± 0.31	0.018
8	25	13.85 ± 5.09	86.15 ± 5.09	8.09 ± 5.61	0.130
9	50	29.91 ± 0.70	70.09 ± 0.70	18.12 ± 1.06	0.001
10	75	21.26 ± 0.57	78.74 ± 0.57	16.26 ± 0.63	< 0.001
11	100	42.39 ± 0.55	57.61 ± 0.55	33.61 ± 0.08	< 0.001
12	250	33.31 ± 2.00	66.69 ± 2.00	28.74 ± 2.40	< 0.001
13	500	63.50 ± 2.69	36.51 ± 2.69	62.81 ± 2.96	< 0.001
14	1000	86.12 ± 0.87	13.87 ± 0.87	87.76 ± 0.95	< 0.001

[a]Data are reported as the average of three trials with calculated standard deviations shown.

Table 4.12. Gel electrophoresis results for 1,3,5-triaza-7-phosphaadmantane sulfide (PTAS) DNA damage assays with 6 μM Cu^{I} and 50 μM H_2O_2.[a]

Gel lane	[PTAS], μM	% Supercoiled	% Nicked	% Damage Inhibition	*p* Value
1: plasmid DNA (p)	0	97.69 ± 3.31	2.31 ± 3.31	–	–
2: p + H_2O_2	0	95.66 ± 0.38	4.34 ± 0.38	–	–
3: p + PTAS + H_2O_2	1000	97.62 ± 1.75	2.38 ± 1.75	–	–
4: p + Cu^{+} + H_2O_2	0	5.31 ± 2.75	94.69 ± 2.75	0	–
5: p + Cu^{+} + H_2O_2 + PTAS	0.1	6.37 ± 3.55	93.63 ± 3.55	-0.84 ± 2.01	0.544
6	1	10.56 ± 7.24	89.44 ± 7.24	-0.71 ± 3.05	0.726
7	10	8.18 ± 7.61	91.82 ± 7.61	3.22 ± 5.42	0.412
8	100	18.59 ± 0.89	81.41 ± 0.89	16.01 ± 0.98	0.001
9	250	36.13 ± 3.34	63.87 ± 3.34	13.76 ± 5.14	0.043
10	500	40.41 ± 2.55	59.59 ± 2.55	20.36 ± 3.93	0.012
11	1000	43.99 ± 2.02	56.01 ± 2.02	43.95 ± 2.22	< 0.001
12	1100	73.53 ± 3.55	26.47 ± 3.55	71.36 ± 5.47	0.002
13	1500	96.16 ± 0.67	3.84 ± 0.67	101.31 ± 0.74	< 0.001

[a]Data are reported as the average of three trials with calculated standard deviations shown.

Table 4.13. Gel electrophoresis results for (2-mercapto-1-methylimidazolyl)pyridine selone ($sepy^{Me}$) DNA damage assays with 6 μM Cu^{I} and 50 μM H_2O_2.[a]

Gel lane	[$sepy^{Me}$], μM	% Supercoiled	% Nicked	% Damage Inhibition	*p* Value
1: plasmid DNA (p)	0	95.76 ± 1.74	4.24 ± 1.74	–	–
2: p + H_2O_2	0	96.71 ± 1.76	3.29 ± 1.76	–	–
3: p + $sepy^{Me}$ + H_2O_2	100	95.92 ± 0.66	4.08 ± 0.66	–	–
4: p + Cu^{+} + H_2O_2	0	7.04 ± 4.12	92.96 ± 4.12	0	–
5: p + Cu^{+} + H_2O_2 + $sepy^{Me}$	0.1	10.02 ± 3.98	89.98 ± 3.98	3.34 ± 1.09	0.034
6	1	12.72 ± 1.70	87.28 ± 1.70	6.27 ± 2.33	0.043
7	10	53.61 ± 3.64	46.39 ± 3.64	51.86 ± 5.99	0.004
8	25	63.61 ± 1.42	36.38 ± 1.42	66.56 ± 1.51	< 0.001
9	50	66.92 ± 0.08	33.08 ± 0.08	66.75 ± 1.85	< 0.001
10	75	75.95 ± 0.87	24.05 ± 0.87	79.66 ± 0.92	< 0.001
11	100	78.52 ± 2.35	21.48 ± 2.35	79.81 ± 3.38	< 0.001
12	250	90.14 ± 0.41	9.86 ± 0.41	94.72 ± 0.43	< 0.001
13	500	92.50 ± 0.73	7.45 ± 0.73	97.28 ± 0.78	< 0.001
14	1000	95.55 ± 0.65	4.44 ± 0.65	100.48 ± 0.69	< 0.001

[a]Data are reported as the average of three trials with calculated standard deviations shown.

Table 4.14. Gel electrophoresis results for ethyl-bis(imidazole) selone (ebis) DNA damage assays with 6 μM Cu^{+} and 50 μM H_2O_2.[a]

Gel lane	[ebis], μM	% Supercoiled	% Nicked	% Damage Inhibition	*p* Value
1: plasmid DNA (p)	0	97.54 ± 0.16	2.46 ± 0.16	–	–
2: p + H_2O_2	0	95.63 ± 0.85	4.37 ± 0.85	–	–
3: p + ebis + H_2O_2	100	98.05 ± 1.71	1.95 ± 1.71	–	–
4: p + Cu^{+} + H_2O_2	0	1.49 ± 1.14	98.51 ± 1.14	0	–
5: p + Cu^{+} + H_2O_2 + ebis	0.1	0.34 ± 0.54	99.66 ± 0.54	-1.19 ± 1.08	0.196
6	1	3.87 ± 2.98	96.13 ± 2.98	2.45 ± 2.00	0.168
7	5	20.56 ± 4.74	79.44 ± 4.74	16.82 ± 5.28	0.031
8	10	40.50 ± 3.18	59.50 ± 3.18	40.43 ± 4.08	0.003
9	25	72.03 ± 3.23	27.97 ± 3.23	74.15 ± 3.60	< 0.001
10	40	78.64 ± 0.65	21.36 ± 0.65	81.52 ± 0.72	< 0.001
11	50	94.93 ± 1.95	5.07 ± 1.95	95.88 ± 0.86	< 0.001
12	75	84.20 ± 1.91	15.80 ± 1.91	96.57 ± 0.70	< 0.001
13	90	89.16 ± 4.32	10.84 ± 4.32	93.24 ± 4.82	< 0.001
14	100	95.18 ± 0.82	4.82 ± 0.82	97.04 ± 2.41	< 0.001

[a]Data are reported as the average of three trials with calculated standard deviations shown.

Table 4.15. Gel electrophoresis results for 1,3,5-triaza-7-phosphaadmantane selenide (PTASe) DNA damage assays with 6 μM Cu^{I} and 50 μM H_2O_2.[a]

Gel lane	[PTASe], μM	% Supercoiled	% Nicked	% Damage Inhibition	*p* Value
1: plasmid DNA (p)	0	97.34 ± 0.79	2.66 ± 0.79	–	–
2: p + H_2O_2	0	98.56 ± 1.17	1.44 ± 1.17	–	–
4: p + PTASe + H_2O_2	1000	98.20 ± 1.45	1.80 ± 1.45	–	–
5: p + Cu^{+} + H_2O_2	0	4.47± 5.65	95.53 ± 5.65	0	–
6: p + Cu^{+} + H_2O_2 + PTASe	1	0.91 ± 1.16	99.09 ± 1.16	-4.13 ± 7.30	0.430
7	5	13.74 ± 2.84	86.26 ± 2.84	3.89 ± 3.32	0.179
8	10	20.85 ± 11.13	79.15 ± 11.13	12.21 ± 13.01	0.245
9	50	21.01 ± 1.12	78.99 ± 1.12	12.39 ± 1.31	0.004
10	75	68.87 ± 7.86	31.13 ±7.86	72.41 ± 8.78	0.004
11	100	95.25 ± 2.38	4.75 ± 2.38	96.92 ± 1.67	< 0.001
12	500	93.13 ± 2.01	6.87 ± 2.01	96.74 ± 2.35	< 0.001
13	1000	91.28 ± 0.34	8.72 ± 0.34	94.57± 0.39	< 0.001

[a]Data are reported as the average of three trials with calculated standard deviations shown.

Table 4.16. Gel electrophoresis results for ergothioneine (ESH) DNA damage assays with 2 μM Fe^{II} and 50 μM H_2O_2.[a]

Gel lane	[ESH], μM	% Supercoiled	% Nicked	% Damage Inhibition	*p* Value
1: plasmid DNA (p)	0	88.25 ± 1.71	11.75 ± 1.71	–	–
2: p + H_2O_2	0	84.42 ± 1.37	15.58 ± 1.37	–	–
3: p + ESH + H_2O_2	1000	88.80 ± 1.00	11.20 ± 1.00	–	–
4: p + Fe^{2+} + H_2O_2	0	20.50 ± 2.29	79.50 ± 2.29	0	–
5: p + Fe^{2+} + H_2O_2 + ESH	0.01	20.89 ± 2.91	79.11 ± 2.91	-0.80 ± 4.59	0.791
6	0.1	21.37 ± 1.89	78.63 ± 1.89	-0.05 ± 2.97	0.979
7	1	29.54 ± 0.61	70.46 ± 0.61	14.06 ± 3.93	0.025
8	10	61.59 ± 2.13	38.41 ± 2.13	64.36 ± 2.81	< 0.001
9	50	72.14 ± 0.21	27.85 ± 0.21	80.00 ± 0.33	< 0.001
10	100	73.22 ± 1.42	26.78 ± 1.42	82.52 ± 1.16	< 0.001
11	1000	76.12 ± 1.53	23.88 ± 1.53	87.00 ± 0.79	< 0.001
12	1500	81.40 ± 1.31	18.61 ± 1.31	94.56 ± 2.06	< 0.001
13	2000	81.56 ± 0.67	18.44 ± 0.67	94.84 ± 1.06	< 0.001

[a]Data are reported as the average of three trials with calculated standard deviations shown.

Table 4.17. Gel electrophoresis results for 2-mercaptoimidazole (2-MerIm) DNA damage assays with 2 μM Fe^{2+} and 50 μM H_2O_2.[a]

Gel lane	[2-MerIm], μM	% Supercoiled	% Nicked	% Damage Inhibition	*p* Value
1: plasmid DNA (p)	0	94.4 ± 0.4	5.6 ± 0.4	–	–
2: p + H_2O_2	0	94.1 ± 0.6	5.9 ± 0.6	–	–
3: p + 2-MerIm + H_2O_2	1000	94.8 ± 1.1	5.2 ± 1.1	–	–
4: p + Fe^{2+} + H_2O_2	0	13.9 ± 1.9	86.1 ± 1.9	0	–
5: p + Fe^{2+} + H_2O_2 + 2-MerIm	0.1	17.1 ± 0.8	82.9 ± 0.8	4.01 ± 3.28	0.168
6	1	39.6 ± 4.3	60.3 ± 4.3	32.19 ± 3.92	0.005
7	10	75.6 ± 2.9	24.4 ± 2.9	76.94 ± 4.25	0.001
8	100	88.2 ± 2.6	11.8 ± 2.6	92.66 ± 3.89	< 0.001
9	1000	91.5 ± 1.1	8.5 ± 1.1	96.77 ± 1.97	< 0.001

[a]Data are reported as the average of three trials with calculated standard deviations shown.

Table 4.18. Gel electrophoresis results for ethyl-bis(imidazole) thione (ebit) DNA damage assays with 2 μM Fe^{2+} and 50 μM H_2O_2.[a]

Gel lane	[ebit], μM	% Supercoiled	% Nicked	% Damage Inhibition	*p* Value
1: plasmid DNA (p)	0	98.77 ± 0.90	1.23 ± 0.90	–	–
2: p + H_2O_2	0	98.75 ± 0.77	1.25 ± 0.77	–	–
3: p + ebit + H_2O_2	100	98.98 ± 0.45	1.02 ± 0.45	–	–
4: p + Fe^{2+} + H_2O_2	0	15.13 ± 1.47	84.87 ± 1.47	0	–
5: p + Fe^{2+} + H_2O_2 + ebit	0.1	12.60 ± 2.04	87.40 ± 2.04	-3.08 ± 4.20	0.332
6	1	14.44 ± 1.70	85.56 ± 1.70	-0.82 ± 0.25	0.030
7	10	32.95 ± 0.66	67.05 ± 0.66	21.21 ± 2.03	0.003
8	25	33.54 ± 1.09	66.45 ± 1.09	30.49 ± 1.18	< 0.001
9	50	42.77 ± 1.04	57.23 ± 1.04	32.96 ± 0.36	< 0.001
10	75	39.47 ± 2.17	60.53 ± 2.17	36.91 ± 2.35	< 0.001
11	100	69.45 ± 1.74	30.55 ± 1.74	64.76 ± 2.23	< 0.001

[a]Data are reported as the average of three trials with calculated standard deviations shown.

Table 4.19. Gel electrophoresis results for methimazole (MetIm) DNA damage assays with 2 μM Fe^{2+} and 50 μM H_2O_2.[a]

Gel lane	[MetIm], μM	% Supercoiled	% Nicked	% Damage Inhibition	*p* Value
1: plasmid DNA (p)	0	94.16 ± 0.50	5.84 ± 0.50	–	–
2: p + H_2O_2	0	83.81 ± 1.76	6.19 ± 1.76	–	–
3: p + MetIm + H_2O_2	1000	93.77 ± 1.24	6.23 ± 1.24	–	–
4: p + Fe^{2+} + H_2O_2	0	7.86 ± 5.53	92.14 ± 5.53	0	–
5: p + Fe^{2+} + H_2O_2 + MetIm	0.1	9.77 ± 5.67	90.23 ± 5.67	2.40 ± 5.54	0.531
6	1	8.49 ± 4.11	91.51 ± 4.11	0.75 ± 2.01	0.584
7	5	36.55 ± 1.18	63.45 ± 1.18	17.03 ± 1.75	0.003
8	10	50.54 ± 0.97	49.46 ± 0.97	56.08 ± 3.16	0.001
9	50	76.65 ± 1.72	23.35 ± 1.72	76.19 ± 2.54	< 0.001
10	100	76.63 ± 1.22	23.37 ± 1.22	90.46 ± 2.40	< 0.001
11	500	88.50 ± 2.73	11.48 ± 2.73	93.70 ± 4.03	< 0.001
12	1000	82.68 ± 1.89	17.32 ± 1.89	98.37 ± 4.34	< 0.001
13	2000	91.40 ± 0.64	8.57 ± 0.64	98.00 ± 0.94	< 0.001

[a]Data are reported as the average of three trials with calculated standard deviations shown.

Table 4.20. Gel electrophoresis results for (2-mercapto-1-methylimidazolyl)pyridine thione (mpy^{Me}) DNA damage assays with 2 μM Fe^{2+} and 50 μM H_2O_2.[a]

Gel lane	[mpy^{Me}], μM	% Supercoiled	% Nicked	% Damage Inhibition	*p* Value
1: plasmid DNA (p)	0	96.38 ± 0.41	3.62 ± 0.41	–	–
2: p + H_2O_2	0	96.25 ± 1.47	3.75 ± 1.47	–	–
3: p + mpy^{Me} + H_2O_2	100	95.87 ± 0.62	4.13 ± 0.62	–	–
4: p + Fe^{2+} + H_2O_2	0	16.39 ± 2.23	83.61 ± 2.23	0	–
5: p + Fe^{2+} + H_2O_2 + mpy^{Me}	0.1	21.01 ± 6.08	78.99 ± 6.08	5.85 ± 5.56	0.210
6	1	19.47 ± 1.91	80.53 ± 1.91	3.86 ± 1.21	0.031
7	10	22.92 ± 2.68	77.08 ± 2.68	8.18 ± 0.96	0.004
8	25	11.28 ± 1.51	88.72 ± 1.51	8.26 ± 1.67	0.013
9	50	23.50 ± 1.86	76.50 ± 1.86	8.90 ± 0.87	0.003
10	75	26.09 ± 2.44	73.91 ± 2.44	24.59 ± 2.69	0.004
11	100	41.04 ± 2.05	58.96 ± 2.05	30.84 ± 1.73	0.001
12	250	44.28 ± 1.33	55.72 ± 1.33	44.65 ± 1.46	< 0.001
13	500	54.60 ± 1.25	45.37 ± 1.25	56.08 ± 1.38	< 0.001
14	1000	53.98 ± 2.25	46.02 ± 2.25	55.36 ± 2.49	< 0.001

[a]Data are reported as the average of three trials with calculated standard deviations shown.

Table 4.21. Gel electrophoresis results for 1,3,5-triaza-7-phosphaadmantane sulfide (PTAS) DNA damage assays with 2 μM Fe^{2+} and 50 μM H_2O_2.[a]

Gel lane	[PTAS], μM	% Supercoiled	% Nicked	% Damage Inhibition	*p* Value
1: plasmid DNA (p)	0	96.45 ± 1.59	3.55 ± 1.59	–	–
2: p + H_2O_2	0	95.32 ± 1.92	4.68 ± 1.92	–	–
3: p + PTAS + H_2O_2	1000	95.39 ± 3.01	4.61 ± 3.01	–	–
4: p + Fe^{2+} + H_2O_2	0	17.71 ± 2.20	82.29 ± 2.20	0	–
5: p + Fe^{2+} + H_2O_2 + PTAS	0.01	6.64 ± 1.05	93.36 ± 1.05	-0.94 ± 1.16	0.295
6	0.1	19.30 ± 4.59	80.70 ± 4.59	2.02 ± 4.69	0.533
7	1	24.48 ± 3.84	75.52 ± 3.84	8.81 ± 2.98	0.036
8	10	30.68 ± 4.14	69.32 ± 4.14	16.77 ± 3.39	0.013
9	100	47.18 ± 2.76	52.82 ± 2.76	37.92 ± 4.94	0.005
10	1000	52.00 ± 3.86	48.00 ± 3.86	44.15 ± 4.05	0.003

[a]Data are reported as the average of three trials with calculated standard deviations shown.

Table 4.22. Gel electrophoresis results for (2-mercapto-1-methylimidazolyl)pyridine selone ($sepy^{Me}$) DNA damage assays with 2 μM Fe^{2+} and 50 μM H_2O_2.[a]

Gel lane	[$sepy^{Me}$], μM	% Supercoiled	% Nicked	% Damage Inhibition	*p* Value
1: plasmid DNA (p)	0	95.78 ± 0.52	4.22 ± 0.52	–	–
2: p + H_2O_2	0	96.58 ± 0.59	3.42 ± 0.59	–	–
3: p + $sepy^{Me}$ + H_2O_2	100	97.01 ± 0.40	2.99 ± 0.40	–	–
4: p + Fe^{2+} + H_2O_2	0	19.09 ± 0.65	80.91 ± 0.65	0	–
5: p + Fe^{2+} + H_2O_2 +$sepy^{Me}$	0.1	22.75 ± 1.51	77.25 ± 1.51	4.69 ± 2.70	0.095
6	1	22.99 ± 2.01	77.01 ± 2.01	5.05 ± 1.84	0.042
7	10	43.26 ± 1.06	56.74 ± 1.06	31.17 ± 1.54	< 0.001
8	25	55.17 ± 1.76	44.83 ± 1.76	46.19 ± 2.23	< 0.001
9	50	57.76 ± 2.03	42.24 ± 2.03	49.91 ± 2.45	< 0.001
10	75	58.64 ± 2.50	41.36 ± 2.50	50.57 ± 3.16	< 0.001
11	100	61.17 ± 3.05	38.83 ± 3.05	54.33 ± 3.83	< 0.001
12	250	64.57 ± 0.23	35.43 ± 0.23	58.07 ± 0.29	< 0.001
13	500	61.80 ± 1.86	38.15 ± 1.86	54.63 ± 2.35	< 0.001
14	1000	66.29 ± 1.70	33.71 ± 1.70	60.24 ± 2.15	< 0.001

[a]Data are reported as the average of three trials with calculated standard deviations shown.

Table 4.23. Gel electrophoresis results for ethyl-bis(imidazole) selone (ebis) DNA damage assays with 2 μM Fe^{2+} and 50 μM H_2O_2.[a]

Gel lane	[ebis], μM	% Supercoiled	% Nicked	% Damage Inhibition	*p* Value
1: plasmid DNA (p)	0	98.02 ± 1.48	1.98 ± 1.48	–	–
2: p + H_2O_2	0	96.65 ± 0.29	3.35 ± 0.29	–	–
3: p + ebis + H_2O_2	100	98.94 ± 1.20	1.06 ± 1.20	–	–
4: p + Fe^{2+} + H_2O_2	0	22.44 ± 8.48	77.56 ± 8.48	0	–
5: p + Fe^{2+} + H_2O_2 + ebis	0.1	21.94 ± 11.46	78.06 ± 11.46	-0.37 ± 4.81	0.906
6	0.2	14.58 ± 1.00	85.42 ± 1.00	3.34 ± 1.17	0.039
7	1	41.84 ± 6.87	58.16 ± 6.87	25.42 ± 1.13	< 0.001
8	2	39.10 ± 2.63	60.90 ± 2.63	31.76 ± 3.05	0.003
9	3	51.58 ± 3.69	48.41 ± 3.69	42.96 ± 4.78	0.004
10	8	73.85 ± 3.65	26.15 ± 3.65	71.77 ± 4.73	0.001
11	10	90.30 ± 3.36	9.70 ± 3.36	88.41 ± 4.40	< 0.001
12	25	86.96 ± 1.11	13.04 ± 1.11	87.23 ± 1.29	< 0.001
13	50	94.72 ± 3.72	5.28 ± 3.72	94.47 ± 3.17	< 0.001
14	100	94.89 ± 2.78	5.11 ± 2.78	94.72 ± 1.96	< 0.001

[a]Data are reported as the average of three trials with calculated standard deviations shown.

Table 4.24. Gel electrophoresis results for 1,3,5-triaza-7-phosphaadmantane selenide (PTASe) DNA damage assays with 2 μM Fe^{2+} and 50 μM H_2O_2.[a]

Gel lane	[PTASe], μM	% Supercoiled	% Nicked	% Damage Inhibition	*p* Value
1: plasmid DNA (p)	0	97.90 ± 1.34	2.10 ± 1.34	–	–
2: p + H_2O_2	0	97.69 ± 0.70	2.31 ± 0.70	–	–
4: p + PTASe + H_2O_2	1000	98.63 ± 0.03	1.37 ± 0.03	–	–
5: p + Fe^{2+} + H_2O_2	0	20.24 ± 3.01	79.76 ± 3.01	0	–
6: p + Fe^{2+} + H_2O_2 + PTASe	0.01	23.84 ± 1.48	76.16 ± 1.48	-2.84 ± 2.11	0.145
7	0.1	24.28 ± 3.82	75.72 ± 3.82	5.23 ± 1.25	0.019
8	1	30.62 ± 5.06	69.38 ± 5.06	13.45 ± 3.30	0.019
9	10	41.59 ± 4.60	58.41 ± 4.60	27.55 ± 4.95	0.011
10	50	40.38 ± 2.37	59.62 ± 2.37	20.81 ± 3.38	0.009
11	100	83.66 ± 1.40	16.34 ± 1.40	81.88 ± 1.62	< 0.001
12	1000	83.26 ± 1.85	16.74 ± 1.85	81.36 ± 2.38	< 0.001

[a]Data are reported as the average of three trials with calculated standard deviations shown.

Table 4.25. Gel electrophoresis results for ergothioneine (ESH) DNA damage assays with 50 μM $[Cu(bipy)_2]^+$ and 50 μM H_2O_2.[a]

Gel lane	[ESH], μM	% Supercoiled	% Nicked	% Damage Inhibition	*p* Value
1: plasmid DNA (p)	0	94.03 ± 0.85	5.97 ± 0.85	–	–
2: p + H_2O_2	0	93.42 ± 1.33	6.58 ± 1.33	–	–
3: p + ESH + H_2O_2	2000	94.61 ± 0.48	5.39 ± 0.48	–	–
4: p + $[Cu(bipy)_2]^+$ + H_2O_2	0	2.74 ± 1.48	97.26 ± 1.48	0	–
5: p + $[Cu(bipy)_2]^+$ + H_2O_2 + ESH	0.1	1.45 ± 1.10	98.55 ± 1.10	-1.42 ± 0.46	0.033
6	1	2.20 ± 1.43	97.80 ± 1.43	-0.60 ± 1.92	0.642
7	2	1.64 ± 1.01	98.36 ± 1.01	-1.21 ± 1.32	0.253
8	5	1.54 ± 1.18	98.46 ± 1.18	-1.32 ± 1.65	0.300
9	10	2.47 ± 2.20	97.53 ± 2.20	-0.30 ± 1.37	0.741
10	50	1.66 ± 1.21	98.34 ± 1.21	-1.19 ± 1.45	0.291
11	100	1.61 ± 1.80	98.39 ± 1.80	-1.24 ± 3.04	0.553
12	500	4.06 ± 1.61	95.94 ± 1.61	1.45 ± 2.50	0.421
13	1000	1.75 ± 1.04	98.25 ± 1.04	-1.09 ± 1.08	0.222
14	2000	2.59 ± 1.15	97.41 ± 1.15	-0.16 ± 2.11	0.905

[a]Data are reported as the average of three trials with calculated standard deviations shown.

Table 4.26. Gel electrophoresis results for 2-mercaptoimidazole (2-MerIm) DNA damage assays with 50 μM $[Cu(bipy)_2]^+$ and 50 μM H_2O_2.[a]

Gel lane	[2-MerIm], μM	% Supercoiled	% Nicked	% Damage Inhibition	*p* Value
1: plasmid DNA (p)	0	94.8 ± 0.5	5.2 ± 0.5	–	–
2: p + H_2O_2	0	94.6 ± 1.3	5.4 ± 1.3	–	–
3: p + 2-MerIm + H_2O_2	1000	94.7 ± 0.6	5.3 ± 0.6	–	–
4: p + $[Cu(bipy)_2]^+$ + H_2O_2	0	7.4 ± 2.0	92.6 ± 2.0	0	–
5: p + $[Cu(bipy)_2]^+$ + H_2O_2 + 2-MerIm	0.1	7.5 ± 2.6	92.6 ± 2.6	0.20 ± 1.45	0.833
6	1	13.6 ± 1.0	86.4 ± 1.0	7.15 ± 1.38	0.122
7	2	6.0 ± 0.5	94.0 ± 0.5	3.40 ± 0.58	0.009
8	5	11.7 ± 1.2	88.3 ± 1.2	9.77 ± 1.37	0.006
9	10	13.4 ± 2.4	86.6 ± 2.4	6.90 ± 1.55	0.016
10	50	8.1 ± 2.9	91.9 ± 2.9	5.69 ± 3.25	0.094
11	100	15.5 ± 2.2	84.5 ± 2.2	9.29 ± 1.44	0.008
12	500	1.0 ± 0.2	99.0 ± 0.2	-2.25 ± 0.23	0.003
13	1000	5.4 ± 1.8	94.6 ± 1.8	2.70 ± 2.09	0.249

[a]Data are reported as the average of three trials with calculated standard deviations shown.

Table 4.27. Gel electrophoresis results for ethyl-bis(imidazole) thione (ebit) DNA damage assays with 50 μM $[Cu(bipy)_2]^+$ and 50 μM H_2O_2.[a]

Gel lane	[ebit], μM	% Supercoiled	% Nicked	% Damage Inhibition	*p* Value
1: plasmid DNA (p)	0	97.52 ± 1.01	2.48 ± 1.01	–	–
2: p + H_2O_2	0	94.78 ± 1.89	5.22 ± 1.89	–	–
3: p + ebit + H_2O_2	100	95.36 ± 0.28	4.64 ± 0.28	–	–
4: p + $[Cu(bipy)_2]^+$ + H_2O_2	0	11.27 ± 7.72	88.73 ± 7.72	0	–
5: p + $[Cu(bipy)_2]^+$ + H_2O_2 + ebit	0.1	15.01 ± 6.04	84.99 ± 6.04	4.38 ± 1.78	0.051
6	1	20.85 ± 11.79	79.15 ± 11.79	11.80 ± 6.53	0.089
7	10	24.61 ± 6.40	75.39 ± 6.40	15.96 ± 2.03	0.005
8	25	23.65 ± 3.22	76.34 ± 3.22	11.93 ± 4.02	0.036
9	50	22.08 ± 8.31	77.92 ± 8.31	13.01 ± 2.21	0.009
10	75	28.55 ± 0.06	71.45 ± 0.06	18.04 ± 0.08	< 0.001
11	100	26.82 ± 5.89	73.18 ± 5.89	18.58 ± 0.83	< 0.001

[a]Data are reported as the average of three trials with calculated standard deviations shown.

Table 4.28. Gel electrophoresis results for methimazole (MetIm) DNA damage assays with 50 μM $[Cu(bipy)_2]^+$ and 50 μM H_2O_2.[a]

Gel lane	[MetIm], μM	% Supercoiled	% Nicked	% Damage Inhibition	*p* Value
1: plasmid DNA (p)	0	94.9 ± 1.0	5.1 ± 1.0	–	–
2: p + H_2O_2	0	94.1 ± 0.5	5.9 ± 0.5	–	–
3: p + MetIm + H_2O_2	2000	94.6 ± 1.0	5.4 ± 1.0	–	–
4: p + $[Cu(bipy)_2]^+$ + H_2O_2	0	3.8 ± 3.9	96.2 ± 3.9	0	–
5: p + $[Cu(bipy)_2]^+$ + H_2O_2 + MetIm	0.1	1.6 ± 0.5	98.4 ± 0.5	-2.57 ± 4.07	0.388
6	1	4.4 ± 2.9	95.6 ± 2.9	0.64 ± 2.16	0.659
7	2	2.5 ± 2.6	97.5 ± 2.6	-1.47 ± 1.51	0.234
8	5	4.9 ± 4.0	95.1 ± 4.0	1.22 ± 2.45	0.479
9	10	4.1 ± 3.0	95.8 ± 3.0	0.29 ± 3.98	0.911
10	50	6.9 ± 1.1	93.1 ± 1.1	3.39 ± 3.30	0.217
11	100	4.9 ± 3.4	95.1 ± 3.4	1.16 ± 3.77	0.647
12	500	1.7 ± 0.2	98.3 ± 0.2	-2.44 ± 4.31	0.430
13	1000	3.5 ± 2.7	96.5 ± 2.7	-0.56 ± 6.97	0.902
14	2000	4.6 ± 3.3	95.4 ± 3.3	0.73 ± 7.09	0.875

[a]Data are reported as the average of three trials with calculated standard deviations shown.

Table 4.29. Gel electrophoresis results for (2-mercapto-1-methylimidazolyl)pyridine thione (mpy^{Me}) DNA damage assays with 50 μM $[Cu(bipy)_2]^+$ and 50 μM H_2O_2.[a]

Gel lane	[mpy^{Me}], μM	% Supercoiled	% Nicked	% Damage Inhibition	*p* Value
1: plasmid DNA (p)	0	97.16 ± 1.67	2.84 ± 1.67	–	–
2: p + H_2O_2	0	96.93 ± 1.57	3.07 ± 1.57	–	–
3: p + mpy^{Me} + H_2O_2	1000	96.87 ± 1.48	3.13 ± 1.48	–	–
4: p + $[Cu(bipy)_2]^+$ + H_2O_2	0	8.46 ± 1.22	91.54 ± 1.22	0	–
5: p + $[Cu(bipy)_2]^+$ + H_2O_2 + mpy^{Me}	0.1	3.81 ± 1.38	96.19 ± 1.38	-5.28 ± 1.60	0.029
6	1	4.21 ± 1.83	95.79 ± 1.83	-4.82 ± 1.69	0.039
7	5	1.9 ± 1.0	98.0 ± 1.0	1.61 ± 1.09	0.125
8	10	11.99 ± 0.37	88.01 ± 0.37	3.99 ± 1.26	0.032
9	50	0.36 ± 0.57	99.64 ± 0.57	2.70 ± 4.56	0.413
10	100	16.41 ± 1.16	83.59 ± 1.16	8.96 ± 2.15	0.019
11	500	38.96 ± 0.52	61.04 ± 0.52	41.79 ± 0.56	< 0.001
13	1000	63.97 ± 2.38	36.03 ± 2.38	62.72 ± 1.86	< 0.001

[a]Data are reported as the average of three trials with calculated standard deviations shown.

Table 4.30. Gel electrophoresis results for 1,3,5-triaza-7-phosphaadmantane sulfide (PTAS) DNA damage assays with 50 μM $[Cu(bipy)_2]^+$ and 50 μM H_2O_2.[a]

Gel lane	[PTAS], μM	% Supercoiled	% Nicked	% Damage Inhibition	*p* Value
1: plasmid DNA (p)	0	95.47 ± 0.81	4.53 ± 0.81	–	–
2: p + H_2O_2	0	95.45 ± 0.53	4.55 ± 0.53	–	–
3: p + PTAS + H_2O_2	2000	95.90 ± 0.85	4.10 ± 0.85	–	–
4: p + $[Cu(bipy)_2]^+$ + H_2O_2	0	8.62 ± 1.87	91.38 ± 1.87	0	–
5: p + $[Cu(bipy)_2]^+$ + H_2O_2 + PTAS	0.01	4.21 ± 3.30	95.79 ± 3.30	1.70 ± 3.54	0.493
6	0.1	7.44 ± 2.63	92.56 ± 2.63	-1.39 ± 3.92	0.602
7	1	8.08 ± 2.83	91.92 ± 2.83	-0.64 ± 3.82	0.799
8	10	5.48 ± 2.79	94.52 ± 2.79	-3.60 ± 1.23	0.037
9	50	6.00 ± 3.79	94.00 ± 3.79	5.63 ± 2.99	0.082
10	100	16.99 ± 10.39	83.01 ± 10.39	9.69 ± 10.96	0.265
11	1000	19.83 ± 2.91	80.17 ± 2.91	12.87 ± 4.39	0.037
12	2000	20.33 ± 2.95	79.67 ± 2.95	18.97 ± 3.16	0.009

[a]Data are reported as the average of three trials with calculated standard deviations shown.

Table 4.31. Gel electrophoresis results for (2-mercapto-1-methylimidazolyl) pyridine selone ($sepy^{Me}$) DNA damage assays with 50 µM $[Cu(bipy)_2]^+$ and 50 µM H_2O_2.[a]

Gel lane	[$sepy^{Me}$], µM	% Supercoiled	% Nicked	% Damage Inhibition	*p* Value
1: plasmid DNA (p)	0	97.56 ± 1.57	2.44 ± 1.57	–	–
2: p + H_2O_2	0	97.69 ± 1.80	2.31 ± 1.80	–	–
3: p + $sepy^{Me}$ + H_2O_2	1000	96.39 ± 0.52	3.61 ± 0.52	–	–
4: p + $[Cu(bipy)_2]^+$ + H_2O_2	0	9.14 ± 1.43	90.86 ± 1.43	0	–
5: p + $[Cu(bipy)_2]^+$ + H_2O_2 + $sepy^{Me}$	0.1	7.99 ± 1.49	92.01 ± 1.49	-1.31 ± 0.92	0.132
6	1	7.84 ± 1.53	92.16 ± 1.53	-1.48 ± 1.00	0.124
7	10	41.74 ± 2.54	58.26 ± 2.54	36.80 ± 2.19	0.001
8	100	91.89 ± 1.96	8.11 ± 1.96	93.46 ± 1.38	< 0.001
9	1000	96.79 ± 2.33	3.21 ± 2.33	98.97 ± 0.65	< 0.001

[a]Data are reported as the average of three trials with calculated standard deviations shown.

Table 4.32. Gel electrophoresis results for ethyl-bis(imidazole) selone (ebis) DNA damage assays with 50 µM $[Cu(bipy)_2]^+$ and 50 µM H_2O_2.[a]

Gel lane	[ebis], µM	% Supercoiled	% Nicked	% Damage Inhibition	*p* Value
1: plasmid DNA (p)	0	99.13 ± 1.05	0.87 ± 1.05	–	–
2: p + H_2O_2	0	99.67 ± 0.23	0.33 ± 0.23	–	–
3: p + ebis + H_2O_2	100	99.24 ± 0.84	0.76 ± 0.84	–	–
4: p + $[Cu(bipy)_2]^+$ + H_2O_2	0	1.30 ± 1.72	98.70 ± 1.72	0	–
5: p + $[Cu(bipy)_2]^+$ + H_2O_2 + ebis	0.1	1.61 ± 1.61	98.39 ± 1.61	0.31 ± 0.47	0.372
6	1	0.23 ± 0.29	99.77 ± 0.29	-1.12 ± 1.91	0.417
7	10	10.68 ± 11.30	89.32 ± 11.30	9.51 ± 11.73	0.295
8	50	39.78 ± 2.93	60.22 ± 2.93	39.24 ± 3.54	0.003
9	100	56.34 ± 2.08	43.66 ± 2.08	56.15 ± 2.43	< 0.001

[a]Data are reported as the average of three trials with calculated standard deviations shown.

Table 4.33. Gel electrophoresis results for 1,3,5-triaza-7-phosphaadmantane selenide (PTASe) DNA damage assays with 50 µM $[Cu(bipy)_2]^+$ and 50 µM H_2O_2.[a]

Gel lane	[PTASe], µM	% Supercoiled	% Nicked	% Damage Inhibition	*p* Value
1: plasmid DNA (p)	0	95.91 ± 0.20	4.09 ± 0.20	–	–
2: p + H_2O_2	0	95.75 ± 0.95	4.25 ± 0.95	–	–
3: p + H_2O_2 + PTASe	1000	93.46 ± 1.53	6.54 ± 1.53	–	–
4: p + Cu^+ + H_2O_2	0	8.26 ± 1.46	91.74 ± 1.46	0	–
5: p + Cu^+ + H_2O_2 + PTASe	0.01	2.88 ± 2.41	97.12 ± 2.41	0.67 ± 2.73	0.712
6	0.1	8.24 ± 1.34	91.76 ± 1.34	-0.03 ± 0.44	0.917
7	1	7.19 ± 4.37	92.81 ± 4.37	-1.22 ± 3.34	0.592
8	10	6.24 ± 4.78	93.76 ± 4.78	-2.29 ± 3.81	0.410
9	50	2.82 ± 2.42	97.18 ± 2.42	2.16 ± 0.77	0.040
10	100	5.05 ± 3.25	94.95 ± 3.25	-3.65 ± 2.02	0.089
11	1000	5.90 ± 2.43	94.10 ± 2.43	-2.72 ± 4.10	0.369
12	2000	4.36 ± 1.40	95.64 ± 1.40	2.35 ± 1.59	0.125

[a]Data are reported as the average of three trials with calculated standard deviations shown.

Table 4.34. Gel electrophoresis results for ergothioneine (ESH) DNA damage assays with 400 µM $[Fe(EDTA)]^{2-}$ and 50 µM H_2O_2.[a]

Gel lane	[ESH], µM	% Supercoiled	% Nicked	% Damage Inhibition	*p* Value
1: plasmid DNA (p)	0	91.78 ± 1.13	8.22 ± 1.13	–	–
2: p + H_2O_2	0	89.95 ± 1.94	10.05 ± 1.94	–	–
3: p + ESH + H_2O_2	2000	91.71 ± 1.15	8.29 ± 1.15	–	–
4: p + $[Fe(EDTA)]^{2-}$ + H_2O_2	0	16.44 ± 4.06	83.56 ± 4.06	0	–
5: p + $[Fe(EDTA)]^{2-}$ + H_2O_2 + ESH	0.1	16.23 ± 2.39	83.77 ± 2.39	-0.35 ± 2.46	0.828
6	1	17.64 ± 3.51	82.36 ± 3.51	1.60 ± 0.67	0.054
7	2	20.89 ± 4.14	79.11 ± 4.14	6.05 ± 0.56	0.003
8	5	19.85 ± 3.60	80.15 ± 3.60	4.63 ± 0.73	0.008
9	10	21.68 ± 1.39	78.32 ± 1.39	7.01 ± 3.27	0.065
10	50	25.05 ± 5.23	74.95 ± 5.23	11.79 ± 2.35	0.013
11	100	30.52 ± 0.76	69.48 ± 0.76	19.05 ± 3.66	0.012
12	500	60.49 ± 2.36	39.51 ± 2.36	59.82 ± 2.97	< 0.001
13	1000	67.73 ± 2.62	32.27 ± 2.62	69.72 ± 1.59	< 0.001
14	2000	71.46 ± 2.32	28.54 ± 2.32	74.82 ± 1.04	< 0.001

[a]Data are reported as the average of three trials with calculated standard deviations shown.

Table 4.35. Gel electrophoresis results for 2-mercaptoimidazole (2-MerIm) DNA damage assays with 400 μM $[Fe(EDTA)]^{2-}$ and 50 μM H_2O_2.[a]

Gel lane	[2-MerIm], μM	% Supercoiled	% Nicked	% Damage Inhibition	*p* Value
1: plasmid DNA (p)	0	95.0 ± 1.4	5.0 ± 1.4	–	–
2: p + H_2O_2	0	94.4 ± 0.7	5.6 ± 0.7	–	–
3: p + 2-MerIm + H_2O_2	1000	94.6 ± 0.4	5.4 ± 0.4	–	–
4: p + $[Fe(EDTA)]^{2-}$ + H_2O_2	0	17.1 ± 1.9	82.9 ± 1.9	0	–
5: p + $[Fe(EDTA)]^{2-}$ + H_2O_2 + 2-MerIm	0.1	20.7 ± 3.2	79.3 ± 3.2	4.72 ± 2.90	0.106
6	1	26.8 ± 0.5	73.2 ± 0.5	12.58 ± 1.59	0.005
7	10	34.0 ± 7.5	66.0 ± 7.5	21.75 ± 11.29	0.079
8	100	51.5 ± 2.5	48.5 ± 2.5	44.54 ± 2.19	< 0.001
9	1000	87.8 ± 0.2	12.2 ± 0.2	91.49 ± 0.99	< 0.001

[a]Data are reported as the average of three trials with calculated standard deviations shown.

Table 4.36. Gel electrophoresis results for ethyl-bis(imidazole) thione (ebit) DNA damage assays with 400 μM $[Fe(EDTA)]^{2-}$ and 50 μM H_2O_2.[a]

Gel lane	[ebit], μM	% Supercoiled	% Nicked	% Damage Inhibition	*p* Value
1: plasmid DNA (p)	0	97.78 ± 0.12	2.22 ± 0.12	–	–
2: p + H_2O_2	0	97.61 ± 2.11	2.39 ± 2.11	–	–
3: p + ebit + H_2O_2	100	96.84 ± 0.09	3.16 ± 0.09	–	–
4: p + $[Fe(EDTA)]^{2-}$ + H_2O_2	0	19.02 ± 2.63	80.98 ± 2.63	0	–
5: p + $[Fe(EDTA)]^{2-}$ + H_2O_2 + ebit	0.1	23.17 ± 3.18	76.83 ± 3.18	5.32 ± 1.53	0.026
6	1	28.39 ± 3.85	71.61 ± 3.85	11.94 ± 2.88	0.019
7	10	31.63 ± 1.35	68.37 ± 1.35	16.02 ± 0.76	< 0.001
8	25	40.35 ± 0.64	59.65 ± 0.64	21.26 ± 0.09	< 0.001
9	50	39.69 ± 2.13	60.31 ± 2.13	26.30 ± 1.04	< 0.001
10	75	45.70 ± 1.58	54.30 ± 1.58	28.59 ± 2.16	0.002
11	100	46.74 ± 2.38	53.26 ± 2.38	35.34 ± 2.44	0.001

[a]Data are reported as the average of three trials with calculated standard deviations shown.

Table 4.37. Gel electrophoresis results for methimazole (MetIm) DNA damage assays with 400 µM $[Fe(EDTA)]^{2-}$ and 50 µM H_2O_2.[a]

Gel lane	[MetIm], µM	% Supercoiled	% Nicked	% Damage Inhibition	*p* Value
1: plasmid DNA (p)	0	93.76 ± 0.32	6.24 ± 0.32	–	–
2: p + H_2O_2	0	85.41 ± 2.81	14.59 ± 2.81	–	–
3: p + MetIm + H_2O_2	2000	93.93 ± 0.97	6.07 ± 0.97	–	–
4: p + $[Fe(EDTA)]^{2-}$ + H_2O_2	0	22.99 ± 1.31	77.01 ± 1.31	0	–
5: p + $[Fe(EDTA)]^{2-}$ + H_2O_2 + MetIm	0.1	23.40 ± 2.63	76.60 ± 2.63	0.70 ± 3.17	0.739
6	1	25.34 ± 2.76	74.66 ± 2.76	3.86 ± 4.60	0.283
7	2	34.12 ± 0.71	65.88 ± 0.71	18.22 ± 0.97	< 0.001
8	5	40.05 ± 1.98	59.95 ± 1.98	26.31 ± 2.70	0.005
9	10	47.87 ± 0.70	52.13 ± 0.70	39.91 ± 3.50	0.002
10	50	54.62 ± 2.83	45.38 ± 2.83	46.18 ± 3.86	0.002
11	100	61.15 ± 1.25	38.85 ± 1.25	61.18 ± 3.95	0.001
12	500	79.90 ± 0.65	20.05 ± 0.65	80.73 ± 0.89	< 0.001
13	1000	82.05 ± 2.59	17.95 ± 2.59	94.63 ± 2.38	< 0.001
14	2000	91.69 ± 1.47	8.31 ± 1.47	96.74 ± 2.00	< 0.001

[a]Data are reported as the average of three trials with calculated standard deviations shown.

Table 4.38. Gel electrophoresis results for (2-mercapto-1-methylimidazolyl)pyridine thione (mpy^{Me}) DNA damage assays with 400 µM $[Fe(EDTA)]^{2-}$ and 50 µM H_2O_2.[a]

Gel lane	[mpy^{Me}], µM	% Supercoiled	% Nicked	% Damage Inhibition	*p* Value
1: plasmid DNA (p)	0	95.86 ± 1.98	4.14 ± 1.98	–	–
2: p + H_2O_2	0	93.77 ± 2.65	6.23 ± 2.65	–	–
3: p + mpy^{Me} + H_2O_2	1000	96.63 ± 1.89	3.37 ± 1.89	–	–
4: p + $[Fe(EDTA)]^{2-}$ + H_2O_2	0	12.40 ± 2.37	87.60 ± 2.37	0	–
5: p + $[Fe(EDTA)]^{2-}$ + H_2O_2 + mpy^{Me}	0.1	14.38 ± 1.14	85.62 ± 1.14	2.38 ± 1.47	0.107
6	1	16.93 ± 1.66	83.07 ± 1.66	5.53 ± 1.34	0.019
7	10	24.05 ± 1.28	75.95 ± 1.28	14.17 ± 3.72	0.022
8	100	41.70 ± 1.87	58.30 ± 1.87	36.07 ± 1.69	< 0.001
9	1000	90.49 ± 0.71	9.51 ± 0.71	96.05 ± 2.20	< 0.001

[a]Data are reported as the average of three trials with calculated standard deviations shown.

Table 4.39. Gel electrophoresis results for 1,3,5-triaza-7-phosphaadmantane sulfide (PTAS) DNA damage assays with 400 μM $[Fe(EDTA)]^{2-}$ and 50 μM H_2O_2.[a]

Gel lane	[PTAS], μM	% Supercoiled	% Nicked	% Damage Inhibition	*p* Value
1: plasmid DNA (p)	0	94.90 ± 0.23	5.10 ± 0.23	–	–
2: p + H_2O_2	0	91.67 ± 1.29	8.33 ± 1.29	–	–
3: p + PTAS + H_2O_2	2000	91.60 ± 0.45	8.40 ± 0.45	–	–
4: p + $[Fe(EDTA)]^{2-}$ + H_2O_2	0	25.33 ± 1.54	74.67 ± 1.54	0	–
5: p + $[Fe(EDTA)]^{2-}$ + H_2O_2 + PTAS	0.01	18.46 ± 1.89	81.53 ± 1.89	-0.71 ± 2.54	0.676
6	0.1	25.63 ± 2.27	74.37 ± 2.27	0.48 ± 1.13	0.538
7	1	28.39 ± 2.24	71.61 ± 2.24	4.63 ± 1.29	0.025
8	10	32.29 ± 2.08	67.71 ± 2.08	10.52 ± 1.12	0.004
9	50	36.14 ± 0.85	63.86 ± 0.85	23.08 ± 1.15	< 0.001
10	100	36.82 ± 0.69	63.18 ± 0.69	17.27 ± 2.36	0.006
11	1000	33.68 ± 1.31	66.32 ± 1.31	12.53 ± 2.46	0.013
12	2000	9.67 ± 2.37	90.33 ± 2.37	-12.56 ± 3.19	0.021

[a]Data are reported as the average of three trials with calculated standard deviations shown.

Table 4.40. Gel electrophoresis results for (2-mercapto-1-methylimidazolyl)pyridine selone ($sepy^{Me}$) DNA damage assays with 400 μM $[Fe(EDTA)]^{2-}$ and 50 μM H_2O_2.[a]

Gel lane #	[$sepy^{Me}$], μM	% Supercoiled	% Nicked	% Damage Inhibition	*p* Value
1: plasmid DNA (p)	0	96.75 ± 1.26	3.25 ± 1.26	–	–
2: p + H_2O_2	0	92.68 ± 0.54	7.32 ± 0.54	–	–
3: p + $sepy^{Me}$ + H_2O_2	1000	97.27 ± 0.57	2.73 ± 0.57	–	–
4: p + $[Fe(EDTA)]^{2-}$ + H_2O_2	0	12.74 ± 0.86	87.26 ± 0.86	0	–
5: p + $[Fe(EDTA)]^{2-}$ + H_2O_2 + $sepy^{Me}$	0.1	13.95 ± 1.83	86.05 ± 1.83	-1.31 ± 0.92	0.132
6	1	20.17 ± 1.56	79.83 ± 1.56	-1.48 ± 1.00	0.124
7	10	72.21 ± 1.17	27.79 ± 1.17	36.80 ± 2.19	0.001
8	100	89.73 ± 1.70	10.27 ± 1.70	93.46 ± 1.38	< 0.001
9	1000	91.24 ± 1.77	8.76 ± 1.77	99.00 ± 0.65	< 0.001

[a]Data are reported as the average of three trials with calculated standard deviations shown.

Table 4.41. Gel electrophoresis results for ethyl-bis(imidazole) selone (ebis) DNA damage assays with 400 μM $[Fe(EDTA)]^{2-}$ and 50 μM H_2O_2.[a]

Gel lane	[ebis], μM	% Supercoiled	% Nicked	% Damage Inhibition	*p* Value
1: plasmid DNA (p)	0	98.06 ± 1.79	1.94 ± 1.79	–	–
2: p + H_2O_2	0	96.57 ± 1.15	3.43 ± 1.15	–	–
3: p + ebis + H_2O_2	100	98.19 ± 1.00	1.81 ± 1.00	–	–
4: p + $[Fe(EDTA)]^{2-}$ + H_2O_2	0	3.71 ± 2.17	96.29 ± 2.17	0	–
5: p + $[Fe(EDTA)]^{2-}$ + H_2O_2 + ebis	0.1	4.73 ± 1.37	95.27 ± 1.37	1.05 ± 3.50	0.520
6	1	7.36 ± 0.75	92.64 ± 0.75	3.84 ± 3.04	0.160
7	10	8.89 ± 1.98	91.11 ± 1.98	5.48 ± 1.12	0.014
8	25	22.22 ± 1.76	77.78 ± 1.76	9.84 ± 2.19	0.016
9	50	14.57 ± 1.75	85.43 ± 1.75	11.48 ± 3.13	0.024
10	75	25.65 ± 2.82	74.35 ± 2.82	14.11 ± 3.50	0.020
11	100	17.26 ± 3.42	82.74 ± 3.42	14.31 ± 5.31	0.043

[a]Data are reported as the average of three trials with calculated standard deviations shown.

Table 4.42. Gel electrophoresis results for 1,3,5-triaza-7-phosphaadmantane selenide (PTASe) DNA damage assays with 400 μM $[Fe(EDTA)]^{2-}$ and 50 μM H_2O_2.[a]

Gel lane	[PTASe], μM	% Supercoiled	% Nicked	% Damage Inhibition	*p* Value
1: plasmid DNA (p)	0	95.97 ± 0.32	4.03 ± 0.32	–	–
2: p + H_2O_2	0	91.98 ± 1.93	8.02 ± 1.93	–	–
3: p + PTASe + H_2O_2	1000	95.27 ± 0.86	4.73 ± 0.86	–	–
4: p + $[Fe(EDTA)]^{2-}$ + H_2O_2	0	22.29 ± 1.90	77.71 ± 1.90	0	–
5: p + $[Fe(EDTA)]^{2-}$ + H_2O_2 + PTASe	0.01	18.46 ± 1.89	81.53 ± 1.89	-0.71 ± 2.54	0.676
6	0.1	20.73 ± 1.98	79.27 ± 1.98	-2.23 ± 3.42	0.376
7	1	31.74 ± 2.45	68.26 ± 2.45	13.46 ± 3.82	0.026
8	10	37.21 ± 0.79	62.79 ± 0.79	21.35 ± 2.90	0.006
9	50	36.14 ± 0.85	63.86 ± 0.85	23.08 ± 1.15	< 0.001
10	100	51.28 ± 1.10	48.72 ± 1.10	41.61 ± 1.22	< 0.001
11	1000	62.03 ± 1.96	37.97 ± 1.96	57.04 ± 1.27	< 0.001
12	2000	9.67 ± 2.37	90.33 ± 2.37	-12.56 ± 3.19	0.021

[a]Data are reported as the average of three trials with calculated standard deviations shown.

Table 4.43. Gel electrophoresis results for ergothioneine (ESH) DNA damage assays with 1450 μM $ONOO^-$.[a]

Gel lane	[ESH], μM	% Supercoiled	% Nicked	% Damage Inhibition	*p* Value
1: plasmid DNA (p)	0	91.91 ± 0.22	8.09 ± 0.22	–	–
2: p + Na_2NO_2	0	91.17 ± 0.35	8.83 ± 0.35	–	–
3: p + KNO_3	0	91.33 ± 1.21	8.67 ± 1.21	–	–
4: p + ESH	1000	90.59 ± 0.95	9.41 ± 0.95	–	–
5: p + $ONOO^-$	0	25.31 ± 5.37	74.69 ± 5.37	0	–
6: p + $ONOO^-$ + ESH	0.1	24.57 ± 2.60	75.43 ± 2.60	-1.36 ± 4.81	0.673
7	1	24.58 ± 1.68	75.42 ± 1.68	-1.41 ± 6.08	0.727
8	5	25.49 ± 3.48	74.51 ± 3.48	0.13 ± 2.89	0.945
9	10	26.02 ± 5.79	73.98 ± 5.79	1.12 ± 0.72	0.114
10	25	30.85 ± 5.14	69.15 ± 5.14	8.43 ± 0.37	< 0.001
11	50	31.66 ± 5.98	68.34 ± 5.98	9.71 ± 1.81	0.011
12	100	40.95 ± 4.50	59.05 ± 4.50	23.76 ± 0.66	< 0.001
13	250	44.84 ± 1.57	55.16 ± 1.57	29.48 ± 3.63	0.005
14	500	54.04 ± 3.57	45.96 ± 3.57	43.63 ± 1.78	< 0.001
15	750	68.03 ± 1.78	31.97 ± 1.78	64.05 ± 2.34	< 0.001
16	1000	75.89 ± 2.73	24.11 ± 2.73	76.50 ± 6.08	0.002
17	2000	93.22 ± 1.41	6.77 ± 1.41	97.21 ± 1.85	< 0.001

[a]Data are reported as the average of three trials with calculated standard deviations shown.

Table 4.44. Gel electrophoresis results for 2-mercaptoimidazole (2-MerIm) DNA damage assays with 1450 μM $ONOO^-$.[a]

Gel lane	[2-MerIm], μM	% Supercoiled	% Nicked	% Damage Inhibition	*p* Value
1: plasmid DNA (p)	0	94.0 ± 2.0	6.0 ± 2.0	–	–
2: p + Na_2NO_2	0	93.1 ± 1.3	6.9 ± 1.3	–	–
3: p + KNO_3	0	92.6 ± 1.0	7.4 ± 1.0	–	–
4: p + ESH	2000	91.8 ± 0.6	8.2 ± 0.6	–	–
5: p + $ONOO^-$	0	27.4 ± 0.5	72.6 ± 0.5	0	–
6: p + $ONOO^-$ + 2-MerIm	0.1	26.9 ± 0.4	73.1 ± 0.4	-0.74 ± 1.43	0.465
7	1	30.2 ± 1.1	69.8 ± 1.1	4.34 ± 1.55	0.039
8	2	28.8 ± 0.4	71.2 ± 0.4	2.19 ± 1.09	0.073
9	5	34.4 ± 6.9	65.6 ± 6.9	10.54 ± 10.03	0.210
10	10	33.9 ± 1.4	66.1 ± 1.4	9.88 ± 1.48	0.007
11	50	35.4 ± 0.6	64.6 ± 0.6	12.15 ± 0.39	< 0.001
12	100	41.2 ± 1.8	58.8 ± 1.8	20.98 ± 3.34	0.008
13	500	59.2 ± 1.2	41.8 ± 1.2	46.89 ± 2.74	0.001
14	1000	85.5 ± 1.7	14.5 ± 1.7	88.39 ± 2.15	< 0.001
15	2000	86.6 ± 0.7	13.4 ± 0.7	90.12 ± 2.73	< 0.001

[a]Data are reported as the average of three trials with calculated standard deviations shown.

Table 4.45. Gel electrophoresis results for ethyl-bis(imidazole) thione (ebit) DNA damage assays with 1450 μM $ONOO^-$.[a]

Gel lane	[ebit], μM	% Supercoiled	% Nicked	% Damage Inhibition	*p* Value
1: plasmid DNA (p)	0	95.54 ± 0.83	4.46 ± 0.83	–	–
2: p + Na_2NO_2	0	94.84 ± 0.79	5.16 ± 0.79	–	–
3: p + KNO_3	0	95.24 ± 0.70	4.76 ± 0.70	–	–
4: p + ebit	100	95.99 ± 0.98	4.01 ± 0.98	–	–
5: p + $ONOO^-$	0	23.82 ± 2.66	76.18 ± 2.66	0	–
6: p + $ONOO^-$ + ebit	0.1	42.12 ± 19.30	57.88 ± 19.30	26.18 ± 25.89	0.222
7	1	36.81 ± 14.89	63.19 ± 14.89	18.37 ± 20.76	0.265
8	10	45.77 ± 3.71	54.23 ± 3.71	30.99 ± 2.98	0.003
9	50	49.25 ± 1.58	50.75 ± 1.58	35.81 ± 0.51	< 0.001
10	100	57.72 ± 4.43	42.28 ± 4.43	47.72 ± 6.27	0.006

[a]Data are reported as the average of three trials with calculated standard deviations shown.

Table 4.46. Gel electrophoresis results for methimazole (MetIm) DNA damage assays with 1450 μM $ONOO^-$.[a]

Gel lane	[MetIm], μM	% Supercoiled	% Nicked	% Damage Inhibition	*p* Value
1: plasmid DNA (p)	0	93.16 ± 0.77	6.84 ± 0.77	–	–
2: p + Na_2NO_2	0	93.10 ± 0.59	6.90 ± 0.59	–	–
3: p + KNO_3	0	92.62 ± 1.08	7.38 ± 1.08	–	–
4: p + MetIm	1000	91.06 ± 1.13	8.94 ± 1.13	–	–
5: p + $ONOO^-$	0	23.39 ± 1.18	76.61 ± 1.18	0	–
6: p + $ONOO^-$ + MetIm	0.1	24.13 ± 3.90	75.87 ± 3.90	0.99 ± 7.02	0.830
7	1	25.96 ± 2.05	74.04 ± 2.05	3.66 ± 4.38	0.285
8	5	30.76 ± 0.59	69.24 ± 0.59	10.57 ± 1.16	0.004
9	10	34.01 ± 5.99	65.99 ± 5.99	15.25 ± 7.61	0.074
10	25	38.76 ± 3.78	61.24 ± 3.78	21.98 ± 6.53	0.028
11	75	35.76 ± 1.70	64.24 ± 1.70	17.77 ± 1.51	0.002
12	100	35.89 ± 1.50	64.11 ± 1.50	17.92 ± 1.79	0.003
13	250	49.92 ± 2.77	50.08 ± 2.77	38.08 ± 2.76	0.002
14	500	61.71 ± 1.99	38.29 ± 1.99	54.99 ± 1.94	< 0.001
15	750	76.31 ± 1.66	23.69 ± 1.66	75.93 ± 2.04	< 0.001
16	1000	83.65 ± 1.45	16.35 ± 1.45	86.46 ± 2.58	< 0.001

[a]Data are reported as the average of three trials with calculated standard deviations shown.

Table 4.47. Gel electrophoresis results for (2-mercapto-1-methylimidazolyl)pyridine thione (mpy^{Me}) DNA damage assays with 1450 µM $ONOO^-$.[a]

Gel lane	[mpy^{Me}], µM	% Supercoiled	% Nicked	% Damage Inhibition	*p* Value
1: plasmid DNA (p)	0	92.85 ± 0.98	7.15 ± 0.98	–	–
2: p + Na_2NO_2	0	92.71 ± 1.73	7.29 ± 1.73	–	–
3: p + KNO_3	0	92.20 ± 2.64	7.80 ± 2.64	–	–
4: p + Mpy^{Me}	1000	92.97 ± 0.53	7.03 ± 0.53	–	–
5: p + $ONOO^-$	0	21.95 ± 3.67	78.05 ± 3.67	0	–
6: p + $ONOO^-$ + mpy^{Me}	0.1	26.84 ± 2.45	73.16 ± 2.45	6.73 ± 7.87	0.277
7	1	26.44 ± 3.32	73.56 ± 3.32	6.34 ± 0.31	< 0.001
8	10	40.17 ± 2.47	59.83 ± 2.47	25.69 ± 1.95	0.002
9	100	42.74 ± 3.08	57.26 ± 3.08	29.22 ± 5.45	0.011
10	1000	77.93 ± 2.23	22.07 ± 2.23	79.11 ± 0.54	< 0.001

[a]Data are reported as the average of three trials with calculated standard deviations shown.

Table 4.48. Gel electrophoresis results for 1,3,5-triaza-7-phosphaadmantane sulfide (PTAS) DNA damage assays with 1450 µM $ONOO^-$.[a]

Gel lane	[PTAS], µM	% Supercoiled	% Nicked	% Damage Inhibition	*p* Value
1: plasmid DNA (p)	0	94.63 ± 1.22	5.37 ± 1.22	–	–
2: p + Na_2NO_2	0	95.90 ± 0.84	4.10 ± 0.84	–	–
3: p + KNO_3	0	95.28 ± 1.42	4.72 ± 1.42	–	–
4: p + PTAS	1000	95.12 ± 0.89	4.88 ± 0.89	–	–
5: p + $ONOO^-$	0	28.13 ± 6.93	71.87 ± 6.93	0	–
6: p + $ONOO^-$ + PTAS	0.1	27.13 ± 7.69	72.87 ± 7.69	-1.44 ± 4.34	0.623
7	1	29.41 ± 7.68	70.59 ± 7.68	1.97 ± 1.40	0.135
8	10	32.53 ± 8.11	67.47 ± 8.11	6.65 ± 2.48	0.043
9	100	43.73 ± 4.83	56.27 ± 4.83	22.96 ± 1.07	< 0.001
10	1000	61.65 ± 2.92	38.35 ± 2.92	49.38 ± 1.80	< 0.001

[a]Data are reported as the average of three trials with calculated standard deviations shown.

Table 4.49. Gel electrophoresis results for (2-mercapto-1-methylimidazolyl)pyridine selone ($sepy^{Me}$) DNA damage assays with 1450 μM $ONOO^-$.[a]

Gel lane	[$sepy^{Me}$], μM	% Supercoiled	% Nicked	% Damage Inhibition	*p* Value
1: plasmid DNA (p)	0	92.30 ± 1.14	7.70 ± 1.14	–	–
2: p + Na_2NO_2	0	91.65 ± 2.33	8.35 ± 2.33	–	–
3: p + KNO_3	0	93.52 ± 1.04	6.48 ± 1.04	–	–
4: p + $sepy^{Me}$	1000	93.02 ± 1.01	6.98 ± 1.01	–	–
5: p + $ONOO^-$	0	22.85 ± 5.14	77.15 ± 5.14	0	–
6: p + $ONOO^-$ + $sepy^{Me}$	0.1	24.20 ± 3.38	75.80 ± 3.38	1.80 ± 2.32	0.311
7	1	24.39 ± 5.60	75.61 ± 5.60	2.27 ± 2.82	0.298
8	10	31.25 ± 3.22	68.75 ± 3.22	12.10 ± 2.18	0.011
9	100	63.59 ± 3.73	36.41 ± 3.73	59.47 ± 4.78	0.002
10	1000	86.48 ± 1.23	13.52 ± 1.23	92.56 ± 1.68	< 0.001

[a]Data are reported as the average of three trials with calculated standard deviations shown.

Table 4.50. Gel electrophoresis results for ethyl-bis(imidazole) selone (ebis) DNA damage assays with 1450 μM $ONOO^-$.[a]

Gel lane	[ebis], μM	% Supercoiled	% Nicked	% Damage Inhibition	*p* Value
1: plasmid DNA (p)	0	95.04 ± 1.67	4.96 ± 1.67	–	–
2: p + Na_2NO_2	0	95.85 ± 0.19	4.15 ± 0.19	–	–
3: p + KNO_3	0	95.05 ± 1.07	4.95 ± 1.07	–	–
4: p + ebis	100	94.93 ± 0.58	5.07 ± 0.58	–	–
5: p + $ONOO^-$	0	24.84 ± 2.99	75.16 ± 2.99	0	–
6: p + $ONOO^-$ + ebis	0.1	27.65 ± 6.95	72.35 ± 6.95	4.06 ± 7.03	0.422
7	1	26.95 ± 3.42	73.05 ± 3.42	2.99 ± 0.81	0.024
8	10	45.48 ± 4.82	54.52 ± 4.82	29.16 ± 3.66	0.005
9	50	50.92 ± 1.99	49.08 ± 1.99	36.68 ± 3.08	0.002
10	100	75.67 ± 2.40	24.33 ± 2.40	71.58 ± 3.22	< 0.001

[a]Data are reported as the average of three trials with calculated standard deviations shown.

Table 4.51. Gel electrophoresis results for 1,3,5-triaza-7-phosphaadmantane selenide (PTASe) DNA damage assays with 1450 μM $ONOO^-$.[a]

Gel lane	[PTASe], μM	% Supercoiled	% Nicked	% Damage Inhibition	*p* Value
1: plasmid DNA (p)	0	93.77 ± 1.22	6.23 ± 1.22	–	–
2: p + Na_2NO_2	0	95.20 ± 1.46	4.80 ± 1.46	–	–
3: p + KNO_3	0	94.43 ± 0.70	5.57 ± 0.70	–	–
4: p + PTASe	1000	93.99 ± 1.81	6.01 ± 1.81	–	–
5: p + $ONOO^-$	0	26.73 ± 2.77	73.27 ± 2.77	0	–
6: p + $ONOO^-$ + PTASe	0.1	25.60 ± 1.56	74.40 ± 1.56	-1.73 ± 2.06	0.283
7	1	28.60 ± 4.60	71.40 ± 4.60	2.84 ± 3.50	0.295
8	10	34.12 ± 3.90	65.88 ± 3.90	10.88 ± 3.64	0.036
9	100	58.26 ± 6.92	41.74 ± 6.92	45.63 ± 11.34	0.020
10	1000	81.01 ± 1.42	18.99 ± 1.42	79.23 ± 2.19	< 0.001

[a]Data are reported as the average of three trials with calculated standard deviations shown.

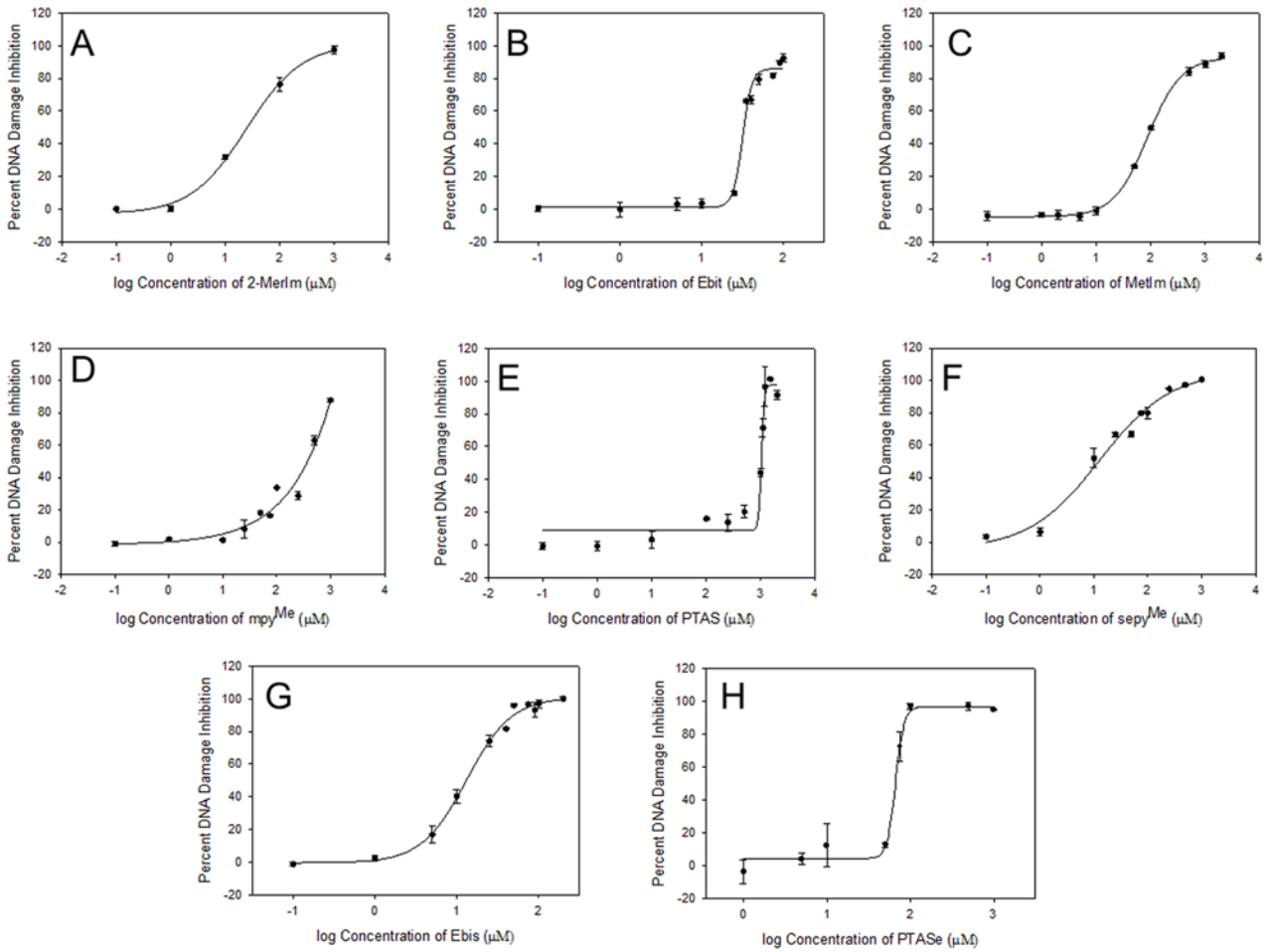

Figure 4.15. Dose-response curves for the prevention of Cu^{I}-mediated DNA damage by A) 2-mercaptoimidazole (2-MerIm), B) ethyl-bis(imidazole) thione (ebit), C) methimazole (MetIm), D) (2-mercapto-1-methyimidazolyl)pyridine thione (mpy^{Me}), E) 1,3,5-triaza-7-phospaadamantane sulfide (PTAS), F) (2-mercapto-1-methyimidazolyl)pyridine selone ($sepy^{Me}$), G) ethyl-bis(imidazole) selone (ebis), and H) 1,3,5-triaza-7-phospaadamantane selenide (PTASe).

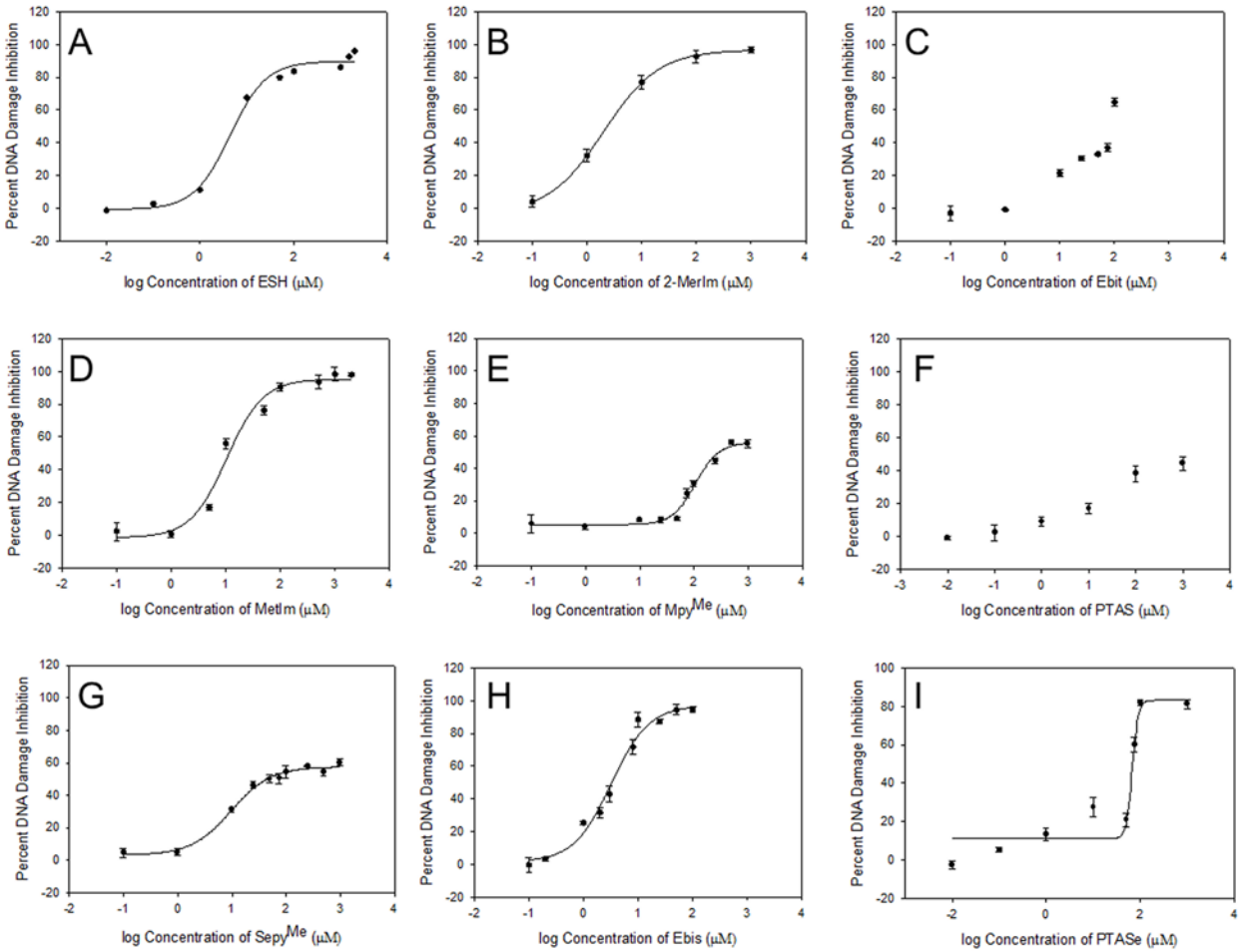

Figure 4.16. Dose-response curves for the prevention of Fe^{I}-mediated DNA damage by A) ergothioneine (ESH), B) 2-mercaptoimidazole (2-MerIm), C) ethyl-bis(imidazole) thione (ebit), D) methimazole (MetIm), E) (2-mercapto-1-methyimidazolyl)pyridine thione (mpy^{Me}), F) 1,3,5-triaza-7-phospaadamantane sulfide (PTAS), G) (2-mercapto-1-methyimidazolyl)pyridine selone ($sepy^{Me}$), H) ethyl-bis(imidazole) selone (ebis), and I) 1,3,5-triaza-7-phospaadamantane selenide (PTASe).

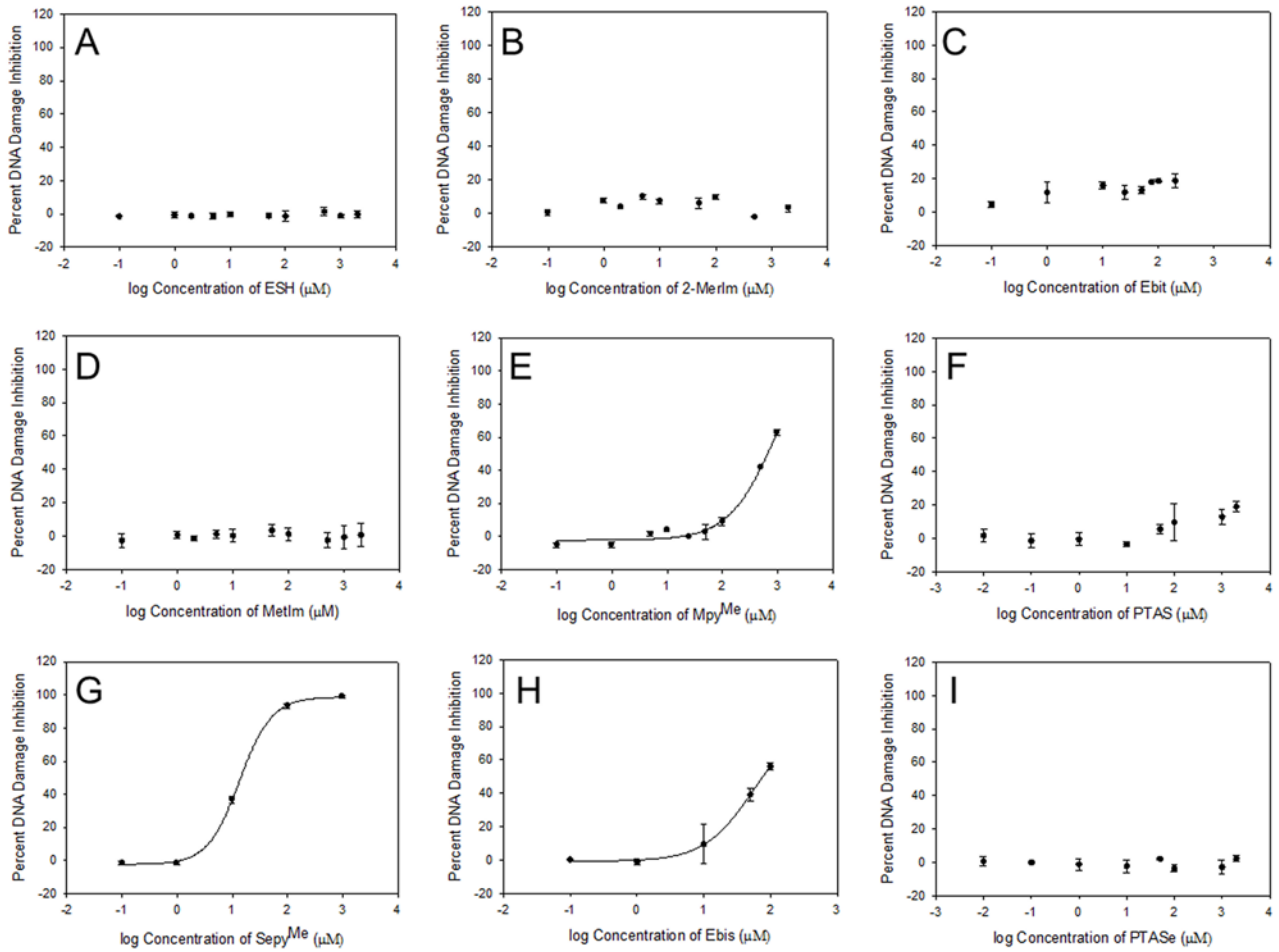

Figure 4.17. Dose-response curves for the prevention of $[Cu(bipy)_2]^+$-mediated DNA damage by A) ergothioneine (ESH), B) 2-mercaptoimidazole (2-MerIm), C) ethyl-bis(imidazole) thione (ebit), D) methimazole (MetIm), E) (2-mercapto-1-methyimidazolyl)pyridine thione (mpy^{Me}), F) 1,3,5-triaza-7-phospaadamantane sulfide (PTAS), G) (2-mercapto-1-methyimidazolyl)pyridine selone ($sepy^{Me}$), H) ethyl-bis(imidazole) selone (ebis), and I) 1,3,5-triaza-7-phospaadamantane selenide (PTASe).

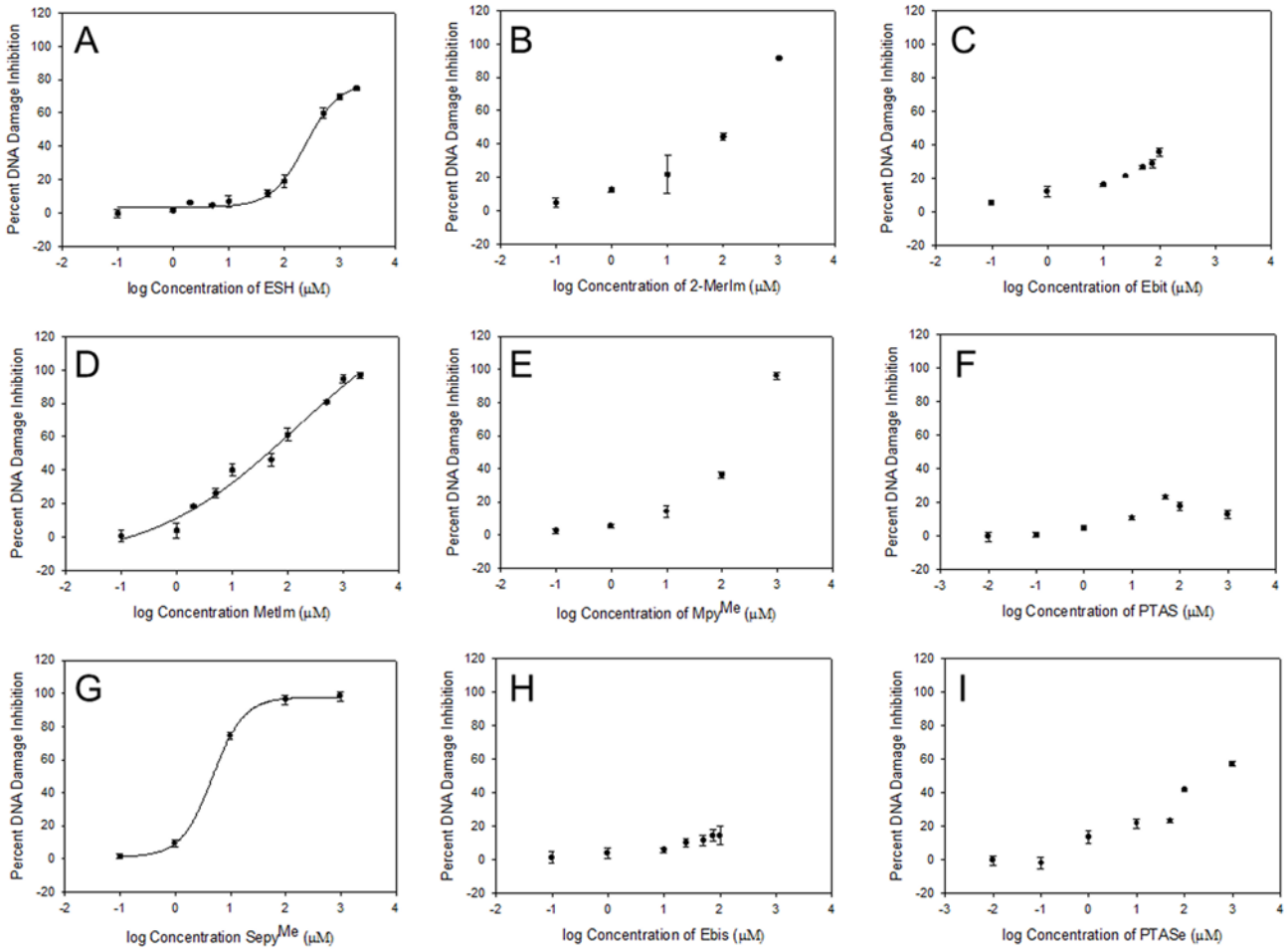

Figure 4.18. Dose-response curves for the prevention of $[Fe(EDTA)]^{2-}$-mediated DNA damage by A) ergothioneine (ESH), B) 2-mercaptoimidazole (2-MerIm), C) ethyl-bis(imidazole) thione (ebit), D) methimazole (MetIm), E) (2-mercapto-1-methyimidazolyl)pyridine thione (mpy^{Me}), F) 1,3,5-triaza-7-phospaadamantane sulfide (PTAS), G) (2-mercapto-1-methyimidazolyl)pyridine selone ($sepy^{Me}$), H) ethyl-bis(imidazole) selone (ebis), and I) 1,3,5-triaza-7-phospaadamantane selenide (PTASe).

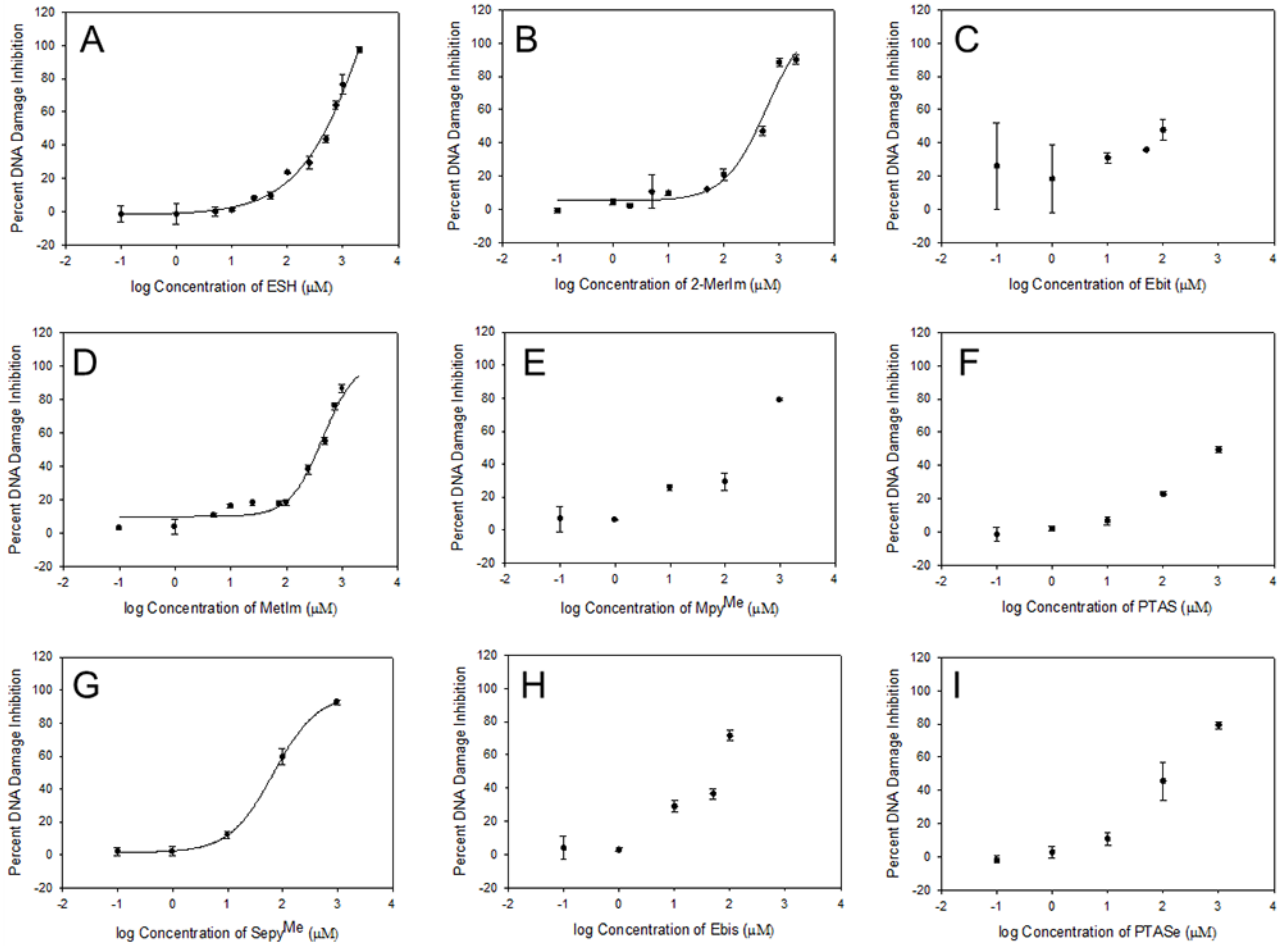

Figure 4.19. Dose-response curves for the prevention of peroxynitrite ($ONOO^-$)-mediated DNA damage by A) ergothioneine (ESH), B) 2-mercaptoimidazole (2-MerIm), C) ethyl-bis(imidazole) thione (ebit), D) methimazole (MetIm), E) (2-mercapto-1-methyimidazolyl)pyridine thione (mpy^{Me}), F) 1,3,5-triaza-7-phospaadamantane sulfide (PTAS), G) (2-mercapto-1-methyimidazolyl)pyridine selone ($sepy^{Me}$), H) ethyl-bis(imidazole) selone (ebis), and I) 1,3,5-triaza-7-phospaadamantane selenide (PTASe).

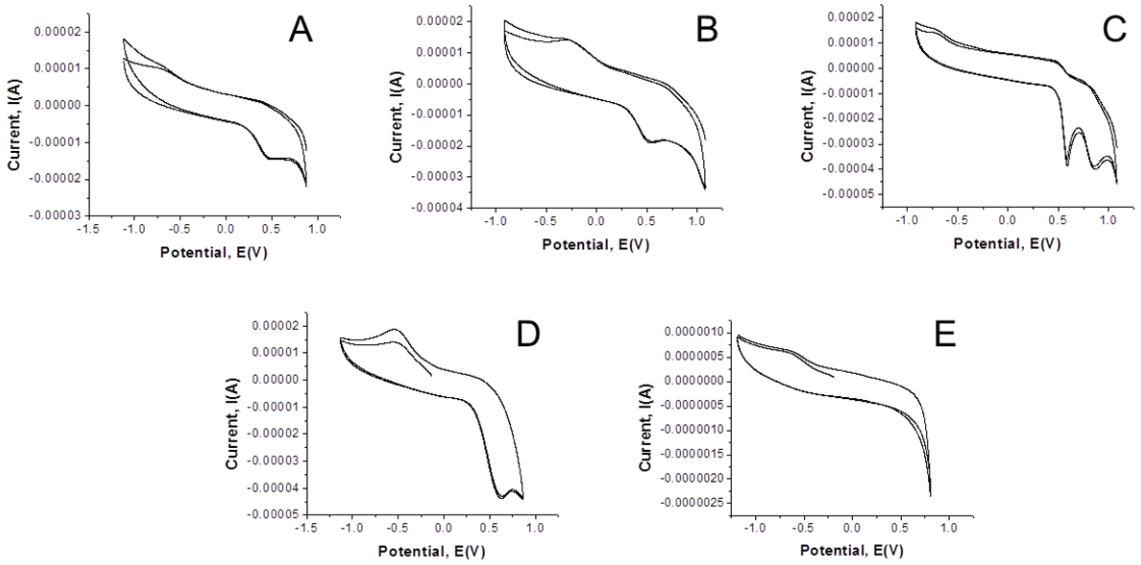

Figure 4.20. Cyclic voltammograms for A) ergothioneine, B) 2-mercaptoimazole, C) ethyl-bis(imidazole) thione, D) methimazole, and E)1,3,5-triaza-7-phosphaadamantane sulfide in MOPS buffer (10 mM, pH =7.0) containing KNO_3 (10 mM) as a supporting electrolyte. Compounds (1 mM) were cycled between -1000 mV and 1000 mV vs. NHE at a scan rate of 100 mV/s.

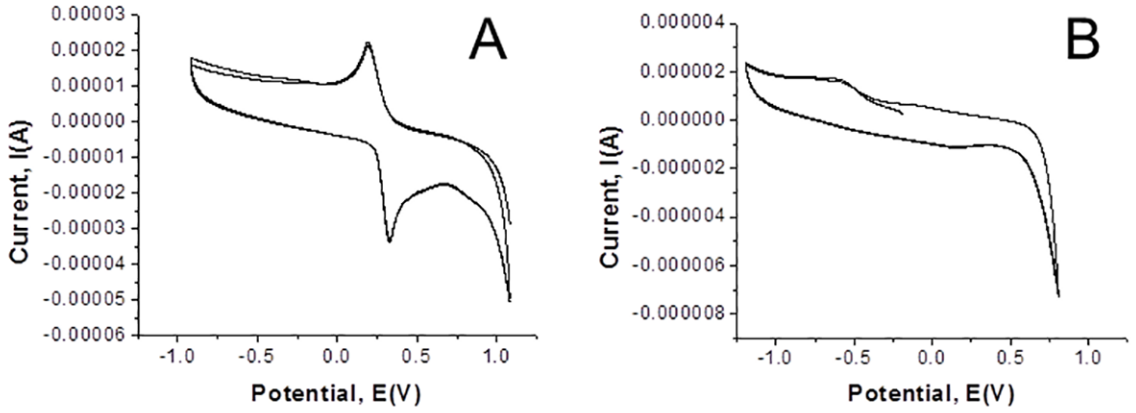

Figure 4.21. Cyclic voltammograms for A) ethyl-bis(imidazole) selone and B) 1,3,5-Triaza-7-phosphaadamantane sulfide in MOPS buffer (10 mM, pH =7.0) containing KNO_3 (10 mM) as a supporting electrolyte. Compounds (1 mM) were cycled between -1000 mV and 1000 mV vs. NHE at a scan rate of 100mV/s.

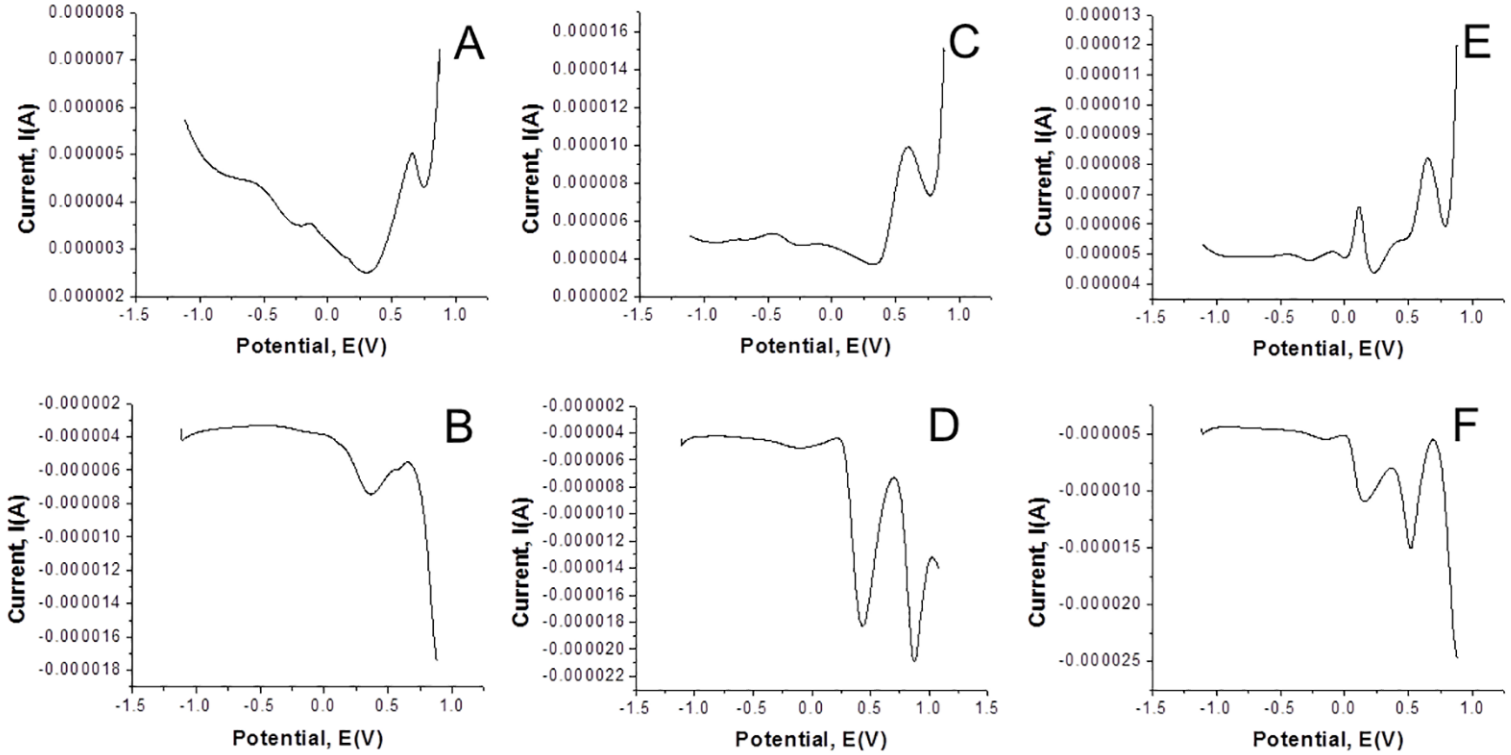

Figure 4.22. Differential pulse voltammetry scans for A) negative scan of ergothioneine, B) positive scan of ergothioneine, C) negative scan of (2-mercapto-1-methyimidazolyl)pyridine thione (Mpy^{Me}), D) positive scan of (2-mercapto-1-methyimidazolyl)pyridine thione (Mpy^{Me}), E) negative scan of (2-mercapto-1-methyimidazolyl)pyridine selone ($Sepy^{Me}$), and F) (2-mercapto-1-methyimidazolyl)pyridine selone ($Sepy^{Me}$) in MOPS buffer (10 mM, pH 7.0) containing KNO_3 (10 mM) as a supporting electrolyte. Compounds (1 mM) were cycled between -1000 mV and 1000 mV vs. NHE, a pulse width of 0.100, a sample width of 0.045, and a pulse period of 0.200 were used.

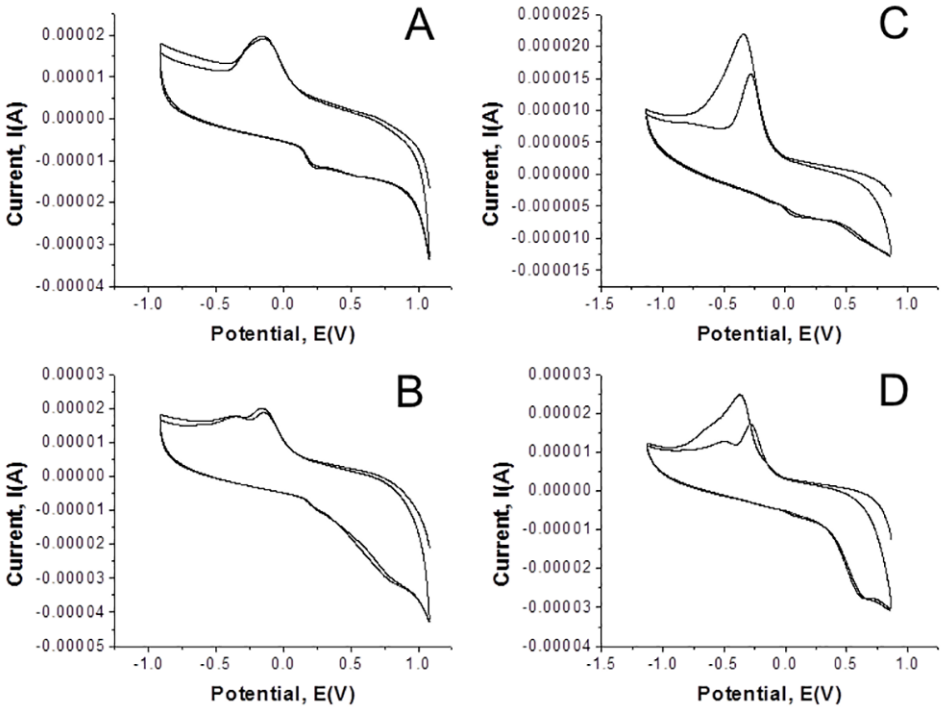

Figure 4.23. Cyclic voltammograms for A) 1:1 Fe:2-mercaptoimidazole, B) 1:6 Fe:2-mercaptoimidazole, C) 1:1 Fe:methimazole, and D) 1:6 Fe:methimazole in MES buffer (10 mM, pH 6.0) containing KNO_3 (10 mM) as a supporting electrolyte. All solutions were cycled between -1000 mV and 1000 mV vs. NHE at a scan rate of 100mV/s.

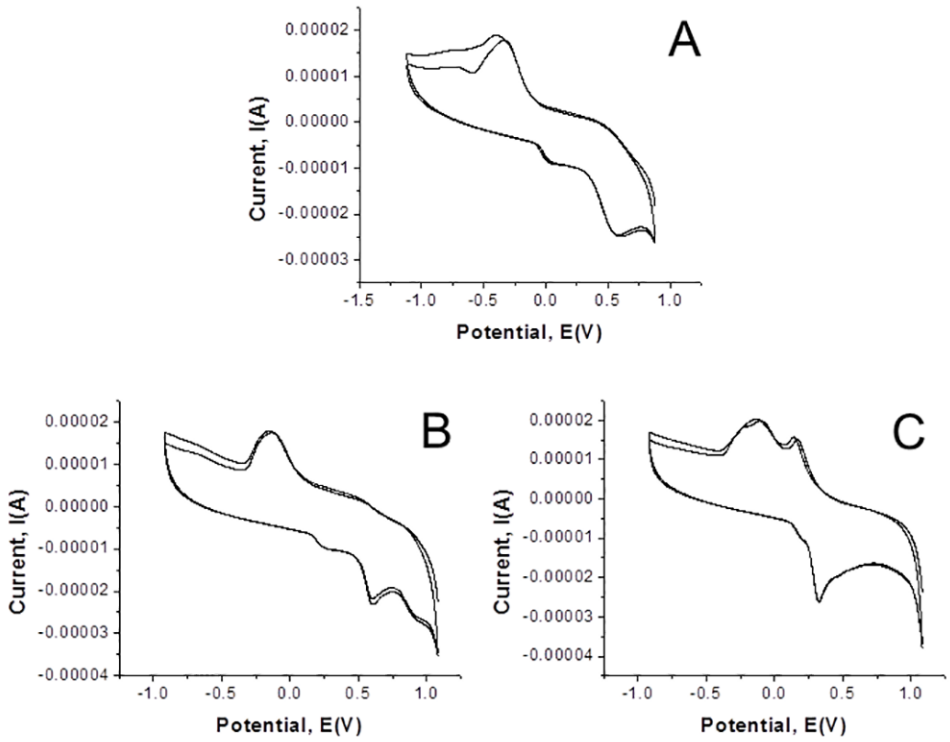

Figure 4.24. Cyclic voltammograms for A) 1:6 Fe:ergothioneine, B) 1:1 Fe:ethyl-bis(imidazole) thione, and C) 1:1 Fe: ethyl-bis(imidazole) selone in MES buffer (10 mM, pH 6.0) containing KNO_3 (10 mM) as a supporting electrolyte. All solutions were cycled between -1000 mV and 1000 mV vs. NHE at a scan rate of 100mV/s.

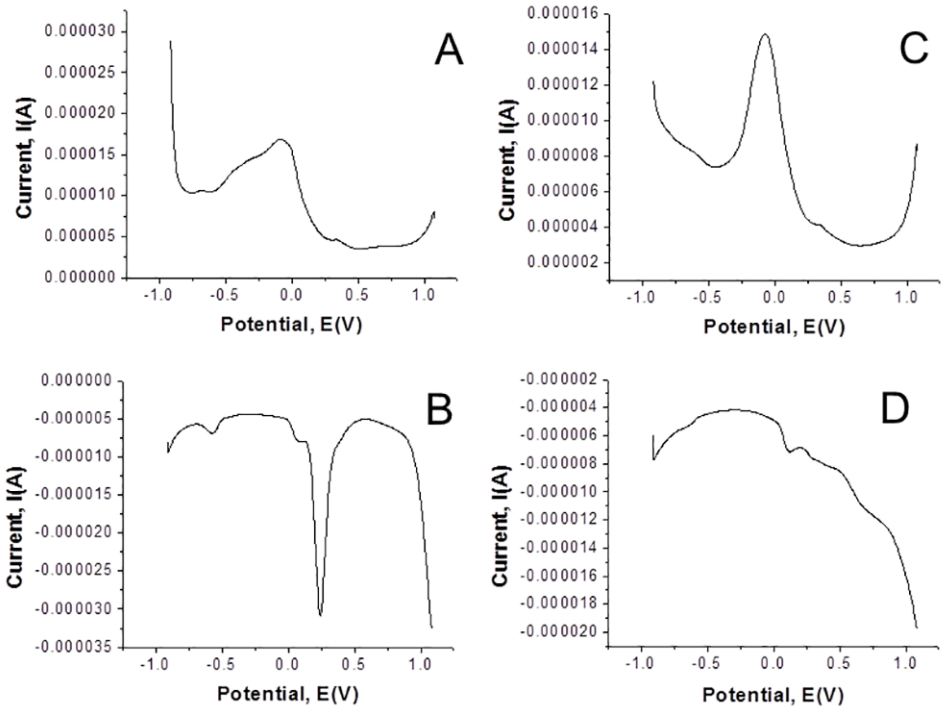

Figure 4.25. Differential pulse voltammetry scans for A) negative scan of 1:1 Fe:ethyl-bis(imidazole) selone, B) positive scan of 1:1 Fe:ethyl-bis(imidazole) selone, C) negative scan of 1:6 Fe:2-mercaptoimidazole, and D) positive scan of 1:6 Fe:2-mercaptoimidazole in MES buffer (10 mM, pH 6.0) containing KNO_3 (10 mM) as a supporting electrolyte. Compounds were cycled between -1000 mV and 1000 mV vs. NHE, using a pulse width of 0.100, a sample width of 0.045, and a pulse period of 0.200.

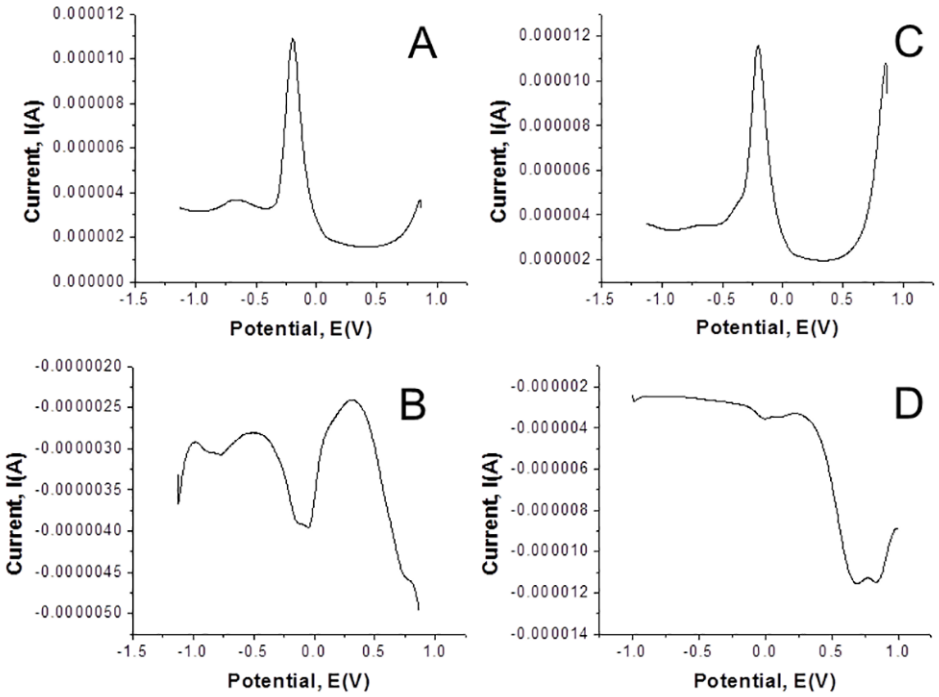

Figure 4.26. Differential pulse voltammetry scans for A) negative scan of 1:1 Fe:methimazole, B) positive scan of 1:1 Fe:methimazole, C) negative scan of 1:6 Fe:methimazole, and D) positive scan of 1:6 Fe:methimazole in MES buffer (10 mM, pH 6.0) containing KNO_3 (10 mM) as a supporting electrolyte. Compounds were cycled between -1000 mV and 1000 mV vs. NHE, using a pulse width of 0.100, a sample width of 0.045, and a pulse period of 0.200.

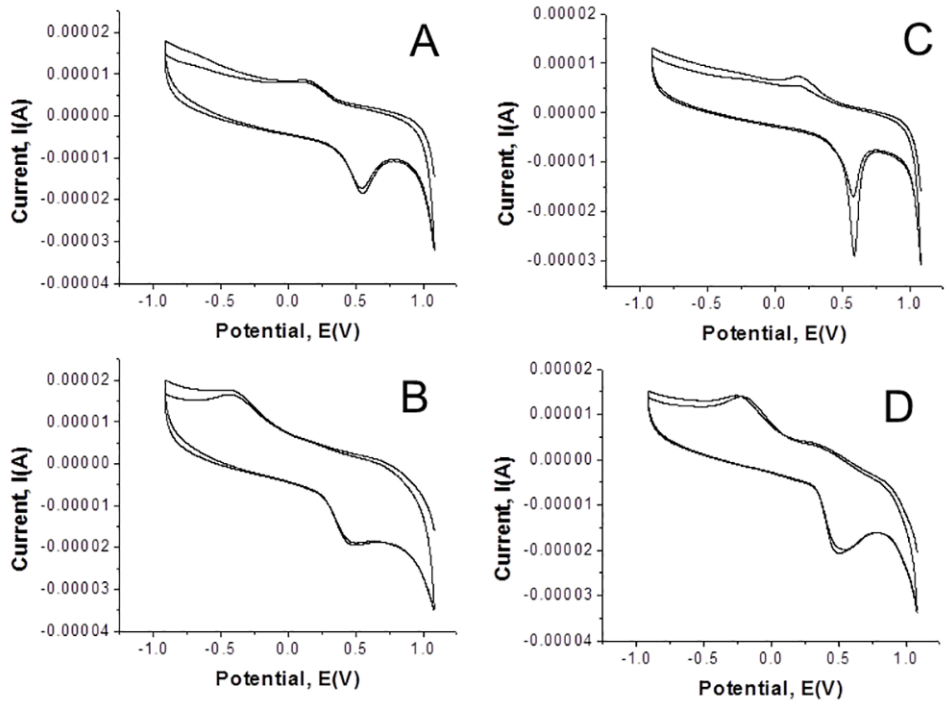

Figure 4.27. Cyclic voltammograms for A) 1:1 Cu:2-mercaptoimidazole, B) 1:4 Cu:2-mercaptoimidazole, C) 1:1 Cu:methimazole, and D) 1:4 Cu:methimazole in MES buffer (10 mM, pH 6.0) containing KNO_3 (10 mM) as a supporting electrolyte. All solutions were cycled between -1000 mV and 1000 mV vs. NHE at a scan rate of 100mV/s.

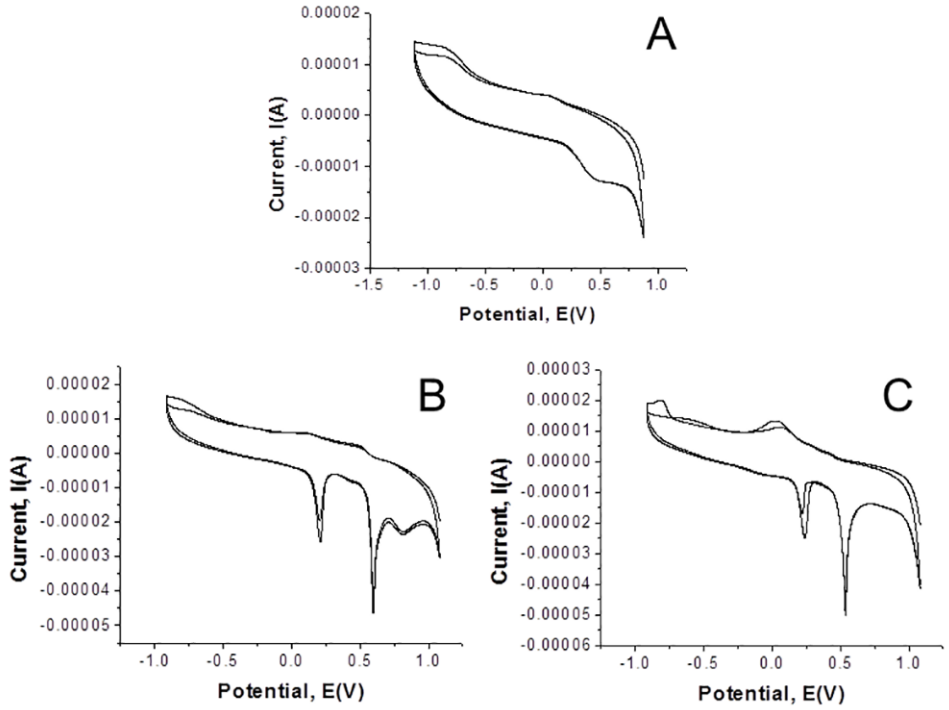

Figure 4.28. Cyclic voltammograms for A) 1:4 Cu:ergothioneine, B) 1:1 Cu:ethyl-bis(imidazole) thione, and C) 1:1 Cu:ethyl-bis(imidazole) selone in MES buffer (10 mM, pH =6.0) containing KNO_3 (10 mM) as a supporting electrolyte. All solutions were cycled between -1000 mV and 1000 mV vs. NHE at a scan rate of 100mV/s.

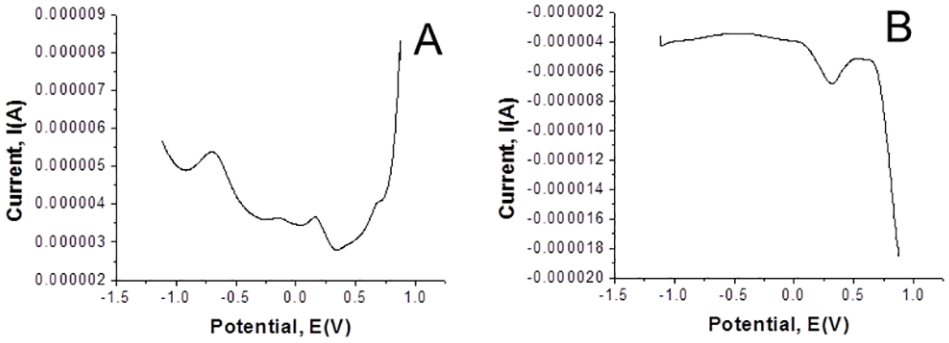

Figure 4.29. Differential pulse voltammetry scans for A) negative scan of 1:4 Cu:ergothioneine, and B) positive scan of 1:4 Cu:ergothioneine in MOPS buffer (10 mM, pH 7.0) containing KNO_3 (10 mM) as a supporting electrolyte. Compounds were cycled between -1000 mV and 1000 mV vs. NHE, using a pulse width of 0.100, a sample width of 0.045, and a pulse period of 0.200.

4.5 References

(1) Valko, M.; Leibfritz, D.; Moncol, J.; Cronin, M. T. D.; Mazur, M.; Telser, J. *Inter. J. Biochem. Cell Biol.* **2007**, *39*, 44-84.

(2) Valko, M.; Rhodes, C. J.; Moncol, J.; Izakovic, M.; Mazur, M. *Chem. Biol. Interact.* **2006**, *160*, 1-40.

(3) Seifried, H. E.; Anderson, D. E.; Fisher, E. L.; Milner, J. A. *J. Nutr. Biochem.* **2007**, *18*, 567-579.

(4) Wilson Tang, W. H. *J. Am. Heart Assoc.* **2012**, *1*, 1-3.

(5) Brewer, A. C.; Mustafi, S. B.; Murray, T. V.; Rajasekaran, N. S.; Benjamin, I. J. *Antioxid. Redox Signal.* **2013**, *18*, 1114-1127.

(6) Beeh, K. M.; Beier, J.; Haas, I. C.; Kornmann, O.; Micke, P.; Buhl, R. *Eur. Respir. J.* **2002**, *19*, 1119-1123.

(7) Battin, E. E.; Brumaghim, J. L. *J. Inorg. Biochem.* **2008**, *102*, 2036-2042.

(8) Battin, E. E.; Brumaghim, J. L. *Cell Biochem. Biophys.* **2009**, *55*, 1-23.

(9) Battin, E. E.; Perron, N. R.; Brumaghim, J. L. *Inorg. Chem.* **2006**, *45*, 499-501.

(10) Battin, E. E.; Zimmerman, M. T.; Ramoutar, R. R.; Quarles, C. E.; Brumaghim, J. L. *Metallomics* **2011**, *3*, 503-512.

(11) Ramoutar, R. R.; Brumaghim, J. L. *J. Inorg. Biochem.* **2007**, *101*, 1028-1035.

(12) Ramoutar, R. R.; Brumaghim, J. L. *Cell Biochem. Biophys.* **2010**, *58*, 1-23.

(13) Ramoutar, R. R.; Brumaghim, J. L. *Main Group Chem.* **2007**, *6*, 143-153.

(14) Akanmu, D.; Cecchini, R.; Aruoma, O. I.; Halliwell, B. *Arch. Biochem. Biophys.* **1991**, *288*, 10-16.

(15) Ey, J.; Schomig, E.; Taubert, D. *J. Agric. Food Chem.* **2007**, *55*, 6466-6474.

(16) Markova, N. G.; Karaman-Jurukovska, N.; Dong, K. K.; Damaghi, N.; Smiles, K. A.; Yarosh, D. B. *Free Radic. Bio. Med.* **2009**, *46*, 1168-1176.

(17) Rahman, I.; Gilmour, P. S.; Jimenez, L. A.; Biswas, S. K.; Antonicelli, F.; Aruoma, O. I. *Biochem. Biophys. Res. Commun.* **2003**, *302*, 860-864.

(18) Briggs, I. *J. Neurochem.* **1972**, *19*, 27-35.

(19) Epand, R. M.; Epand, R. F.; Wong, S. C. *J. Clin. Chem. Clin. Biochem.* **1988**, *26*, 623-626.

(20) Yamashita, M.; Yamashita, Y.; Ando, T.; Wakamiya, J.; Akiba, S. *Biol. Trace Elem. Res.* **2013**, *156*, 36-44.

(21) Klein, M.; Ouerdane, L.; Bueno, M.; Pannier, F. *Metallomics* **2011**, *3*, 513-520.

(22) Yamashita, Y.; Yabu, T.; Yamashita, M. *World J. Biol. Chem.* **2010**, *1*, 144-150.

(23) Yamashita, Y.; Yamashita, M. *J. Biol. Chem.* **2010**, *285*, 18134-18138.

(24) Kimani, M. M.; Bayse, C. A.; Stadelman, B. S.; Brumaghim, J. L. *Inorg. Chem.* **2013**, *52*, 11685-11687.

(25) Que, E. L.; Domaille, D. W.; Chang, C. J. *Chem. Rev.* **2008**, *108*, 1517-1549.

(26) Yang, L.; McRae, R.; Henary, M. M.; Patel, R.; Lai, B.; Vogt, S.; Fahrni, C. J. *Proc. Nat. Acad. Sci. USA* **2005**, *102*, 11179-11184.

(27) Jhurry, N. D.; Chakrabarti, M.; McCormick, S. P.; Holmes-Hampton, G. P.; A., L. P. *Biochemistry* **2012**, *51*, 5276-5284.

(28) Ma, Y.; Liu, Z.; Hider, R. C.; Petrat, F. C. *Anal. Chem. Insights* **2007**, *2*, 61-67.

(29) Weiss, G.; Fuchs, D.; Hausen, A.; Reibnegger, G.; Werner, E. R.; Werner-Felmayer, G.; Wachter, H. *Exp. Hematol.* **1992**, *20*, 605-610.

(30) Angel, I.; Bar, A.; Horovitz, T.; Taler, G.; Krakovsky, M.; Resnitsky, D.; Rosenberg, G.; Striem, S.; Friedman, J. E.; Kozak, A. *Drug Dev. Res.* **2002**, *56*, 300-309.

(31) Keyer, K.; Imlay, J. A. *Proc. Natl. Acad. Sci. USA* **1996**, *93*, 13635-13640.

(32) Perry, G.; Cash, A. D.; Srinivas, R.; Smith, M. A. *Drug Dev. Res.* **2002**, *56*, 293-299.

(33) Park, S.; Imlay, J. A. *J. Bacteriol.* **2003**, *185*, 1942-1950.

(34) Bar-Or, D.; Thomas, G. W.; Rael, L. T.; Lau, E. P.; Winkler, J. V. *Biochem. Biophys. Res. Commun.* **2001**, *282*, 356-360.

(35) Halliwell, B.; Gutteridge, J. B. *Methods. Enzymol.* **1990**, *186*, 1-85.

(36) Tanaka, S.; Haruma, K.; Yoshihara, M.; Kajiyama, G.; Kira, K.; Amagase, H.; Chayama, K. *J. Nutr.* **2006**, *136*, 821S-826S.

(37) Fleischauer, A. T.; Arab, L. *J. Nutr.* **2001**, *131*, 1032S-1040S.

(38) Pinto, J. T.; Rivlin, R. S. *J. Nutr.* **2001**, *131*, 1058S-1060S.

(39) Clark, L. C.; Dalkin, B.; Krongrad, A.; Combs, G. F., Jr.; Turnbull, B. W.; Slate, E. H.; Witherington, R.; Herlong, J. H.; Janosko, E.; Carpenter, D.; Borosso, C.; Falk, S.; Rounder, J. *Br. J. Urol.* **1998**, *81*, 730-734.

(40) Combs, G. F.; Jr *Brit. J. Cancer* **2004**, *91*, 195-199.

(41) Lippman, S. M.; Klein, E. A.; Goodman, P. J.; Lucia, M. S.; Thompson, I. M.; Ford, L. G.; Parnes, H. L.; Minasian, L. M.; Gaziano, J. M.; Hartline, J. A.; Parsons, J. K.; Bearden, J. D., III; Crawford, E. D.; Goodman, G. E.; Claudio, J.; Winquist, E.; Cook, E. D.; Karp, D. D.; Walther, P.; Lieber, M. M.; Kristal, A. R.; Darke, A. K.; Arnold, K. B.; Ganz, P. A.; Santella, R. M.; Albanes, D.; Taylor, P. R.; Probstfield, J. L.; Jagpal, T. J.; Crowley, J. J.; Meyskens, F. L., Jr.; Baker, L. H.; Coltman, C. A., Jr. *J. Am. Med. Assoc.* **2009**, *301*, 39-51.

(42) Reid, M. E.; Duffield-Lillico, A. J.; Slate, E.; Natarajan, N.; Turnbull, B.; Jacobs, E.; Combs, G. F.; Alberts, D. S.; Clark, L. C.; Marshall, J. R. *Nutr. Cancer* **2008**, *60*, 155-163.

(43) Zimmerman, M. T.; Stadelman, B. S.; Brumaghim, J. L. *In preparation*.

(44) Bhabak, K. P.; Mugesh, G. *Chem. Eur. J.* **2010**, *16*, 1175-1185.

(45) Henle, E. S.; Luo, Y.; Linn, S. *Biochemistry* **1996**, *35*, 12212-12219.

(46) Liu, X.; Millero, F. J. *Geochim. Cosmochim. Acta* **1999**, *63*, 3487-3497.

(47) Perron, N. R.; Hodges, J. N.; Jenkins, M.; Brumaghim, J. L. *Inorg. Chem.* **2008**, *47*, 6153-6161.

(48) Koppenol, W. H.; Moreno, J. J.; Pryor, W. A.; Ischiropoulos, H.; Beckman, J. S. *Chem. Res. Toxicol.* **1992**, *5*, 834-842.

(49) Radi, R.; Peluffo, G.; Alvarez, M. N.; Naviliat, M.; Cayota, A. *Free Radic. Biol. Med.* **2001**, *30*, 463-488.

(50) Briviba, K.; Tamler, R.; Klotz, L. O.; Engman, L.; Cotgreave, I. A.; Sies, H. *Biochem. Pharmacol.* **1998**, *55*, 817-823.

(51) Daiber, A.; Zou, M. H.; Bachschmid, M.; Ullrich, V. *Biochem. Pharmacol.* **2000**, *59*, 153-160.

(52) Kumar, S.; Singh, H. B.; Wolmershäuser, G. *Organometallics* **2006**, *25*, 382-393.

(53) Padmaja, S.; Squadrito, G. L.; Lemercier, J. N.; Cueto, R.; Pryor, W. A. *Free Radic. Biol. Med.* **1996**, *21*, 317-322.

(54) Sies, H.; Klotz, L. O.; Sharov, V. S.; Assmann, A.; Briviba, K. *Z Naturforsch.: Biosci.* **1998** *C*, *53*, 228-232.

(55) Woznichak, M. M.; Overcast, J. D.; Robertson, K.; Neumann, H. M.; May, S. W. *Arch. Biochem. Biophys.* **2000**, *379*, 314-320.

(56) De Silva, V.; Woznichak, M. M.; Burns, K. L.; Grant, K. B.; May, S. W. *J. Am. Chem. Soc.* **2004**, *126*, 2409-2413.

(57) Epe, B.; Ballmaier, D.; Roussyn, I.; Briviba, K.; Sies, H. *Nucleic Acids Res.* **1996**, *24*, 4105-4110.

(58) Beckman, J. S.; Beckman, T. W.; Chen, J.; Marshall, P. A.; Freeman, B. A. *Proc. Natl. Acad. Sci. USA.* **1990**, *87*, 1620-1624.

(59) Christian, G. D. *Analytical Chemistry*, 4th ed.; John Wiley & Sons: New York, 1980, p. 616.

(60) Smolenski, P.; Jaros, S. W.; Pettinari, C.; Lupidi, G.; Quassinti, L.; Bramucci, M.; Vitali, L. A.; Petrelli, D.; Kochel, A.; Kirillov, A. M. *Dalton. Trans.* **2013**, *42*, 6572-6581.

(61) Smolenski, P.; Kochel, A. *Polyhedron* **2010**, *29*, 1561-1566.

(62) Rabinovich, D. Chemistry Department, University of UNC at Charlotte, Charlotte, NC. Personal Communication, October 2011.

(63) Kimani, M. M.; Brumaghim, J. L.; VanDerveer, D. *Inorg. Chem.* **2010**, *49*, 9200-9211.

(64) Kimani, M. M.; Wang, H. C.; Brumaghim, J. L. *Dalton Trans.* **2011**, *41*, 5248-5259.

(65) Boghaei, D. M.; Farvid, S. S.; Gharagozlou, M. *Spectrochim. Acta* **2007**, *A 66*, 650-655.

(66) Brown, A. P.; Anson, F. C. *Anal. Chem.* **1977**, *49*, 1589-1595.

(67) Bhabak, K. P.; Satheeshkumar, K.; Jayavelu, S.; Mugesh, G. *Org. Biomol. Chem.* **2011**, *9*, 7343-7350.

(68) Pierre, J. L.; Fontecave, M. *Biometals* **1999**, *12*, 195-199.

(69) Jai, W.-G.; Huang, Y.-B.; Lin, Y.-J.; Jin, G.-X. *Dalton Trans.* **2008**, *41*, 5612-5620.

(70) Keith, W. G.; Powell, R. E. *J. Chem. Soc.* A **1969**, 90.

(71) Hughes, M. N.; Nicklin, H. G. *J. Chem. Soc.* A **1971**, 164-168.

(72) Bard, A. J.; Faulkner, L. R. *Electrochemical Methods, Fundamentals and Applications*; Second ed.; Wiley: New York, 2004, p 286-293.

(73) Bard, A. J.; Faulkner, L. R. *Electrochemical Methods, Fundamentals and Applications*; Second ed.; Wiley: New York, 2004, p 808.

CHAPTER FIVE

INVESTIGATIONS INTO THE FUNCTIONS OF CLOTRIMAZOLE AND PSEUDOEPHEDRINE-DERIVATIVE METAL COMPLEXES: ELECTROCHEMICAL AND COPPER OXIDATIVE DNA DAMAGE STUDIES

5.1. Introduction

A vast amount of research has been focused on the use of organometallic and inorganic metal complexes as drugs for the treatment of cancer, largely due to the success of cisplatin.[1-3] However, there are numerous non-metal-containing drugs such as clotrimazole and pseudoephedrine that possess metal binding sites, and yet the effect of metal coordination on their function has been relatively unexplored. This is of particular concern since redox-active transition metals such as Fe^{II} and Cu^{I} can generate damaging hydroxyl radical ($^{\bullet}OH$) when exposed to hydrogen peroxide *via* the Fenton and Fenton-like reactions, respectively.[4-6]

Clotrimazole (Figure 5.1) is an antifungal agent and calmodulin antagonist,[7,8] and it can reduce the viability of MCF-7 human breast cancer cells by inducing detachment of 6-phosphofructo-1-kinase, aldolase, and glycolytic enzymes from the cytoskeleton.[9] Penso and Beitner reported similar activity in LL/2 Lewis lung carcinoma cells and CT-26 colon adenocarcinoma cells.[10] Clotrimazole can also deplete intracellular Ca^{II} concentrations in acute lymphoblastic leukemia cells, resulting in apoptosis.[11] Since clotrimazole contains metal-coordinating atoms, metal binding and generation of $^{\bullet}OH$ or other reactive oxygen species may contribute to its antifungal and other toxic effects.

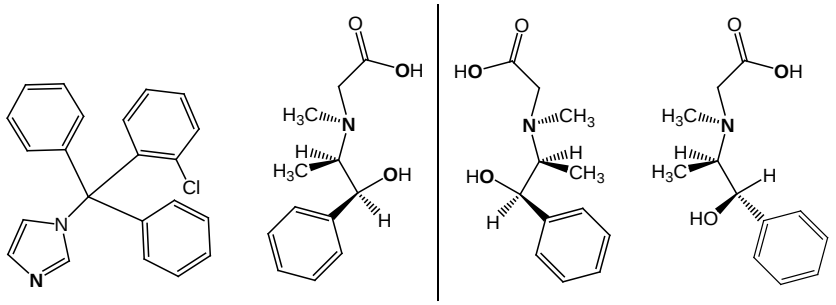

Figure 5.1. Structures of clotrimazole (clotri) and chiral pseudoephedrine derivatives *N*-[2-hydroxy-1(*R*)-methyl-2(*R*)-phenylethyl]-*N*-methylglycine [*R*,*R*(-)(H_2cpse)], *N*-[2-hydroxy-1(*S*)-methyl-2(*S*)-phenylethyl]-*N*-methylglycine [*S*,*S*(-)(H_2cpse)], and *N*-[2-hydroxy-1(*S*)-methyl-2(*R*)-phenylethyl]-*N*-methylglycine [*S*,*R*(-)(H_2ceph)]. Metal coordinating atoms in each ligand are highlighted in bold type.

In vitro studies with clotrimazole (clotri) determined that its cytotoxic properties were substantially enhanced upon addition of $CdCl_2$ or $PbCl_2$.[12] This synergistic advantage was also observed with $ZnCl_2$, with the added benefit of faster apoptosis induction.[13] Previous studies by Barba-Behrens *et al.* reported the successful synthesis, identification, and cytotoxic properties of Cu^{II}, Co^{II}, Zn^{II}, and Ni^{II} clotri complexes with HeLa (cervix-uterine), PC3 (prostate), and HCT-15 (colon) carcinoma cells.[14] However, no studies have focused on understanding the mechanisms behind the cytotoxic activity of these novel metal-clotri complexes.

Pseudoephedrine (Figure 5.1) is commonly used as a nasal decongestant, stimulant,[15] or an antitussive drug.[16,17] Yet, little is known about how its function may be altered in the presence of biological transition metals. Thus, copper complexes of pseudoephedrine derivatives (Figure 5.1) were studied for their electrochemical properties and ability to promote oxidative DNA damage. These derivatives have a carboxylic-acid-containing substituent bound to the nitrogen, thus providing a possible third coordination site in addition to the hydroxyl oxygen and nitrogen.[18]

Electrochemical studies were conducted on $[Cu(clotri)_3(NO_3)][NO_3]\cdot 2H_2O$, $Cu_3(R,R(-)\text{-cpse})_3$ and $Cu_3(S,S(+)\text{-cpse})_3$ to determine their potential ability to readily undergo oxidation and reduction within the redox window of Fenton-like reactions. Gel electrophoresis studies were conducted on these Cu^{II} complexes to assess their ability to generate the hydroxyl radical ($^{\bullet}OH$) when hydrogen peroxide is added, resulting in DNA damage. Since DNA contains the cellular genetic map, significant DNA damage may result in harmful mutations, leading to the onset of various diseases. If these complexes promote $^{\bullet}OH$ generation then it is possible that they can cause cellular oxidative damage leading to apoptosis. Studies with clotrimazole and pseudoephedrine derivatives and their metal complexes were performed in collaboration with Dr. Noráh Barba-Behrens (Universidad Nacional Autónoma de México). The work on the clotrimazole and its metal complexes presented in this Chapter soon will be submitted for publication in a special issue of *Dalton Transactions* focusing on DNA-binding metal complexes (Betanzos-Lara, S.; Chmel, N. P.; Zimmerman, M. T.; Barrón-Sosa, L. R.; Garino, C.; Salassa, L.; Rodger, A., Brumaghim, J.; Gracia-Mora, I.; Barba-Behrens, N. "Redox-active and DNA-binding coordination complexes of clotrimazole," *Dalton Trans.*, manuscript in preparation).

5.2. Results and Discussion

5.2.1. Electrochemical studies of clotrimazole-metal complexes. Cyclic voltammetry (CV) experiments were conducted on the clotri complexes of Zn^{II}, Co^{II}, and Cu^{II} to determine their electrochemical properties (Table 5.1). Experiments were

Table 5.1. Electrochemical potentials (versus NHE) from cyclic voltammetry studies of the tested complexes in acetonitrile.

Compound	Ep_a **(V)**	Ep_c **(V)**	ΔE **(V)**	$E_{1/2}$ **(V)**
$Zn(clotri)_2Cl_2$	—	—	—	—
$Zn(clotri)_2Br_2$	1.021[a]	0.591[a]	0.435[a]	0.806[a]
$[Zn(clotri)_3(NO_3)][NO_3]\cdot 5H_2O$	—	—	—	—
$Co(clotri)_2Cl_2$	-0.238[b], 0.997[c], 1.206[a]	—	—	—
$Co(clotri)_2Br_2$	-0.038[b], 0.648[c], 0.948[a]	-1.612[b], 0.376[c]	1.574[b], 0.272[c]	-0.825[b], 0.512[c]
$Co(clotri)_3(NO_3)_2$	-0.296[b]	-1.669[b]	1.373[b]	-0.982[b]
$Cu(clotri)_2Cl_2\cdot 5H_2O$	-0.512[d], -0.082[e]	-1.192[d], -0.379[e]	0.680[d], 0.297[e]	-0.852[d], -0.239[e]
$Cu(clotri)_2Br_2\cdot 5H_2O$	-0.479[d], 0.018[e], 0.962[a]	-1.407[d], -0.297[e], 0.614[a]	0.928[d], 0.279[e], 0.348[a]	-0.943[d], -0.139[e], 0.788[a]
$[Cu(clotri)_3NO_3][NO_3]\cdot 2H_2O$	-0.441[d], 0.117[e], 0.693[a]	-1.603[d], -0.141[e], 0.338[a]	1.162[d], 0.258[e], 0.355[a]	-1.022[d], -0.012[e], 0.515[a]

[a]Potentials from the clotri ligand. [b]Potentials from the $Co^{II/0}$ couple. [c]Potentials from the $Co^{III/II}$ couple. [d]Potentials from the $Cu^{I/0}$ couple. [e]Potentials from the $Cu^{II/I}$ couple.

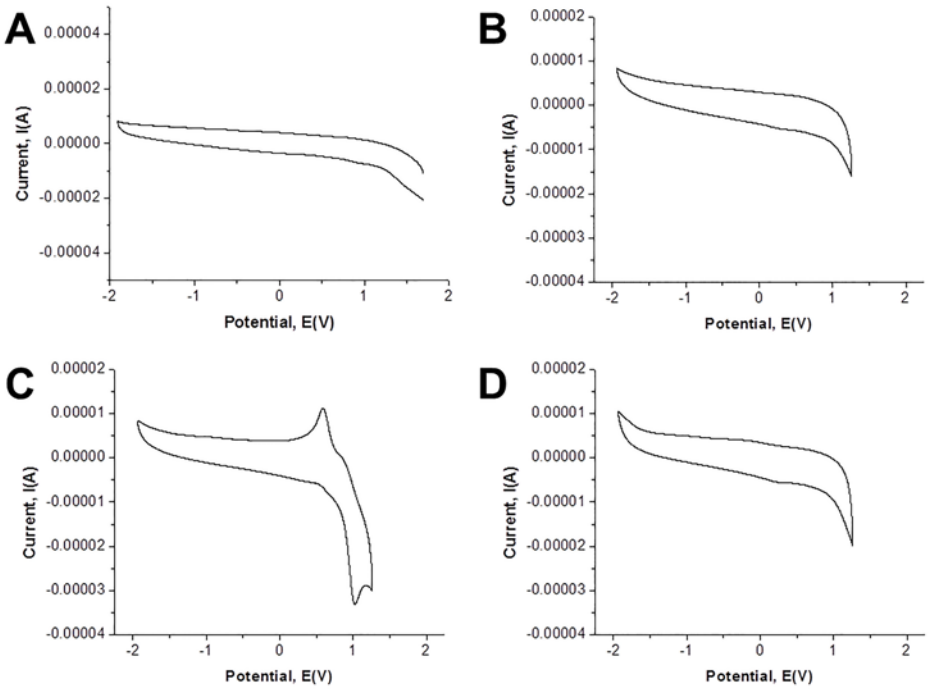

Figure 5.2. Cyclic voltammograms vs. NHE for A) clotrimazole, B) $[Zn(clotri)_2Cl_2]$, C) $[Zn(clotri)_2Br_2]$, and D) $[Zn(clotri)_3NO_3]$. Samples are 1 mM in acetonitrile with 0.1 M $TBAPF_6$ as the supporting electrolyte.

performed in acetonitrile unless otherwise specified, and all potentials are normalized to the normal hydrogen electrode (NHE). Electrochemical studies of the clotri ligand show that this ligand is redox-inactive within the investigated window (Figure 5.2A).

The cyclic voltammograms for $Zn(clotri)_2Cl_2$ and $[Zn(clotri)_3(NO_3)][NO_3]$ (Figures 5.2A and 5.2C) show no electrochemical activity. In contrast, studies of the analogous $Zn(clotri)_2Br_2$ complexshow a cathodic wave at 1.021 V and an anodic wave at 0.591 V (Figure 5.2 B), with an $E_{1/2}$ value of 0.806 V. This redox couple is attributed to the clotri ligand, in agreement with previous studies involving metal coordinated histidine and imidazole-derived ligands.[19,20]

However, Nair and Ray[21] reported a $Zn(furfural\text{-}histidine)_2$ complex with N2O2 coordination where the voltammogram exhibited an irreversible two-electron cathodic

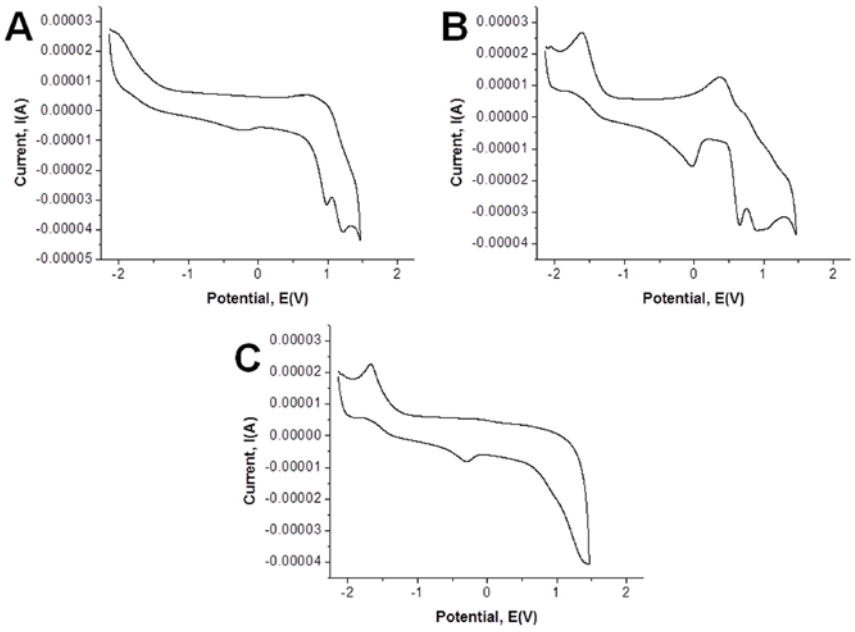

Figure 5.3. Cyclic voltammograms vs. NHE for A) $Co(clotri)_2Cl_2$, B) $Co(clotri)_2Br_2$, and C) $Co(clotri)_3(NO_3)_2$. Samples are 1 mM in acetonitrile with 0.1 M $TBAPF_6$ as the supporting electrolyte.

wave at -0.900 V for the Zn^{II} to Zn^0 reduction. In contrast the clotri ligand only has a single N atom of the histidine ring capable of coordination, with no O coordination sites. Additionally, the $[Zn(clotri)_3(NO_3)][NO_3]$ complex contains a third clotri ligand, compared to the two clotri ligands in the chloride or bromide complexes, and binding of this additional clotri ligand may also shift the $Zn^{II/0}$ redox couple outside the investigated window.

Cyclic voltammetric studies of $Co(clotri)_2Cl_2$ (Figure 5.3A) show an anodic wave at 1.206 V, indicating oxidation of the clotri ligand, and anodic waves at 0.977 V and -0.238 V that represent the oxidation of Co^{II} to Co^{III} and Co^0 to Co^{II}, respectively. Differential pulse voltammetry (DPV) studies (Figures 5.4A and 5.4B) confirm both oxidation and reduction waves for the ligand-based potentials of the clotri complex.

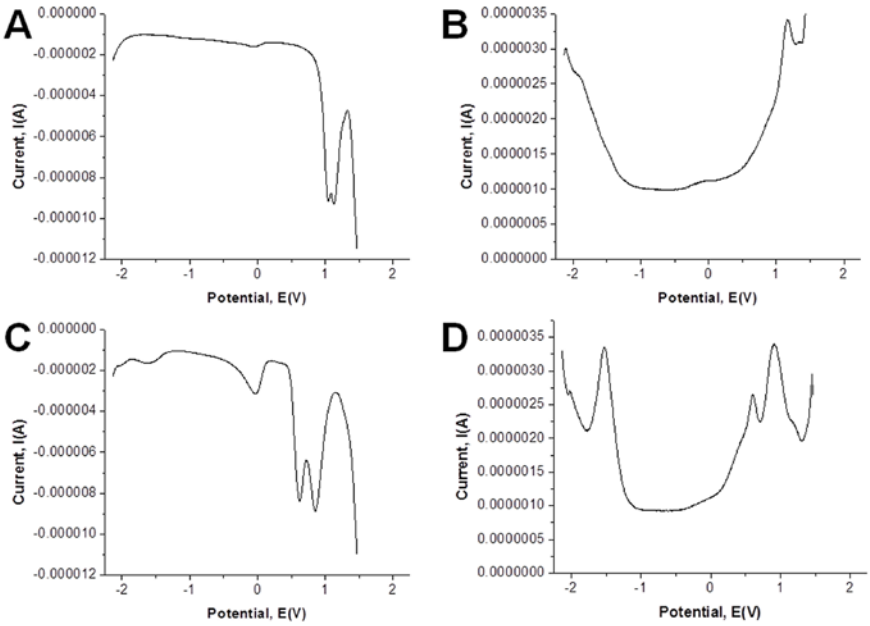

Figure 5.4. Differential pulse voltammetry vs. NHE for A) $Co(clotri)_2Cl_2$ positive scan, B) $Co(clotri)_2Cl_2$ negative scan, C) $Co(clotri)_2Br_2$ positive scan, and D) $Co(clotri)_2Br_2$ negative scan. Samples are 1 mM in acetonitrile with 0.1 M $TBAPF_6$ as the supporting electrolyte.

Electrochemical studies of the bromide complex, $Co(clotri)_2Br_2$, reveal both $Co^{III/II}$ and $Co^{II/0}$ redox couples, in addition to oxidation of the clotri ligand (Figure 5.3B). The quasi-reversible $Co^{II/0}$ redox couple with a cathodic wave at -1.612 V and an anodic wave at -0.038 V has an $E_{1/2}$ value of -0.825 V. The $Co^{III/II}$ redox couple has an $E_{1/2}$ value of 0.512 V, and the oxidation of the clotri ligand occurs at 0.948 V. DPV studies (Figures 5.4C and 5.4D) confirm the reduction of the clotri ligand in addition to the $Co^{III/II}$ and $Co^{II/0}$ redox couples for this bromide complex. The cyclic voltammogram for the nitrate complex, $Co(clotri)_3(NO_3)_2$, exhibits only the $Co^{II/0}$ redox couple ($E_{1/2}$ = -0.982 V), whereas DPV studies also show waves for the $Co^{III/II}$ couple and the clotri ligand (Figures 5.5A and 5.5B).

A comparison of the anodic waves for the $Co^{II/3I}$oxidation of $Co(clotri)_2Cl_2$ and

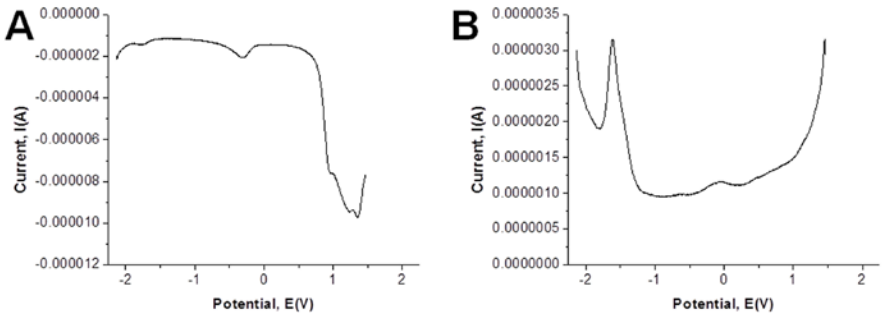

Figure 5.5. Differential pulse voltammetry vs. NHE for A) $Co(clotri)_3(NO_3)_2$ positive scan and B) $Co(clotri)_3(NO_3)_2$ negative scan. Samples are 1 mM in acetonitrile with 0.1 M $TBAPF_6$ as the supporting electrolyte.

$Co(clotri)_2Br_2$ reveals that the chloride complex more readily undergoes oxidation to hard Co^{III} relative to borderline Co^{II} compared to the bromide complex, as expected by hard-soft acid-base theory. These electrochemical results therefore demonstrate that the halide ligand significantly affects the electrochemical properties of the cobalt center.

Araujo *et al.*[19] reported a conjugated bis(imino)pyridine ligand (2,6-bis[1-(4-R-phenylimino)ethyl]pyridine) with 3N donors and two coordinated chlorides (or bromides) bound to a Co^{II} center, and observed a one-electron $Co^{III/II}$ redox couple by cyclic voltammetry. Their studies revealed a more negative $E_{1/2}$ value for the $Co^{III/II}$ redox couple ($E_{1/2}$ value of 0.153 V), compared to the $Co(clotri)_2Br_2$ complex, consistent with our results indicating that the clotri ligand stabilizes the higher oxidation states of cobalt.

Electrochemical studies were also conducted on analogous clotri-Cu^{II} complexes. In acetonitrile, $Cu(clotri)_2Cl_2$ (Figure 5.6A) exhibits both quasi-reversible $Cu^{II/I}$ and $Cu^{I/0}$ redox couples with $E_{1/2}$ values of -0.239 V and -0.852 V, respectively. However, these potentials are weaker than expected due to precipitation observed after the initial scan. In contrast, the $Cu(clotri)_2Br_2$ complex (Figure 5.6B) clearly shows $Cu^{II/I}$ and $Cu^{0/I}$ redox couples in addition to redox activity of the clotri ligand. The cathodic wave at -1.407 V

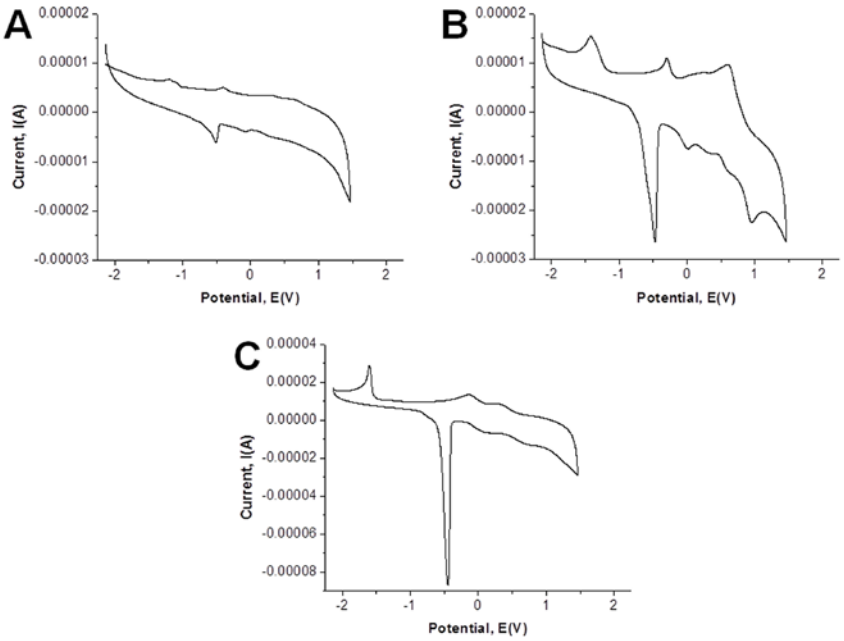

Figure 5.6. Cyclic voltammograms vs. NHE for A) Cu (clotri)$_2$Cl$_2$•5H$_2$O, B) Cu(clotri)$_2$Br$_2$•5H$_2$O, and C) [Cu(clotri)$_3$NO$_3$][NO$_3$]. Samples are 1 mM in acetonitrile with 0.1 M TBAPF$_6$ as the supporting electrolyte.

and the anodic wave at -0.479 V form the quasi-reversible $Cu^{I/0}$ redox couple for the bromide complex, with an $E_{1/2}$ value of -1.022 V. The sharp shape of the anodic wave at -0.479 V is characteristic of Cu^0 to Cu^I oxidation due to the copper stripping from the carbon working electrode.[22] The anodic wave around 0.190 V and the cathodic wave around 0.620 V are attributed to possible formation of an electrochemically active acetonitrile complex upon clotri dissociation. The quasi-reversible $Cu^{II/I}$ and clotri redox couples have $E_{1/2}$ values of -0.139 V, and 0.788 V, respectively.

The [Cu(clotri)$_3$(NO$_3$)][NO$_3$] complex exhibits a strong quasi-reversible redox couple for the $Cu^{I/0}$ couple ($E_{1/2}$ = -1.022), and two weaker quasi-reversible redox couples for both the $Cu^{II/I}$ and clotri couples ($E_{1/2}$ values of -0.012 V and 0.515 V, respectively). It has the most positive $E_{1/2}$ value for the $Cu^{II/I}$ redox couple (-0.012 V), followed by the bromide and chloride complexes ($E_{1/2}$ values of -0.139 V and -0.239 V, respectively),

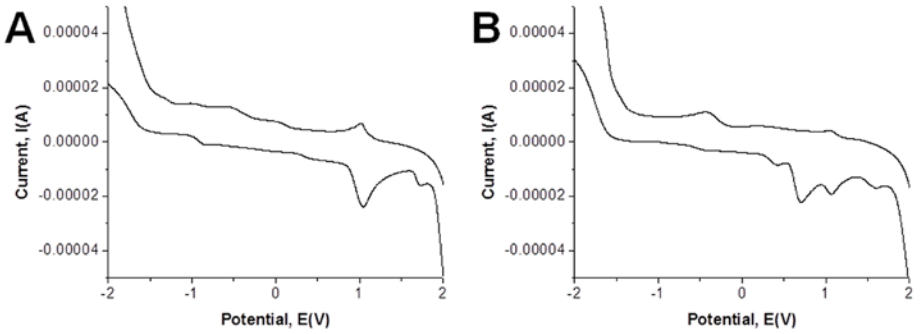

Figure 5.7. Cyclic voltammograms of A) $[Cu(clotri)_2Cl_2]$ and B) $[Cu(clotri)_2Br_2]$. Samples are 1 mM in dichloromethane with 0.1 M $TBAPF_6$ as the supporting electrolyte.

indicating that the hard chloride ligands stabilize borderline Cu^{II} relative to the soft Cu^{I}. Interestingly, the $[Cu(clotri)_3(NO_3)][NO_3]$ complex containing a hard nitrate ligand stabilizes soft Cu^{I} relative to the borderline Cu^{II} ion. Thus, the three clotri ligands present in the nitrate complex have a greater influence on the electrochemical properties of the Cu^{II} center than the halide ligands.

Additional studies were conducted on both the $Cu(clotri)_2Cl_2$ and $Cu(clotri)_2Br_2$ complexes in dichloromethane, since both remain in solution over the course of the electrochemical experiments using this solvent. Neither of these complexes exhibits the $Cu^{I/0}$ redox couple in CH_2Cl_2. Under these conditions, $Cu(clotri)_2Cl_2$ has a significant redox wave at the positive end of the voltammogram (Figure 5.7), consistent with a clotri-based redox couple ($E_{1/2}$ value of 1.002 V; Table 5.2). In comparison, $Cu(clotri)_2Br_2$ exhibits both the clotri and $Cu^{II/I}$ redox couples (Figure 5.7B; $E_{1/2}$ values of 1.057 V and 0.768 V, respectively).

Table 5.2. Electrochemical potentials (versus NHE) of the complexes investigated in dichloromethane.

Compound	Ep_a (V)	Ep_c (V)	ΔE (V)	$E_{1/2}$ (V)
$Cu(clotri)_2Cl_2 \cdot 5H_2O$	1.034[b]	0.970[b]	0.064[b]	1.002[b]
$Cu(clotri)_2Br_2 \cdot 5H_2O$	0.703[a], 1.070[b]	0.834[a], 1.044[b]	0.131[a], 0.026[b]	0.768[a], 1.057[b]

[a]Potentials of the $Cu^{II/I}$ couple. [b]Potentials of the clotri ligand.

Studies by Neelakantan *et al.*[20] found the anodic wave for oxidation of Cu^{I} to Cu^{II} for a Cu^{II}-pyridoxine-imidazole complex (with 2O and 1N donor ligands, respectively) appears around 0.503 V (versus NHE). Miyamoto *et al.*[23] also found that coordination to tri(2-pyridylthio)methyl, a tridentate imidazole ligand, caused $Cu^{I/II}$ oxidation to occur around 0.480 V when Cu^{II} was coordinated to either bromide or chloride. However, this anodic wave is observed over the range of -0.082 V to 0.117 V for the Cu^{II}-clotri complexes. The negative shifts of these anodic waves for the Cu^{II}-clotri complexes compared to the Cu^{II}-pyridoxine-imidazole complex and tri(2-pyridylthio)methyl complexes indicate that additional imidazole-based ligand coordination stabilizes higher copper oxidation states. Our results indicate that the borderline clotri ligand has a stronger effect than the anionic halide or nitro ligands on the electrochemical potential of Cu^{II}, since addition of a third clotri ligand stabilizes Cu^{II} relative to Cu^{I}. When only two clotri ligands are present, in the case of the $Cu(clotri)_2Br_2$ complex, the $E_{1/2}$ value is shifted more positively, favoring Cu^{I} relative to Cu^{II}.

5.2.2. Electrochemical studies of chiral pseudophedrine derivatives. Electrochemical studies were performed on chiral H_2cpse ligands (Figure 5.1), the four mononuclear Cu^{II} complexes, and the two trinuclear Cu^{II} complexes listed in Table 5.3. Pseudophedrine derivatives and metal complexes were synthesized and characterized by the Barba-Behrens group.[18] All experiments were conducted in degassed methanol due to limited solubility of both the ligands and their copper complexes in other solvents.

Cyclic voltammograms of (+)*S*,*S*-H_2cpse, (-)*R*,*S*-H_2cpse, and (+)*S*,*R*-H_2cpse all exhibit a single irreversible oxidation wave (Figure 5.8) with Ep_a values of 0.926, 0.871,

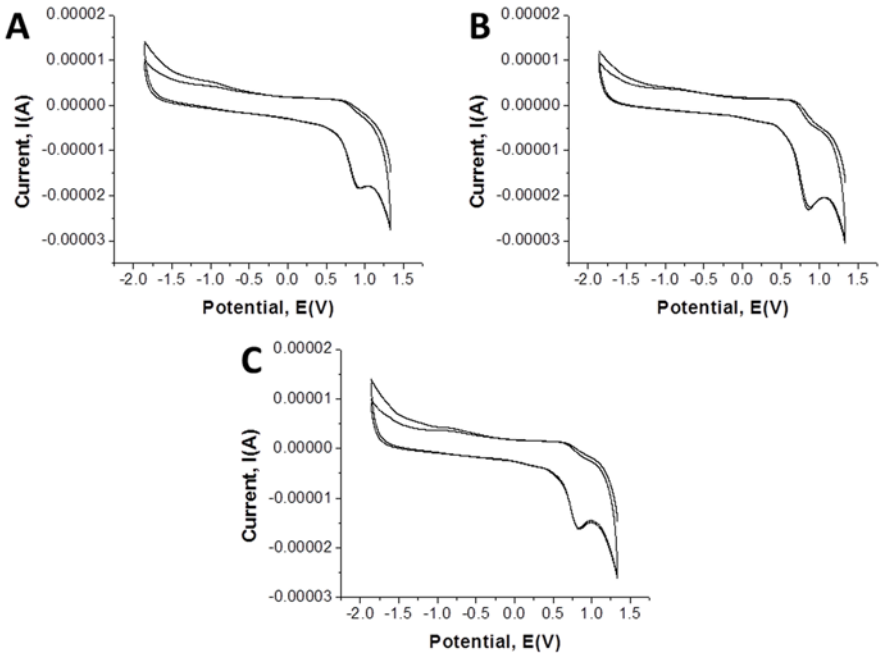

Figure 5.8. Cyclic voltammograms vs. NHE for the ligands A) (+)*S*,*S*-H_2cpse, B) (-)*R*,*S*-H_2cpse, and C) (+)*S*,*R*-H_2cpse. Samples are 1 mM in methanol with 0.1 M tetrabutylammonium hexafluorophosphate as the supporting electrolyte.

and 0.831 V, respectively. This difference of almost 100 mV for oxidations of these chiral ligands is significant, and it would be informative to also test the (-)*R*,*R*-H_2cpse ligand to determine its oxidation potential, although samples of this ligand were not available from our collaborator. Few articles investigate the electrochemical activity of chiral metal complexes with N and O donor ligands,[24,25] and no reports specifically discuss the electrochemical activity of the unbound chiral compounds.

Cpse and ceph ligands have the same structure, but Barba-Behrens *et al.*[26] reported that the ceph ligands can show bidentate coordination to Cu^{II}, binding through only the nitrogen and the carboxylate oxygen atoms (Figure 5.1).[18] Oxidation waves for the ligand are only observed for the Cu(*S*,*S*(-)Hcpse)$_2$ and Cu(*R*,*S*(-)Hcpse)$_2$ complexes. There is no change for the ligand potential in the *S*,*S* complex compared to the unbound *S*,*S*(+)H_2cpse, but a positive shift of 0.135 V is observed for coordinated *R*,*S*(-)H_2cpse in

the *R,S* complex. The quasi-reversible $Cu^{II/I}$ redox couples for Cu(*S,S*(+)Hcpse)$_2$ and Cu(*R,R*(-)Hcpse)$_2$ are similar ($E_{1/2}$ of -0.520 and -0.524 V, respectively; Figure 5.9); however, the quasi-reversible $Cu^{I/0}$ couples vary by 0.047 V ($E_{1/2}$ values of -0.095 and -0.142 V, respectively). Thus, the oxidation waves for the $Cu^{II/I}$ and $Cu^{I/0}$ redox couples of Cu(*R,S*(-)Hceph)$_2$ are shifted more positively than the oxidation waves observed for the diastereomeric Cu(*S,S*(+)Hcpse)$_2$ and Cu(*R,R*(-)Hcpse)$_2$ complexes (Table 5.3), resulting in more positive $E_{1/2}$ values for both copper redox couples of Cu(*R,S*(-)Hceph)$_2$.

In contrast, Cu(*S,R*(+)Hceph)$_2$ only shows a $Cu^{I/0}$ redox couple with similar Ep_c and $E_{1/2}$ values to those observed for its diasteromer Cu(*R,S*(-)Hceph)$_2$ (Table 5.3). The diastereomers Cu(*R,R*(-)Hcpse)$_2$ and Cu(*S,S*(+)Hcpse)$_2$ differ by -0.047 V for the $Cu^{II/I}$ redox couple. Comparison to Cu(*R,S*(-)Hceph)$_2$, reveals a shift in the $Cu^{II/I}$ $E_{1/2}$ value of +0.039 V compared to Cu(*S,S*(+)Hcpse)$_2$, and +0.086 V compared to Cu(*R,R*(-)Hcpse)$_2$. These significant shifts indicate that ligand chirality affects the electrochemical properties of the coordinated Cu^{II} and that H_2ceph stabilizes Cu^{I} over Cu^{II} relative to the H_2cpse ligands.

Niklas *et al.*[27] reported only the $Cu^{II/I}$ redox couple for chiral and achiral derivatives of [bis(picolyl)amino]acylglycine ethyl ester and [bis(picolyl)amino]-acylphenylalanine methyl ester complexes of Cu^{II}, complexes with square pyramidal or distorted octahedral geometry and N3O coordination; additional ligands such as acetonitrile, oxygen, and chloride aid in stabilizing these geometries. These studies were conducted under similar conditions to our studies (in methanol with 0.1 M tetrabutylammonium hexafluorophosphate as the supporting electrolyte and potentials vs.

Table 5.3. Electrochemical potentials (versus NHE) from cyclic voltammetry studies of the tested complexes in methanol.

Compound	Ep_a **(V)**	Ep_c **(V)**	ΔE **(V)**	$E_{1/2}$ **(V)**
(+)*S*,*S*-H_2cpse	0.926	—	—	—
(-)*R*,*S*-H_2cpse	0.871	—	—	—
(+)*S*,*R*-H_2cpse	0.831	—	—	—
Cu(*S*,*S*(+)Hcpse)$_2$	0.075[a], 0.264[b], 0.926	-1.115[a], -0.454[b]	1.040[a], 0.718[b]	-0.520[a], -0.095[b]
Cu(*R*,*R*(-)Hcpse)$_2$	0.075[a], 0.178[b]	-1.124[a], -0.461[b]	1.049[a], 0.639[b]	-0.524[a], -0.142[b]
Cu(*R*,*S*(-)Hceph)$_2$	0.075[a], 0.264[b], 0.966	-0.918[a], -0.375[b]	0.843[a], 0.639[b]	-0.413[a], -0.056[b]
Cu(*S*,*R*(+)Hceph)$_2$	0.098[a]	-0.903[a]	0.805[a]	-0.402[a]
Cu_3(*S*,*S*(+)-cpse)$_3$	0.145[a], 0.414[b]	-1.399[a], -0.982[a], -0.430[b]	1.254[a], 0.837[a], 0.844[b]	-0.627[a], -0.415[a], -0.008[b]
Cu_3(*R*,*R*(-)-cpse)$_3$	0.193[a]	-1.321[a], -0.958[a], -0.445[b]	1.514[a], 1.151[a]	-0.564[a], -0.383[a]

[a]$Cu^{I/0}$ potential. [b]$Cu^{II/I}$potential.

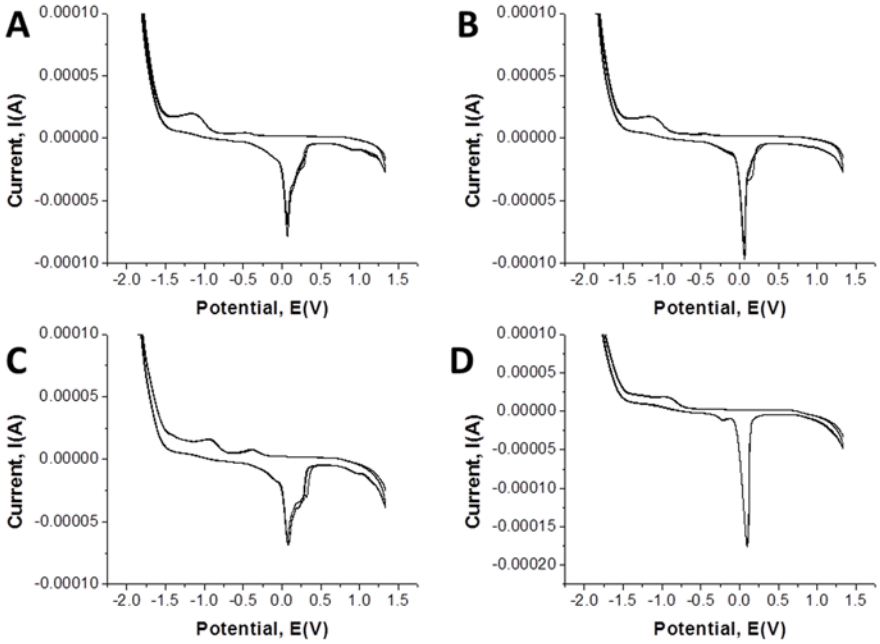

Figure 5.9. Cyclic voltammograms vs. NHE for A) Cu(*S*,*S*(+)Hcpse)$_2$, B) Cu(*R*,*R*(-)Hcpse)$_2$, C) Cu(*R*,*S*(-)Hceph)$_2$ and D) Cu(*S*,*R*(+)Hceph)$_2$. Samples are 1 mM in methanol with 0.1 M tetrabutylammonium hexafluorophosphate as the supporting electrolyte.

normal hydrogen electrode), but with a smaller electrochemical window of -0.4 to 0.2 V. No electrochemical data were reported for the uncoordinated ligands, and no observed redox waves in the copper complex voltammograms were assigned to either ligand. The $Cu^{II/I}$ $E_{1/2}$ values reported for the complexes by Niklas *et al.* are between -0.16 V and -0.10 V,[27] and are relatively similar to the $E_{1/2}$ values determined for the $Cu^{II/I}$ couples of Cu(*S*,*S*(+)Hcpse)$_2$ and Cu(*R*,*R*(-)Hcpse)$_2$ ($E_{1/2}$ values of -0.142 and -0.095 V, respectively). The significant shift observed for the $Cu^{II/I}$ redox couple (between -0.104 V and -0.044 V) $E_{1/2}$ value of Cu(*R*,*S*(-)Hcpse)$_2$ compared to the complexes reported by Niklas *et al.* is likely attributed to the presence of the borderline nitrogen donor pyridines in the [bis(picolyl)amino]acylglycine ethyl ester and [bis(picolyl)amino]-acylphenylalanine methyl ester for stabilizing Cu^{II} substantially more than Cu^{I}. The

absence of a visible $Cu^{II/I}$ redox couple for Cu(*S*,*R*(+)Hceph)$_2$ is surprising, since the geometry and Cu^{II} coordination is the same as in Cu(*R*,*S*(+)Hceph)$_2$; thus, chirality must be a significant factor in the electrochemical potentials of these mononuclear copper complexes.

Similar electrochemical studies were conducted on the trinuclear copper complexes Cu_3(*S*,*S*(+)-cpse)$_3$ and Cu_3(*R*,*R*(-)-cpse)$_3$ (Figure 5.10), in which the H_2cpse ligands are doubly deprotonated.[18] No ligand-based oxidative waves are observed in the voltammograms of these trinuclear complexes. The voltammogram of Cu_3(*S*,*S*(+)-cpse)$_3$ exhibits three reductive waves but only two oxidative waves. The two reductive waves at -1.399 and -0.952 V are attributed to the reduction of Cu^I to Cu^0, similar in shape to the $Cu^{I/0}$ reductive wave observed for the mononuclear copper complexes (Figure 5.9). The third reductive wave at -0.430 V is attributed to the reduction of Cu^{II} to Cu^I. The oxidative wave at 0.145 V is attributed to the oxidation of Cu^0 to Cu^I, and the wave at 0.414 V is attributed to the oxidation of Cu^I to Cu^{II}; however, the $Cu^{0/I}$ oxidative wave is

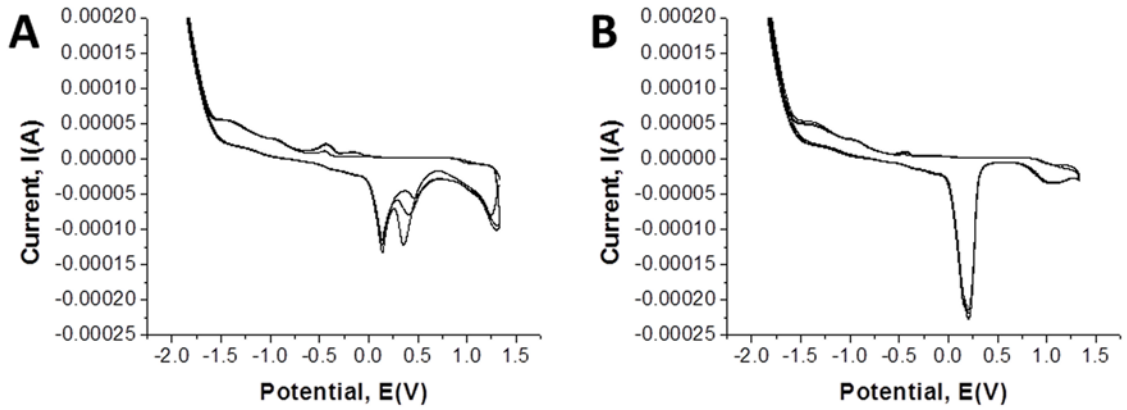

Figure 5.10. Cyclic voltammograms vs. NHE for A) Cu_3(*S*,*S*(+)-cpse)$_3$] and B) Cu_3(*R*,*R*(-)-cpse)$_3$. Samples are 1 mM in methanol with 0.1 M tetrabutylammonium hexafluorophosphate as the supporting electrolyte.

broader than expected, suggesting that all three Cu^{II} centers are not chemically equivalent.

Two reductive waves are observed in the voltammogram of $Cu_3(R,R(-)\text{-cpse})_3$, but $Cu_3(R,R(-)\text{-cpse})_3$ exhibits a single broad oxidative wave at 0.193 V, caused by the overlapping of the Cu^{I} stripping and Cu^{II} oxidation waves. Comparison of the $Cu^{I/0}$ $E_{1/2}$ values of $Cu(S,S(+)\text{Hcpse})_2$ and $Cu(R,R(-)\text{Hcpse})_2$ to their respective trinuclear copper complexes reveal a shift of -0.127 V for the $Cu^{I/0}$ $E_{1/2}$ value of $Cu_3(S,S(+)\text{-cpse})_3$ and of -0.040 V for $Cu_3(R,R(-)\text{-cpse})_3$. Previous studies with of a trinuclear Cu^{II} complex with tetradenate aromatic ligands (three nitrogen and one oxygen donor atoms) showed three oxidative waves for each of the three $Cu^{II/I}$ redox couples.[28] However, these studies did not reveal redox activity for the $Cu^{I/0}$ couple, and did not identify any waves attributed to ligand electrochemistry. Our studies with these trinuclear complexes suggest that the three Cu^{II} centers behave differently and that the overall effect of ligand chirality on the redox activity of the Cu^{II} centers is significant. $Cu(R,S(-)\text{Hceph})_2$ exhibits the largest shift in the $Cu^{II/I}$ redox couple compared to $Cu(S,S(+)\text{Hcpse})_2$ and $Cu(R,R(-)\text{Hcpse})_2$ and only differs from the H_2cpse ligands through chirality.

5.2.3. DNA damage studies. Gel electrophoresis studies were performed on three Cu^{II} complexes listed in Table 5.4 to determine their ability to promote oxidative DNA damage caused by Cu^{I}/H_2O_2 (pH 7). Due to their limited aqueous solubility, these complexes were first dissolved in ethanol (5 mL) and then diluted with water (20 mL) for these studies (200 μM final concentration). In all cases, ascorbic acid (1.25 equiv) was added to the Cu^{II} complexes to reduce the copper to radical-generating Cu^{I}.

Table 5.4. Effective concentration (EC_{50}) values for DNA damage and electrochemical potentials (versus NHE) of the complexes in methanol.

Compound	EC_{50} (μM)	$E_{1/2}$ (V)
$[Cu(clotri)_3(NO_3)][NO_3]\cdot 2H_2O$	10.47 ± 0.01	-0.515[a], -0.012[b]
$Cu_3(S,S(+)\text{-cpse})_3$	15.14 ± 0.02	-0.627[a], -0.415[a], -0.008[b]
$Cu_3(R,R(-)\text{-cpse})_3$	21.72 ± 0.03	-0.564[a], -0.383[a]

[a]$Cu^{I/0}$ potential. [b]$Cu^{II/I}$ potential.

DNA damage caused by increasing concentrations of $[Cu(clotri)_3(NO_3)][NO_3]$ and ascorbic acid with H_2O_2 is shown in Figure 5.11. Lane 2 shows that hydrogen peroxide alone does not result in DNA damage, but reducing Cu^{II} to form Cu^{I} in the presence of H_2O_2 results in DNA damage (lane 3).

Upon adding increasing concentrations of $[Cu(clotri)_3(NO_3)][NO_3]$, DNA damage is significantly increased, with ~90 % DNA damage at 50 μM. Clotri alone shows no ability to damage DNA at these concentrations (data not shown) or over the 30 min reaction time. This is not surprising, since previous studies have shown clotrimazole reduces the viability of human breast cancer cell line (MCF-7) in both dose- and time-dependent responses (EC_{50} of 89 ± 5 μM at 90 ± 7 min).[9] Likewise, Barba-Behrens *et al.* reported EC_{50} values between 12-52 μM for clotri toxicity in HeLa (cervix-uterine), PC3 (prostate), and HCT-15 (colon) cancer cell lines after treatment for 24 h.[14] Figure 5.12A shows a best-fit dose-response curve for DNA damage by

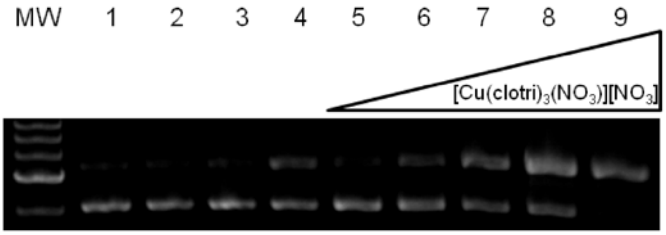

Figure 5.11. Gel electrophoresis image of Cu^{I}-mediated DNA damage by $[Cu(clotri)_3(NO_3)][NO_3]\cdot 2H_2O$ in MOPS buffer (10 mM, pH 7). Lane: MW = 1 kb molecular weight marker; lane 1: plasmid DNA (p); lane 2: p + H_2O_2; lane 3: p + compound + H_2O_2; lane 4: p + ascorbate (AA, 7.5 μM) + $CuSO_4$ (6 μM) + H_2O_2 (50 μM); lanes 5-9: p + increasing compound concentration + AA + H_2O_2: 1 (lane 5), 5 (lane 6), 10 (lane 7), 25 (lane 8), and 50 μM (lane 9) $[Cu(clotri)_3(NO_3)][NO_3]\cdot 2H_2O$, respectively.

[Cu(clotri)$_3$(NO$_3$)][NO$_3$], resulting in a calculated concentration required to promote 50% DNA damage (EC$_{50}$) of 10.47 ± 0.01 µM.

Similar studies were conducted with Cu$_3$(*R*,*R*(-)-cpse)$_3$ and Cu$_3$(*S*,*S*(+)-cpse)$_3$, to determine their ability to promote DNA damage; EC$_{50}$ plots for these complexes are shown in Figure 5.12. Cu$_3$(*R*,*R*(-)-cpse)$_3$ and Cu$_3$(*S*,*S*(+)-cpse)$_3$ promote DNA damage with EC$_{50}$ values of 21.72 ± 0.03 µM and 15.14 ± 0.02 µM, respectively (Table 5.4). The only difference between these two complexes is the chirality of the coordinated H$_2$cpse ligands, yet they have statistically different EC$_{50}$ values. Thus, chirality plays asignificant role in the DNA damaging ability of these copper complexes.

The obtained DNA damage results correlate well with previously published growth inhibition data for these complexes in HeLa (cervical-uterine), PC3 (prostate),

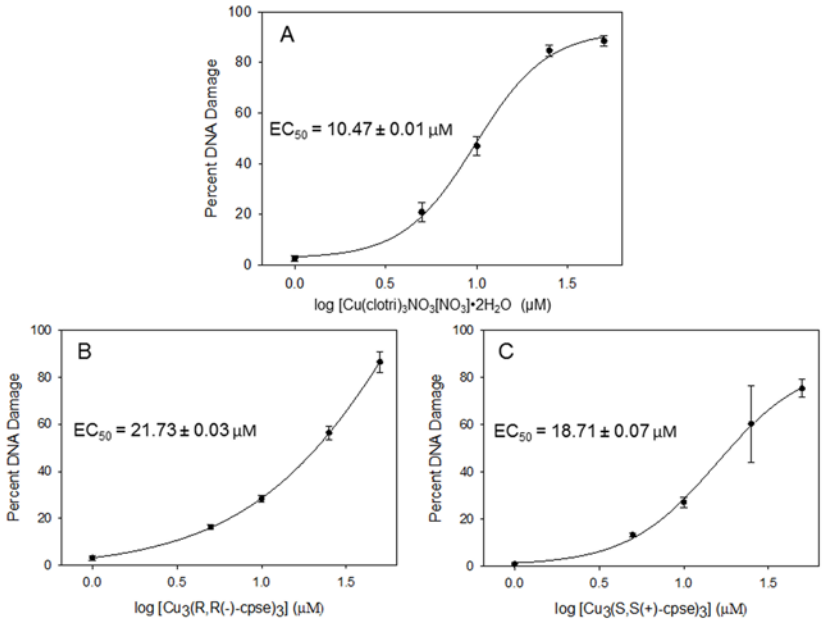

Figure 5.12. Dose-response curves for DNA damage by A) [Cu(clotri)$_3$(NO$_3$)][NO$_3$], B) Cu$_3$(*R*,*R*(-)-cpse)$_3$, and C) Cu$_3$(*S*,*S*(+)-cpse)$_3$.

and HCT-15 (colon) cancer cell lines.[14] Cu^{II} compounds $[Cu(clotri)_2Cl_2]$ and $[Cu(clotri)_3(NO_3)][NO_3]$ exhibit generally lower IC_{50} values (3.2-8.2 μM) compared with Co^{II} complex $[Co(clotri)_2Cl_2]$ and $[Co(clotri)_3(NO_3)_2]$ (IC_{50} values of 7.0-27.0 μM), suggesting that DNA interactions might be the cause of these compounds' cytotoxicity. Electrochemical results also correlate with the reported cytotoxicity, since $[Cu(clotri)_2Cl_2]$, $[Cu(clotri)_2Br_2]$, and $[Cu(clotri)_3(NO_3)][NO_3]$ were the most cytotoxic clotri complexes,[14] and these Cu^{II} complexes readily undergo reduction to Cu^{I} ($Cu^{II/I}$ potentials of -0.239 to -0.012 V) at biologically attainable potentials. Cellular Cu^{I} is known to generate hydroxyl radical that causes DNA damage and death,[29] and this reaction primarily occurs in biological systems if the metal redox potentials are between –0.324 to 0.460 V.[30] The less electrochemically accessible $Co^{III/II}$ potentials (0.512 V for the cobalt chloride complex and only an oxidation potential of 0.977 V for the cobalt bromide complex) lie outside the biological window for hydroxyl radical generation, so these complexes are less likely to cause cellular damage by ROS generation. Unsurprisingly, the redox inactive Zn^{II} complexes were found to be the least cytotoxic.[31] Correlation of the cellular toxicity results with the electrochemical redox potentials for these complexes suggest that some of these compounds may cause cell death by generating reactive oxygen species.

$Cu_3(S,S(+)\text{-cpse})_3$ has slightly more negative $E_{1/2}$ values for the $Cu^{II/I}$ redox couple compared to $[Cu(clotri)_3(NO_3)][NO_3]$ (Table 5.4), indicating that Cu^{II} is favored more upon coordination by the H_2cpse ligand. When this complex is reduced by ascorbic acid, the resulting Cu^{I} species should be more susceptible to oxidation by H_2O_2, resulting in

greater hydroxyl radical formation and oxidative DNA damage. The $E_{1/2}$ value for the $Cu^{II/I}$ couple for $[Cu(clotri)_3(NO_3)][NO_3]$ and $Cu_3(S,S(+)\text{-cpse})_3$ falls within the biological electrochemical window for the Fenton-like reaction (-0.324 V < $E_{1/2}$ < 0.460 V),[30] as would be expected from the observed DNA damage. Given the degree of DNA damage observed at relatively low concentrations of these copper complexes, it is likely that copper-mediated oxidative DNA damage plays a significant role in their cytotoxicity.

5.3. Conclusions

We have shown that clotrimazole when bound to transition metals Co^{II} and Cu^{II} exhibits the ability to stabilize the higher (harder) oxidation state of the respective metals over the lower (softer) oxidation state. Gel studies with labile clotri in the presence of H_2O_2 did not result in oxidative damage to plasmid DNA within the 30 min reaction window, and is in agreement with previous studies that found the cytotoxic ability of clotri was both dose- and time-dependent. However, $[Cu(clotri)_3(NO_3)][NO_3]$ treated with ascorbic acid and H_2O_2 resulted in significant oxidative DNA damage at low concentrations, suggesting that the cytotoxic ability of clotri is amplified in the presence of copper, and is primarily dose-dependent.

In contrast, the electrochemical studies with chiral pseudophedrine analogs favor Cu^{I} over Cu^{II}, whereas previous studies have shown that similar ligands with borderline nitrogen donor pyridines favor Cu^{II}. This preference of the Cu^{I} oxidation state is likely due to the absence of aromatic nitrogen binding sites in the pseudophedrine analogs. DNA damage studies revealed the ability of $Cu_3(R,R(-)\text{-cpse})_3$ and $Cu_3(S,S(+)\text{-cpse})_3$ to

promote oxidative damage at low concentrations, exhibiting 50% effective concentrations between 10-24 μM.

This work has provided evidence that drugs with metal coordination sites promote oxidative damage in a dose-dependent manner when a redox active metal is present. In addition, the potential of the $Cu^{I/II}$ couple for these complexes fall within the biological window for $^{\bullet}OH$ generation, suggesting that their cytotoxic properties may be due in part to ROS generation.

5.4. Materials and Methods

Materials. Potassium nitrate was from Fisher. MOPS was obtained from Alfa Aesar. All compounds clotrimazole and pseudoephedrine-derived compounds were provided by Dr. Noráh Barba-Behrens (Universidad Nacional Autónoma de México). Acetonitrile was obtained from BDH. Tetrabutylammonium hexafluorophosphate ($TBAPF_6$) was obtained from Alfa Aesar and was purified by recrystallizing in a 3:1 mixture of ethanol:deionized water. Plasmid DNA (pBSSK) was purified from DH1 *E.* coli competent cells using a 5 Prime PerfectPrep^{TM} Spin Kit (250 count, Fisher). NaCl (99.999%), glycerol, and bromophenol blue were all from Alfa Aesar. Yeast extract, 30% H_2O_2, sodium EDTA, tryptone (peptone), $CuSO_4 \cdot 5H_2O$, agarose, and dichoromethane were all from Fisher. Glucose and ampicillin were from EMD. Ethidium bromide and agar were from Lancaster. Ethanol (200 proof) and ascorbic acid were from Acros Organics. Xylene cyanol FF was from J. T. Baker. Tris hydrochloride and microcentrifuge tubes were from VWR. A NANOpure Diamond water deionization

system (Barnstead Internationl, Dubuque, IA) was used to prepare deionized H_2O (diH_2O). Degassed diH_2O was prepared by bubbling with N_2 gas for at least 4 h. Metal-free microcentrifuge tubes were prepared by washing the tubes in 1 M HCl for ~1 h, and then triple rinsing three times with diH_2O.

Electrochemical Studies. Cyclic voltammetry (CV) and differential pulse voltammetry (DPV) experiments were conducted with a CH Electrochemical Analyzer (CH Instruments, Inc.) in dry, degassed acetonitrile (or dichloromethane) with $TBAPF_6$ (0.1 M) as a supporting electrolyte. Final concentrations of all compounds were 1 mM, with a final volume of 5 mL. All samples were degassed for 10 min with N_2 before each experiment. CV experiments were conducted with a scan rate of 100 mV/s. DPV experiments were conducted on all samples and confirmed all waves observed in the cyclic voltammograms. A pulse amplitude of 0.020 V and a pulse width of 0.050 were used for all DPV experiments, in conjunction with a sample width of 0.020 and a pulse period of 0.100. Samples of each complex were cycled between -1.6 V and 1.6 V using a glassy carbon working electrode, a Pt counter electrode, and a Ag/AgCl (+0.197 V vs. NHE[32]) reference electrode. All acetonitrile and dichloromethane experiments were externally referenced to ferrocene (0.593 V vs. Ag/AgCl[33]).

Plasmid transfection, amplification, and purification. Tris-EDTA buffer (pH 8.01) was used to elude the plasmid from the spin columns. Plasmid was dialyzed against 130 mM NaCl for 24 h at 4°C to ensure all Tris-EDTA buffer and metal contaminates were removed. Plasmid concentration at 260 nm and absorbance ratios of $A_{250}/A_{260} \leq 0.95$ and $A_{260}/A_{280} \geq 1.8$ were determined via UV-vis for DNA used in all

experiments. Plasmid purity was determined through digestion (0.1 pmol) with *Sac 1* and *KpN1* in a mixture of NEB buffer and bovine serum albumin was conducted at 37°C for 90 min. Comparison to an undigested plasmid sample and a 1 kb molecular weight marker was performed using gel electrophoresis.

DNA damage gel electrophoresis experiments. Deionized H_2O, MOPS buffer (10 mM, pH 7.39), NaCl (130 mM), ethanol (0.02-0.86 M), ascorbate (7.5-62.5 μM), and the indicated concentrations of the Cu^{II} complexes (1-50 μM) were combined in a microcentrifuge tube and allowed to stand for 5 min at room temperature. Plasmid (pBSSK; 0.1 pmol in 130 mmol NaCl solution) was then added to the reaction mixture and allowed to stand for 5 min at room temperature. Hydrogen peroxide (50 μM) was added and allowed to react at room temperature for 30 min, and then EDTA (50 μM) was added to quench the reaction. All given concentrations were final concentrations in a 10 μL volume. Samples were loaded into a 1% agarose gel in TAE running buffer; and damaged and undamaged plasmid DNA was separated by electrophoresis (140 V for 30 min). Gels were then stained using ethidium bromide and imaged under UV light. The amounts of nicked (damaged) and circular (undamaged) DNA were quantified using UViProMW (Jencons Scientific Inc., 2007). The intensity of the circular plasmid band was multiplied by 1.24, due to the different binding abilities of ethidium bromide to supercoiled and nicked plasmid DNA.[34,35]

Calculating percent inhibition of DNA damage. The formula 1-[%N-%B]*100 was used to calculate percent DNA damage inhibition; %N = percent of nicked DNA in lanes 6 and higher, and %B = the percent of nicked DNA in the Cu^{I}/H_2O_2 or Fe^{II}/H_2O_2

control lane (lane 5). All percentages were corrected for residual nicked DNA (lane 2) prior to calculation. Results were obtained from an average of three trials, with indicated standard deviations.

5.5. References

(1) Kelland, L. *Nat. Rev. Cancer* **2007**, *7*, 573-584.

(2) Tan, C. P.; Lu, Y. Y.; Ji, L. N.; Mao, Z. W. *Metallomics* **2014**, *6*, 978-995.

(3) Wang, D.; Lippard, S. J. *Nat. Rev. Drug Discov.* **2005**, *4*, 307-320.

(4) Henle, E. S.; Han, Z.; Tang, N.; Rai, P.; Luo, Y.; Linn, S. *J. Bio. Chem.* **1999**, *274*, 962-971.

(5) Henle, E. S.; Linn, S. *J. Bio. Chem.* **1997**, *272*, 19095-19098.

(6) Imlay, J. A. *Annu. Rev. Microbiol.* **2003**, *57*, 395-418.

(7) MacNeil, S.; Dawson, R. A.; Crocker, G.; Tucker, W. F.; Bittiner, B.; Singleton, J. G.; Hunter, T.; Tierney, D. F. *Br. J. Dermatol.* **1993**, *128*, 143-150.

(8) Wilson, D.; Hebecker, B.; Moyes, D. L.; Miramon, P.; Jablonowski, N.; Wisgott, S.; Allert, S.; Naglik, J. R.; Hube, B. *Antimicrob. Agents Chemother.* **2013**, *57*, 5178-5180.

(9) Meira, D. D.; Marinho-Carvalho, M. M.; Teixeira, C. A.; Veiga, V. F.; Da Poian, A. T.; Holandino, C.; de Freitas, M. S.; Sola-Penna, M. *Mol. Genet. Metab.* **2005**, *84*, 354-362.

(10) Penso, J.; Beitner, R. *Mol. Genet. Metab.* **2002**, *76*, 181-188.

(11) Ito, C.; Tecchio, C.; Coustan-Smith, E.; Suzuki, T.; Behm, F. G.; Raimondi, S. C.; Pui, C. H.; Campana, D. *Leukemia* **2002**, *16*, 1344-1352.

(12) Oyama, T. M.; Oyama, T. B.; Oyama, K.; Matsui, H.; Horimoto, K.; Nishimura, Y.; Oyama, Y. *Toxicology* **2006**, *228*, 269-279.

(13) Oyama, Y.; Matsui, H.; Morimoto, M.; Sakanashi, Y.; Nishimura, Y.; Ishida, S.; Okano, Y. *Toxicol. Lett.* **2007**, *171*, 138-145.

(14) Betanzos-Lara, S.; Gomez-Ruiz, C.; Barron-Sosa, L. R.; Gracia-Mora, I.; Flores-Alamo, M.; Barba-Behrens, N. *J. Inorg. Biochem.* **2012**, *114*, 82-93.

(15) Gillies, H.; Derman, W. E.; Noakes, T. D.; Smith, P.; Evans, A.; Gabriels, G. *J. Appl. Physiol.* **1996**, *81*, 2611-2617.

(16) Minamizawa, K.; Goto, H.; Ohi, Y.; Shimada, Y.; Terasawa, K.; Haji, A. *J. Pharmacol. Sci.* **2006**, *102*, 136-142.

(17) Raviteja, K. H.; Nasare, M.; Prasad, V. V. L. N.; Diwan, P. V. *Br. J. Pharma. Res.* **2014**, *4*, 418-428.

(18) Ávila-Torres, Y.; López-Sandoval, H.; Mijangos, E.; Quintanar, L.; Rodríguez, E. E.; Flores-Parra, A.; Contreras, R.; Vicente, R.; Rikken, G. L. J. A.; Barba-Behrens, N. *Polyhedron* **2013**, *51*, 298-306.

(19) Araujo, C. M.; Doherty, M. D.; Konezny, S. J.; Luca, O. R.; Usyatinsky, A.; Grade, H.; Lobkovsky, E.; Soloveichik, G. L.; Crabtree, R. H.; Batista, V. S. *Dalton Trans.* **2012**, *41*, 3562-3573.

(20) Neelakantan, M. A.; Sundaram, M.; Nair, M. S. *J. Chem. Eng. Data* **2011**, *56*, 2527-2535.

(21) Nair, M. S.; Raj, C. R. S. *J. Coord. Chem.* **2009**, *17*, 2903-2908.

(22) Falcomer, V. A.; Lemos, S. S.; Batista, A. A.; Ellena, J.; Castellano, E. E. *Inorg. Chim. Acta* **2006**, *359*, 1064-1070.

(23) Miyamoto, R.; Santo, R.; Matsushita, T.; Nishioka, T.; Ichimura, A.; Teki, Y.; Kinoshita, I. *Dalton Trans.* **2005**, 3179-3186.

(24) Dai, Z.; Xu, X.; Canary, J. W. *Chirality* **2005**, *17*, S227-S233.

(25) Srinivasan, S.; Athappan, P. *Trans. Metal Chem.* **2001**, *26*, 588-593.

(26) Castro, M.; Cruz, J.; Lopez-Sandoval, H.; Barba-Behrens, N. *Chem. Commun.* **2005**, 3779-3781.

(27) Niklas, N.; Hampel, F.; Walter, O.; Gunter, L.; Alsfasser, R. *Eur. J. Inorg. Chem.* **2002**, *7*, 1839-1847.

(28) Feldscher, B.; Stammler, A.; Bögge, H.; Glaser, T. *Polyhedron* **2011**, *30*, 3038-3047.

(29) Ramirez, D. C.; Mejiba, S. E.; Mason, R. P. *J. Biol. Chem.* **2005**, *280*, 27402-27411.

(30) Pierre, J. L.; Fontecave, M. *Biometals* **1999**, *12*, 195-199.

(31) Kapitza, S.; Jakupec, M. A.; Uhl, M.; Keppler, B. K.; Marian, B. *Cancer Lett.* **2005**, *226*, 115-121.

(32) Bard, A. J.; Faulkner, L. R. *Electrochemical Methods, Fundamentals and Applications*; Second ed.; Wiley: New York, 2004, pp 286-293.

(33) Connelly, N. G.; Geiger, W. E. *Chem. Rev.* **1996**, *96*, 877-910.

(34) Hertzberg, R. P.; Dervan, P. B. *J. Am. Chem. Soc.* **1982**, *104*, 313-315.

(35) Lloyd, R. S.; Haidle, C. W.; Robberson, D. L. *Biochemistry* **1978**, *17*, 1890-1896.

CHAPTER SIX

DNA DAMAGE PREVENTION ABILITIES OF MULTIFUNCTIONAL SELENIUM AND SULFUR COMPOUNDS AND THE ROLE OF REDOX-ACTIVE METALS IN THE BIOLOGICAL ACTIVITY OF CLOTRIMAZOLE AND PSEUDOEPHEDRINE-DERIVED COMPOUNDS

6.1. Conclusions

The primary cause of DNA damage under oxidative stress conditions is metal-mediated formation of $^{\bullet}OH$ from H_2O_2 reduction,[1-3] and this damage is an underlying cause of many chronic diseases.[4-8] Both metal ions and ROS are required for cellular functions, so cells have many mechanisms to maintain metal and ROS homeostasis. During oxidative stress, however, levels of ROS can rise faster than cellular antioxidants can scavenge them. Oxidative damage can quickly spiral out of control when metal-chelating proteins are damaged, releasing redox-active metals such as Fe^{II} and Cu^{I}.[9-11] Interest in endogenous and exogenous sulfur and selenium antioxidants arose from their natural roles in maintaining cellular homeostasis, previously observed anticancer properties, the biological abundance of sulfur- and selenium-containing amino acids, and their ability to treat and prevent many chronic diseases.[12,13]

Previous studies determined that sulfur- and selenium-containing amino acids and their derivatives more effectively prevent Cu^{I}-mediated DNA damage than Fe^{II}-mediated DNA damage, and demonstrated that copper coordination is necessary, but not sufficient, for their observed antioxidant activity.[14-18] Electrochemical studies of these sulfur and selenium antioxidants revealed that the majority of the selenium compounds are readily

oxidized, an indication of potential ROS scavenging properties, but only two of the sulfur compounds exhibited any redox behavior (Chapter 2) under the conditions used. Since DNA damage prevention is observed for sulfur compounds that are redox-inactive and not all redox-active selenium compounds prevent DNA damage, metal binding rather than ROS scavenging was determined to be the primary mechanism for sulfur selenium antioxidant prevention of metal-mediated DNA damage.

Due to the promising antioxidant behavior quantified for sulfur- and selenium-containing amino acids, the abilities of *N*,*N*'-dimethylimazole thione (dmit) and selone (dmise) to prevent metal-mediated DNA damage were also investigated. These thione and selone compounds are similar to the antithyroid drug methimazole and the naturally occuring thione- and selone-containing amino acids ergothioneine and selenoneine. Dmit and dmise inhibit Cu^{I}-mediated DNA damage (IC_{50} = 1550 μM and ~240 μM, respectively; Chapter 3), but in contrast to all other sulfur and selenium antioxidants tested for prevention of metal-mediated DNA damage, dmit and dmise are more potent inhibitors of Fe^{II}-mediated DNA damage (IC_{50} = 89.1 μM and 3.2 μM, respectively; Chapter 3). Additional mass spectrometry studies confirmed their ability to coordinate both Cu^{I} and Fe^{II}. Interest in these two compounds was further peaked upon observing prevention of oxidative damage when their ability to bind Cu^{I} or Fe^{II} was removed by using $[Cu(bipy)_2]^{+}$ and $[Fe(EDTA)]^{2-}$ to generate DNA-damaging hydroxyl radical, suggesting that these antioxidants can effectively scavenge $^{\bullet}OH$ in addition to binding copper and iron to prevent DNA damage. This idea was reinforced by the fact that dmit prevents peroxynitrite ($ONOO^{-}$)-mediated DNA damage under metal-free conditions,

albeit at higher concentrations (> 100 μM). Similar to previous DNA damage prevention studies, the selenium-containing dmise was more effective than the sulfur-containing dmit at preventing DNA damage from all sources. Thus, the research described in Chapter 3 has identified the first multifunctional sulfur and selenium antioxidants that prevent metal-mediated DNA damage by metal coordination at very low micromolar concentrations and by ROS scavenging at concentrations over 100 μM.

Since dmit and dmise prevent DNA damage by multiple antioxidant mechanisms, further studies were conducted on structurally similar compounds to determine: 1) if they possess similar multifunctional antioxidant properties, 2) if they have similar antioxidant mechanisms (metal coordination, targeted scavenging of ROS, etc.) for DNA damage prevention, and, 3) if there are relationships between structure and antioxidant activity. In contrast to the sulfur and selenium amino acid compounds,[14-16] every sulfur and selenium compound studied in Chapter 4 prevents both Cu^{I}- and Fe^{II}-mediated DNA damage with IC_{50} values ranging from 12-1023 μM and 2.3-1000 μM, respectively. Additionally, the majority of these compounds, with the exception of ethyl-bis(imidazole) thione and (2-mercapto-1-methylimidazolyl) pyridine thione, more effectively prevent DNA damage by Fe^{II} than by Cu^{I} ;. As observed for dmit and dmise in Chapter 3, antioxidant behavior is also observed for these thione and selone compounds when $[Cu(bipy)_2]^{+}$, $[Fe(EDTA)]^{2-}$, and $ONOO^{-}$ cause the DNA damage but at substantially higher concentrations compared to DNA damage from Cu^{I} and Fe^{II}. Therefore, the thione, selone and related compounds investigated in Chapter 4 utilize multiple mechanisms to prevent oxidative DNA damage.

Comparing results from the sulfur-containing compounds from Chapter 4, it is

evident that methylation of the imidazole nitrogens plays a significant role in DNA damage prevention, since the non-methylated ergothioneine and 2-mercaptoimazole have the lowest IC_{50} values with both Cu^{I} and Fe^{II}, followed by the mono-methylated methimazole and ergothioneine. Nitrogen methylation accounts for an average 5-fold increase in activity for compounds with no methylation compared to mono-methylated compounds and an average 15-fold increase in activity compared to di-methylated compounds. The potentially aromatic thiones 2-MerIm and MetIm are active at concentrations 12 times lower than the non-aromatic sulfide PTAS for inhibition of both copper- and iron-mediated DNA damage. The largest contributor to thione antioxidant activity is denticity; compounds that possess more than one possible metal binding site typically require concentrations 48-fold less than compounds with only one metal binding site. Denticity also has a significant impact on selenium antioxidant prevention of Cu^{I}-mediated DNA damage, followed by selenium functional group (C=Se or P=Se; accounting for an approximately 4-fold difference in activity). As is typical,[14-18] the selenium-containing compounds were 6-to-27-fold more effective than analogous sulfur-containing compounds at preventing metal-mediated DNA damage.

Mass spectrometry studies revealed that the majority of the compounds form complexes with Cu^{I} and Fe^{II}, supporting the relationship between metal coordination and DNA damage prevention (Chapter 4). Electrochemical studies revealed that many of these compounds are readily oxidized, indicative of ROS scavenging capabilities. When Cu^{I} or Fe^{II} is added to solutions of these antioxidants, most were found to stabilize Cu^{II} and Fe^{II} relative to Cu^{I} and Fe^{III}, but the $Cu^{II/I}$ and $Fe^{III/II}$ potentials in the presence of

these antioxidants fall within the redox window of the biological Fenton and Fenton-like reactions, suggesting that thione- and selone-metal binding to prevent metal redox cycling is not a major mechanism for antioxidant activity. The primary antioxidant mechanism at very low micromolar concentrations is through metal coordination (targeted scavenging), whereas ROS scavenging is active at high concentrations. These are the first studies that have observed multifunctional sulfur and selenium compounds capable of preventing multiple types of metal- and nonmetal-mediated DNA damage.

The most exciting breakthrough from this work is the determination of a relationship between chemical structure and antioxidant activity, which has been difficult to observe in previous research due to the limited structural diversity of the antioxidants studied. The most pertinent chemical properties observed in this work are nitrogen methylation > denticity > aromaticity > S/Se speciation, and these results will allow researchers to develop compounds of interest that are highly potent inhibitors of oxidative damage, instead of the time consuming process of investigating compounds one by one. Since many of the sulfur and selenium compounds discussed in Chapters 3 and 4 are analogs of both natural and pharmaceutical compounds, this work will also allow effective development and execution of animal and clinical trials for prevention and treatment of diseases caused by oxidative stress.

Similar to sulfur and selenium antioxidant activity, interactions of redox-active biological metal ions with known drugs and anticancer agents is not well explored. In Chapter 5, electrochemical studies of clotrimazole, an antifungal agent, with $Cu^{II/I}$ and $Co^{II/I}$ showed that the higher oxidation state is stabilized more than the lower oxidation

state upon clotrimazole coordination. In addition, DNA damage studies with $[Cu(clotri)_3(NO_3)][NO_3] \cdot 2H_2O$ revealed that the Cu^{II} center is readily reduced by ascorbic acid, and when treated with H_2O_2, can generate DNA damaging $^{\bullet}OH$. These results support previous studies that clotrimazole-metal complexes kill cancer cells[19,20] and suggest that the observed cytotoxic activity may be due to apoptosis caused by cellular DNA damage.

Pseudophedrine is a stimulant and antitussive drug that can potentially coordinate metal ions. Studies of pseudoephedrine-derived Cu^{II} complexes (Chapter 5) revealed their ability to stabilize Cu^{I} relative to Cu^{II}, likely due to these ligands' lack of aromatic nitrogen binding sites. Little is known about interactions of pseudoephedrine and redox-active metals, but DNA damage studies conducted on $Cu_3(R,R(-)\text{-cpse})_3$ and $Cu_3(S,S(+)\text{-cpse})_3$ revealed their ability to generate $^{\bullet}OH$, resulting in effective concentrations for 50% oxidative DNA damage between 10-24 μM. These studies of clotrimazole and pseudoephedrine-derived metal complexes illustrated how redox-active metal binding can amplify known cytotoxic properties (clotrimazole), or result in unexpected cytotoxic properties (pseudoephedrine). This information is crucial for the future development of effective cytotoxic metal complexes as antifungal and anticancer agents and for the development of drugs that have minimum adverse reactions in the presence of biologically relevant metal ions.

6.2. References

(1) Bar-Or, D.; Thomas, G. W.; Rael, L. T.; Lau, E. P.; Winkler, J. V. *Biochem. Biophys. Res. Commun.* **2001**, *282*, 356-360.

(2) Imlay, J. A. *Annu. Rev. Microbiol.* **2003**, *57*, 395-418.

(3) Imlay, J. A. *Annu. Rev. Biochem.* **2008**, *77*, 755-776.

(4) Brewer, G. J. *Exp. Biol. Med.* **2007**, *232*, 323-335.

(5) Collins, C. A.; Fry, F. H.; Holme, A. L.; Yiakouvaki, A.; Al-Qenaei, A.; Pourzand, C.; Jacob, C. *Org. Biomol. Chem.* **2005**, *3*, 1541-1546.

(6) De Flora, S.; Izzotti, A. *Mutat. Res.* **2007**, *621*, 5-17.

(7) Fry, F. H.; Holme, A. L.; Giles, N. M.; Giles, G. I.; Collins, C.; Holt, K.; Pariagh, S.; Gelbrich, T.; Hursthouse, M. B.; Gutowski, N. J.; Jacob, C. *Org. Biomol. Chem.* **2005**, *3*, 2579-2587.

(8) Loft, S.; Deng, X. S.; Tuo, J.; Wellejus, A.; Sorensen, M.; Poulsen, H. E. *Free Radic. Res.* **1998**, *29*, 525-539.

(9) Angel, I.; Bar, A.; Horovitz, T.; Taler, G.; Krakovsky, M.; Resnitsky, D.; Rosenberg, G.; Striem, S.; Friedman, J. E.; Kozak, A. *Drug Dev. Res.* **2002**, *56*, 300-309.

(10) Keyer, K.; Imlay, J. A. *Proc. Natl. Acad. Sci. USA* **1996**, *93*, 13635-13640.

(11) Perry, G.; Cash, A. D.; Srinivas, R.; Smith, M. A. *Drug Dev. Res.* **2002**, *56*, 293-299.

(12) Kieliszek, M.; Blazejak, S. *Nutrition* **2013**, *29*, 713-718.

(13) Zwolak, I.; Zaporowska, H. *Cell Biol. Toxicol.* **2012**, *28*, 31-46.

(14) Battin, E. E.; Brumaghim, J. L. *J. Inorg. Biochem.* **2008**, *102*, 2036-2042.

(15) Battin, E. E.; Perron, N. R.; Brumaghim, J. L. *Inorg. Chem.* **2006**, *45*, 499-501.

(16) Battin, E. E.; Zimmerman, M. T.; Ramoutar, R. R.; Quarles, C. E.; Brumaghim, J. L. *Metallomics* **2011**, *3*, 503-512.

(17) Ramoutar, R. R.; Brumaghim, J. L. *J. Inorg. Biochem.* **2007**, *101*, 1028-1035.

(18) Ramoutar, R. R.; Brumaghim, J. L. *Main Group Chem.* **2007**, *6*, 143-153.

(19) Betanzos-Lara, S.; Gomez-Ruiz, C.; Barron-Sosa, L. R.; Gracia-Mora, I.; Flores-Alamo, M.; Barba-Behrens, N. *J. Inorg. Biochem.* **2012**, *114*, 82-93.

(20) Meira, D. D.; Marinho-Carvalho, M. M.; Teixeira, C. A.; Veiga, V. F.; Da Poian, A. T.; Holandino, C.; de Freitas, M. S.; Sola-Penna, M. *Mol. Genet. Metab.* **2005**, *84*, 354-362.

APPENDIX A

COPYRIGHT PERMISSION FOR PRESENTED WORK

Chapter One (Figures 1.4 and 1.6)

Copyright Clearance Center RightsLink®

Home | Account Info | Help

ACS Publications

Title: Oxidation of Biologically Relevant Chalcogenones and Their Cu(I) Complexes: Insight into Selenium and Sulfur Antioxidant Activity

Author: Martin M. Kimani, Craig A. Bayse, Bradley S. Stadelman, and Julia L. Brumaghim

Publication: Inorganic Chemistry

Publisher: American Chemical Society

Date: Oct 1, 2013

Copyright © 2013, American Chemical Society

Logged in as:
Matthew Zimmerman
Account #:
3000778920

LOGOUT

PERMISSION/LICENSE IS GRANTED FOR YOUR ORDER AT NO CHARGE

This type of permission/license, instead of the standard Terms & Conditions, is sent to you because no fee is being charged for your order. Please note the following:

- Permission is granted for your request in both print and electronic formats, and translations.
- If figures and/or tables were requested, they may be adapted or used in part.
- Please print this page for your records and send a copy of it to your publisher/graduate school.
- Appropriate credit for the requested material should be given as follows: "Reprinted (adapted) with permission from (COMPLETE REFERENCE CITATION). Copyright (YEAR) American Chemical Society." Insert appropriate information in place of the capitalized words.
- One-time permission is granted only for the use specified in your request. No additional uses are granted (such as derivative works or other editions). For any other uses, please submit a new request.

If credit is given to another source for the material you requested, permission must be obtained from that source.

BACK | CLOSE WINDOW

Chapter Two


Copyright Clearance Center
RightsLink
Home
Account Info
Help
Metallomics
Title: Preventing metal-mediated oxidative DNA damage with selenium compounds
Author: Erin E. Battin,Matthew T. Zimmerman,Ria R. Ramoutar,Carolyn E. Quarles,Julia L. Brumaghim
Publication: Metallomics
Publisher: Royal Society of Chemistry
Date: Feb 2, 2011
Copyright © 2011, Royal Society of Chemistry
Logged in as:
Matthew Zimmerman
Account #:
3000778920
LOGOUT
This reuse request is free of charge. Please review guidelines related to author permissions here:
http://www.rsc.org/AboutUs/Copyright/Permissionrequests.asp
BACK
CLOSE WINDOW
Copyright © 2014 Copyright Clearance Center, Inc. All Rights Reserved. Privacy statement.
Comments? We would like to hear from you. E-mail us at customercare@copyright.com